

UNIVERSITY OF OKLAHOMA

GRADUATE COLLEGE

BACTERIAL FLAGELLA TEMPLATED SYNTHESIS OF HYBRID
NANOMATERIALS BY BIOMIMETIC MINERALIZATION IN MILD CONDITIONS

A DISSERTATION

SUBMITTED TO THE GRADUATE FACULTY

in partial fulfillment of the requirements for the

Degree of

DOCTOR OF PHILOSOPHY

By

DONG LI
Norman, Oklahoma
2011

BACTERIAL FLAGELLA TEMPLATED SYNTHESIS OF HYBRID
NANOMATERIALS BY BIOMIMETIC MINERALIZATION IN MILD CONDITIONS

A DISSERTATION APPROVED FOR THE
DEPARTMENT OF CHEMISTRY AND BIOCHEMISTRY

BY

Dr. Chuanbin Mao, Chair

Dr. Paul F. Cook

Dr. Philip E. Klebba

Dr. Wai Tak Yip

Dr. Roger G. Harrison Jr.

© Copyright by DONG LI 2011

All Rights Reserved.

ACKNOWLEDGEMENTS

First, I would like to express my sincere thanks to my research advisor Dr. Chuanbin Mao for his encouragement, patience and guidance throughout the progress of this study, for his unconditional support during all these years, and for being an excellent mentor. He also gave me the freedom to carve out my own path, even if it meant the path was uncertain at times. Without his unflagging support and encouragement over the years, I would not have made it this far.

To my Ph.D. committee members, I wish to wholeheartedly thank for their excellent suggestions and kind help when I met some difficulties in my life. I am extremely grateful to Dr. Philip E. Klebba and Dr. Salette M. C. Newton who gave me valuable guidance and support when I study flagella display. Without their help, none of this would have been possible. I also wish to thank Dr. C. LeRoy Blank for his sincere help when I took teach test.

I owe an immense debt of gratitude to Dr. Preston Larson and Mr. Gregory W. Strout for their scientific support and untiring help for TEM and SEM examination. I extend my sincere thanks to Dr. Ann H. West for her kind help and support when I study in her lab in the first year.

I am grateful to all my friends and my lab mates for their ready help and cooperation. Last, but certainly not least, I would like to express my endless gratitude to my family, friends and colleagues, for their support and encouragement throughout these really difficult years.

TABLE OF CONTENTS

ACKNOWLEDGEMENTS.....	IV
TABLE OF CONTENTS.....	V
LIST OF TABLES.....	IX
LIST OF FIGURES.....	X
LIST OF ABBREVIATIONS.....	XIII
ABSTRACT.....	XVI
Chapter 1 Flagella-Templated Nanomaterials Synthesis and Assembly.....	1
1. 1 Introduction.....	1
1. 2 Biology and structure of flagella.....	2
1. 3 Flagella assembly.....	8
1. 4 Peptide display on flagella.....	9
1. 5 Biomedical application of flagella.....	11
1. 6 Nanomaterials on flagella template.....	12
1. 7 Assembly of flagella based nanomaterials.....	23
1. 8 Outlook.....	27
Chapter 2 Biomimetic Nucleation and Growth of Bone Mineral on Bone Protein-Derived Peptides Displayed on Bacterial Flagella with Further Assembly.....	29
2. 1 Introduction.....	29
2. 2 Materials and methods.....	32
2. 2. 1 Display of bone protein derived peptides from type I collagen and BSP on bacterial flagellar surface.....	32
2. 2. 2 Purification of bacterial flagella:.....	35
2. 2. 3 Flagella examination by optical and electron microscopy:.....	36
2. 2. 4 Western blot analysis:.....	36
2. 2. 5 Nucleation of flagella in supersaturated HAP solution:.....	36
2. 2. 6 Flagella assembly with nucleation of HAP:.....	37
2. 3 Results.....	37
2. 4 Discussion.....	46
Chapter 3 Biomimetic Mineralization of Engineered Flagella Combined with Spontaneous Self-Assembly.....	52
3. 1 Introduction.....	52

3. 2 Materials and methods	54
3. 2. 1 Flagella display and purification:	54
3. 2. 2 Flagella nucleation:.....	54
3. 2. 3 Coating of flagella, type I collagen and polylysine on cell culture plate:	55
3. 2. 4 BMSCs isolation and culture:.....	55
3. 2. 5 Proliferation assay by Methylthiazoletetrazolium (MTT) test:	55
3. 2. 6 Scanning Electron Microscopy (SEM) examination:.....	56
3. 2. 7 Immunofluorescence examination:.....	56
3. 3 Result and Discussion	57
Chapter 4 Osteogenic Differentiation of Rat Bone Marrow Stem Cells on Biomimetic Nano-Structured Substrates Generated by Bioengineered Flagella.....	75
4. 1 Introduction	75
4. 2 Materials and Methods.....	77
4. 2. 1 Layer-by-layer preparation of flagella based substrate:	77
4. 2. 2 BMSCs isolation and culture:.....	78
4. 2. 3 Proliferation assay by MTT test:	79
4. 2. 4 SEM examination:	79
4. 2. 5 Immunofluorescence of OPN and OCN:.....	79
4. 2. 6 Quantitative Real-time PCR:.....	80
4. 2. 7 Mineralized bone matrix formation assay:	80
4. 2. 8 Statistical analysis:	81
4. 3 Results	81
4. 3. 1 Characterization of flagella coated substrates	81
4. 3. 2 Morphology studies of BMSCs	82
4. 3. 3 Proliferation of BMSCs on flagellar substrates	85
4. 3. 4 Gene expression by immunofluorescence	86
4. 3. 5 Quantitative real-time PCR	89
4. 3. 6 Mineralized calcium-containing matrix formation.....	92
4. 4 Discussion	93
4. 5 Conclusion.....	98

Chapter 5 Effects of Phosphorylation of Bioengineered Flagella on Biomimetic Mineralization	99
5. 1 Introduction	99
5. 2 Materials and Methods	100
5. 2. 1 Flagella Display:	100
5. 2. 2 <i>Salmonella</i> flagella purification:	101
5. 2. 3 Phosphorylation of bioengineered flagella and examination:	101
5. 2. 4 Nucleation of flagella in supersaturated HAP solution:	101
5. 3 Results and Discussion	102
Chapter 6 Assembly of Bioengineered Flagella/Collagen Hybrid with Biomimetic Mineralization	107
6. 1 Introduction	107
6. 2 Materials and Methods	108
6. 2. 1 Surface display of flagella and bioengineered flagella isolation:	108
6. 2. 2 Assembly of bioengineered flagella/collagen hybrid and biomimetic nucleation:	109
6. 2. 3 BMSCs isolation and culture:	109
6. 2. 4 SEM examination:	109
6. 3 Results and Discussions	110
Chapter 7 Morphology-Controlled Synthesis of Silica Nanotubes through pH-Sensitive Flagella	114
7. 1 Introduction	114
7. 2 Materials and Methods	116
7. 2. 1 Flagella display and purification of flagella:	116
7. 2. 2 Synthesis of silica on wild type and bioengineered flagella templates:	118
7. 3 Results and Discussion	118
Chapter 8 Biotemplated Synthesis of Hollow Bilayer of TiO ₂ /SiO ₂ Nanotubes at Ambient Conditions	134
8. 1 Introduction	134
8. 2 Materials and Methods	136
8. 2. 1 <i>Salmonella</i> flagella purification:	136
8. 2. 2 TiO ₂ /SiO ₂ growth on flagella templates:	136

8. 2. 3 Calcinations of the bilayer of TiO ₂ /SiO ₂ nanotubes at different temperatures:	137
8. 2. 4 Materials Characterization:.....	137
8. 3 Result and Discussion	137
8. 4 Conclusions	150
REFERENCES:	151

LIST OF TABLES

Table 1.1: Summary of nanomaterials prepared using engineered flagella nanotubes as scaffolds.....	13
Table 2.1: Inserted sequences in recombinant plasmid.....	33
Table 5.1: Secondary structure prediction of peptides displayed on flagella.....	106
Table 7.1: Inserted sequences in recombinant plasmid.....	116

LIST OF FIGURES

Figure 1.1: Schematic diagram of the bacterial flagellum.	3
Figure 1.2: Protein structure of flagellin.	7
Figure 1.3: Protein structure of flagella filament.	8
Figure 1.4: Diagram of <i>FliC</i> conserved and variable regions.	10
Figure 1.5: TEM images of flagella mediated inorganic nanotubes.	16
Figure 1.6: Metal nanoparticles and nanotubes synthesized on bioengineered flagella.	18
Figure 1.7: Metal nanoparticles synthesized histidine loop flagella.	19
Figure 1.8: SEM images of the obtained hybrid flagella/silica nanotubes by using different flagella as templates.	21
Figure 1.9: Low and high magnification TEM images of silica nanotubes using Fla-KKCC as templates in the presence of or without DTT.	21
Figure 1.10: TEM images of the silica nanotubes calcined at different temperatures.	22
Figure 1.11: SEM images of amorphous TiO ₂ nanotubes on flagella.	23
Figure 1.12: Coexistence between isotropic and conical phase in flagella SJW1103 at 20 mg/ml imaged with a polarization microscope.	24
Figure 1.13: TEM images of disulfide cross-linked Cys loop flagella bundles stained with 2 % phosphotungstic acid (pH 7.5)	25
Figure 1.14: Topographic AFM image of the second layer of the arginine–lysine peptide loop flagella and schematic illustration of layer-by-layer assembly of the arginine–lysine peptide loop flagella through molecular complementarity.	26
Figure 2.1: Positions of different regions within type I collagen in bone.	31
Figure 2.2: Protein sequences and positions of inserted peptides displayed on flagella.	34
Figure 2.3: Bacterial motility assay in 24 h.	37
Figure 2.4: Silver staining of bacterial flagella before and after purification.	38
Figure 2.5: SDS-PAGE electrophoresis of <i>FliC</i> and Western blotting of recombinant <i>FliC</i>	39
Figure 2.6: TEM images of flagella with N-terminal of type I collagen and C-terminal of type I collagen soaked in 4 mM supersaturated HAP precursor solution for 9 days.	40
Figure 2.7: TEM images and SAED patterns of flagella with E8 and GPP8 soaked in 4 mM supersaturated HAP precursor solution at different time intervals.	41
Figure 2.8: TEM images of high concentration of flagella with E8 nucleated in 4 mM supersaturated HAP precursor solution.	42
Figure 2.9: TEM images of Ca ²⁺ induced bioengineered flagella bundles with E8.	43
Figure 2.10: TEM images of self-assembled flagella bundles with E8 induced at 4 mM of CaCl ₂	44
Figure 2.11: FTIR analysis of flagella.	44
Figure 2.12: TEM images of flagella bundles with E8 soaked in supersaturated HAP solution with EDX and SAED analysis.	45
Figure 2.13: TEM images of ribbon-like flagella bundles displayed with E8 soaked in HAP precursor solution for 3 days with SAED analysis.	46
Figure 2.14: Oriented nucleation of HAP on the surface of flagella.	51
Figure 3.1: TEM micrographs of flagella in 4 mM supersaturated HAP precursor solution.	59

Figure 3.2: TEM micrographs of different magnification of flagella bundles formed in HAP precursor solution.....	60
Figure 3.3: TEM micrographs of bioengineered flagella under different concentration of CaCl ₂	63
Figure 3.4: TEM images of flagella at different concentrations of CaCl ₂	64
Figure 3.5: Turbidity measurement of different concentration of CaCl ₂ with flagella (65 and 130 µg/ml) at 320 nm.....	64
Figure 3.6: Schematic illustration of bundle formation of flagella was induced by Ca ²⁺	66
Figure 3.7: Immunofluorescence images of BMSCs on different materials substrate after 24 h culture.....	67
Figure 3.8: Bright field microscopy of BMSCs on different materials scaffold and control after 24 h.....	69
Figure 3.9: Immunofluorescence images of BMSCs on flagella scaffold after 24 h culture.....	69
Figure 3.10: SEM micrographs of BMSCs on collagen and flagella coated substrate.....	70
Figure 3.11: Surface spreading area and proliferation study of BMSCs on different materials coated substrate.....	70
Figure 3.12: Differentiation of BMSCs on collagen and flagella coated substrates were analyzed for gene expression by immunostaining for 7 and 14 days.....	72
Figure 3.13: Aggregated nodule-like cluster of BMSCs on flagella coated substrates were analyzed by immunostaining.....	73
Figure 4.1: Schematic illustration of the formation of the flagella substrate using layer-by-layer method.....	78
Figure 4.2: AFM micrographs of flagella surfaces prepared by layer-by-layer method.....	82
Figure 4.3: Bright field Microscopy of BMSCs on flagella and polylysine coated substrates prepared by LBL at 24 h.....	83
Figure 4.4: BMSCs morphology on flagella coated substrates using SEM.....	85
Figure 4.5: SEM topographies of polylysine coated substrate and BMSCs.....	85
Figure 4.6: Proliferation of BMSCs on flagella coated substrates with control.....	86
Figure 4.7: Cells grown on flagella and polylysine coated substrates were analyzed for gene expression by immunostaining for 7, 14 and 21 days.....	88
Figure 4.8: Light microscopy of calcified nodule-like structures formed on M-RGDE8.....	89
Figure 4.9: Real-time PCR analysis for Runx2, OPN, OCN and type I collagen (Col I) gene expression on flagella and polylysine coated substrate at different time points.....	91
Figure 4.10: Real-time PCR analysis for Runx2, OPN, OCN and type I collagen (Col I) gene expression on flagella and polylysine coated substrates.....	92
Figure 4.11: Mineralization derived from different flagella coated substrates and polylysine coated surface assayed by Alizarin red S at 14 days.....	93
Figure 4.12: TEM images of bacterial flagella from wild type <i>Salmonella</i>	94
Figure 5.1: Phosphorylation of bioengineered flagella by CK2.....	103
Figure 5.2: TEM images of bioengineered flagella after biomimetic mineralization in supersaturated HAP solution with prior and after phosphorylation.....	104
Figure 5.3: High magnification of mineralized flagella after phosphorylation.....	105
Figure 6.1: TEM micrographs of flagella/collagen composite.....	110

Figure 6.2: TEM micrographs of flagella with CBM.	111
Figure 6.3: TEM micrographs of flagella/collagen hybrid mineralized in supersaturated HAP solution with SAED.	112
Figure 6.4: Bright field microscopy images of BMSCs on flagella/collagen composite.	113
Figure 6.5: SEM micrographs of BMSCs on flagella/collage composite.	113
Figure 7.1: White precipitates formed after the reaction at different pHs.	120
Figure 7.2: TEM images of the resulting silica nanotubes on wild type flagella templates at different pHs.	121
Figure 7.3: TEM images of precipitates formed at different pHs.	122
Figure 7.4: Higher magnification of SNTs on wild type flagella templates at different pHs.	123
Figure 7.5: pH changes before and after the reaction.	125
Figure 7.6: TEM images of different morphology with various surface features of SNTs on wild type flagella templates.	126
Figure 7.7: TEM images of SNTs on wild type flagella template with different surface features and thickness.	127
Figure 7.8: The morphology and surface features of SNTs on negatively charged bioengineered flagella.	129
Figure 7.9: The morphology and surface features of SNTs on positively charged bioengineered flagella.	130
Figure 7.10: TEM images of SNTs on GPP8 flagella template.	131
Figure 7.11: SNTs morphology on bioengineered flagella with mixed polar peptides from type I collagen.	131
Figure 7.12: TEM images of SNTs on pili template.	132
Figure 8.1: Schematic representation of the procedure for fabrication bilayer titania/silica nanotubes and subsequent calcination.	138
Figure 8.2: SEM micrographs of flagella mediated titania and bilayer titania/silica nanotubes with EDX analysis.	139
Figure 8.3: TEM micrographs of titania nanotubes.	140
Figure 8.4: TEM micrographs of titania nanotubes based on other biological templates.	141
Figure 8.5: TEM micrographs of bilayer titania/silica nanotubes.	142
Figure 8.6: TEM micrographs of titania and titania with thin layer of silica nanotubes annealed at low temperature.	143
Figure 8.7: TEM micrographs of titania/silica nanotubes calcined at different temperatures.	144
Figure 8.8: TEM micrographs of thicker layer of silica on titania layer nanotubes calcined at 800 °C.	145
Figure 8.9: HRTEM micrograph with EDX analysis of calcined at 500 °C titania/silica nanotubes.	145
Figure 8.10: HRTEM micrograph with EDX analysis of titania/silica nanotubes before calcination.	147
Figure 8.11: HRTEM analysis of titania/silica nanotubes for the phase transition.	148
Figure 8.12: SEM micrographs of silica and silica/titania nanotubes using flagella as templates with EDX analysis.	150

LIST OF ABBREVIATIONS

AcAc	Acetylacetone
AFM	Atomic force microscopy
APTES	Aminopropyltriethoxysilane
Asp	Aspartic acid
BGA 75	Bone acidic glycoprotein 75
BMP-2	Bone morphogenetic protein-2
BMSCs	Bone marrow derived stem cells
BSA	Bovine serum albumin
BSP	Bone sialoprotein
CBM	Collagen-binding motif
CD	Circular dichroism
CDT	Covalent DNA display
CK2	Casein Kinase II
CPT3	Cholera toxin peptide 3
DMEM	Dulbecco's Modified Eagle Medium
DMSO	Dimethyl sulfoxide
DPP	Phosphophoryn
DSP	Dentin Sialoprotein
DTT	Dithiothreitol
ECM	Extracellular matrix
EDX	Energy dispersive X-ray
FBS	Fetal bovine serum
FliC	Flagellin

FTIR	Fourier transform infrared spectroscopy
GEPIs	Polypeptides called genetically engineered proteins for inorganics
Glu	Glutamic acid
HAP1 or HAP2	Hook-associated proteins-1 or -2
Hyp	Hydroxyproline
LBL	Layer-by-layer
MTT	Methylthiazoletetrazolium
NCPs	Non-collagenous macromolecules proteins
NHS-PEO ₄ -biotin	<i>N</i> -hydroxysulfosuccinimide-polyethyleneoxide-biotin
OCN	Osteocalcin
OGP	Osteogenic peptide
OPN	Osteopontin
PA.	Peptide-amphiphiles
PBS	Phosphate-buffered saline
PD	Phage display
PGA	Polyglycolic acid
PLA	Polylactic acid
PLGA	Copolymers of PLA and PGA
PLLA	L-lactic acid
Pro	Proline
QDs	Quantum dots
SAED	Selected area electron diffraction
SDS-PAGE	Sodium dodecyl-sulfate polyacrylamide gel electrophoresis
SEM	Scanning Electron Microscopy
Ser	Serine

TBT	Titanium IV butoxide
TEOS	Tetraethoxysilane
Titania, TiO ₂	Titanium oxide
TLR5	Toll-like receptor 5
TMV	Tobacco mosaic virus
UA	Uranyl acetate

ABSTRACT

Biological template directed nanomaterials have unique properties. Under genetic control, they can specifically interact with other macromolecules or inorganics. Moreover, the biologically based materials are easily assembled into nano-, micro- and macro-scales in a hierarchical manner because of their inherent self-assembly characteristics via molecular recognition. By integrating molecular biology, chemistry and materials science, we can control peptide-material interactions with a genetic approach. This approach provides unprecedented opportunities to design and synthesize novel nanomaterials. Bacterial flagella are composed of thousands of flagellin (*FliC*) proteins through self-assembly. By means of genetic engineering called peptide display, a foreign peptide can be inserted on *FliC* and finally displayed on the surface of bacterial flagella. At the same time, it is surface-exposed. The bio-engineered flagella can be used as a display tool for extracellular secretions, live vaccines, protein-ligand interactions, peptide display libraries, and so forth. Recently, flagella-templated synthesis and assembly of inorganic nanomaterials have exhibited a variety of promising applications as nanotubes or nanowires.

Chapter 1 is a literature review that introduces the basis and use of genetically engineered flagella, and the recent progress for flagella based synthesis and assembly of nanomaterials is summarized. Identification of domains that are responsible for the nucleation of hydroxyapatite (HAP) is explored in chapter 2 using flagella surface display technique. A bacterial flagellum has a long threadlike structure that is similar to the shape of type I collagen in bone. Because the nucleation of HAP initiates at the hole zone of type I collagen, N-, C-terminal, part of N-, C-Zone around the hole zone, and a central

repetitive (Gly-Pro-Pro)₈ (GPP8) were displayed on the surfaces of flagella. Some of the negatively charged non-collagen proteins are also considered to be involved in the nucleation process. Eight glutamic acid residues (E8) from bone sialoprotein (BSP), which are considered to be one of the most important promoters for HAP nucleation, were displayed on the surface of flagella. After nucleation in an HAP supersaturated solution, flagella with E8 and GPP8 sequences were found to be nucleated by nano-leveled HAP crystals. After the E8 flagella were assembled into bundles induced by calcium ions, we found the crystallographic *c* axes of the HAP nanocrystals were preferentially aligned with the long axes of the flagella. This arrangement is similar to the molecular level of bone. The nucleation of HAP with the spontaneous self-assembly of bioengineered flagella is discussed in chapter 3. Using a biomimetic strategy, at a high concentration, the GPP8 flagella can spontaneously self-assemble into parallel ordered structures that resemble the arrangement of type I collagen fibrils with HAP in bone. Meanwhile, the crystallographic *c*-axes of HAP are parallel to the long axes of the flagella. The biomineralized flagella can support bone marrow stem cell (BMSC) adhesion and growth. In osteogenic media, the flagella promote differentiation of BMSCs toward osteoblasts. In chapter 4, we introduce the BMSCs differentiation on the integrin-binding motif Arg-Gly-Asp (RGD) and 8 glutamic acids displayed flagella scaffold. Our results indicate that the cells are viable on flagella surfaces and show an enhanced growth rate on RGD peptide enriched flagella surfaces. Immunofluorescence and quantitative real-time PCR (q-PCR) analysis revealed that the up-regulation and early expression of osteogenic specific markers (osteopontin, OPN and osteocalcin, OCN) in cells on bioengineered flagella than on those of wild type and control. We propose the surface

chemistry and microenvironment generated by flagella can be recognized by BMSCs and trigger osteogenic signaling pathways.

Phosphorylation is a very important post-translational modification and important for mediating the HAP nucleation in bone tissue. In chapter 5, phosphorylation of serines displayed on flagella surfaces by casein kinase II (CK2) is demonstrated. After phosphorylation, the mineralization of bioengineered flagella was highly increased. Moreover, the poly-glutamic acids displayed on flagella exhibited a higher ability for the nucleation of HAP than did poly-aspartic acids. Because collagen is limited to induce apatite formation from metastable calcium phosphate solutions directly, in chapter 6, a collagen-binding motif (CBM) from OPN is displayed on flagella. The flagella can co-assembled with type I collagen to form hybrid bundles with enhanced HAP nucleation ability.

Flagella were also used as efficient biological templates for synthesis of silica nanotubes (SNTs) in aqueous solution under mild conditions. In chapter 7, the morphology of SNTs was tuned by adjusting the pH of the solution. The morphology and surface features of SNTs could also be controlled by the modification of the surface chemistry of flagella with the surface display technique. Finally, a variety of quite different morphologies and surface features of SNTs were obtained. In chapter 8, bilayer $\text{TiO}_2/\text{SiO}_2$ nanotubes mediated by flagella as templates are demonstrated using a new sol-gel method. The reaction was carried out in aqueous solution under ambient conditions. The thickness of either layer is controllable by varying the concentrations of the precursor solution or reaction time. After calcination at 500 °C, the organic flagella templates were removed. At the same time, the inner TiO_2 layer became crystalline phases and dispersed inside the

SiO₂ matrix close to the central pore. The outer SiO₂ shell was still amorphous but supported TiO₂ nanoparticles as a “skeleton”.

Chapter 1 Flagella-Templated Nanomaterials Synthesis and Assembly

1. 1 Introduction

Because nanometer leveled materials have unique properties, they lead to a vast range of applications, including chemical, biological, medical, and electronics [1-8]. However, with chemical and physical methods, sometimes the size and shape of nanomaterials are hard to be controlled in order to gain homologous distribution. Furthermore, stringent conditions are often required with limited quantities and quality [9-11]. Due to the nonspecific interactions and uncontrolled agglomerations between nanoparticles, they seldom self-assemble into higher ordered structures [1, 11, 12]. Practical strategies are needed for the control and fabrication of large-scale nanostructures and the ordered assembly of materials in two and/or three dimensions (2D and 3D).

On the other hand, organisms can be considered precisely organized and assembled nano-machines. With billions of years of evolution, nature has provided us many different kinds of biomaterials. Most of these naturally occurring materials are at the nanometer level with specific dimensions. Using these biological materials as templates or scaffolds, it is much easier to fabricate uniform and homologous hybrid materials. Usually, these materials can self-assemble from the molecular to the nano-, micro- and macro-scales in a hierarchical manner under controlled size, morphology and organization with intricate and delicate structures [9, 11, 13-15]. Combining molecular biology and genetic approaches, the characteristics of these biomaterials can be modulated, such as self-assembly, hybrid formation and surface chemistry.

In biological tissues, especially hard tissues, there are many hybrid systems. That is, in addition to the organic phase, primarily proteins, there are also inorganics within a complex organic matrix, such as HAP, silica, magnetite and calcite [16-18]. All of these biological tissues are synthesized in aqueous environments using biomacromolecules, primarily proteins, but also carbohydrates, lipids and polysaccharides incorporated into inorganic materials [16, 19, 20]. The inorganics are synthesized via enzymatic or non-enzymatic reactions. By means of self- and co-assembled subunits through the molecular recognition of inorganics by protein, these organic-inorganic materials assemble into

short- and long-range ordered structures. Proteins or peptides control and direct the specific nucleation or interact with inorganics, usually as an integral structure in their biological functions and physical performances leading to specific and controllable functions [9, 10, 15, 16, 18, 20].

For the fabrication of hybrid nanomaterials, proteins or peptides specifically binding to a target are selected and/or designed. Next, these specific proteins or peptides with biological activity and binding propriety are used as erectors or assemblers to form ordered organic-inorganic hybrid materials [7, 9, 10, 14, 16]. A number of self-assembly proteins, peptides and nanometer leveled organisms are selected for nanotechnology, such as DNA, phage, virus and flagella [21-26]. In this chapter, flagella as templates for nanomaterials synthesis and assembly will be summarized.

1.2 Biology and structure of flagella

Flagella are the organelles of locomotion for most bacteria, which make them transform from “plant” to “animal”. A bacterial flagellum is a helix-shaped long filament with uniform thickness. When rotated by the motor at the base, it works as a propeller. With flagella, bacteria can swim to favorable circumstances. This behavior is called chemotaxis or thermotaxis [27-30]. The number, length and diameter of flagella on a cell differ among species. The diameter of a flagellum is about 10-20 nm and the length of the filament can be up to 10 μm . Flagella are free at one end and the other end attach to the cell. The flagellum is divided into three parts: the filament, the hook and the basal body (Figure 1.1) [31]. The basal body is a transmembrane with a stable core and fragile components that easily detach from the core. It consists of a rod and a series of rings (the motor and the switch complex) that anchor the flagellum to the cell wall and the cytoplasmic membrane [32]. As a molecular motor, it enables the flagellum to rotate and propel the bacterium through the surrounding fluid. In fact, the flagellar motor rotates very rapidly at about 20,000 rpm, but energy consumption is only around 10^{-16} W and energy conversion efficiency is close to 100 %. The average speed of flagellar swimming is around 50 $\mu\text{m}/\text{sec}$. The hook is short, highly curved and flexible that links the filament and the basal body. The filament is the rigid, helical structure that extends from the cell surface [28, 33, 34].

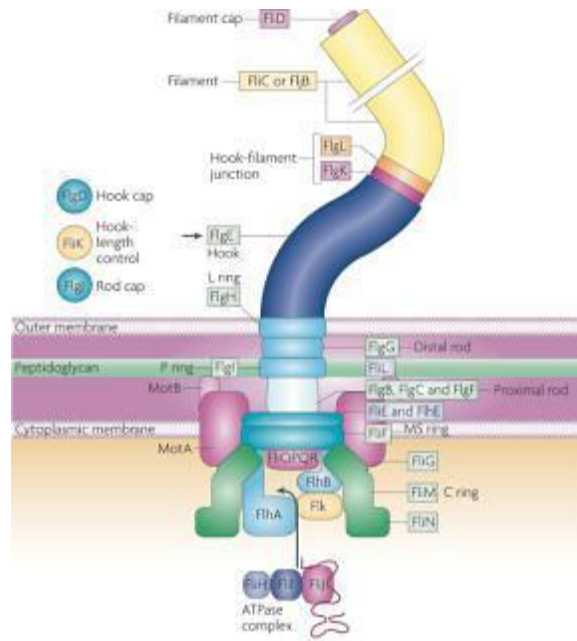


Figure 1.1: Schematic diagram of the bacterial flagellum. Different colors represent different protein components (Reprinted with permission from Fabienne et al. Nature Reviews Microbiology 6, 455-465 (2008))

The flagellum is composed of about 25 different proteins by self-assembly. In *Salmonella*, about 50 genes are arranged in clusters, making 17 operons, and the operons are divided into three classes according to the order of expression [34-37]. The expression of these three classes is highly controlled in a hierarchical manner. The master operon in the highest class controls over the rest of the second class. In turn, the second class regulates the expression of operons at lower classes [31, 37, 38]. The flagella assemble in a step-by-step manner. The basal structure and the hook are assembled first, following the gene expression for the filament parts. First of all, the rotor ring (*FliF*), a membrane protein, is expressed and self-assembled into an MS ring complex in the cytoplasmic membrane. Then, other protein molecules, including MotA and MotB, attach to the ring one by one from the base to the tip to construct the motor structure. *FliG*, *FliM* and *FliN* form a bell-shaped structure called C ring, which is around the rim of the complex extending to the cytoplasm. As helical propellers, the flagellar filaments are built on this C ring motor structure. These proteins translocate from inside the cell to the periplasm and outside the cell through the central channel, located at the center of the C

ring. *FlgB*, *FlgC*, *FlgG* and *FlgF* which compose the rod export to the periplasmic space first. *FliL*, a flagellum-specific ATPase, provides energy for this selective and active transportation process. After the assembly of the rod, P and L rings are formed to make a hole through the outer membrane. The P and L rings help transfer other proteins and grow the hook at the tip of the rod [39]. The hook is assembled from approximately 100 copies of *FlgE*. At the same time, *FlgD* attaches at the tip of the growing hook. Then *FlgC* polymerizes at the free end of the hook between the junction proteins and *FlgD*. Between the hook and the filament, there are also two junction proteins called HAP1 and HAP2 (hook-associated proteins). During synthesis of the flagellar filament, *FliC* molecules come out of the ribosome and pass through the membrane, and “finally” are transported through the hollow core of the filament, where they attach to the growing tip of the filament, causing it to lengthen, where they self-assemble in a helical manner with the help of a cap complex (*FliD*) [40]. Precise recognition of the template structure by component proteins allows this highly ordered self-assembly process to proceed without error. The flagellar filament is made of 20,000 to 30,000 copies of *FliC* polymerized into a helical tube structure with 15 μm long, 12-25 nm in diameter [33, 35, 38, 41-46]. The cap is a pentameric, stool-like complex made of HAP2. Flexible stepping movements accompanied by rotation of the whole cap promote the efficient self-assembly of *FliC* molecules. Without *FliD*, *FliC* monomers secrete into the growth medium directly and unable to assemble into filament [47-49].

Even though the filament is composed of chemically identical molecules, it has a supercoiled structure caused by two different swim patterns –“run” and “tumble” [43, 50]. Bacterial cells swim actively by rotating a bundle of flagella. The motor switches its direction every few seconds to change the swimming direction of the cells as bacteria seek better environments. Reversal of the motor rotation causes a structural change in the flagellar filament from a left-handed to a right-handed helical form. This makes the flagellar bundle fall apart, propelling force imbalanced, leading to changes in the swimming direction. At the same time, the reversal rotation produces a twisting force and changes the flagella from a run to a tumble [34, 46, 51].

The tubular structure of a flagellar filament is assembled with roughly 11 subunits-*FliC* per 2 turns of the 1-start helix [52]. It is a nearly longitudinal helical array of subunits. Dr. Namba's group [53-58] tried to understand the structure of *FliC*, the assembly and switching mechanism responsible for these structural changes. In order to analyze the structure in atomic detail with X-ray crystallography, *FliC* has to be crystallized. However, its strong tendency to polymerize makes crystallization difficult and *FliC* monomers exhibit a mixture of different conformations. It takes many years to crystallize *FliC* and analyze its structure. In 1989 [58], the structure and subunits of bacterial flagellar filaments were first resolved by X-ray fibre diffraction, but the resolution was low (20 Å). In 1995 [59], a resolution of ~11 Å of a bacterial flagellar filament of *Salmonella typhimurium* was reconstructed with the aid of analysis by electron micrographs. An α -helix to the inner tube, two α -helices to the outer tube and a fourth α -helix to the spacer were identified on each *FliC* monomer. Using liquid helium in the cryostage to reduce radiation damage and a stable field emission source to increase the image quality, a higher quality density map (9 Å) of the R-type filament from *S. Typhimurium* was solved [53, 60]. Four distinct domains, D0, D1, D2 and D3 were identified from the density map with the interlocked α -helical segments of the core portion. According to the left- and right-handed twist of the protofilaments respectively, they have two slightly different conformations, named L and R types. The repeat distance observed in the structure of the L-type protofilament is 5.27 nm, while it is 5.19 nm in the R-type, the difference being only 0.08 nm. The mixture of protofilaments with different lengths produces the helical tube structure of the filament. When the 11 protofilament strands transform from the L-type into the R-type, normally left-handed flagellar filament turns into right-handed helical forms.

Because the full length of *FliC* is highly likely to polymerize into a filament through the interaction of the N- and C- terminal chains, in 2000, a 41 kDa fragment of *Salmonella FliC* without both the amino- and carboxyl- terminal ends was crystallized [54]. In 2001, the structure of this segment was analyzed at 2.0 Å resolutions, which directly revealed the protofilament structure [55]. This fragment looks like a boomerang or an aircraft which is composed of two wings and a short body. The three-dimensional space of the wing is about 70*25*20 Å.

Because the terminal chains in the inner core also have important roles in filament formation and assembly regulation, the complete atomic model of the R-type bacterial flagellar filament was reported in 2003 using electron cryomicroscopy [56]. The distribution of domains and secondary structures along the amino acid sequence is summarized in Figure 1. 2. The atomic model with 4 Å resolution shows intricate molecular packing and an α -helical coiled coil, which are formed by the terminal chains in the inner core of the filament. The four linearly connected domains labeled D0, D1, D2 and D3 are arranged from inside to outside of the filament. Domains D2 and D3 form the projection on the filament surface. The overall shape of *FliC* looks like an uppercase Greek gamma (Γ). The domain D0, which is located in the inner side of the flagellum, is completely investigated. In domain D0, the two terminal chains form an α -helical coiled coil. The N-terminal starts from Gln 2 and extends up to Ser 32, and the C-terminal starts from Ala 459 and extends to Ser 491. The diameter of the filament is about 24 nm and the central channel is about 2 nm [56].

Domain D1 comprises an N-terminal segment from Ala 44 to Gln 176, and a C-terminal segment from Asn 406 to Glu 454. It comprises three α -helices and a unique β -turn/ β -hairpin/ α -helix motif. The structure of the N-terminal chain forms two α -helices and β -hairpin. The first N-terminal α -helix in domain D1 (ND1a) (44–99) extends through the long axis of this domain, followed by a loop connecting to the second, shorter α -helix (ND1b) (104–129). The β -hairpin (140–160) is flanked by two distorted β -turns (131–134 and 135–138) on the N-terminal side, and slightly more than one turn of the α -helix (163–168) on the C-terminal side. This α -helix is followed by an extended chain (170–176). The C-terminal chain forms an α -helix (406–447). This rod-like domain is hydrophobic along its central axis [55, 56].

Domain D2 is also composed of two parts: Lys 177 to Gly 189, and Ala 284 to Ala 401 which are made up of mostly β -strands except for one short α -helix (285–289) and one short α -helix (288–298). These β -strands are best described as a series of randomly oriented β -hairpins and some of them are involved in three-stranded β -sheets. This domain has three hydrophobic regions, two of which form enclosed hydrophobic cores. Domain D2 can be divided into two compact subdomains, D2a and D2b (Figure 1. 2B).

Through their hydrophobic interaction, subdomains form domain D2. The third hydrophobic region of domain D2 is formed as part of this interface [55].

Domain D3 is located in the center of the protein from Tyr 190 to Val 283. It also consists of mostly β -strands with one short stretch of a helical fold (199-209). Domain D3 is made of four β -strands and one helical strand, which encloses 15 hydrophobic side chains in its core. A cross β -motif located at the two ends of domain D1 connects to D2. The connecting domains between D2 and D3 (Gly 189 to Thr 193 and Val 281 to Ser 285) form a short β -strand. In addition, a section of this fold can be described as a series of randomly oriented β -hairpins [55]. This domain can display up to 302 amino acids without losing its ability to form filaments, although the filaments are significantly more unstable than those of wild-type *FliC* [61].

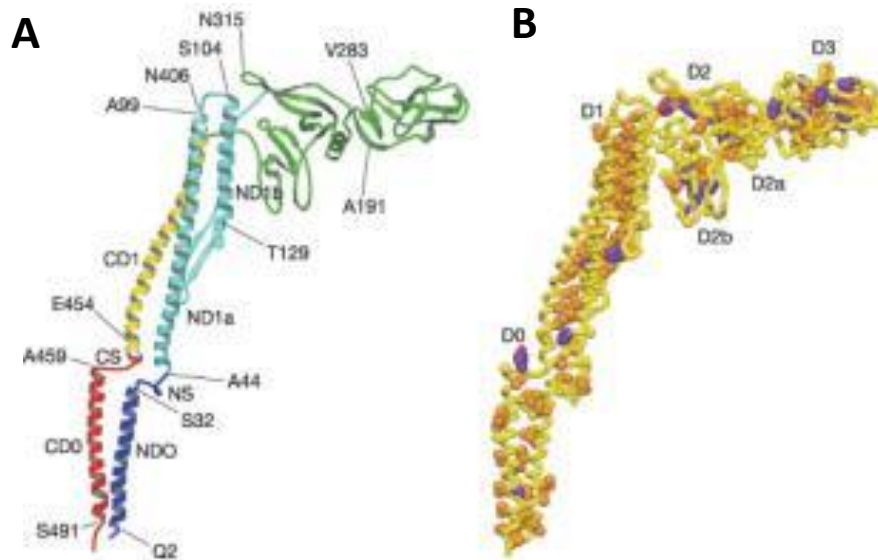


Figure 1.2: Protein structure of flagellin. A) Stereo diagram of the C backbone. The chain is colored as follows: residues 1–44, blue; 44–179, cyan; 179–406, green; 406–454, yellow; 454–494, red; B) Distribution of hydrophobic side chains, mainly showing hydrophobic cores that define

1. 3 Flagella assembly

The molecular packing pattern of the end-on view from the distal end of the flagellum is shown in Figure 1. 3 [56]. It shows the concentric double-tubular structure in which domains D0 and D1 are tightly packed into the core; however domains D2 and D3 are relatively separated to each other. They project out from the filament core. The diameter of the filament is about 240 Å with an inner channel at about 20 Å. From inside and outside views of the filament (Figure 1. 3B, C), both domains D0 and D1 have axial and lateral intersubunit interactions. Because the outer-tube domain is responsible for the formation of L- and R- type conformation, it indicates that the axial interactions between intersubunits are located D1 domains along the protofilament. The interactions are formed between the first N-terminal α -helix (Asn 56 to Asp 69) and the β -turns/ β -hairpin motif (Phe 132 to Asp 151) in the D1 upper subunit domain and by short segments of two N-terminal α -helices with a short loop connecting these α -helices (Gln 89 to Asp 107), Leu 408 and Gln 409 of the C-terminal α -helix and Asn 315 of domain D2 of the lower subunit.

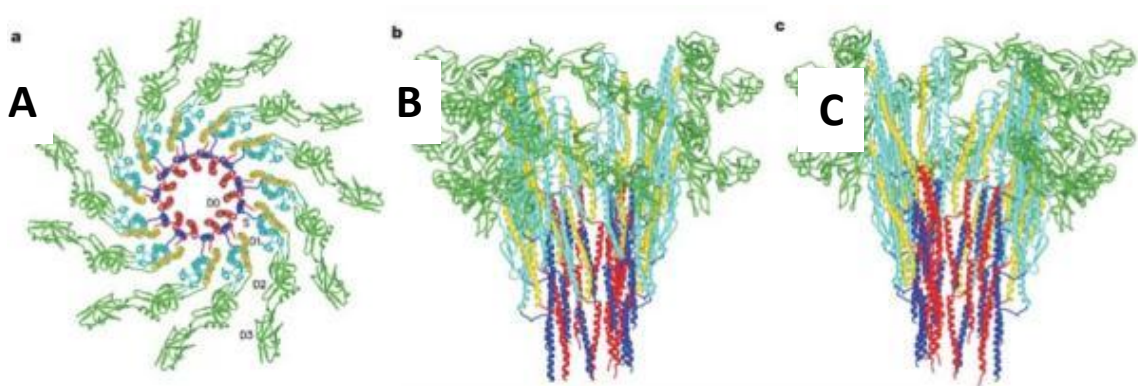


Figure 1.3: Protein structure of flagella filament. A) End-on view from the distal end of the filament. Eleven subunits are displayed. B) Side view from outside the filament. Three protofilaments on the far side have been removed for clarity. C) Side view from inside the filament. Three protofilaments on the near side have been removed. Top and bottom of the side view images correspond to the distal and proximal ends of the filament, respectively. The chain is color coded as in Fig. 2a. (Reprinted with permission from Yonekura et al. Nature 424, 643-650 (2003))

The protofilaments assembled into the supercoiled forms of the flagellar filament are constructed by two distinct L- and R-type conformations of *FliC* arranged in a very organized manner. In straight filaments, 11 protofilaments per 2 turns of the 1-start helix form a helical assembly and packed tightly with a half-subunit stagger to form the concentric double-tubular structure. Domain D1 interacts with each other along the 11- and 5-start directions only. Along the 5-start helix, the β -hairpin of domain D1 interacts with ND1a and ND1b of subunit 0. Subunit 11 intervenes in the space between subunits 0 and 6, or subunit 17 would come into the open space between subunits 6 and 12. Within the outer tube, the intersubunit interactions are mostly polar-polar or charge-polar, but within the inner tube and between the inner and outer tubes, there are mostly hydrophobic interactions [40, 44, 62].

1.4 Peptide display on flagella

Using natural peptides or organisms as scaffolds or templates for the synthesis of inorganics is not enough because one peptide is hard to interact with multiple inorganics. Usually, the interactions between bio-templates and inorganics are like antigen/antibody or receptor/ligand. We need to select or design peptides with specific binding activity to functional targets [1, 10, 12, 15]. By combining genetic tools and biological techniques, there are three ways to select or design specific peptides [63]. The first one is using the candidate sequences existed in natural proteins or peptides. The second one is using the artificial designed sequences. The third one is using the biopanning method to select specific polypeptides binding their target [12, 64-67]. The selected short polypeptides called genetically engineered proteins for inorganics (GEPIs) bind to a specific surface, size, or morphology of an inorganic compound, promote the assembly of intricate, hybrid organic-inorganic structures. In this approach, a large, random library of peptides with the same number of amino acids, but varying compositions, is screened to identify specific sequences that strongly bind to an inorganic material of practical interest. The common libraries are phage display (PD) and cell surface display including flagella display [1, 12].

Up to now, many polypeptides that can interact with or promote synthesis of inorganics or other nanometer-leveled materials are identified. Moreover, with surface display, the

higher ordered assembly and arrangement of these materials may be induced in a controlled manner. These technologies include virus/phage display, cell display, ribosomal display, mRNA display and covalent DNA display (CDT) [68-79]. The PD by far is the most utilized technique for nanotechnology [75].

In this chapter, the flagella display technique with applications will be summarized. Based on genetic in-frame fusion, a carrier protein that consists of a target sequence fused within some region of *FliC*, however, without affecting the assembly of the flagella. At the same time, the fused peptide is surface-exposed. Traditionally, flagella display technology is used for basic microbiological research, molecular biology, vaccinology, constructions of random peptide libraries, and biotechnology [80, 81]. In recent years, with the development of nanotechnology and biotechnology, more novel applications are explored such as diagnostic purposes, as biocatalysts, as template for synthesis of inorganic nanotubes, as well as tissue engineering.

As mentioned above, the D0 and D1 domains are important for *FliC* polymerization by intersubunit interactions at the highly conserved portion, whereas in the central region of *FliC*, the amino acid sequences are highly variable (Figure 1. 4) and up to 187 amino acid residues in *E. coli FliC* can be deleted without loss of function and flagellar polymerization [82, 83].

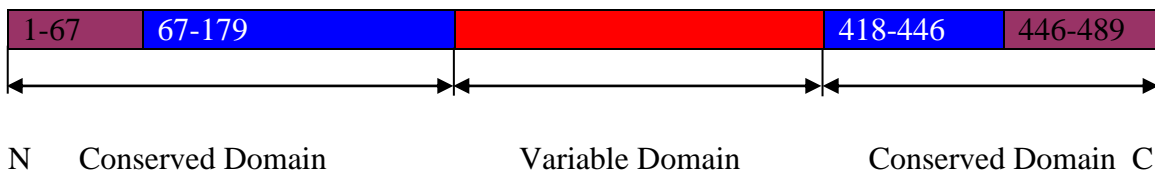


Figure 1.4: Diagram of *FliC* conserved and variable regions

Based on this characteristic, the foreign peptide is inserted in this variable domain of *FliC* and finally, transformed into *Salmonella* host strain with a $\Delta FliC$ mutation. Thousands of copies of the fusion *FliC* along the flagellar filament are expressed by complementation of the $\Delta FliC$ mutation with the hybrid *FliC* gene.

1. 5 Biomedical application of flagella

Kuwajima et al first reported hybrid flagella by inserting a lysozyme-derived fragment into the central region of the flagellin in 1988 [84]. Since then, display of other short peptides as antigenic epitopes on flagella was reported [81, 85-87]. Flagella are potent immunogens and prove to be safe as vaccines in phase I clinical trials in human being [88]. Actually, the whole bacteria with hybrid flagella were used as live vaccine. They are cheap and can provide unlimited supply using the bacterial vaccine strain [86].

Adhesive proteins on the surface of bacteria are essential to interact with host tissues for further infection. Thousands of copies of adhesive peptides on flagella can provide an alternative way of intervention in the infectious process [86]. Flagella display is also used to analyze protein-protein interactions such as adhesion-receptor interactions. Because multiple copies are displayed on surfaces of flagella simultaneously, this system creates high affinity interaction even if the single bacterial adhesion shows low affinity to its receptor [81].

Similar to PD, a library of flagella display was developed by Lu and coworkers in 1995 [89]. In this system, a random library of 1.77×10^8 individual dodecapeptides was expressed in the thioredoxin active site loop in *FliC*, named FliTrx. This active site consists of a short disulfide-bonded loop protruding from the flagella surface and enables to express conformational constrained peptides. By interaction between the library and immobilized ligands, only specific peptides bound to the targets can be selected. The weak or non-binders are washed out in mild conditions. This step is repeated several times at harder conditions to enrich the tighter binders. Finally, the peptides which tightly interact with the desired ligands are selected from the original library. It is a powerful tool for biotechnological and biological applications including the protein-ligand interactions, antibody-binding epitope screening and isolation and evolution of proteins or enzymes. A series of papers reported the adhesive dodecapeptides by this library mainly on eukaryotic proteins [90-106].

The flagella display can also be used to export foreign heterologous proteins. Normally, expression of foreign proteins is based on fusions encoding secreted carrier proteins or use of fusions with secretion signals or motifs of well-characterized protein secretion

pathways. The flagellar axial proteins are exported through central channel and assembled at the distal end of the filament. This process is directed by the flagella type III export apparatus. This system translocates effector proteins from the cytoplasm to the exterior of the bacterial cell and into eukaryotic target cells without involvement of periplasmic intermediates [107]. HAP2 is very important for flagellar filaments grew. After deletion of the HAP2 structural gene of *Salmonella*, *FliC* monomers excrete into the culture medium directly [47, 48]. However, when the purified HAP2 was added into the mutant, polymerization of flagellar filament becomes normal [108]. As a result, the HAP2 deleted flagellum-based system can be applied for extracellular exportation of heterologous proteins [109, 110]. Comparing to the versatile type I secretion system in Gram-negative bacteria, this system exports much higher concentrations of extra-cellular heterologous proteins [111].

1. 6 Nanomaterials on flagella template

The recent application of flagella is using them as templates or scaffolds for the synthesis of inorganic nanotubes or organic nanotubes. There are some advantages compared to other surface display techniques: 1) Thousands of copies of foreign peptides can be displayed on the surfaces of flagella with homogeneous surface modification and provide multivalent interactions; 2) Flagella can be easily detached from bacterial cells to obtain a large amount of highly purified materials; 3) Different polypeptides can be displayed on the same flagellar filament or simultaneous displayed on *FliC* and *FliD* separately which make them with multi-functions; 4) Normally, 10-40 amino acid residues are long enough for peptide display. However, sometimes, longer peptides are needed because some interactions may need secondary or ternary dimensional structures. In flagella display system, up to 302 residues can be displayed on the surfaces of flagella [61]; 5) The arrangement of *FliC* is very organized after self-assembled into filament. It is about 5.4 nm between adjacent D3 domains on the surfaces of flagella [112]. Any modifications on this domain will generate the same periodicity of spacing; 6) Comparing to PD, flagella display only needs one step replication with infection.

Table 1.1: Summary of nanomaterials prepared using engineered flagella nanotubes as scaffolds

Peptide type	Peptide sequences	Combination target	Methods	Aim or results	References
Peptide loop	histidine loop (GHHHHHH) ₄	Au (gold)	synthesis of gold nanoparticles on flagella by reduction of Au(I) ions	linear flagella-Au nanotube with discrete gold nanoparticles attached	Kumara et al 2007
	arginine-lysine loop (RKRKRKR)	Au (gold) nanoparticles	synthesized 3 and 10 nm gold nanoparticles covalently attached by amine coupling to arginine-lysine peptide loop flagella	aggregates of linear flagella-Au large bundles	
	histidine loop (GHHHHHH) ₄	Cu (copper)	Synthesis copper nanoparticles on flagella by reduction of Cu(II) ions	linear flagella-Cu nanotube bundles with discrete Cu nanoparticles and single linear Cu nanotubes	
	aspartic acid-glutamic acid loop (HDEDEDEG) ₃	Co (cobalt)	synthesis of cobalt nanoparticles on flagella by reduction of Co(II) ions	ordered array of Co nanoparticles on Asp-Glu loop flagella nanotubes	
	histidine loop (GHHHHHH) ₄	Co (cobalt)	synthesis of cobalt nanoparticles on flagella by reduction of Co(II) ions	fractal-like dense assembly of flagella with cobalt to form nanoparticle composite	
		Pd (palladium)	synthesis of palladium nanoparticles on flagella by reduction of Pd(II) ions	single flagella-Pd nanoparticles	
		Cd (cadmium)	synthesis of cadmium nanoparticles on flagella by reduction of Cd (II) ions	ordered array of nanoparticles on single and aggregated flagella nanotube fragments	
	aspartic acid-glutamic acid loop (HDEDEDEG) ₃	Ag (silver)	synthesis of silver on flagella by reduction of Ag(I) ions	aggregated bundles and arrays of Ag-flagella nanowires	
	arginine-lysine loop (RKRKRKR)	Silica	Synthesis silica nanotube with sodium silicate (Na ₂ SiO ₃) or tetraethyl orthosilicate (Si(OC ₂ H ₅) ₄) by amine coupling to arginine-lysine peptide loop flagella	Separated nanotubes formed by Na ₂ SiO ₃ , but Si(OEt) ₄ generate clumped pattern	Kumara et al 2007
	Tyrosine-serine-glycine loop (HYSYGYSYGYSY)	Titanium oxide	Synthesis titanium oxide nanotubes with titanium (IV) ethoxide in ethanol by sol-gel process	Single titanium oxide nanotube	
aspartic acid-glutamic acid loop	hydroxyapatite	Synthesis nanotubes by reaction of CaCl ₂ with Na ₂ HPO ₄	Tubular apatite structures formed on flagella.		

Peptide type	Peptide sequences	Combination target	Methods	Aim or results	References
	(HDEDEDEG) ₃			Finally arrays of mineral nanocrystals were presented	
	aspartic acid-glutamic acid loop (HDEDEDEG) ₃	polyaniline	Flagella were fixed on TEM grid. Aniline was coated followed by Tris (2, 2'-bipyridine) dichlororuthenium (II) hexahydrate.	aggregated bundles of flagella coated by polyaniline	
	histidine loop (GHHHHHH) ₄	ZnS/Mn quantum dots	synthesized 3 nm nanoparticles attached to flagella	ordered array of nanoparticles on single flagella	Kumara et al 2007
ZnS quantum dots		Synthesis nanoparticles by reaction of ZnSO ₄ with Na ₂ S on flagella	aggregates of linear flagella with discrete ZnS nanoparticles attached		
CdTe quantum dots		Synthesis nanoparticles on flagella by CdTe QDs capped with L-cystine	linear flagella nanotube with discrete CdTe nanoparticles attached		
	Wild type	Pd(II)	Synthesis nanoparticles on flagella by reduction of Pd(II) ions	Thick layer of Pd coated on flagella	Deplanche et al. 2008
	(CCCCCCCCCCCC)	Au(III)	Synthesis nanoparticles on flagella by reduction of Au(III) ions	Nanoparticles attached on surface of flagella	
	Wild type	TiO ₂	Synthesis nanotubes on flagella by hydrolysis of TiCl ₄ in aqueous solution	Linear separated nanotubes	Hesse et al 2009
	KKKKKKKKKKCCCCCCCC	SiO ₂	Synthesis nanotubes on flagella by hydrolysis of tetraethoxysilane in aqueous solution	Linear pearl-necklace-like flagella nanotube.	Wang et al 2009
	DPEPRREVCELDPD CDE	SiO ₂	Synthesis nanotubes on flagella by hydrolysis of tetraethoxysilane in aqueous solution	Linear pearl-necklace-like flagella nanotube with tadpole structures	
	Wild Type	SiO ₂	Synthesis nanotubes on flagella by hydrolysis of tetraethoxysilane in aqueous solution	Linear pearl-necklace-like flagella nanotube with cyclic morphology	

Kumara et al [26] reported the synthesis of inorganic nanotubes, nanoparticles and organic nanotubes using bioengineered flagella (FliTrx system) as template. The FliTrx system is from Invitrogen, was designed to display of constrained loop peptides on the surface of bacterial flagella. The fusion peptides are inserted into the solvent-accessible active site region of thioredoxin with the peptide sequence –Cys32-Gly33-***-Pro34-Cys35-. Silica bionanotubes formed on cationic “Arg-Lys” loop peptide (RKRKRKR) with four guanidine and three amine functional groups which displayed on the surface of

flagella. However, the morphology of silica nanotubes is different with two kinds of precursors: Na_2SiO_3 or $\text{Si}(\text{OEt})_4$. Single nanotube was formed by Na_2SiO_3 , but $\text{Si}(\text{OEt})_4$ generates more cross-linked patterns (Figure 1. 5A, B). The positively charged surfaces of flagella may attract and bind the first layer of silicate ions followed further mineralization on the initial layer of the silica. Because Ti(IV) ions are prefer to bind hydroxyl groups than carboxylate groups, a poly Tyr loop peptide with phenol side chains groups (Figure 1. 5D), alternating with three serine and glycine residues (HYSYGYSYGYSY) is displayed on flagella. This type of flagella can initiate formation of titania bionanotubes using titanium (IV) ethoxide in ethanol as precursor solution (Figure 1. 5C). Because the negatively charged proteins are very important for biomineralization of HAP, three repeats of the anionic ASP-Glu sequences (HDEDEDEG)₃ have been displayed on surface of flagella. After the flagella are placed on holey carbon grid and air dried, 5 μl of 10 mM CaCl_2 is placed at one side of the grid following 5 μl of 10 mM Na_2HPO_4 on the other side. Hydroxyapatite nanoparticles nucleate on anionic flagella with a time dependent manner but the nanocrystals are randomly oriented (Figure 1. 5E). Most recently, we displayed 8 glutamic acids which are from BSP on flagella without constrained peptide loops. After nucleated within a HAP precursor solution, we also observed HAP nanocrystals nucleation on the flagella surface. Polyaniline can be coated on anionic Asp-Glu loop peptide flagella. In this process, anilinium ions may polymerize on flagella by ionic interactions and π - π stacking of the aromatic rings (Figure 1. 5F).

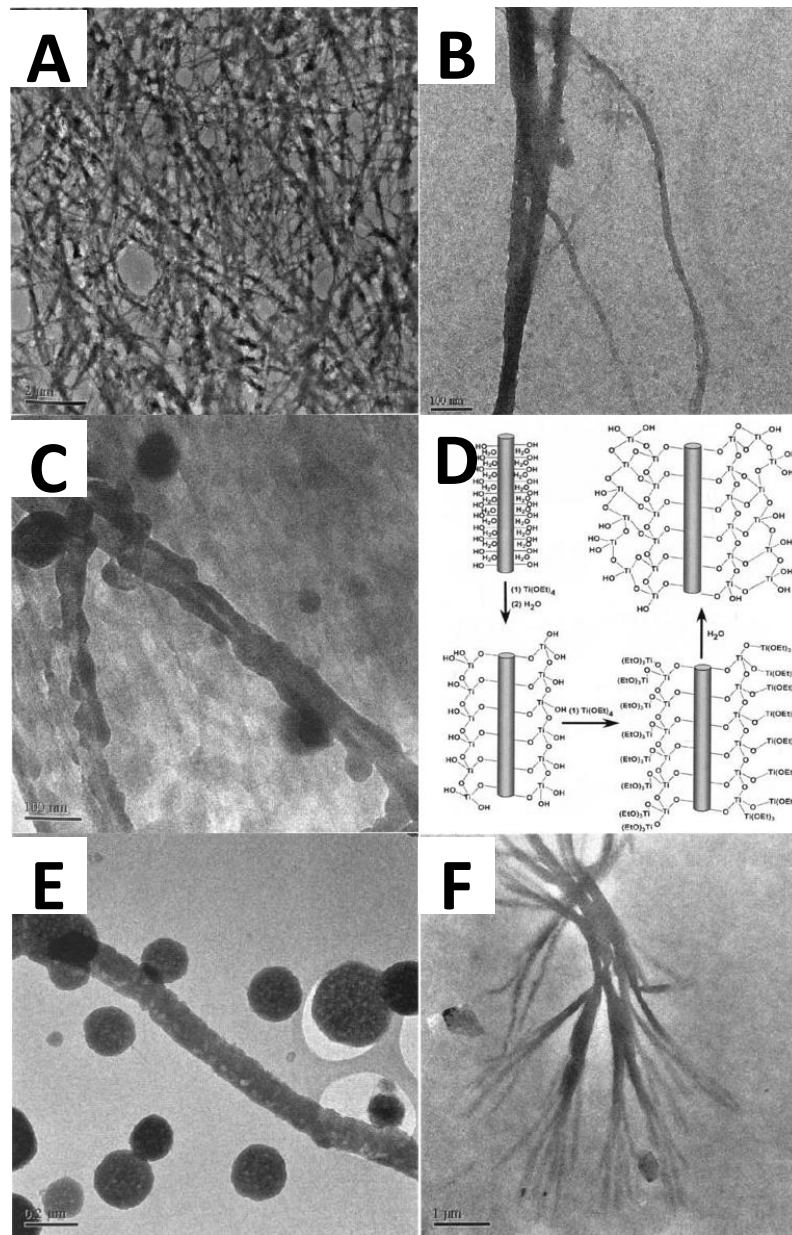


Figure 1.5: TEM images of flagella mediated inorganic nanotubes. A) Silica biomineralization on cationic Arg-Lys loop flagella with tetraethoxysilane. B) Silica formation with sodium silicate. C) TiO₂ nanotubes synthesized on Tyr-Ser-Gly loop flagella. D) Mechanism illustration of TiO₂ synthesis by sol-gel process on flagella. E) Hydroxyapatite nanocrystals synthesized on anionic Asp-Glu loop flagella after 20 minutes exposure to mineralization solution. F) Polyaniline nanowires synthesized on anionic Asp-Glu loop flagella. (Reprinted with permission from Kumara et al. Journal of nanoscience and nanotechnology 7, 2260-72 (2007))

The genetically engineered flagella were also used as scaffolds for the self-assembly of metal nanoparticles and nanotubes [113]. Three different types of loop peptides are applied in this report. One is a 4 time insert of a one glycine, six histidine loop (“His loop”) peptide containing imidazole groups (GHHHHHH)₄. The second one is a 3 time insert of an anionic “Asp-Glu loop” peptide composed of one histidine residue, three aspartic acid residues, three glutamic acid residues, and one glycine residue (HDEDEDE)₃. The third one is a single insert of a cationic “Arg-Lys loop” peptide encoding four arginine residues with guanido side chain groups and three lysine residues with amine side chain groups (RKRKRKR). After soaked into solutions of various metal ions (Co(II), Cu(II), Cd(II), Ag(I), and Pd(II)) and under controlled reduction by NaBH₄ or hydroquinone, genetically engineered flagella were coated by ordered nanoparticles or nanotubes (Figure 1. 6). In most cases, only nanoparticles are aligned on flagella. On histidine loop flagella, Au nanoparticles with 5.93 (±1.48) nm in diameter aligned on the surface of the flagella scaffold to form an ordered array as shown in Figure 1. 6A. Copper, cobalt, palladium and cadmium nanoparticles were generated on histidine loop peptide flagella. An ordered array of Co nanoparticles was also produced by reduction of Co(II) on Asp-Glu loop flagella (Figure 1. 6C, D, E, F, H). Ag(I) was formed a layer of metal on aspartic acid-glutamic acid loop peptide flagella resulting formation of nanowires (Figure 1. 6G). In another approach, synthesized Au nanoparticles with 3 or 12 nm in diameters were functionalized by 10-thioldecanoic acid. Then the nanoparticles were mixed with the positively charged arginine-lysine loop flagella. A thick layer of Au nanoparticles attached on the flagella bundles with 500 nm diameter were shown in Figure 1. 6B.

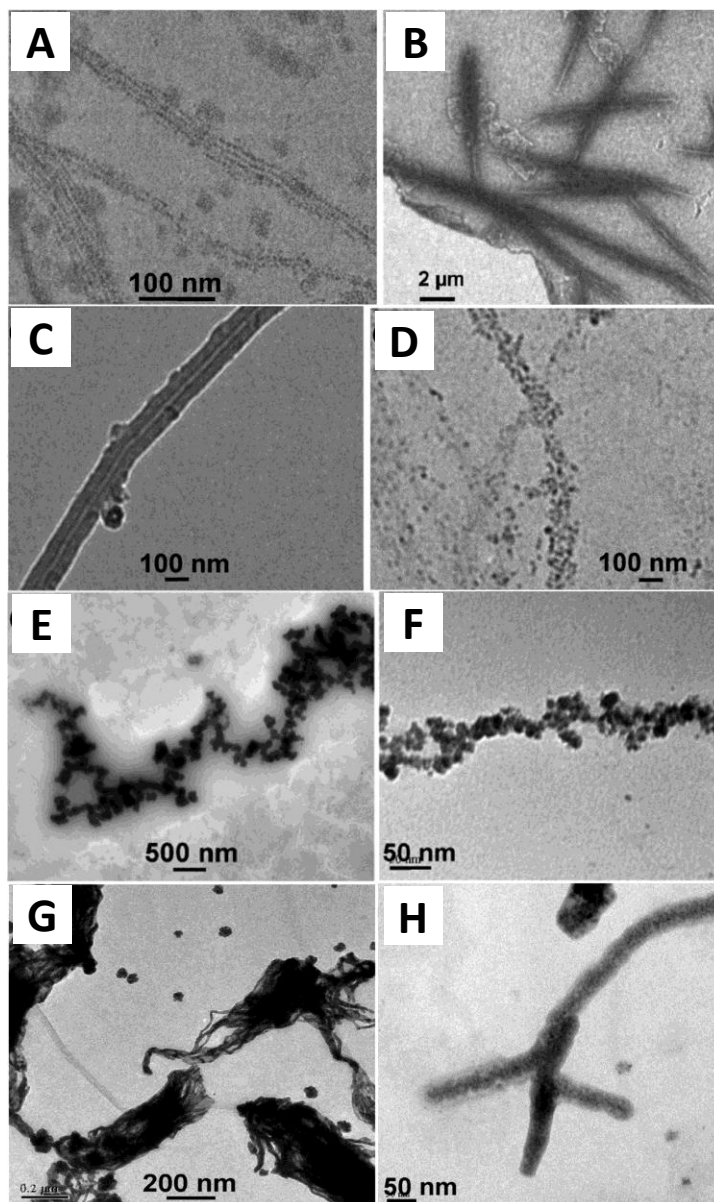


Figure 1.6: Metal nanoparticles and nanotubes synthesized on bioengineered flagella. A) Gold nanoparticles were synthesized on a histidine loop peptide flagella. B) Gold nanoparticles attached by covalent attachment to Arg-Lys peptide loop flagella. C) Copper nanotubes synthesized by reduction of Cu(II) on histidine loop flagella. D) Copper nanoparticles synthesized by reduction of Cu(II) on histidine loop flagella. E) Cobalt nanoparticles synthesized by reduction of Co(II) on histidine loop flagella. F) Palladium nanoparticles synthesized by reduction of Pd(II) on histidine loop flagella. G) Silver nanowires synthesized on flagella with glutamic acid-aspartic acid loop peptides.

H) Cadmium nanoparticles synthesized on histidine loop flagella. (Reprinted with permission from Kumara et al. Chemistry of Materials 19, 2056-2064 (2007))

Deplanche et al [114] demonstrated Pd(0) nanoparticles could completely cover *D. desulfuricans* flagellar filaments by the H₂-mediated reduction of [Pd(NH₃)₄]Cl₂. However, No Au (0) could be formed using HAuCl₄. Using engineered flagella with cysteine-derived thiol residues in the *E. coli* *FliC* protein as the template, stabilized Au (0) nanoparticles at 20–50 nm in diameters could be obtained on the surface of flagella.

Integration of engineered flagella with quantum dots (QDs) was demonstrated recently for further potential applications, such as imaging, sensors, light emitting diodes, solar cells and molecular electronics [115]. Flagella with 4× insert variant with 24 histidine residues (GHHHHH)₄ were isolated. ZnS/Mn QDs with an average size of 3 nm are self-assembled on flagella with poly-histidine residues loop peptides (Figure 1. 7). Direct synthesis of ZnS nanoparticles on immobilized His-loop flagella was also demonstrated. The flagella were fixed on holey carbon grid. One side was placed by ZnSO₄ and the other side was placed by Na₂S. TEM images of ZnS nanoparticles on flagella are shown in Figure 1. 7B. CdTe QDs capped with L-cysteine can also bind to the flagella with His-loop with about 2.4 nm separation (Figure 1. 7C). Negatively charged flagella can assemble with cationic liposomes loaded with a model drug. It may provide a novel way for photodynamic cancer therapy [116].

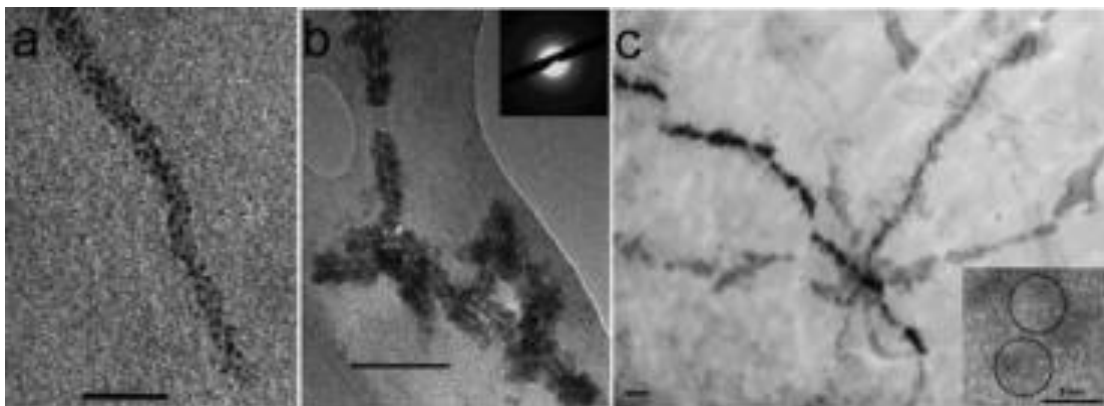


Figure 1.7: Metal nanoparticles synthesized on histidine loop flagella. A) TEM image of ZnS/Mn nanoparticles immobilized on a histidine loop flagella scaffold (scale bar 50 nm). B) TEM image of ZnS nanoparticles synthesized on a flagella scaffold (scale bar 100 nm); C) TEM image of CdTe QDs capped with L-cysteine bound to the flagella with His-loop (scale bar 100 nm).

(inset) electron diffraction pattern indicating Wurtzite structure. C) TEM image of CdTe nanoparticles immobilized on a histidine loop flagella scaffold (scale 100 nm); (inset) high-resolution TEM image of CdTe nanoparticles immobilized on a flagella template (scale bar 5 nm). (Reprinted with permission from Kumara et al. *Journal of Physical Chemistry* 111, 5276-5280 (2007))

By using another flagella display technique without constrained loop peptide, Wang et al [117] coated site-specific silica sheaths on flagellar surface. The proposed mechanism is that aminopropyltriethoxysilane (APTES) absorbed on the surface of flagella through hydrogen bonding or electrostatic interactions between the amino group of APTES and protein of flagella to form nuclei, followed polycondensation of tetraethoxysilane (TEOS) on these nuclei. It is easy to produce a large amount of silica nanotubes by this method close to room temperature and neutral pH in aqueous solution. The morphology of as-synthesized silica nanotubes using flagella template can be tuned by different surface charges. One type of genetically engineered flagella (termed Fla-KKCC) is displayed a peptide with a sequence -Lys-Lys-Lys-Lys-Lys-Lys-Lys-Lys-Lys-Lys-Cys-Cys-Cys-Cys-Cys-Cys-Cys-Cys-Cys-, which has two domains (positively charged due to the Lys and thiol-rich due to the Cys). Another type of engineered flagella (termed Fla-OCN) is displayed a peptide with a sequence of -Asp-Pro-Glu-Pro-Arg-Arg-Glu-Val-Cys-Glu-Leu-Asp-Pro-Asp-Cys-Asp-Glu-, which has negatively charged residues (Asp and Glu) and strong nucleophilic residues (Arg and Cys). The third one is wild type flagella. After coating, all of them give pearl-necklace-like silica fibers as shown in Figure 1. 8. However, the morphology of these silica fibers is quite different. Silica fibers on wild type flagella are cyclic (Figure 1. 8A) while those on flagella with Fla-KKCC are straighter (Figure 1. 8B). On Fla-OCN displayed flagella, large silica spheres usually formed at one end of the fibers (Figure 1. 8C). The silica-flagella hybrid nanotubes were also examined by TEM (Figure 1. 9). Uniform pore size of 14 ± 0.5 nm was observed. In the present of dithiothreitol (DTT), silica nanotubes formed by single flagellum (Figure 1. 9A, B). Without DTT, silica nanotubes prepared by Fla-KKCC flagella formed larger pore sizes than single flagellum due to the formation of flagellar bundles through the formation of disulfide bond between neighboring flagella (Figure 1. 9C). Large silica

spheres were observed at the intersection points (with arrows) on wild-type flagella templated silica nanotubes (Figure 1. 9D).

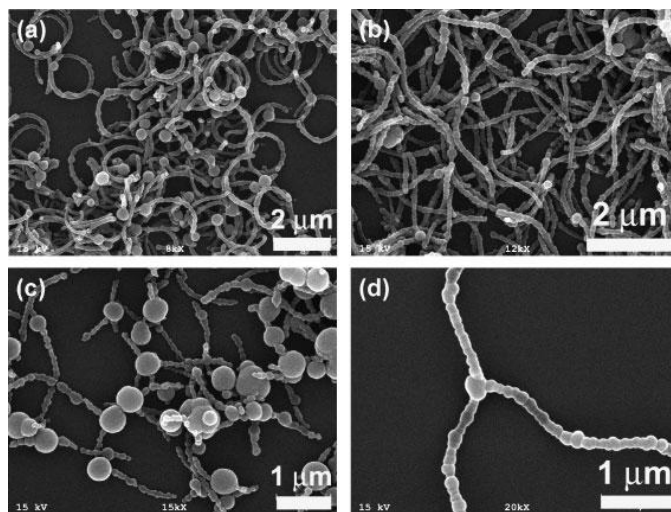


Figure 1.8: SEM images of the obtained hybrid flagella/silica nanotubes by using different flagella as templates: A) wild type flagella; B) Fla-KKCC flagella; C) Fla-OCN flagella. D) The detailed pearl-necklace-like silica nanotubes and the intersection structure.

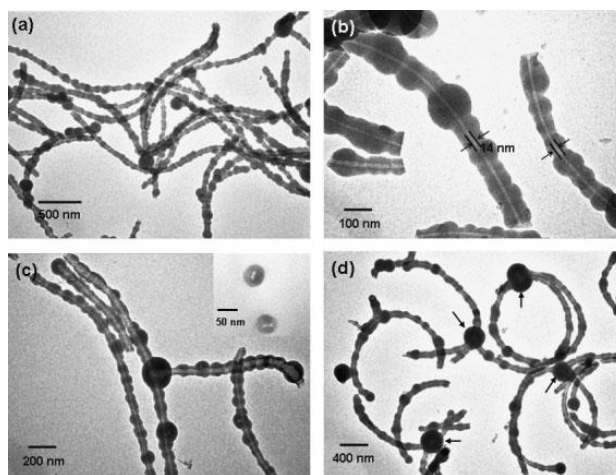


Figure 1.9: A) Low and B), high magnification TEM images of silica nanotubes using Fla-KKCC as templates in the presence of DTT. C) TEM images of the silica nanotubes without DTT. Two flagella in the silica nanotubes were observed at the cross section. D) wild-type flagella template silica nanotubes.

The flagella template inside the silica/flagella nanotubes can be removed after calcination at high temperatures (Figure 1. 10). Under higher temperature (800 °C), a periodic nanohole array along the silica shell was formed with a center-to-center spacing of approximately 79 nm. This kind of nanotube can selectively uptake QDs to the inner channels. Moreover, the outer wall of the nanotubes can be coated by Au nanoparticles. This distinct functional nanotube may have potential applications in the fabrication of photonic crystals and plasmonic waveguides.

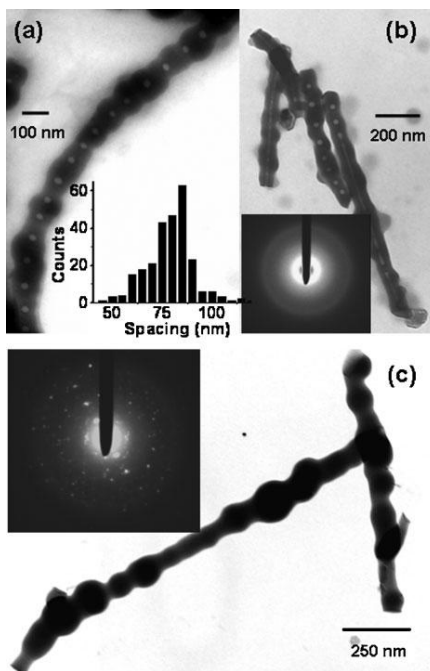


Figure 1.10: TEM images of the silica nanotubes calcined at different temperatures. A) The 1D periodic array of nanoholes along silica fiber which was calcined at 800 °C for 4 h. B) Silica nanotubes calcined at 800 °C for 1 h. C) Crystalline silica fibers formed after calcination of silica nanotubes at 950 °C for 4 h.

Recently, Hesse et al [118] showed the formation of TiO₂ nanotubes on wild type flagella using titanium chloride aqueous solution as a precursor solution at pH 2.5 (Figure 1. 11A, B, C). At 40 °C, a layer of TiO₂ was coated on flagellar surfaces. However, nanocrystalline TiO₂ was formed on flagella at 50 °C. After annealing at 200 °C, amorphous TiO₂ converted into nanoparticles. The filament diameter is less than 200 nm (Figure 1. 11D). However, the diameter of filament increased to ~300 nm at 400 °C

(Figure 1. 11E). The advantage of this method is that wild type flagella can be deposited by TiO₂ without any genetic modification. Moreover, this process is done at low temperature in aqueous solution and it is similar to that of biominerals in Nacre, sea urchin spine and sponge spicule.

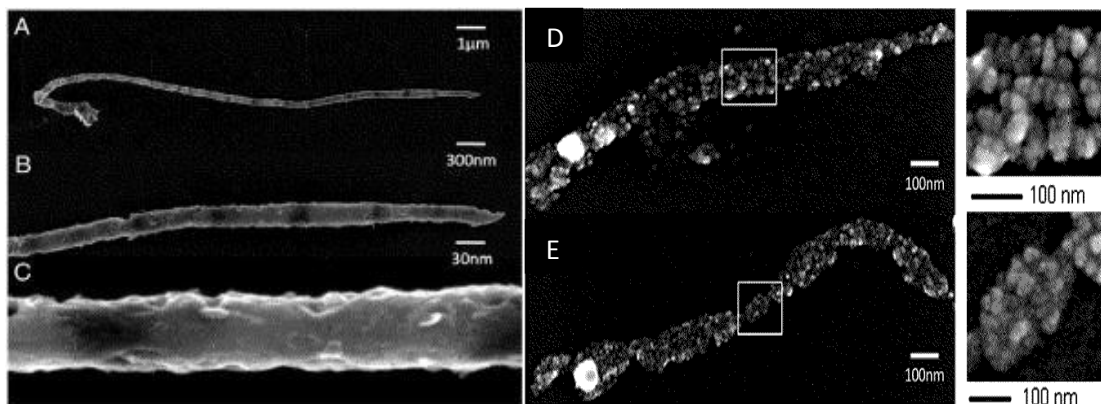


Figure 1.11: SEM images of amorphous TiO₂ nanotubes on flagella. (Reprinted with permission from Hesse et al. *Materials Science & Engineering* 29, 2282-2286 (2007))

1. 7 Assembly of flagella based nanomaterials

Assembly of nanomaterials in a highly ordered and organized fashion is very challenging. Nanomaterials can be assembled by covalent or non-covalent interactions between individual molecules such as electrostatic interaction, H-bond, hydrophobic or hydrophilic interaction, ligand/receptor interaction and chemical bond. In recent years, the nanostructured materials with self-assembly inspired from nature gain more and more attention [119-121]. It is well-known, high concentration of M13 bacteriophage could self-assemble into highly order liquid-crystal phase [122]. Barry et al [123] also found highly concentrated helical flagella isolated from *Salmonella typhimurium* could form liquid crystalline phase (Figure 1. 12). When the concentrations are under 17 mg/ml, wild-type flagella SJW1103 form isotropic phase. With increasing the concentrations of flagella, bright birefringent droplets appeared from a dark isotropic background with a well-defined striped pattern with a 2.4 μm periodicity. Uniform birefringent formed when the concentration of flagella was above 29 mg/ml. Fluorescence labeled flagella indicated that the filaments were always in phase with respect to each other.

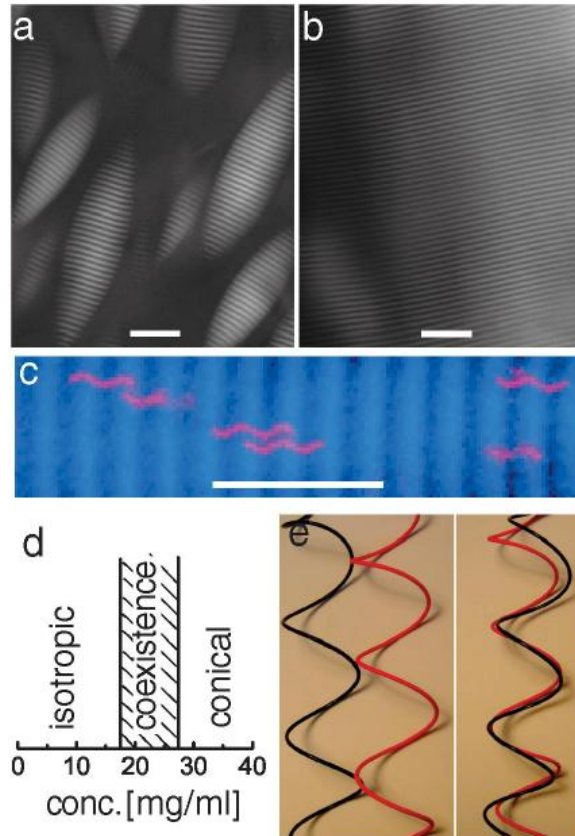


Figure 1.12: A) Coexistence between isotropic and conical phase in flagella SJW1103 at 20 mg/ml imaged with a polarization microscope. The scale bar is 20 μm ; B) A single phase imaged with a polarization microscope; the scale bar is 20 μm ; C) Fluorescently labeled flagella dissolved in a conical phase of unlabeled flagella. The fluorescent image was overlaid above a polarization microscope image. The scale bar is 10 μm ; D) Tentative phase diagram of flagella SJW1103; E) Excluded volume between two helical rods out of phase and in phase with respect to each other. (Reprinted with permission from Barry et al. Physical Review letters 96, 018305-1-4 (2006))

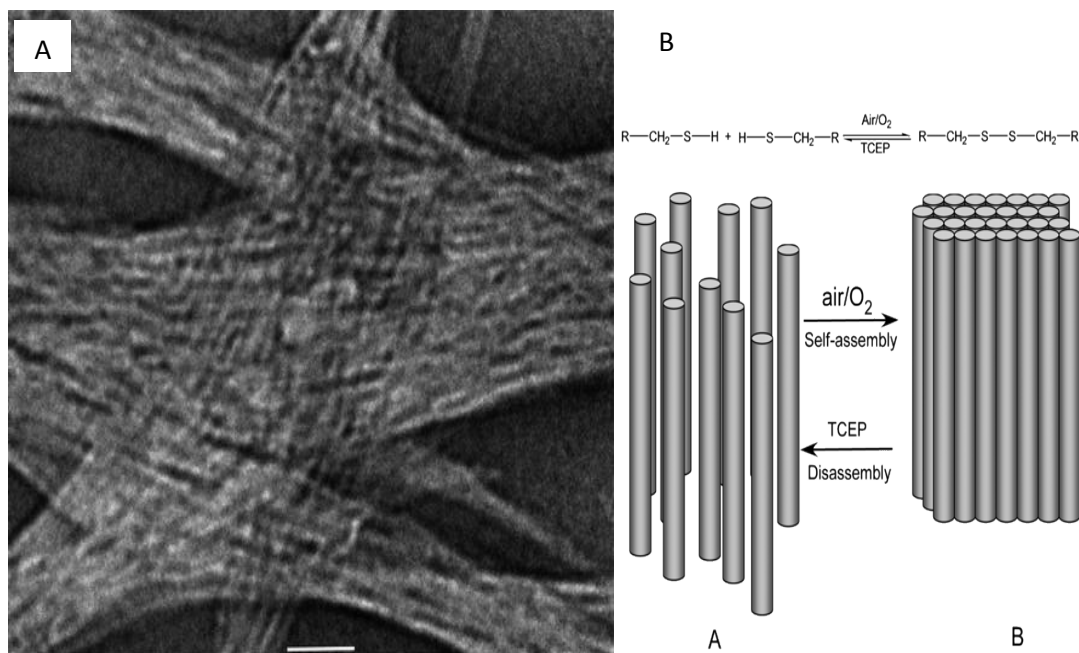


Figure 1.13: A) TEM images of disulfide cross-linked Cys loop flagella bundles stained with 2 % phosphotungstic acid (pH 7.5) (scale bar 100 nm); B) Assembly and disassembly of flagella bundle (A) Disassembly upon addition of a reducing agent. (B) Flagella nanotube bundle formation upon oxidative disulfide bond formation. (Reprinted with permission from Kumara et al. Nano Letters 6, 2121-2129 (2006))

Flagella can also be assembled into higher ordered structures with surface chemistry modification by flagella display. After displayed with “Cys-loop” containing 6 or 12 thiol side chains (-His-Cys-Cys-Cys-Cys-Cys-Cys-), the flagella can self-assemble into bundles in parallel via formation of disulfide bonds between neighboring flagella along the axis of the bundles (Figure 1. 13) [25]. The flagella bundles can be up to 10 μm in length and 200 nm in diameter. Under reducing environment, the bundles can be disassembled into individual flagella. Other bioengineered flagella with negatively or positively charged peptide loops or with six histidine loop peptide, however, cannot form large bundles. Bioengineered flagella can also be assembled by layer-by-layer (LBL) method on a gold-coated mica and quartz surfaces in a bottom-up manner. The flagella with arginine-lysine loops are assembled by LBL through molecular complementary interactions between biotin and streptavidin (Figure 1. 14A). The gold-plated mica plates were incubated with a mixture of undecanethiol with an ethanolic solution of η -octane

thiol to form amine-terminated surface. Then, the amine-terminated surface was linked by *N*-hydroxysulfosuccinimide-polyethyleneoxide-biotin (NHS-PEO₄-biotin). On the other side, positively charged flagella with arginine-lysine peptide loop flagella were also biotinylated by NHS-PEO₄-biotin. Ester groups of *N*-hydroxysulfosuccinimide react with amine group on lysine to form amide bonds. For LBL assembly, the biotinylated gold-plated mica plates were coated by a layer of streptavidin followed by a layer of biotinylated flagella. Multiple layers were produced by repeating the same procedure. A schematic representation of LBL assembly of biotinylated flagella are shown in Figure 1. 14B. Negative charged flagella with glutamic acid-aspartic acid peptides loops can be assembled by electrostatic attraction to protonated amine groups on polyethyleneimine (Figure 1. 14C) [124]. A schematic illustration of the electrostatic LBL assembly process is shown in Figure 1. 14D.

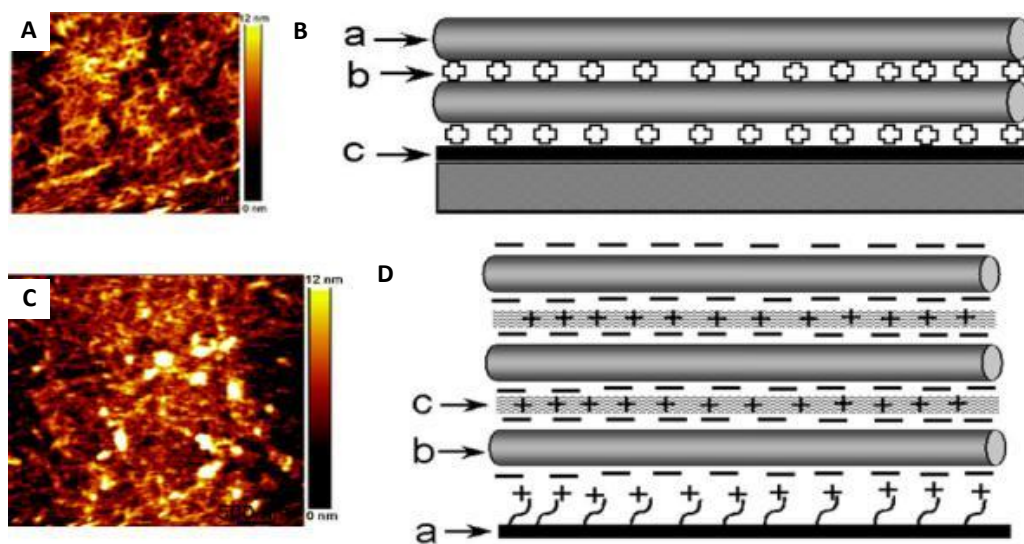


Figure 1.14: A) Topographic AFM image of the second layer of the arginine–lysine peptide loop flagella. B) Schematic illustration of layer-by-layer assembly of the arginine–lysine peptide loop flagella through molecular complementarity. (a) Top layer of biotinylated flagella; (b) Middle layer of streptavidin; and (c) bottom layer on biotinylated amine-terminated mixed SAM on gold; C) Topographic AFM image of the second layer of glutamic acid–aspartic acid peptide loop flagella; D) Schematic illustration of layer-by-layer assembly of flagella by electrostatic attraction: (a) quartz with positively charged amine groups; (b) flagella with glutamic acid–aspartic acid

peptide loops assembled on (a) by electrostatic attraction; and (c) polyethyleneimine adsorbed on (b) through electrostatic attraction. (Reprinted with permission from Kumara et al. *Biomacromolecules* 8, 3718-3722 (2007))

1. 8 Outlook

With surface display, bioengineered flagella can be used for identification of peptide-ligand interactions, vaccine carriers, secretion tools for foreign proteins, and so forth [86, 93]. Based on random peptide library screening, more and more polypeptides with functional groups will be identified and displayed on flagella, which will lead to more applications.

Two different peptides in separate *FliC* subunits can be displayed on the same flagellum filament simultaneously, which becomes a double-hybrid display system [61, 125]. Or *FliD*, like *FliC*, also includes conserved and less conserved regions. With amino acid analysis of *FliD* N- and C- terminal regions, which are located in the leg-like domains of the cap, are more conserved. These domains make contact with the distal ends of the flagella. However, in the plate-like structure of the cap, the sequences are more variable, and can be partially deleted or inserted by foreign polypeptides. By combining the *FliC* double-display technique, a triple-display technique was developed by Majander [126] in which three foreign peptides are simultaneously expressed within the same flagellum. This technique makes flagella as multi-functional tools. As vaccines, specific adhesion polypeptides to their targets can be displayed on *FliD* for specific attachment. At the same time, *FliC* can carry two different antigenic epitopes. It may also be applied to gene or drug delivery as a carrier for diagnostic or therapeutic purposes. For examples, polypeptides recognized by target cells are displayed on *FliD*. The polypeptides that can combine with drugs or genes are displayed on *FliC*.

Flagella are easily depolymerized into monomeric *FliCs* under acidic conditions or at high temperatures. Interestingly, *FliC* can re-polymerize into flagella again in salts under neutral pH and sometimes with the aid of short flagella fragments as seeds. In addition, *FliC* from different strains can initiate copolymerization [127]. Two or more kinds of engineered *FliCs* can be mixed together and copolymerize into hybrid flagella, providing more freedom and flexibility for further applications.

With the combination of molecular biology and bionanotechnology, using genetic methods and/or design, more and more peptides are being selected for specific binding to targets. In recent years, a variety of targets, including noble metals, metals, oxide and nitride semiconductors, minerals and some other substrates, were selected. Most of the processes are accomplished at ambient conditions by molecular biomimetics. This approach makes it possible to fabricate more novel flagella/inorganic hybrid materials at the molecular and nanometer levels by display sequences selectively binding to the targets. With the combination of double or triple display, different polypeptides that recognize more than one target can be displayed. This may permit organized assembly of nanocomposite materials at higher levels, resulting in a variety of new applications, such as biomimetics, tissue engineering, and “bottom up” assembly. These hybrid flagella are promising for diagnostic purposes, the construction of biocatalysts, advanced biosensors, bioreactors, bioadsorbents, random peptide libraries, nanotubes, nanowires and in other biotechnological approaches [128].

Chapter 2 Biomimetic Nucleation and Growth of Bone Mineral on Bone Protein-Derived Peptides Displayed on Bacterial Flagella with Further Assembly

2. 1 Introduction

It is promising to fabricate biocompatible and biodegradable scaffolds for bone repair and regeneration. New bone can build on them and ,finally, defective bone tissue can be replaced [129]. However, constructing a nanocomposite mimicking both the composition and organization of bone is challenging. Bone is a dynamic, highly vascularized tissue mainly composed of inorganic mineral-HAP ($\text{Ca}_{10}(\text{PO}_4)_6(\text{OH})_2$) and organic scaffold-type I collagen [130]. From a material science point of view, bone tissue is an inorganic–organic hybrid nanocomposite material containing multiple levels of hierarchical structure in an organized fashion. At the lowest level of organization, the HAP nanocrystallites (20-80 nm long, 2-5 nm thick) are assembled along the fibrous collagen molecules [131, 132]. With the development of tissue engineering, especially combined with bionanotechnology, designing artificial biomaterials at the nano-level that can interact with and replace ECM becomes feasible [133, 134]. In contrast with conventional methods, these novel materials can mimic the complex and delicate structure of bone at the nanoscale level via a “bottom up” approach [134]. Recently, we demonstrated the orientated nucleation of HAP nanocrystals on native or bioengineered phage and spider silk [135-137].

In this study, bacterial flagella filaments are utilized to mimic collagen fibrils at the lowest level of bone tissue structure. Using peptide display technique, peptides from bone proteins were displayed on flagella surface: First, to identify the peptides or domains are responsible for mineral nucleation from bone protein-derived peptides using flagella display; Second, to build structurally and functionally bone-like materials at the nanometer level. The bacterial flagellum is a long filament composed of several thousand copies of bacterial *FliC* major proteins as well as some other minor proteins, such as a pentamer of the tip-associated *FliD* protein. The linear tubular structure of a flagellum has a repeat of 11 monomers per two turns through self-assembly via non-covalent interactions between α -helical and coiled-coil motifs [56]. Each flagellum is about 10-15

μm in length with an outer diameter of 12-25 nm and an inner diameter of 2-3 nm. The N- and C- terminal regions of *FliC* located in the inner tube are highly conserved, whereas the central region of *FliC* is surface-exposed and contains highly variable sequences [81]. Based on genetic approach, a foreign peptide can be inserted into the variable region of *FliC* and, thus, displayed on the surface-exposed portions of flagella. This technique is called peptide display. Up to 302 amino acid residues have been successfully displayed on the surface of flagella, without preventing flagellar polymerization and functions [81]. The recombinant bacterial flagella were used as live vaccines to evoke humoral and cellular immune responses [138]. Recently the bioengineered flagella mediated synthesis of inorganic and organic nanotubes has been reported [139-144].

In bone tissue, type I collagens are parallel to each other, forming thicker fibrils in a hexagonal array. The type I collagen molecules align with each other and pack precisely into the so-called quarter-staggered mode, exhibiting a characteristic D-banding that exhibits the alternating hole or gap (47 nm in length) and overlap (20 nm in length) zones [129, 145]. Biomineralization occurring on the collagen fibrils includes the nucleation of HAP nanocrystals in the appropriate microenvironment and assembly within collagen fibrils. To date, however, the direct evidence and precise chemical mechanisms of HAP nanocrystal nucleation are still not clear. Most of the previous reports suggest that HAP nanocrystals are initially nucleated at the hole zone of the collagen fibrils [145-148], especially at the defined region-e and d bands, which contain the charged amino acid side chains [149]. However, Maitland and Arsenault [150] found the apatite crystals occurring at both the hole and overlap zones during the early stage of mineralization in an asymmetric pattern. *In vitro*, type I collagen can also mediate nucleation of HAP nanocrystals [149], but it is still a mystery as to which domains or sequences on type I collagen can direct initial apatite nucleation precisely [151]. It is proposed that potential sites of HAP nucleation occur on the charged amino acid residues of type I collagen including glutamic and aspartic acid, lysine, arginine, hydroxylysine and histidine [152].

The type I collagen molecule is mainly composed of repeated Gly-X-Y (where X is often proline and Y is often hydroxyproline) sequences with small non-helical domains at the

N- and C-terminals. Accordingly, the total N-, C-terminals and partial N-, C-zones enriched with polar amino acid residues, are displayed on flagella. Because the biomineralization initiates at both the hole and overlap zones, an 8 repetitive Gly-Pro-Pro (GPP8) sequence is also designed to be displayed on flagella (Figure 2. 1).

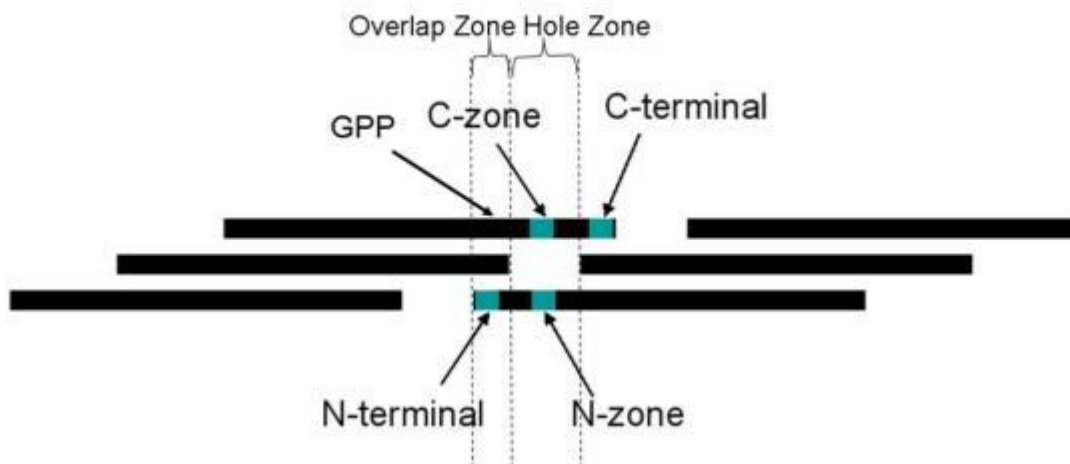


Figure 2.1: Position of different domains within type I collagen fibrils in bone tissue. Partial N, C-zones located at the hole zone are selected. N, C- terminals located at the overlap zone are selected. A 8 repetitive GPP resemble to the central portion of type I collagen is designed.

It is well established that *in vivo*, type I collagen itself is not the only contributor for HAP nucleation. Many non-collagenous proteins are also very important during the biomineralization process to regulate HAP nucleation and the growth of the mineral phase [129, 151, 153]. OPN and OCN are the prominent non-collagenous proteins that are thought to regulate HAP nucleation due to the presence of the acidic amino acids [154, 155]. As a very important nucleator, BSP can bind to type I collagen fibrils forming a complex as a nucleator to induce the nucleation of HAP nanocrystals [156]. Moreover, the X-ray crystal structure of OCN indicates that it coordinates with 5 calcium ions in a spatial orientation corresponding to calcium ion positions in the HAP crystal lattice [155]. He et al [157] reported that the dentin matrix protein 1 (DMP1), which is also an acidic non-collagen protein, could also nucleate HAP *in vitro*. *In vivo*, non-collagenous proteins are morphologically, structurally, and functionally connected to collagen fibrils, which facilitate primary crystal formation and subsequent crystal growth on collagen. A

possible mechanism is that these anionic groups induce a local supersaturation of Ca^{2+} followed by phosphates, especially in the intermolecular β -sheet acidic domains [157-161]. Therefore, we also displayed a peptide encoding 8 glutamic acid residues (E8) from BSP on flagella. Studying the nucleation ability of these bioengineered flagella is carried out in supersaturated HAP precursor solution at room temperature.

2. 2 Materials and methods

2. 2. 1 Display of bone protein derived peptides from type I collagen and BSP on bacterial flagellar surface

2. 2. 1. 1 Digestion of original plasmid:

The vector pLS411 contains the gene of *FliC* in which most of the central hypervariable region has been deleted and replaced with a 45 bp oligonucleotide encoding a foreign peptide (Cholera toxin peptide 3, CPT3). This epitope is inserted by restriction sites *Xho* I and *Bgl* II [138]. In order to insert the new sequences that are selected from bone related proteins, the pLS411 was digested by restriction enzymes *Xho* I and *Bgl* II (New England Biolabs, NEB) at 37 °C for 2 h, and then run on 1 % agarose gel. After purification by Gel Extraction Kit (QIAGEN), the plasmid with *Xho* I and *Bgl* II restriction sites was collected.

2. 2. 1. 2 Preparation of DNA fragments and cloning:

Cloning DNA fragment preparation: The single-stranded oligonucleotides that encode target peptides including restriction sites of *Xho* I and *Bgl* II at the ends were synthesized (Invitrogen). The forward and reverse single-stranded oligonucleotides were mixed together at a final concentration of 100 mM. After annealing, they formed complementary double-stranded DNA with a restriction site of *Xho* I at the 5'-end as well as *Bgl* II site at the 3'-end. HAP most likely interacts with charged or polar amino acids [152]. Therefore, the sequences encoding 17 amino acids of N-terminal and 26 amino acids of C-terminal of type I collagen near the very end, which are rich in charged and polar amino acids, are displayed on flagella respectively. Similarly, partial N-zone and C-zone of type I collagen are selected and displayed. Moreover, a 72 bp nucleotide encoding 8 repeated GPP peptides is displayed on flagella. The total selected sequences from type I collagen and E8 from BSP are listed in Table 2. 1 and the positions of these sequences are depicted by Figure 2. 2.

Table 2.1: Inserted sequences in recombinant plasmid

Name	Oligonucleotides	Encoded amino acids
GPP8	5' - GA TCT GGA CCA CCT GGT CCA CCT GGT CCT CCA GGT CCA CCT GGA CCA CCT GGT CCA CCT GGT CCT CCA GGT CCA CCT C -3' 5' - TC GAG AGG TGG ACC TGG AGG ACC AGG TGG ACC AGG TGG TCC AGG TGG ACC TGG AGG ACC AGG TGG ACC AGG TGG TCC A-3'	GPPGPPGPPGPPGPPGPPGPPGPP
N-terminal	5' -GA TCT CAG CTG TCT TAT GGC TAT GAT GAG AAA TCA ACC GGA GGA ATT TCC GTG CCT C-3' 5' -TC GAG AGG CAC GGA AAT TCC TCC GGT TGA TTT CTC ATC ATA GCC ATA AGA CAG CTG A-3'	QLSYGYDEKSTGGISVP
C-terminal	5' -GA TCT CAG CGC TGG TTT CGA CTT CAG CTT CCT GCC CCA GCC ACC TCA AGA GAA GGC TCA CGA TGG TGG CCG CTA C-3' 5' -TC GAG TAG CGG CCA CCA TCG TGA GCC TTC TCT TGA GGT GGC TGG GGC AGG AAG CTG AAG TCG AAA CCA GCG CTG A-3'	SAGFDFSFLPQPPQEKAHDGGRYIRA

Name	Oligonucleotides	Encoded amino acids
E8	5' –GA TCT CGA GGT GAT GAA GAG GAA GAG GAA GAG GAA GAA C-3' 5' –TC GAG TTC TTC CTC TTC CTC TTC CTC TTC ATC ACC TCG A-3'	EEEEEEEE
N-zone	5' –GA TCT GGT TTG GAT GGT GCC AAG GGA GAT GCT GGT CCT GCT GGT CCT AAG GGT GAG CCT GGC AGC CCT GGT GAA AAT C-3' 5' –TC GAG ATT TTC ACC AGG GCT GCC AGG CTC ACC CTT AGG ACC AGC AGG ACC AGC ATC TCC CTT GGC ACC ATC CAA ACC A-3'	GLDGAKGDA GPAGPKGEPGSPGEN
C-zone	5' –GA TCT GGA CCC CAA GGC CCA CGT GGT GAC AAG GGT GAG ACA GGC GAA CAG GGC GAC AGA GGC ATA AAG GGT CAC CGT C-3' 5' –TC GAG ACG GTG ACC CTT TAT GCC TCT GTC GCC CTG TTC GCC TGT CTC ACC CTT GTC ACC ACG TGG GCC TTG GGG TCC A-3'	GPQPGDGETGEQDGRGIKTHR

N-terminal

162 alsygydek stggisvpgp
181 mgpsgprglp gppgapppqg fggppgepge pgasgpmgpr gppgppgkng ddgeagkpgr
241 pgergppgpq garglpntag lpgmkghrgf sldgakgda gpagpkgepg spgengapga
301 mgprglpger grpgapdag argndgatga agppgptgpa pppgfpavag akgeagppgp
361 rgsegppgvr gepgpppag aagpagnpa dgppgakgan gapgia.....
.....
961 vglpgqrger gfpglpssg epkkgppsga sgergppgpm gppglagppg esgregapga
1021 egspgrdgsp gakedrgeta pagppganga pagppvgpa gksgrgetg pagpagpvgp
1081 vgargpapq gprgdkgetg eqgdrgikh rfgsflgpp pppgspeeg psgasppagp
1141 rgppgsagap gkdglnglp pigppprgr tgdagpvpp gpppppppp ppsagdfsf
1201 lpqppqekah dgryyra

C-terminal

Figure 2.2: Protein sequences and positions of inserted peptides displayed on flagella. (The whole N-zone and C-zone regions were marked by underline)

Ligation and transformation: The double-stranded oligonucleotides were ligated into *Xho* I and *Bgl* II linearized pLS411 by T4 ligase (Invitrogen) at room temperature for 1 h. Then, the plasmids were transformed into competent *E. coli* DH5 α . Finally, the recombinant plasmids were transformed into *FliC* deficient *Salmonella* strain SL5928 by electroporation. SL5928 is an *aroA* live-vaccine strain of *Salmonella* Dublin. Because its only *FliC* gene- *fliC*(g, p) has been replaced via transduction by *fliC*(i)::Tn10, an allele inactivated by transposon insertion, the functional flagella cannot be expressed [138].

Selection and motility assay: The ampicillin-resistant clones with recombinant plasmid were selected and confirmed by sequencing. In order to ascertain whether the recombinant strain could assemble flagella with motile function, the clones were cultured in semisolid medium (1 % tryptone; 1.5 % NaCl; 0.35 % agar) for a cell motility test. *Salmonella* SL5928 with the recombinant plasmid was inoculated by stabbing the center of the medium to a depth beyond the midway point and then cultured at 37 °C for 24-48 h. Only the bacteria with functional flagella assembled on their surfaces are motile in the media, providing an easy method to verify synthesis and assembly of the engineered flagella. Motility of *Salmonella* was tracked visually by observing the diffusion growth from the center of the plate. Finally, the entire plate will be covered by diffused growth. If no functional flagella were synthesized and protruded from the cell surface, the clone of the bacteria would be kept in the center.

2. 2. 2 Purification of bacterial flagella:

SL5928 with recombinant plasmid was inoculated into semisolid medium and incubated at 37 °C until it reached the edge of the plate. The cells from the advancing edge of growth were inoculated into 1 L of LB containing L-ampicillin (100 μ g/ml) and incubated at 37 °C with shaking (250 rpm). When the OD of the cell culture reached about 0.6-0.8, the bacteria were harvested by centrifugation at 6000 g for 15 min, washed three times with phosphate-buffered saline (PBS, pH 7.2) and finally suspended in 25 ml of PBS. The flagella were detached from the cells by vigorous vortex at the highest speed for 3 times (30 sec/each time). The supernatant containing the sheared flagella was separated by centrifugation at 12,000 \times g for 40 min. The purity of the isolated flagella

was subjected to sodium dodecyl-sulfate polyacrylamide gel electrophoresis (SDS-PAGE).

2. 2. 3 Flagella examination by optical and electron microscopy:

Flagella were examined with silver staining. A drop of purified flagella (15 μ l) were mounted on carbon grid and air dried. The sample was then stained with 1 % (wt/vol) uranyl acetate (UA) for 30 s [162] and observed with transmission electron microscopy (TEM, Zeiss 10).

2. 2. 4 Western blot analysis:

In order to confirm the insert peptides on flagella, the flagella with GPP8 and E8 were subjected to Western blot examination. The purified flagella were denatured for 5 min at 95 °C and applied to 10 % of the SDS-PAGE at 200 V for 40 min. Then, the proteins were transferred to PVDF membrane at 30 V, 90 mA for overnight in a methanol buffer. The membrane was sealed in a plastic bag with 5 ml blocking buffer (10 % defat milk in PBS) for 1 h at room temperature with agitation on an orbital shaker. After washed with PBS containing 0.05 % Tween 20 (TTBS), the membrane was incubated for 1 h at room temperature with diluted (1: 1000) primary polyclonal antibody (rabbit anti- type I collagen or rabbit anti-BSP) (Sigma-Aldrich) in blocking buffer. The membrane was then washed with TTBS and incubated with alkaline phosphatase-conjugated goat anti-rabbit antibody (Sigma-Aldrich) (1: 2000 diluted in TTBS) for 1 h at room temperature under constant agitation. Finally, the blotting bands were visualized by incubation with chromogenic substrates-NBT/BCIP for 30 min at room temperature in the dark.

2. 2. 5 Nucleation of flagella in supersaturated HAP solution:

Supersaturated HAP solution (4 mM) was prepared as described [163] from HAP powder (Sigma-Aldrich). The bioengineered flagella (30 μ l, 50 μ g/ml) were mixed with 500 μ l of supersaturated HAP solution and incubated for various periods of time at room temperature. Wild type flagella are used as a control. A drop of mixture was mounted on the carbon TEM grids. After carefully rinsed with ddH₂O, these samples were examined with TEM (Zeiss 10 and JEOL 2000-FX).

2. 2. 6 Flagella assembly with nucleation of HAP:

The assembly of flagella was based on our previous report with some modification [136]. Briefly, the CaCl₂ solution (100 mM) was adjusted to pH=9.5 by NaOH because the flagella are stable at pH=2-10 [164]. The solution was then diluted into different concentrations with water and mixed with purified flagella. The bundled flagella were collected by centrifugation (10,000 g for 10 min) and washed with water. Finally, the flagella bundles were incubated in supersaturated HAP solution at room temperature.

2. 3 Results

The plasmids were sequenced at each step to confirm the identity of the inserts (data not shown). The stains with recombinant plasmids were cultured on semi-solid media with a negative control strain SL5928. After incubated at 37 °C for 1 day, all of recombinant strains diffused from the inoculated site, but the negative control SL5928 only formed a colony in the center of the plate due to its lack of motility. The motility assay confirmed that the flagella polymerized from the engineered bacterial flagellin were functional. However, the diffusion speeds of the recombinant stains varied from each other as well as from the control. For example, the strain with E8 spread faster than that with GPP8 (Figure 2. 3).

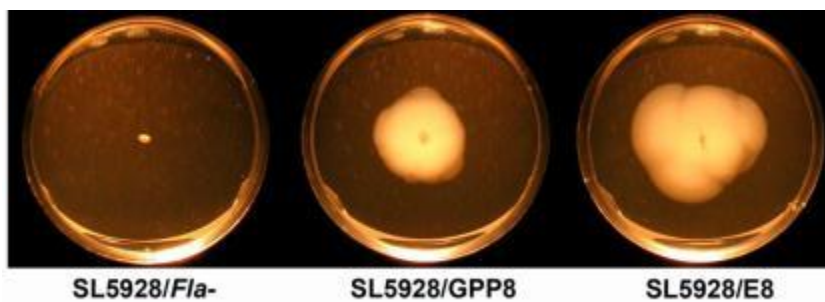


Figure 2.3: Bacterial motility assay in 24 h. No spreading of SL5928 strain as the negative control. Flagella with E8 spread faster than that with GPP8

Before and after the bacterial flagella were purified from bacteria, they were examined and verified using silver nitrate staining. Over ten flagella were observed on the surface of a single bacterium at SL5928 with E8 (Figure 2. 4A). Other strains show similar results but with fewer and shorter flagella (data not shown). After purification, a large

amount of flagella with characteristic sinusoidal morphology were observed at a very high degree of purity (Figure 2. 4B). Under TEM, flagella exhibited a more linear structure after staining by UA with 15 ± 0.5 nm in diameter and 2-4 micrometers in length (Figure 2. 4C).

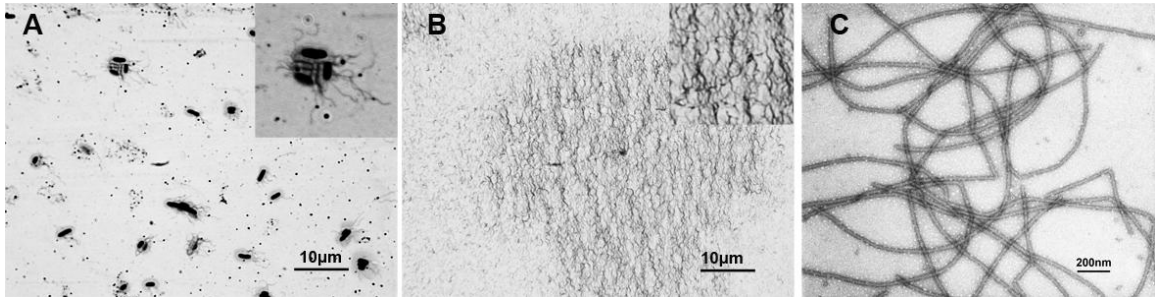


Figure 2.4: A) Silver staining of bacterial flagella before purification (insert: higher magnification). B) Silver staining of bacterial flagella after purification (insert: higher magnification). C) TEM images of purified flagella

After purification, the recombinant flagella was subjected to SDS-PAGE analysis and only showed one band with a molecular weight of about 55 kDs on the gel (Figure 2. 5A). It indicates that *FliC* was isolated with a very high degree of purity. Bovine serum albumin (BSA) at 66 kDs and SL5930 were used as a control. Strain SL5930 is a pBR322 derivative also containing flagellin gene with a 48 bp deletion in hyper variable region [165]. Other recombinant flagella with N-, C-terminal, N-, C-zone inserts also exhibit very similar molecular weight band on the SDS-PAGE gel (data not shown). *FliC* with GPP8 or E8 against anti-type I collagen and BSP polyclonal antibody showed a very clear blotting band. GPP8 *FliC* blotting band presented a higher intensity than did that of BSP *FliC*. The low affinity of anti-BSP antibody may be ascribed to the fact that E8 is only composed of a short part of BSP. The initial concentration of GPP8 and E8 flagella were adjusted to the same concentration (1.6 mg/mL) and loaded 8 μl on the gel. No blotting band is visible with wild-type *FliC* (Figure 2. 5B).

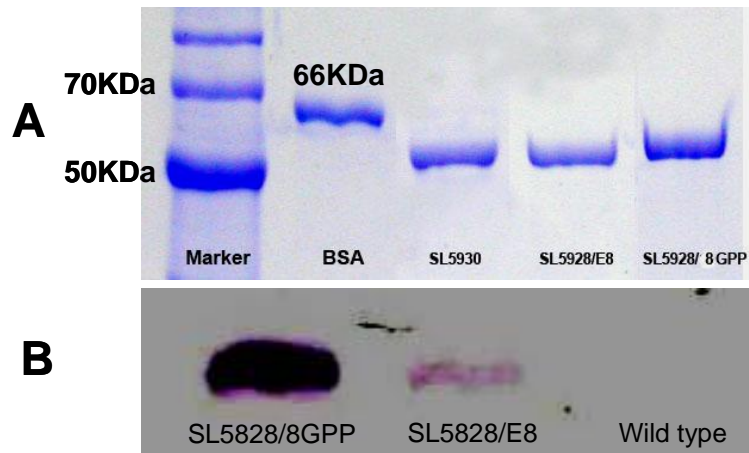


Figure 2.5: A) SDS-PAGE electrophoresis of *FliC*. (8 μ l/sample). Molecular weight of BSA is 66 kDa. SL5930 encodes flagellin protein with a 48 bp deletion in the center of hypervariable region (Control). The molecular weight of SL5928/E8 and SL5928/GPP8 are close to that of SL5930. B) Western blotting of recombinant *FliC*. A clear band can be observed for SL5928/GPP8 and SL5928/E8. Wild type *FliC* was used as a control.

After being soaked in supersaturated HAP precursor solution at 3, 6 and 9 days, the flagella were examined by TEM. In the control, there was no visible mineralization on wild type flagella until the ninth day (data not shown). Similar results were observed for the engineered flagella that contain N-, C-terminal in 9 days. A very thin layer of amorphous mineral deposited on the surface of the flagella with N-, C-zone inserts and created a low contrast image (Figure 2. 6). Because the flagella are invisible under TEM without staining, UA stained flagella were used as controls for each sample. Purified flagella were detected on all samples and had no obvious difference between each other (data not shown).

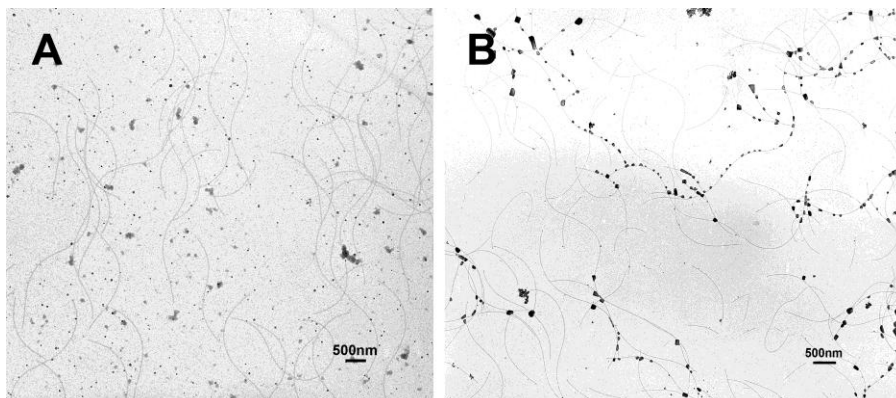


Figure 2.6: TEM images of flagella with N-zone of type I collagen A) and C-zone of type I collagen B) soaked in 4 mM supersaturated HAP precursor solution for 9 days.

For recombinant flagella with E8 and GPP8 sequences, inorganic minerals, which make the flagella visible directly under TEM, were observed on the surface of the flagella after 3 days. From selected area electron diffraction (SAED) analysis, only amorphous minerals were formed at this time (Figure 2. 7A, B). After 6 days, the E8 and GPP8 flagella were shown to be aligned with crystalline minerals which were revealed by SAED analysis. However, the flagellar surfaces were not totally covered by minerals. A lot of gaps can be observed along the flagella (Figure 2. 7C, D). After 9 days, an entire layer of polycrystalline minerals was observed on the flagella displaying E8 and GPP8 sequences with diameters of 46 ± 5 nm and 38 ± 4 nm respectively (Figure 2. 7E, F). In the SAED patterns, the presence of the (211) and (002) planes indicates that the polycrystalline minerals are composed of HAP. However, stronger patterns were observed consistently on E8 flagella than those on GPP8 flagella at each time interval. Interestingly, at high concentration, E8 flagella show strong tendency to form bundle-like structures after soaked in supersaturated HAP solution (Figure 2. 8). However, the bundle-like structures were staggered to each other forming network structures.

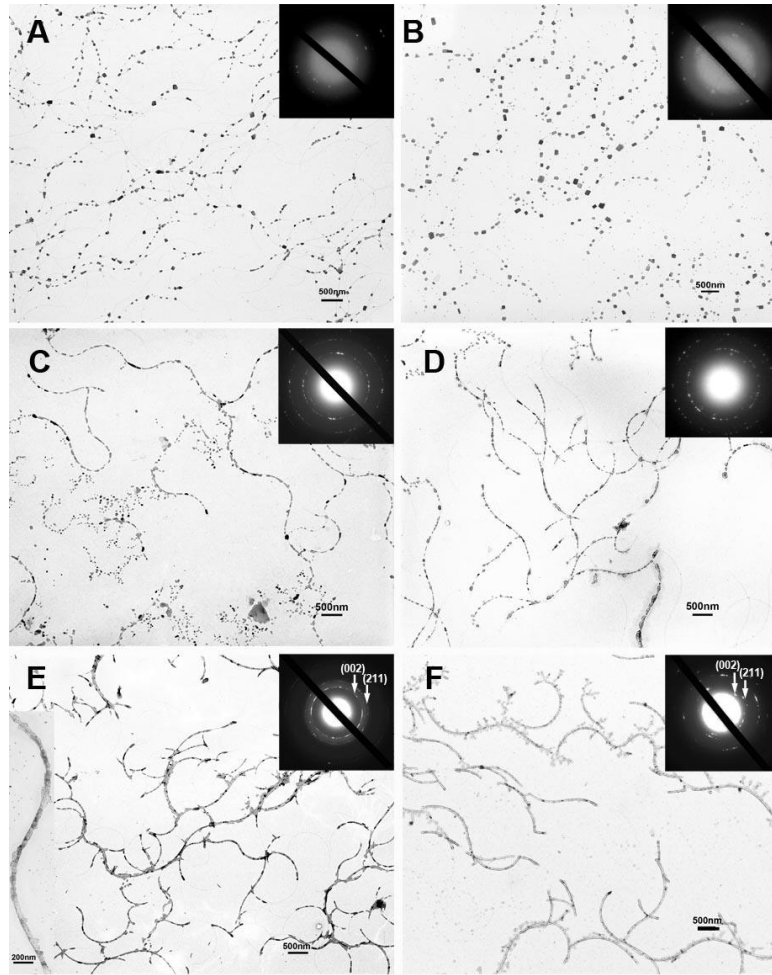


Figure 2.7: TEM images and SAED patterns of E8 and GPP8 flagella soaked in 4 mM supersaturated HAP precursor solution at different time intervals. A, B) After 3 days, flagella with E8 (A) and GPP8 (B) in supersaturated HAP solution. Almost no crystals nucleated. C, D) After 6 days, flagella with E8 (C) and GPP8 (D). Some crystals nucleated with amorphous mineral. E, F) After 9 days flagella with E8 (E) with high magnification (insert) and GPP8 (F). HAP crystals nucleated on the surface of flagella. Stronger SAED pattern was observed on E8 flagella than on GPP8 flagella.

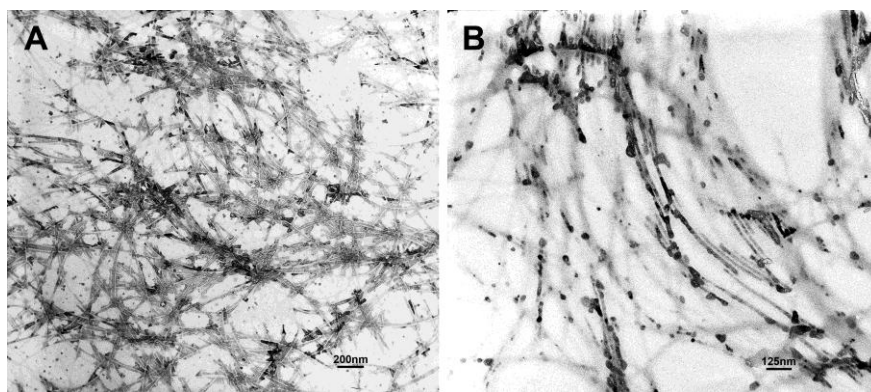


Figure 2.8: TEM images of high concentration of flagella with E8 nucleated in 4mM supersaturated HAP precursor solution. A: Bundle-like structures of flagella can be observed at some areas. B: high magnification of bundle-like flagella.

In order to obtain parallel bundles for the purpose of identifying the relative orientation of the mineral crystals with respect to flagella, flagella bundles induced by Ca^{2+} were investigated. Because the E8 flagella exhibited stronger nucleation of polycrystalline minerals, they were selected to be assembled into bundles for further analysis. At a high concentration of CaCl_2 (0.5 M), flagella totally depolymerized into monomers [166]. Thus, much lower concentrations of CaCl_2 were used in our study; however, we still found partial depolymerization of the E8 flagella at concentrations of CaCl_2 over 7 mM (Figure 2. 9D). Interestingly, below 7 mM of CaCl_2 , bundles of flagella could be observed and exhibited a Ca^{2+} concentration dependent manner (Figure 2. 9). After multiple experiments with different concentrations of CaCl_2 , 4 mM CaCl_2 was determined to be optimal and was used for the this study. After staining with 1 % UA, parallel bundle structures of flagella were observed. Some flagella packed into flat ribbons structures up to 200 nm in diameter (Figure 2. 10). At higher concentrations of Ca^{2+} , the bundled flagella straightened and almost lost the characteristic curly morphology. The correlations of Ca^{2+} with flagella with E8 were examined by Fourier transform infrared spectroscopy (FTIR). After mixed 4 mM CaCl_2 with E8 flagella, the observed peak at 1657 cm^{-1} predominantly corresponding to the C=O stretch for pure E8 flagella shifted to 1629 cm^{-1} for flagella/ Ca^{2+} (Figure 2.10). The red shift indicates that the C=O bonds in E8 flagella were weakened because of the formation of chelate bonds between Ca^{2+} and C=O bonds [167, 168]. This implies that the carbonyl groups on the

surfaces of E8 flagella were ionized by the coordination of Ca^{2+} . At the same time, the peak at 1528 cm^{-1} , which corresponds to a combination of the N–H in-plane bend and the C–H stretch, almost disappeared due to the decrease in intensity (Figure 2. 11).

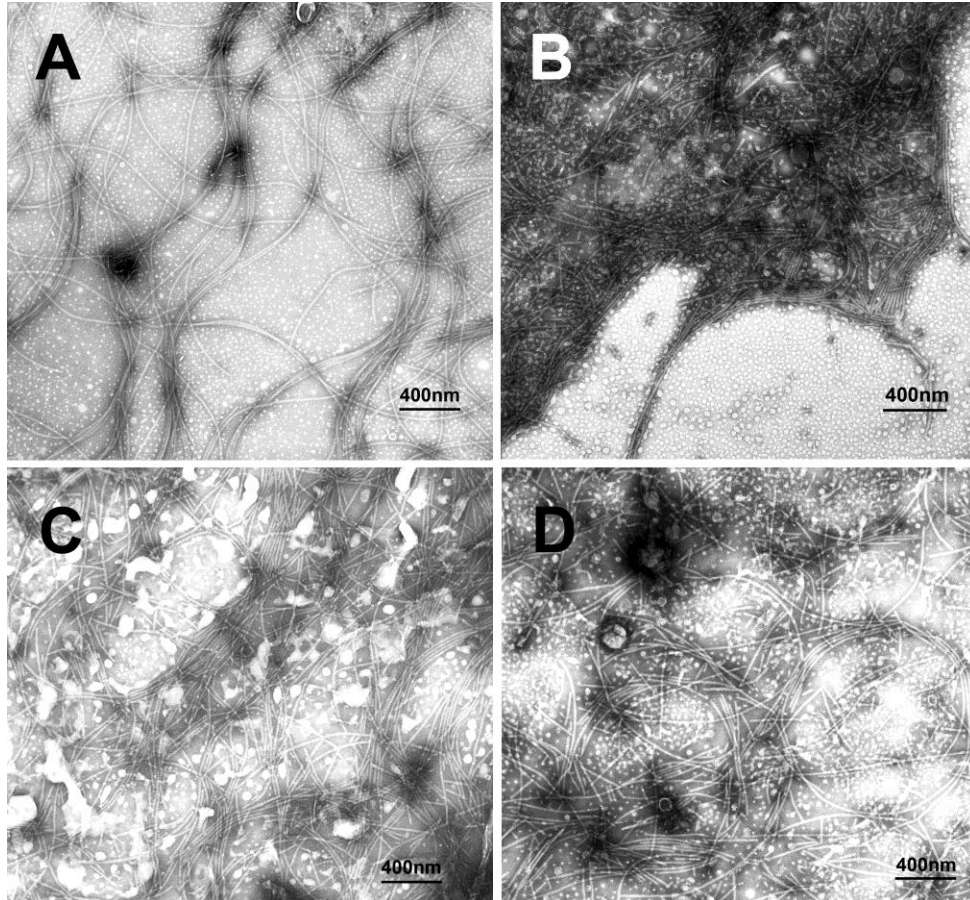


Figure 2.9: TEM images of Ca^{2+} induced E8 bioengineered flagella bundles. A) 2 mM of CaCl_2 . Some flagella formed narrow bundles by side-by-side aggregation. B) 4 mM. Thick bundles of flagella can be observed. C) 6 mM. Some flagella bundles can be observed and a small amount of flagella start to broke into small ones. D) 8 mM. About half of the flagella were degraded into short ones. Some bundles can still be observed.

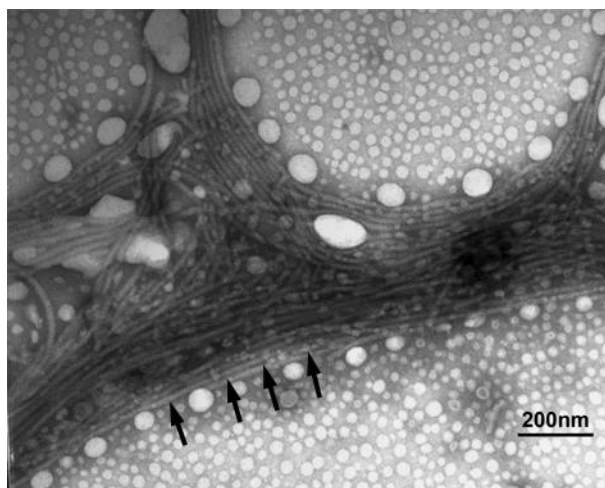


Figure 2.10: TEM images of self-assembled flagella bundles with E8 induced at 4 mM of CaCl_2 . Parallel flagella bundles formed with side-by-side aggregation (marked by arrows).

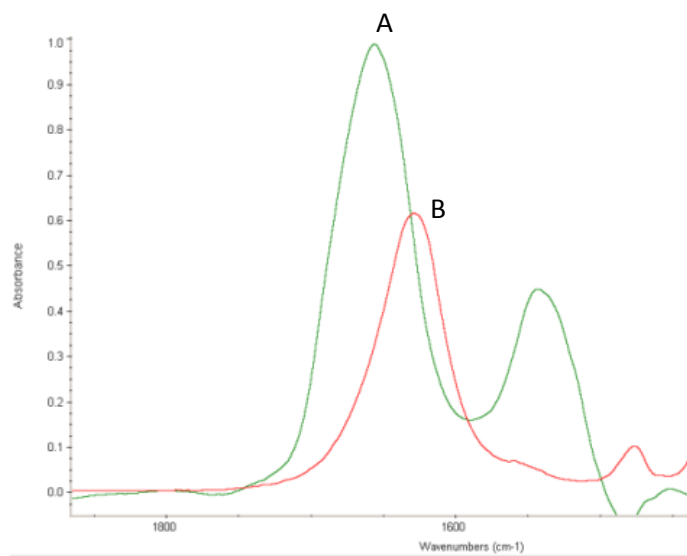


Figure 2.11: FTIR analysis of flagella. A) Purified flagella with E8. B) Flagella with E8 mixed with 4 mM CaCl_2

The flagella bundles were collected by centrifugation. After being carefully washed with pure water, the bundles were immersed in 4 mM supersaturated HAP solution. After one day, amorphous minerals with tiny inorganic nanoparticles nucleated and aligned on flagella (Figure 2. 12A). Meanwhile, the flagella bundles became “loose” after soaking in

HAP precursor solution and the flagella recovered the characteristic curly morphology. Plate-shaped polycrystalline mineral could be observed throughout the surface of flagella thick bundles after 3 days (Figure 2. 12B). The minerals were characterized by energy-dispersive X-ray spectroscopy (EDX) (Figure 2. 12D). It revealed a Ca/P ratio of 1.65 ± 0.05 , which is close to the theoretical value of HAP with a formula of $\text{Ca}_{10}(\text{PO}_4)_6(\text{OH})_2$ (Ca/P ≈ 1.67). Some minor Na and Cl precipitated from supersaturated HAP precursor solution and were present in the minerals. The copper and silicon detected by EDX came from the sample substrate. Narrower mineralized flagella bundles could also be observed on the same TEM sample, (Figure 2. 12C). SAED analysis revealed that preferential alignment of the HAP crystallographic *c*-axis parallel with the long axis of flagella bundles (Figure 2. 12C insert). The diffraction arcs corresponding to the (002) and (004) plane demonstrated the *c*-axis preferred orientation of HAP nanocrystals.

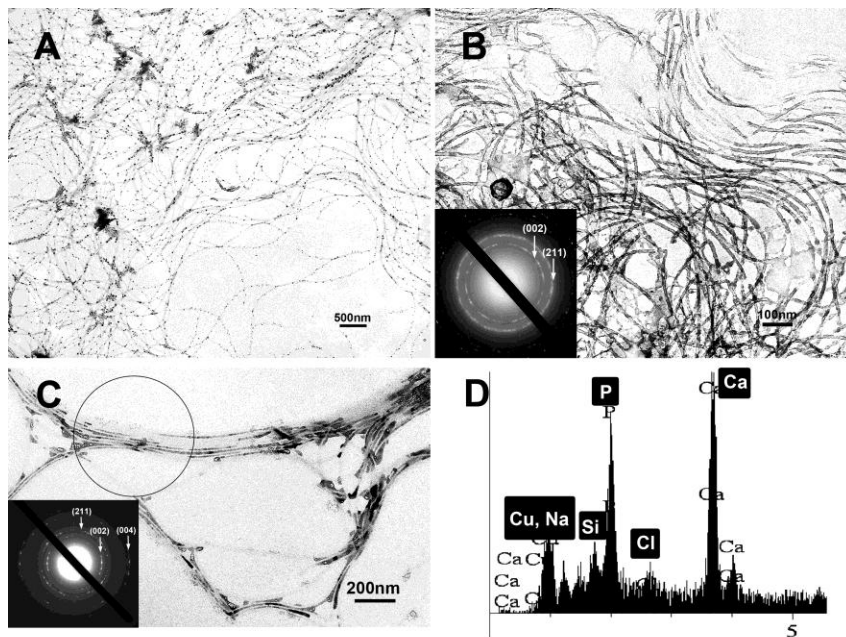


Figure 2.12: TEM images of flagella bundles with E8 soaked in supersaturated HAP solution with EDX and SAED analysis. A) 1 day of flagella bundles with E8 in supersaturated HAP solution. Nanometer-levelled minerals nucleated on the surface of flagella. B) 3 days of flagella bundles in supersaturated HAP solution. The bundles became “loose” and nucleated by a nanoscale HAP crystalline. C) Narrow flagella bundles with SAED pattern (insert) taken from the highlighted sections. The arc of (002)

and (004) indicated the oriented nucleation of HAP. D) EDX analysis of the flagella bundles.

When the E8 flagella were incubated in supersaturated HAP precursor solution, occasionally, ribbon-like flagella bundles could be observed directly (Figure 2. 13). They might be formed by super-flagella [169]. SAED pattern also revealed a short arc of the (002) and (004) planes of HAP, indicating the preferred orientation along the long axis of the flagella bundles.

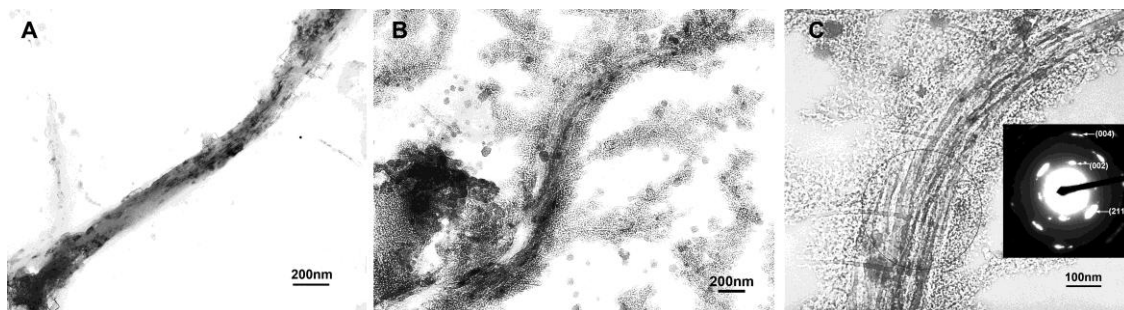


Figure 2.13: (A, B) TEM images of ribbon-like flagella bundles displayed with E8 soaked in HAP precursor solution for 3 days. They might be formed by super-flagella. (C) SAED analysis also showed short arc of (002) and (004) planes, indicating the preferred orientation along the long axis of the flagella bundles.

2. 4 Discussion

Biom mineralization of bone is a very complex process, which involves cell-mediated deposition of HAP crystalline materials within the ECM in an organized fashion [151]. Although the peptides displayed on flagella surfaces may exhibit different conformations from those in the native bone proteins, we believe the displayed peptides used here can provide more information to aid in the understanding of the nucleation of HAP *in vitro*. Each flagellar filament is a nanofiber assembled from thousands of subunits. Because the *FliCs* are organized along the filament during the self-assembly, the peptide displayed on each subunit will be naturally organized and uniformly distributed throughout the surface of flagella. By biomimetic nucleation, the peptide which serves as the nucleator to direct mineral nucleation can be identified. Moreover, the mineralized flagella resemble that the

lowest level of hierarchical organization of bone in which type I collagen fibrils are mineralized with HAP nanocrystals [131, 149].

The role of collagen in bone mineralization has been controversial [149, 151, 152, 170]. The domains of collagen that initiate HAP nucleation are unclear. *In vitro*, collagen itself could be nucleated in SBF solution [153]. Because the initial mineralization site is located at the hole zone of type I collagen, the hole zone domain of type I collagen may participate in the process of mineralization [149, 171]. The overlap zone is also reported to be involved in the nucleation process of HAP in an asymmetric pattern. Except for these domains, the major portion of type I collagen is composed of repeating G-X-Y sequence which is proposed to provide the organizational framework and spatial constraint for crystal deposition. The exact role and mechanism of this repeating sequence is not very clear [151].

In this work, different domains from type I collagen including 8 GPP repeats, N-, C-terminals and N-, C-zone of type I collagen are displayed on the surface of different engineered flagella and investigated to elucidate which domains or portions can promote the nucleation of HAP. Surprisingly, our results show that among all the type I collagen-derived sequences displayed on flagella, GPP8 exhibited HAP nucleation ability. Even still, the ability of GPP8 to initiate HAP nucleation is much weaker than that of the E8 flagella. *In vivo*, the second proline of the GPP sequence is usually hydroxylated into 4-hydroxyprolyl residues. The hydroxyl group is also considered to be involved in HAP nucleation through the formation of hydrogen bond with HAP crystals [172]. Proline residues affect the calcium-binding activity of rotavirus VP7 outer capsid protein [173]. The conformation change of poly-prolines induced by calcium chloride indicate the interaction between proline and Ca^{2+} [174]. Most recently, Chung [175] et al identified a 12-residue peptide binding to (100) single-crystal HAP using PD. The peptide resembled the tri-peptide repeat sequences (Gly-Pro-Hyp) in type I collagen. Moreover, the synthesized peptide could mediate HAP nucleation *in vitro* which may be ascribed to the cooperative non-covalent interaction of the peptide with HAP. We may only surmise a similar mechanism on flagella with GPP8, but the exact mechanism is still not clear.

In our experiment, no crystals were nucleated on the surface of flagella with N-, C-terminal sequences, so the two regions may be eliminated from the biomineralization process. Although there are some polar amino acids in the N-, C- terminals, the specific conformation of protein or peptides may be very important for HAP nucleation according to previous research [152, 157]. The N-, C-zone sequences displayed on flagella also have some polar amino acids. Moreover, they are similar to the tri-peptide repeat sequences (G-X-Y) of type I collagen (Table 2. 1). Both polar amino acids [149] and collagen like sequences [175] may assist the nucleation of inorganic minerals.

Except for collagen, many kinds of non-collagenous macromolecular proteins participate in the control of HAP nucleation and growth of the mineral phase [176]. These proteins are morphologically, structurally, and functionally connected to the collagen fibers and may regulate the nucleation of HAP within collagen fibers either to promote or inhibit the formation of the initial crystalline structure [177]. OCN [138], OPN, osteonectin (ONN), BSP, phosphophoryn (DPP) and chondrocalcin (CC) [178] were examined at a wide range of concentrations. BSP and DPP exhibited nucleation activity at minimum concentrations of 0.3 $\mu\text{g/ml}$ and 10 $\mu\text{l/ml}$ respectively, but OCN, OPN, ONN and CC have no nucleation activity at concentrations up to 100 $\mu\text{g/ml}$. Moreover, BSP can bind to collagen to form a complex and this complex might serve as a nucleator to induce formation of HAP crystals [179].

BSP is highly glycosylated, tyrosine-sulfated and serine-phosphorylated sialoprotein which exclusively exists in mineralized tissues such as bone and teeth. Notably, there are two polyglutamic acid regions, which are located in the N-terminal of the molecule. They are predicted to form an α -helical structure which may provide an appropriate spacing of the γ -carboxylate groups for binding Ca^{2+} ions in the dimensions of the HAP crystals [160, 161, 172]. Through comparison between native and recombinant BSP without post-translational modification in a steady-state agarose gel system for HAP nucleating activity, recombinant BSP is less potent than native bone BSP, suggesting that some of the strong mineral-binding properties are determined directly by a specific sequence in the protein [159]. Moreover, the replacement of the single domain with either polyaspartic acid (poly[D]) or polyalanine (poly[A]) does not alter nucleating activity.

When both domains were replaced with poly[D] within recombinant BSP, no nucleating activity was found. Synthetic poly[D] did not show nucleating activity *in vitro*, in fact to inhibit HAP formation [176]. The possible reason is that synthetic poly[D] is more likely to form a random coil conformation. Synthetic poly[E] can form an α -helical conformation by itself *in vitro*, so it does not lose its nucleating activity [180] and a sequence of at least eight contiguous glutamic acid residues may be required for the nucleation of HAP [160].

After the flagella were engineered to display 8 glutamic acid residues on their surface, they showed a very strong ability to induce HAP nucleation. It is proposed that local ions are highly concentrated at the interface of flagella and HAP precursor solution. An initial accumulation or nucleation of the Ca^{2+} on the negatively charged $-\text{COO}^-$ surfaces results in the availability of nucleation sites through electrostatic potential interactions. This is followed by PO_4^{3-} incorporation at the nucleation sites [156, 159-161, 176]. As a result, the degree of supersaturation is increased at the interface between flagella and solution, leading to the site-specific nucleation of HAP on the flagella. The interaction of the negatively charged flagella surface with Ca^{2+} was confirmed by the self-assembly of flagella with E8 into bundles in a Ca^{2+} concentration dependent manner. Divalent metal ions or positively charged polymers can induce protein fibers to aggregate laterally and assemble into net-like paracrystals or side-by-side bundles [181]. Recently, we demonstrated the assembly of bacteriophage bundles was induced by a high concentration of Ca^{2+} [136]. However, high concentration of Ca^{2+} resulted in depolymerization of flagella fibers [166]. Fortunately, in our study, the lateral aggregation of E8 flagella was induced by a much lower concentration of Ca^{2+} (2 mM). In order to induce the self-assembly of flagella bundles, the optimized concentration of Ca^{2+} is about 4 mM. The bundle-like aggregation of the E8 flagella within 4 mM supersaturated HAP precursor solution may be based on similar mechanism. The negatively charged flagella may prefer adsorbing Ca^{2+} , which induced the self-assembly of flagella. However, due to the effects of negatively charged PO_4^{3-} in the precursor solution, the bundles become smaller and are not parallel to each other.

After the bundled flagella by Ca^{2+} biomineralized in HAP precursor solution, interestingly, the *c*-axes of the HAP crystals oriented along the long axes of flagella bundles. It is consistent with previous research using other fiber bundles [136, 158]. This structure is similar to that of HAP crystals in bone in which HAP nanocrystals are also preferentially parallel with their *c*-axis to the long axes of the collagen fibrils [147]. The crystallographic orientation of HAP can be controlled by the aligned carboxyl groups generated by the arachidic acid monolayers [172]. The glutamic acids displayed on the surface of flagella is also very organized and aligned on the surface of flagella which may result in oriented nucleation and growth of HAP. The other possible mechanism is that HAP may nucleate within and grow along the channels between two neighboring flagella fibers in the bundles [142].

The design of individual small molecules with the specific properties of natural biomaterials using a “bottom-up” approach is a novel strategy in bionanotechnology [182]. By combining nature’s biological materials with synthetic macromolecules and inorganics at a nanoscale, hybrid molecular biomimetics is emerging as a promising methodology. Biologically derived materials usually have unique functional properties at the nanometer level [183]. On the other hand, biomaterials can form highly organized patterns from molecular to the nano-, micro- and macro- scale. The bacterial flagellum with tubular structure is formed by *FliC* monomers self-assembly. With the help of Ca^{2+} , flagella can be assembled into higher ordered bundles.

Bacterial surface display technology is typically applied in basic microbiology, molecular biology, vaccinology and biotechnology [138]. Recently, bioengineered flagella as template for synthesis of metal nanoparticles and nanotubes have been reported [139]. In this study, bioengineered flagella can be assembled into bundles with orientated nucleation of HAP nanocrystals along their long axes by biomimetic nucleation (Figure 2. 14). The biomineralized flagella bundles may serve as building blocks for further assembly into a scaffold for bone tissue engineering. There also have some other merits to using bioengineered flagella as building blocks: 1) The bacterial flagella can be disassembled into monomers at pH 2 and reassembled into integrated flagella at pH 7 which are similar to the designed amphiphile fibers [158]; 2) the bacterial flagella can

form an organized 2D or 3D structure at a very high concentration by liquid crystal formation [123] or by the display of cysteine residues on the surface of flagella to generate stable bundles [184].

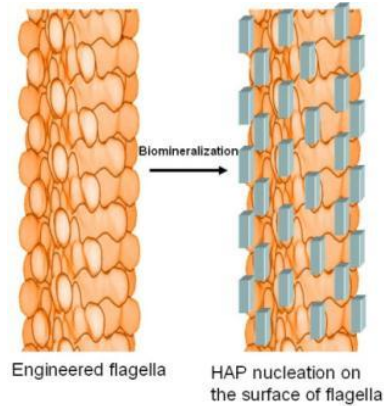


Figure 2.14: Oriented nucleation of HAP on the surface of flagella.

In conclusion, different portions of type I collagen and functional domains of non-collagen protein were successfully displayed on the surface of flagella without losing the motile function. HAP nanocrystals can be nucleated on the surface of engineered flagella with E8 or GPP8 sequences. Oriented nucleation of HAP polycrystalline were observed on E8 flagella after assembling into bundles. The preferred orientation resembles HAP crystals in bone. The mineralized bioengineered flagella mimic some aspects of the lowest levels of ECM organization in natural bone.

Chapter 3 Biomimetic Mineralization of Engineered Flagella Combined with Spontaneous Self-Assembly

3. 1 Introduction

Although a wide range materials designed to substitute natural bone have been developed over the last several decades, many of them differ, at times drastically, from natural bone tissue in aspects such as composition and structure. Due to their biocompatible and biodegradable properties, synthetic polymers such as polyfumarates, polylactic acid (PLA), polyglycolic acid (PGA), copolymers of PLA and PGA (PLGA), and polycaprolactone have been used in a variety of methods for bone tissue engineering [185]. These synthetic polymers are also of interest due to their ability to be assembled into two or three-dimensional (2D or 3D) scaffolds. The main approaches include layer-by-layer fabrication, electrospinning, hydrogel and sol-gel process. There are also many naturally occurring biomaterials derived mainly from proteins such as collagen, gelatin, albumin and polysaccharides that have been used as bone substitute scaffold [185, 186]. Nevertheless, most of above scaffolds just randomly pack together into network matrix not like the oriented collagen fibrils in bone. Manipulation of these molecules to simulate the same degree of bone organization at 2D or 3D, however, has remained a challenge.

Natural bone is a nanocomposite material of organic collagen nanofibers in intimate contact with inorganic HAP nanocrystals [147]. In order to discover a material that emulates the unique mechanical properties of bone, various combinations of HAP with synthetic and natural materials have been extensively investigated. Among the methods currently employed, the biomimetic “bottom-up” approach especially with nanoscale features has gained much attention due to its ability to mimic the organization and/or structures of natural bone [187]. Biomimetic nanocomposites are perceived to be superior in many aspects such as large surface area-to-volume ratio and excellent mechanical strength. Moreover, they can be synthesized under mild physiological conditions in aqueous environments at low temperature and still achieve hierarchical organization with complex morphology and controlled size. A current trend in novel bone materials design and fabrication is to take advantage of molecules that possess the ability to self-assemble into the higher ordered structures. A variety of collagen-like peptides, self-assembled

peptide or peptide amphiphile based systems are used as building-blocks to direct hierarchical structures in a highly controlled fashion [158, 188-192]. In addition to self-assembly, some of the molecules also contain other specific functions. For example, the RGD domain displayed on peptide amphiphile promotes preosteoblastic cells adhesion [193]. The phosphoserine residue can mediate HAP nucleation [158]. Recently, naturally occurring fibers such as silk, spider silk, phage and virus which all self-assembled from monomers in an ordered fashion were investigated as potential materials for bone tissue engineering [137, 194-196]. We also demonstrated that the bioengineered flagella with eight continuous GPP or glutamic acid peptides can induce the formation of HAP nanocrystals on their surfaces.

In this chapter, the spontaneous assembly of bioengineered bacterial flagella containing a collagen-like peptide in a very organized fashion was demonstrated. Bacterial flagellum, the appendage that enables bacteria to swim in aqueous environments, is a helical nanotube that is self-assembled from *FliC*s and some other proteins. Flagellum has an outer diameter of about 12–25 nm, an inner diameter of 2 nm, and a length of up to 10-15 μm . *FliC* proteins have highly conserved N- and C- terminal regions and a central region that has a highly variable amino acid sequence. The *FliC* proteins self-assemble to form flagellum, a helical fiber that contains 11 subunits per 2 turns. *FliC* is a globular protein in which the N- and C- terminal regions, termed D0 and D1, bind together by non-covalent interactions and face the center of the flagellum helix. The solvent-exposed, center region of *FliC*, termed the D2 and D3 domains, can be modified by the insertion or deletion of peptide sequences without losing the self-assembly properties. In this study, we introduced a type I collagen-like sequence (Gly-Pro-Pro)₈ (Named GPP8) to the dispensable region (D2 and D3) of flagella. After being mixed with supersaturated HAP precursor solution, the bioengineered flagella with GPP8 can nucleate HAP nanocrystalline on their surface and spontaneously self-assemble into an ordered monolayer structure which resembles the organization of natural bone. Meanwhile, this scaffold can support BMSCs growth, proliferation and differentiation.

3. 2 Materials and methods

3. 2. 1 Flagella display and purification:

Genetic display of a foreign peptide on flagella has been described elsewhere [142]. Briefly, the original vector pLS411, which contains the gene for *FliC* with a multicloning site that includes restriction enzymes of *Xho* I and *Bgl* II located in the hypervariable region of *FliC* was digested (New England Biolabs) at 37 °C for 2 h. Then, the 72 bp nucleotide sequence encoding 8 repeated GPP units was synthesized (Invitrogen) with restriction sites, *Xho* I and *Bgl* II, at the ends. The synthesized oligonucleotides were inserted in the linearized vector pLS411 by T4 ligase and transformed into competent cells of *FliC* deficient *Salmonella* SL5928. Strain SL5928 is an *aroA* live-vaccine strain of *Salmonella* Dublin. Because its only *FliC* gene- *FliC*(g,p) has been replaced via transduction by *FliC*(i)::Tn10, an allele inactivated by transposon insertion, the functional flagella cannot be expressed. Finally, the ampicillin-resistant clones with recombinant plasmid were selected and confirmed by sequencing. Because only the bacteria with functional flagella can swim in the semisolid medium, the clones were cultured in semisolid medium (1 % tryptone; 1.5 % NaCl; 0.35 % agar) for cell motility test to confirm assembly of recombinant flagella.

The bioengineered bacterial flagella were detached from the bacterial cells by vigorous shaking through vortex at highest speed 3 times (30 sec/each time). The supernatant containing the sheared flagella was separated by centrifugation at 12,000 g for 20 min. The flagella were precipitated at 100,000 g for 2 h and dissolved in ddH₂O.

3. 2. 2 Flagella nucleation:

Supersaturated HAP solution (4 mM) was prepared as described [13] from HAP power (Sigma). 20 µl of flagella was mixed with different volumes of supersaturated HAP solution and incubated for various periods of time at room temperature. After 6 days, a drop of aqueous solution was mounted on the carbon TEM grid. After being carefully rinsed with double distilled water and dried at room temperature, these grids were subjected to TEM (Zeiss 10) measurements operated at 80 kV.

3. 2. 3 Coating of flagella, type I collagen and polylysine on cell culture plate:

Coating of flagella on cell culture plate was prepared according our recent report [194]. Sterile-filtered polylysine solution (0.01 %) (Sigma-Aldrich) aliquots to the 24 or 96 well cell culture plate (350 μ l/well for 24 well and 100 μ l/well for 96 well) for 30 min, allowing for the adsorption of the first cationic polyelectrolyte layer to the substrate. The polylysine was then removed and the plates were dried under a pressurized air stream. Flagella in water or supersaturate HAP solution was added into each well and was incubated at room temperature for 20 min. Flagella were removed and the plates were dried under a pressurized air stream. The previous steps were repeated three times and the final layer was coated with flagella. Type I collagen solution form rat tail (Sigma-Aldrich) was diluted with 20 mM acetic acid was coated on cell culture plate. One layer of polylysine coated coverslips was used as control.

3. 2. 4 BMSCs isolation and culture:

Primary BMSCs were isolated from the bone marrow from the femur of young adult female Fisher 334 rats (Harlan) based on previously described method [33]. Briefly, the isolated bone marrow cells were washed several times with Dulbecco's Modified Eagle Medium (DMEM; GIBCO BRL, Grand Island, NY, USA). After cell viability tested and the density of the cells confirmed using trypan blue staining, cells were maintained in DMEM (low glucose) supplemented with 10 % fetal bovine serum (FBS) (Invitrogen), penicillin G 100 U/mL, streptomycin 100 μ g/mL, and amphotericin B 0.25 μ g/mL. The cells were incubated in humidified atmosphere containing 5 % CO₂ at 37 °C. The non-adherent cells were removed after three days by changing the culture media. The BMSCs passage was performed no more than three times after isolation and before use.

3. 2. 5 Proliferation assay by Methylthiazoletetrazolium (MTT) test:

BMSCs were plated at a density of 4×10^3 cells/well in 96-well plates in DMEM for 72 h. 3-(4, 5-dimethyl thiazol-2-yl)-2, 5-diphenyl tetrazolium bromide (MTT) (5mg/ml, 20 μ l/well, Sigma-Aldrich) was added to the cell cultures and incubated for 4 h at 37 °C. All of the solution was then dumped and dimethyl sulfoxide (DMSO) (150 μ l/well, Sigma-Aldrich) was added to each well and agitated for 30 seconds to dissolve the crystals. The

absorbance was measured at 490 nm using a Biotek spectrophotometric microplate reader.

3. 2. 6 Scanning Electron Microscopy (SEM) examination:

BMSCs were seeded on flagella or collagen at a density of 1×10^4 cells/ml in a 24-well culture plate with a pre-cleaned cover-slip in each well. After being cultured for 24 h, the cells were washed with PBS and fixed with 2.5 % glutaraldehyde in $0.1 \times$ PBS for 1 h. The cells were washed again with PBS and then dehydrated in a graded series of ethanol (50 %, 70 %, 90 %, and 100 %) for 30 min each. The samples were further dehydrated by a supercritical point CO₂ dryer. The morphology of BMSCs was observed using SEM (XL30, FEI Corporation). Cell surface area was calculated by the computer-assisted planimetry from at least forty five cells per sample in the SEM micrographs using the automated measure function of Image J (downloaded from the National Institute of Health, Bethesda, MD, USA, free download available at <http://rsb.info.nih.gov/ij/>).

3. 2. 7 Immunofluorescence examination:

The cells were cultured in a 24-well plate with a round pre-cleaned cover-slip in each well and terminated at 7 and 14 days in osteogenic media. The cells were washed 2 times by PBS and fixed using 70 % ethanol in PBS for 30 min at room temperature. After being washed by PBST buffer ($1 \times$ PBS containing 0.05 % Tween-20), the samples were then introduced the permeability for 5min (0.1 % Triton X-100 in $1 \times$ PBS solution). Afterwards, the samples were blocked in 5 % BSA (Sigma-Aldrich) for 1 h at room temperature. The primary anti-OPN antibody (1: 500, Abcam Biotechnology) and anti-OCN antibody (1: 1000, Santa Cruz Biotechnology) diluted in 5 % BSA were incubated with cells overnight at 4 °C. After being washed 3 times for 5 min by $1 \times$ PBST, secondary antibodies of Goat anti-rabbit IgG-TRITC (1: 500, Santa Cruz Biotechnology) at 1:100 dilutions in blocking buffer were then incubated for 1 h at room temperature. Filamentous actin was stained with FITC-conjugated phalloidin (1: 40, Invitrogen) in PBS and nuclei were stained with DAPI (1: 1000, Chemicon). The coverslips with samples were then inverted onto glass slides, mounted and the images were collected by a fluorescence microscope (N-storm, Nikon Microsystems).

3. 3 Result and Discussion

Nature provides us tremendous materials with delicate structures and spectacular properties. Amazingly, most natural materials are only assembled by simple molecules from nano-, micro- to macro-dimensions with hierarchical structures. A current trend in materials design and production is to take advantage of natural materials with hybridized functions and biocompatibility. Meanwhile, most of biomaterials can be harvested in large amount with ease. Fabrication of bone substitute materials that mimic the structure, composition and biological features of natural bone tissue is very attractive research field. There are several key characteristics that are very important for biomimicking bone materials. First, it is vital that the materials possess intimate interaction with nanoscale calcium phosphate minerals or can accumulate and nucleate calcium phosphate from precursor solution. Second, the materials should be able to self-assemble spontaneously into organized, especially hierarchical, structures, which are similar to the organization of natural bone. Generally, materials that exhibit organized arrangement at the nanoscale have better mechanical properties [197]. Third, the materials must have good biocompatibility and can support cell attachment and growth.

In this study, bioengineered flagella are utilized as the basic building blocks of bone materials. Recently, we have confirmed that after the flagella were modified to display eight continuous GPP peptides, the flagella was able to nucleate calcium phosphate nanocrystals on their surfaces after being soaked in supersaturated HAP solution. Interestingly, the flagella formed parallel bundles in HAP precursor solution in a concentration dependent manner. Higher concentrations of flagella induced more bundle formation (Figure 3. 1). The initial concentration of flagella was 800 $\mu\text{g/ml}$ (10 μl) and mixed with different volumes of HAP precursor solution (1000, 800, 600, 400, 200 and 100 μl). After being incubated at room temperature for 6 days, the flagella were observed by TEM. At the lowest concentration of flagella, only monodisperse flagella were observed. A layer of inorganic minerals nucleated on the surfaces of flagella surface (Figure 3. 1A). As the concentration of the flagella was increased, flagella started to aggregate and the minerals nucleated between neighboring flagella forming more and more bundled flagella with parallel structures(Figure 3. 1B, C, D, E). At the highest flagella concentration, almost all flagella aggregated into parallel bundles (Figure 3. 1F)

with characteristic curly morphology of flagella. The bundled flagella at different magnifications are shown in Figure 3. 2. Most flagella bundles were covered by a layer of mineral which enhanced the contrast under TEM (Figure 3. 2A). SAED analysis verified that the mineral was composed of HAP by the presence of 211, 002 and 004 plane (Figure 3. 2A insert). The diameter of flagella is about 15 nm. After carefully measuring distance between neighboring flagella, the channels between flagella filled by calcium phosphate are 25 ± 10 nm in diameter. Figures 3. 2B, C and D exhibit the magnification of the mineralized flagella bundles. In order to identify the correlations between the HAP crystal orientation and the long axis of the flagella, the SAED pattern was analyzed at the relative straight bundle part of flagella. It indicated the ring-shaped diffraction ascribed to the 211 plane and two pairs of arc-shaped diffraction corresponding to the 002 and 004 planes. This data demonstrated the crystallographic *c*-axes of HAP are parallel to the long axes of the flagella.

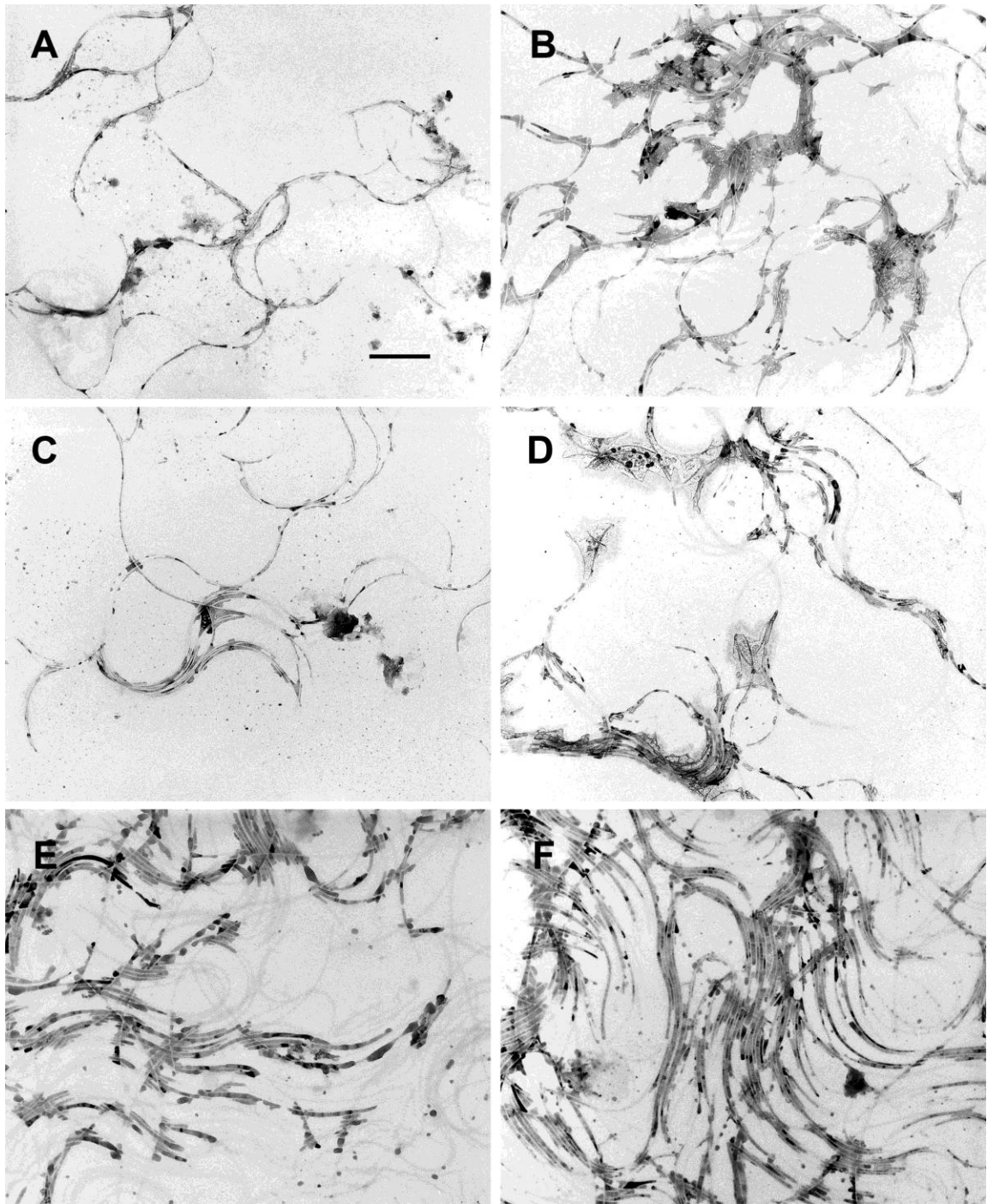


Figure 3.1: TEM micrographs of flagella in 4mM supersaturated HAP precursor solution. Flagella mixed with different ratio of HAP precursor solution: A) 1:100; B) 1:80; C) 1:60 D) 1:40 E) 1:20; F) 1:10 (Scale bar is 400 nm).

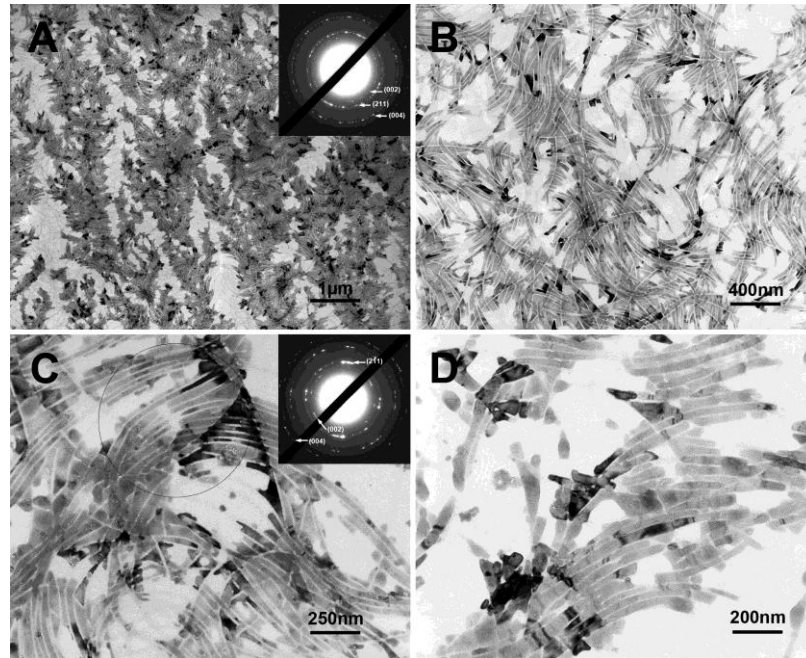


Figure 3.2: TEM micrographs of different magnification of flagella bundles formed in HAP precursor solution. A) SAED pattern show (002) and (211) plane corresponding to HAP crystals (Insert). C) Inset is the SAED patterns taken from the highlighted section. Two pairs of arc-shaped diffraction corresponding to the 002 and 004 planes of HAP indicate the crystallographic c -axes of HAP are parallel to the long axes of the flagella.

In a control experiment, neither nucleation of HAP on flagella nor ordered assembly was observed after wild type flagella mixed with 4 mM supersaturated HAP solution (data not shown). This illustrated that the displayed GPP8 sequences play an important role in the nucleation of HAP crystalline and side-by-side alignment. Type I collagen consists of two identical $\alpha 1(I)$ chains and one $\alpha 2(I)$ chains. Each of the three chains has a left-handed helix which all intertwines in a right-handed fashion to form a triple-helix. A distinctive feature of type I collagen in the triple helical region is the repeated amino acid sequence (Gly-X-Y), in which X and Y can be any amino acid but are often either proline (Pro) or hydroxyproline (Hyp), respectively. Hyp is involved in the formation and stabilization of the triple helix and, at the same time, helps the self-assembly of fibril formation [198]. The pure helical region without the non-helical ends can still self-assemble into the triple helical structure [199]. This indicates that there is a specific interaction between the Gly-X-Y sequences. A variety of strategies have been developed using short, synthetic

collagen-like proteins or triple-helical peptides to investigate collagen's structure and how it assembles [200-205]. Previous studies demonstrated that (Pro-Pro-Gly)₁₀ and (Pro-Pro-Gly)₂₀ can assemble into collagen-like triple-helical structures in aqueous solution with appropriate salt concentrations [206-208]. These sequences can also form larger micro-crystalline segments, which are lateral aggregations of fibers in parallel or anti-parallel fashion at about 4 °C [206]. Crystal structure analysis of the collagen-like peptide revealed that the triple helix structure is stabilized by interchain hydrogen bonds between C=O and N-H groups [209]. Type I collagen also spontaneously self-assembles into fibrils with a characteristic binding pattern which is considered to be an entropy-driven process through inter-molecular hydrogen bonds [210]. Electrostatic and hydrophobic interactions are also involved in the self-assembly [211-214]. Meanwhile, hydroxyproline might contribute the correct fibril formation [198]. In our results, apparently, the distances between neighboring flagella is much larger than distance of the hydrogen bonds inside the triple-helix of collagen or inter collagen molecules in each fibril. TEM micrographs also revealed that the purified bioengineered flagella do not self-assemble into fibrils spontaneously even at a very high flagella concentration (1000 µg/ml) in water (data not shown). This indicates that the HAP precursor solution plays an important role in the organized self-assembly of bioengineered flagella.

The HAP precursor solution is mainly composed of Ca²⁺ and PO₄³⁻. In order to determine which ions promote the self-assembly of flagella, different concentrations of CaCl₂ were mixed with flagella (Figure 3. 3). At low CaCl₂ concentration (1 mM), some lateral aggregation of flagella was observed (Figure 3. 3A). With increased CaCl₂ concentration (2 mM and 3 mM), more bundles could be observed and flagella became more compacted (Figure 3. 3B, C). At 4 mM of CaCl₂, ribbon-like structures appeared due to parallel aggregation between neighboring flagella and the flagella became "straight". At the same time, some of flagella broke into much short fragments (Figure 3. 3D). More flagella depolymerized with increase of CaCl₂ concentration but "compact" flagella bundles formed (Figure 3. 3E, F). Functioning as a "salting-inner", high concentration of Ca²⁺ (0.5 M) resulted in the entire depolymerization of flagella [166]. When the concentration of CaCl₂ was reached to 10 mM, all flagella have depolymerized into short fragments. Surprisingly, some thick and more compact bundles were still

observed (Figure 3. 3G). Some linear structures with a diameter similar to the flagella fragments can be identified on the bundles. We believe these big bundles reassembled from the small flagella fragments or the flagella monomers-*FliCs*. More TEM micrographs of partially depolymerized flagella fragments and thicker ribbon-like bundles of flagella are shown in Figure 3. 4A and B. After increasing the concentration of CaCl_2 to 20 mM, only thick and compact bundles were observed and all flagella fragments disappeared. The fragments may be totally depolymerized or reassembled into bundles (Figure 3. 3H). More TEM micrographs of bundles were shown in Figure 3. 4C and D. The bundles exhibited some linear structures with curly morphology but no structures like the flagella fragments were observed. The bundle formation of flagella with increase of CaCl_2 concentration was also confirmed by a turbidity study at 320 nm (Figure 3.5). Two different concentrations of flagella (65 and 130 $\mu\text{g/ml}$) have been studied. At both concentrations of flagella, initially, the turbidity increased depending on the concentration of CaCl_2 . However, the turbidity started to decrease at high concentration of CaCl_2 which may be induced by depolymerization of flagella. Divalent metal ions or positively charged polymers can induce protein fibers to assemble into bundles by lateral aggregation [181, 215, 216]. Biological fibers such as phage and pili can also be assembled into bundles by Ca^{2+} or positively charged polymers [136, 217]. The lateral packing of phage nanofibers in CaCl_2 solution was proposed by the electrostatic interaction of Ca^{2+} to the negatively charged phage [136]. The lateral side-by-side assembly of flagella induced by CaCl_2 might partially depend on a similar mechanism due to the large surface exposed domains (D2 and D3 from 405 aa-454 aa in the wild type of flagella) [56].

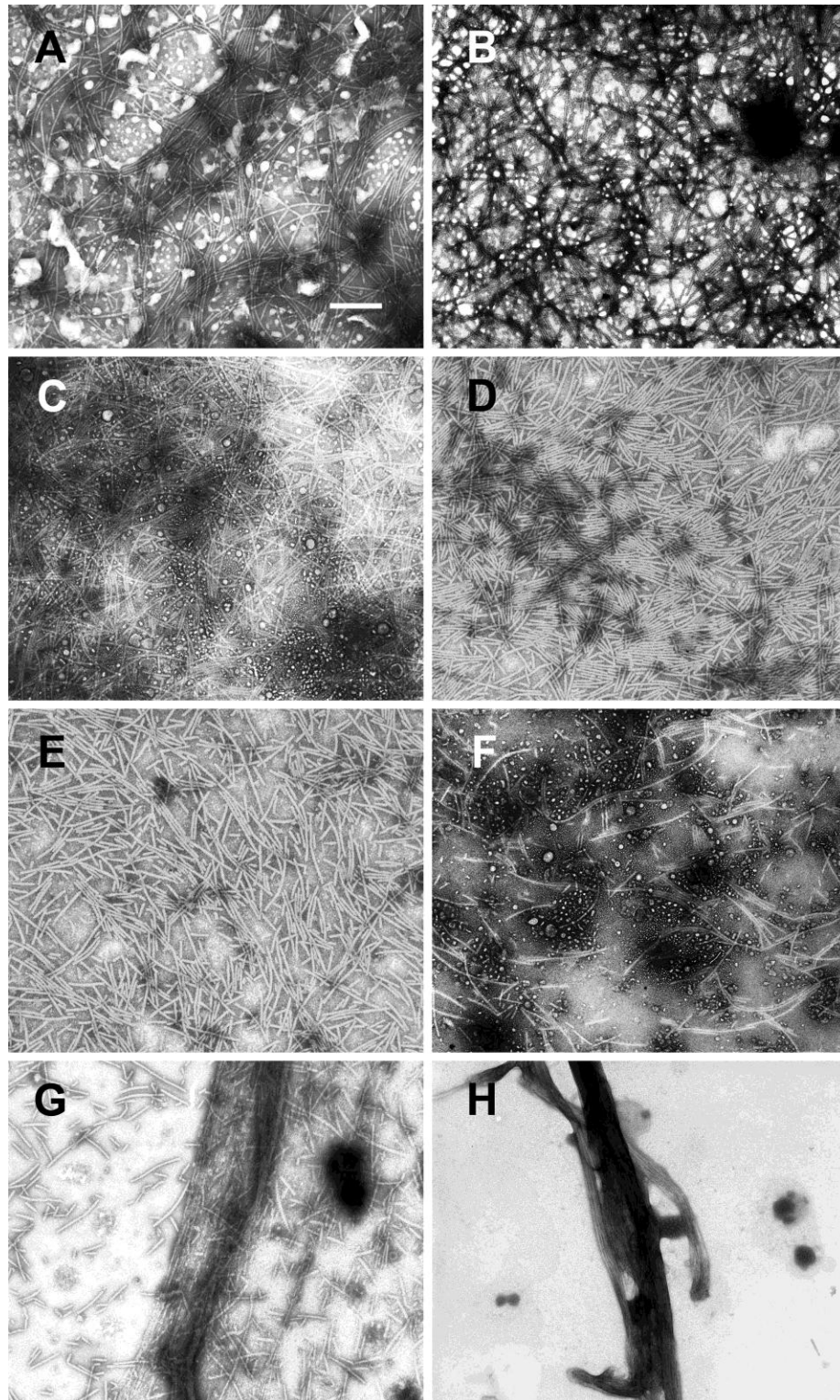


Figure 3.3: TEM micrographs of bioengineered flagella under different concentration of CaCl_2 . Concentration of CaCl_2 : A) 1 mM; B) 2 mM; C) 3 mM; D) 4 mM; E) 6 mM; F) 8 mM; G) 10 mM; H) 20 mM (Scale bar is 400 nm)

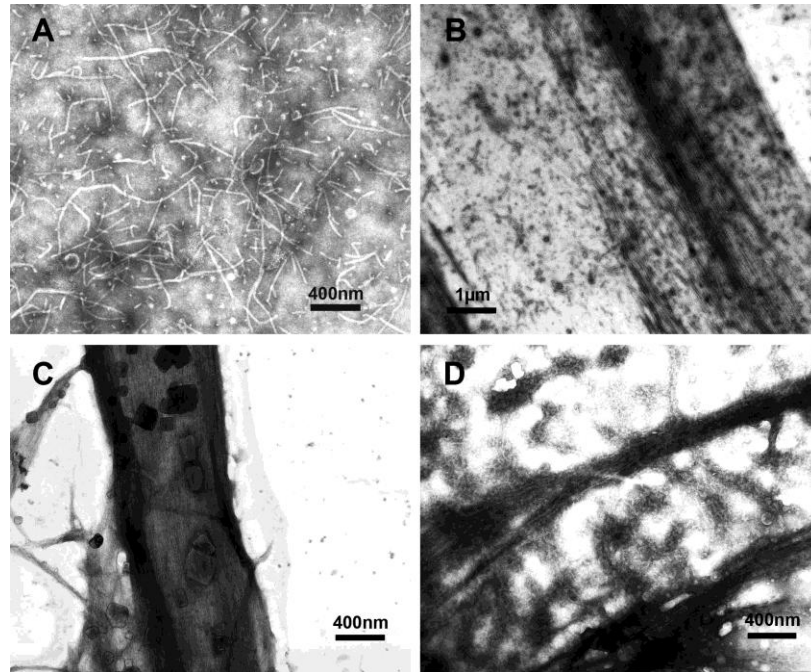


Figure 3.4: TEM images of flagella at different concentrations of CaCl_2 ; A) Flagella depolymerized into short fragments at 10 mM CaCl_2 ; B) Ribbon-like bundle of flagella under 10 mM CaCl_2 ; C) and D) bundles formed by flagella fragments or *FliCs* under 20 mM CaCl_2 .

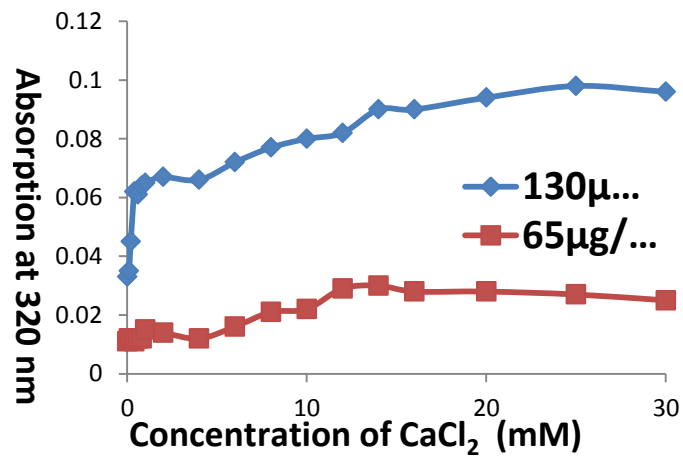


Figure 3.5: Turbidity measurement of different concentration of CaCl_2 with flagella (65 and 130 $\mu\text{g/ml}$) at 320 nm [218].

Previous research demonstrated that Ca^{2+} promotes fibril formation of type I collagen *in vitro*. Ca^{2+} may bind to carbonyl groups of acidic amino acids by ionic interaction in

collagen [219]. Urry first proposed neutral sites for Ca^{2+} binding sites in elastin and collagen [220]. Zhang et al revealed that Ca^{2+} chelate with carbonyl oxygen on collagen molecules by FTIR spectrum leading to a red shift of the amide I band [168]. CD spectra and turbidity measurements in situ have suggested the interaction between Ca^{2+} and collagen molecules induce the conformation change of collagen during the initial stage of biomineralization [221]. Molecular modeling and theoretical study of the collagen like peptide-PPG also revealed that cations bind to carbonyl groups and the final position of calcium ions was similar to that in HAP crystal [222, 223]. We believe the interaction between displayed GPP8 on flagella and Ca^{2+} based on the similar mechanism. During the early stages of biomineralization in supersaturated HAP solution, the calcium ions first chelate with carbonyl groups located on GPP8 sequence. This is followed by phosphate neutralization, which results in the formation of calcium phosphate. Based on the above experimental data and previous research, the side by side aggregation and ordered alignment of bioengineered flagella in supersaturated HAP solution during biomineralization has been proposed (Figure 3. 6). The bundle formation induced by Ca^{2+} is shown in Figure 3. 6A. Calcium ions chelate with carbonyl groups on one flagellum and neighboring flagellum which promote the side-by-side aggregation. At the same time, water molecule mediated hydrogen bonds may also help the ordered alignment of collagen [210]. The same bonds might also form between displayed GPP peptide. In supersaturated HAP solution, after Ca^{2+} coordinated with flagella, phosphate will be electrostatically attracted to the flagella surface resulting in supersaturation at the interface and formation of calcium phosphate nuclei. Subsequently, more ions will accumulate on the nuclei and calcium phosphate will grow preferentially along the flagella surface and in the channels between neighboring flagella in the bundles. With more calcium phosphate formation, more minerals filled the channels of neighboring flagella and the distance between neighboring flagella was broadened (Figure 3. 6B). Our previous study on bioengineered flagella with 8 glutamic acids also formed bundles induced by CaCl_2 . After being soaked in supersaturated HAP solution, the bundles of flagella became “loose” and the HAP nanocrystals nucleate between neighboring flagella in the bundles. The oriented nucleation and growth of HAP along flagella surface with GPP may be similar to the nucleation of HAP on collagen surface.

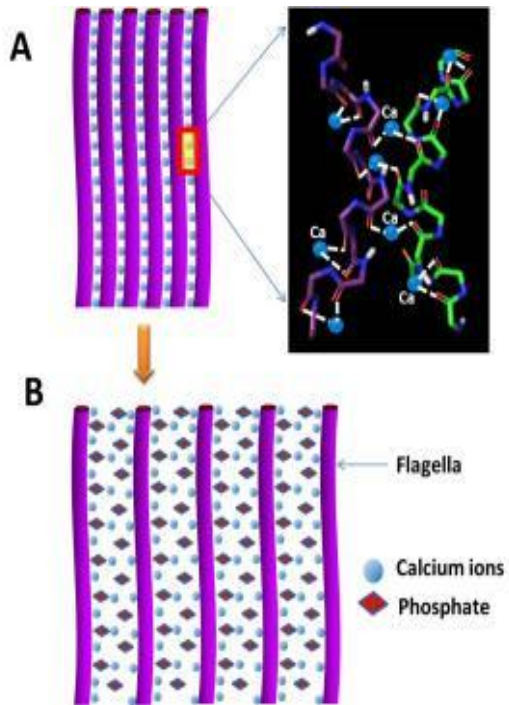


Figure 3.6: Schematic illustration of bundle formation of flagella was induced by Ca^{2+} (A) and calcium phosphate formation in supersaturated HAP precursor solution (B).

Bone marrow derived stem cells (BMSCs) can sense the topographies, surface chemistry and microenvironment during proliferation and differentiation [195, 224-226]. *In vivo*, since the cells locate and directly interact with the nanoscale extra-cellular matrix in bone tissue, the nano-leveled materials with biomimetic features often exhibit an excellent physiochemical environment that promotes cell adhesion, proliferation and differentiation [227, 228]. Naturally occurring biomaterials such as phage, virus, silk, spider silk also present good cytocompatibility to which the cells can adhere and on which cells can grow [194-196]. Meanwhile, the signaling motifs displayed on the surface of materials can direct cell behavior in a controlled manner. Here, the BMSCs behavior on bacterial flagella scaffold was first reported.

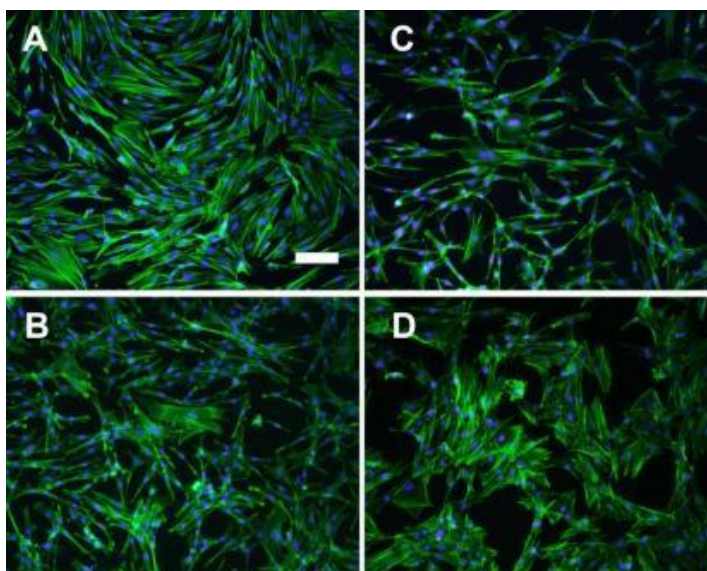


Figure 3.7: Immunofluorescence images of BMSCs on different materials substrate after 24 h culture. A) BMSCs on type I collagen; B) BMSCs on polylysine; C) BMSCs on flagella; D) BMSCs on plastic cell culture plate (Scale bar is 100 μm). In all images, cell nuclei are stained by DAPI (blue) and F-actin is stained by FITC-labeled phalloidin (green).

LBL assembly of nanobiomaterials has been shown to be an effective approach to generate nanometer-scale films in our previous research [194]. Here, the biomineralized flagella with GPP8 were coated on polylysine functionalized substrate. After this was repeated three times, the final layer was coated with the GPP8-modified flagella. The initial interactions between cells and substrate decide cell behavior. 24 h after the BMSCs were seeded on flagella surface, the morphology of BMSCs was characterized by bright field and fluorescence microscopy (Figure 3. 7 and 3. 8). Cells spread on flagella surface but not as good as on other substrates such as on type I collagen and polylysine. Type I collagen exhibited high affinity to BMSCs. Most BMSCs presented spindle-like morphology and some of the cells are parallel to each other (Figure 3. 7A and 3. 8A). Polylysine also promotes the cell attachment and adhesion and BMSCs exhibited a well-spread morphology (Figure 3. 7B and 3. 8B). BMSCs were less spread on flagella coated substrate and exhibited a range of morphologies from spindle to polygonal morphology (Figure 3. 7C and 3. 8C). Sometimes, the curly BMSCs were observed (Figure 3. 9). Most BMSCs show polygonal morphology and are well-spread on plastic cell culture

plate (Figure 3. 7D and 3. 8D). SEM micrographs of BMSCs on collagen and flagella also revealed similar morphology to the ones under light microscopy (Figure 3. 10A and C). BMSCs anchored on the substrates by filopodia-like extensions. The collagen or flagella coated substrates were observed at higher magnification. Collagen coated substrate exhibited curly ribbon-like structures which should be formed by collagen fibrils (Figure 3. 10B). Flagella coated substrate show very rough surfaces due to the biomineralized flagella surface coated by calcium phosphate minerals (Figure 3. 10D). Combining TEM and SEM results of different materials coated substrates, it can be concluded that the morphology of BMSCs on collagen and flagella is induced by the contact guidance response [229]. Surface spreading area of BMSCs measurements confirmed that the bioengineered flagella spread significantly less than did the control ($P < 0.05$). The surface area of BMSCs on collagen and polylysine is less than on the control but there is no significant difference (Figure 3. 11A). The proliferation of BMSCs on different substrates was also studied after 3 days culture (Figure 3. 11B). The growth rate of the BMSCs on the flagella scaffold was much lower than that of ones on other substrates ($P < 0.05$). Type I collagen and polylysine promote cell proliferation but no significant difference was observed when compared to the control. The above results demonstrate that cells can attach and growth on the topographies generated by biomineralized flagella. However, it is not as good as collagen or polylysine coated substrates. The flagella may not very favorable for cell adhesion and proliferation but they still are viable.

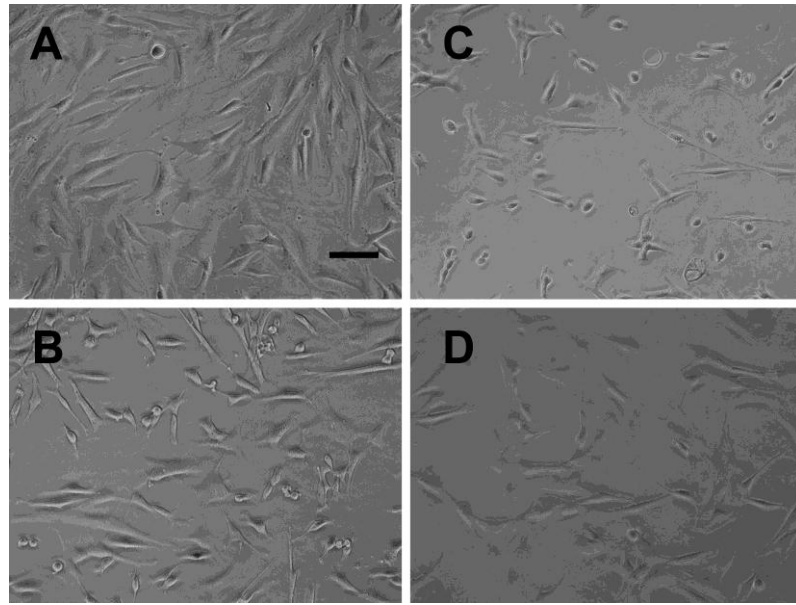


Figure 3.8: Bright field microscopy of BMSCs on different materials scaffold and control after 24 h. A) BMSCs on type I collagen; B) BMSCs on polylysine; C) BMSCs on flagella; D) BMSCs on plastic cell culture plate. Scale bar is 100 μm .

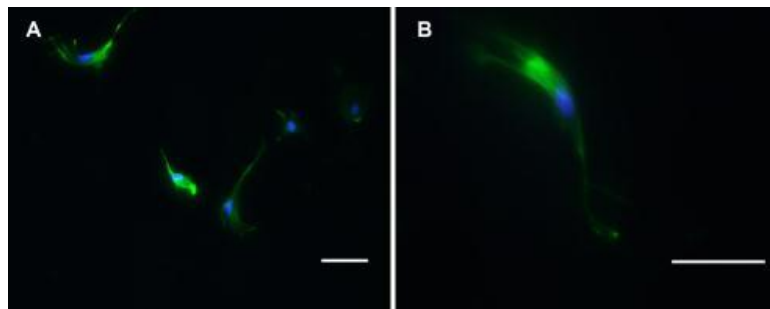


Figure 3.9: Immunofluorescence images of BMSCs on flagella scaffold after 24 h culture. In some areas, curly morphology of BMSCs was observed. The BMSCs may attach the curly portion of flagella bundles and induced by the contact guidance response. (Scale bar is 100 μm). In all images, cell nuclei are stained by DAPI (blue) and F-actin is stained by FITC-labeled phalloidin (green).

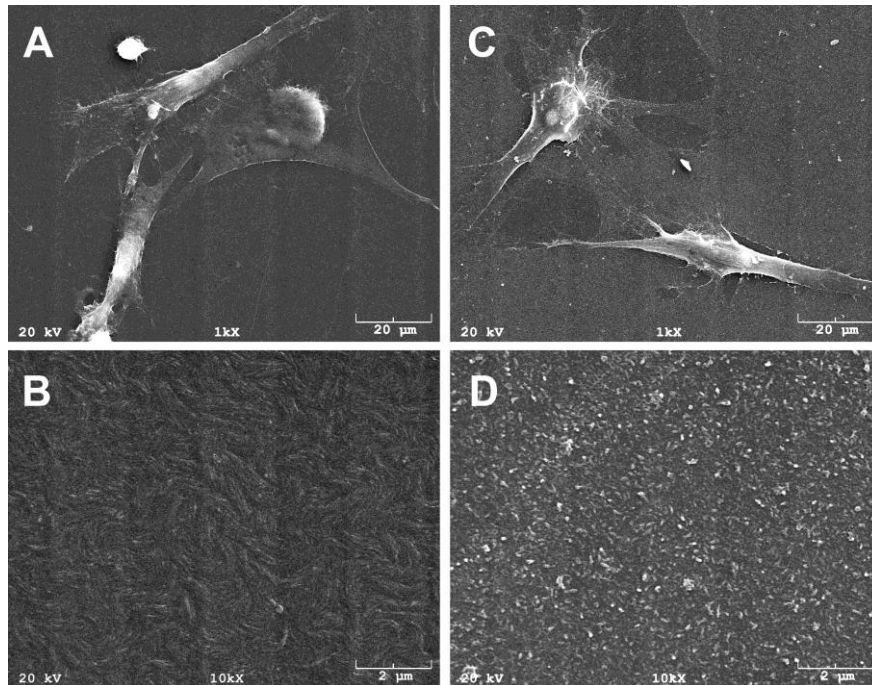


Figure 3.10: SEM micrographs of BMSCs on collagen and flagella coated substrate. A) BMSCs on collagen coated substrate; B) SEM micrograph of collagen coated substrate; C) BMSCs on biomineralized flagella coated substrate; D) SEM micrograph of biomineralized flagella coated substrate.

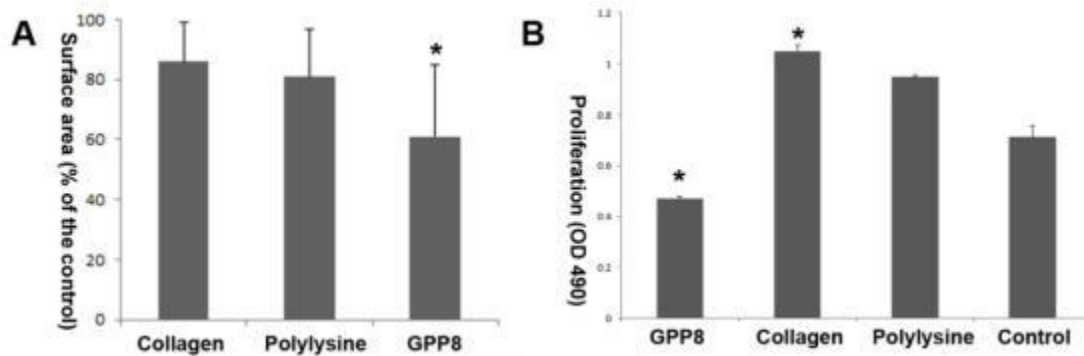


Figure 3.11: Surface spreading area and proliferation study of BMSCs on different materials coated substrate. A) Surface area of BMSCs relative to control. Cells are less-spread on flagella coated substrate (compared with control group, *P<0.05); B) BMSCs proliferation on different materials coated substrate. Collagen and polylysine promote the cells proliferation (compared with control group, *P<0.05). However, flagella inhibit BMSCs growth compared to control (*P<0.05).

BMSCs differentiation toward osteoblast was marked by osteogenic gene expression. The extent of BMSCs differentiation on biomineralized flagella was examined by osteogenic markers-OPN and OCN by immunofluorescence. Cell cultures were terminated at 7 and 14 days and OPN and OCN gene expression were characterized in BMSCs in order to detect early differentiation toward osteoblasts. As shown in Figure 3. 12, under osteogenic media, BMSCs can express both of OPN and OCN. After 7 days, a higher level of OPN and OCN expression was detected in BMSCs on flagella than on the other substrates. Polylysine also promoted the early differentiation of BMSCs which is consistent with recent report [230]. After 14 days, the osteogenic gene expression of BMSCs on type I collagen increased greatly. Recently, Tsai et al reported that type I collagen promotes osteogenesis by ERK and Akt pathways [231]. BMSCs on flagella and polylysine still had a high level of OPN and OCN expression. As the osteogenic culture of BMSCs on the flagella coated substrate progressed from 7 to 14 days, at some areas, cells started to aggregate and form calcified nodule-like structures. The high OPN and OCN gene expression inside the formed nodules indicated the high level of differentiation of BMSCs on this scaffold (Figure 3. 13). It is well known, the calcium phosphate such as HAP highly enhances BMSCs differentiation toward osteoblasts. The immunofluorescence examination of BMSCs on flagella demonstrated that the nanotopographies produced by flagella in combination with calcium phosphate generated microenvironment promote the early differentiation of BMSCs.

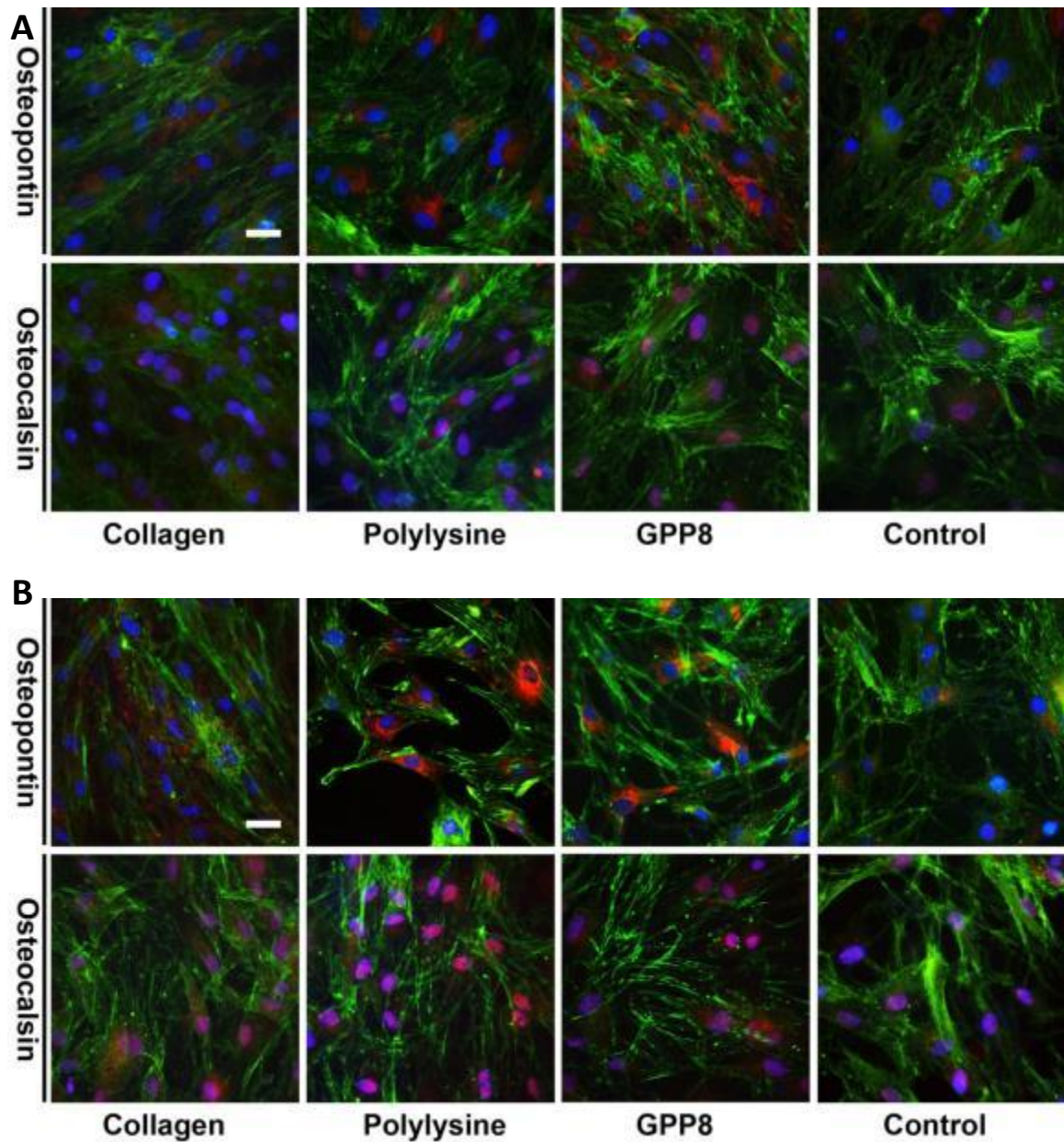


Figure 3.12: Differentiation of BMSCs on collagen and flagella coated substrates were analyzed for gene expression by immunostaining for 7 and 14 days: A) BMSCs growth for 7 days; B) BMSCs growth for 14 days (Scale bar is 25 μm). Color representation: cell nuclei are stained by DAPI (blue) and the F-actin of cells are stained by FITC-labeled phalloidin (green), OPN and OCN are stained by rhodamine-labeled antibody (red).

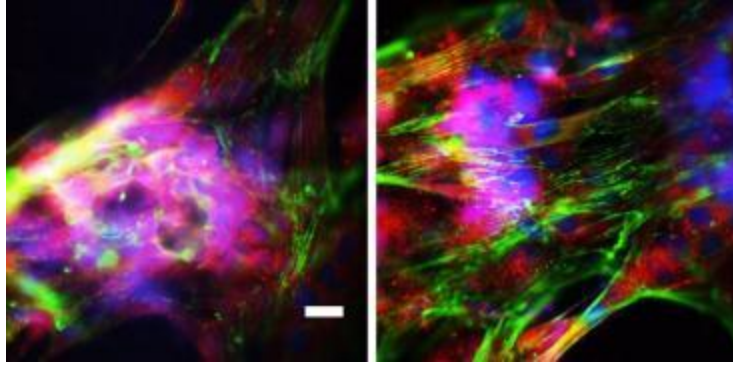


Figure 3.13: Aggregated nodule-like cluster of BMSCs on flagella coated substrates were analyzed by immunostaining: A) OPN gene expression; B) OCN gene expression (Scale bar is 25 μm). Color representation: cell nuclei are stained by DAPI (blue) and the F-actin of cells are stained by FITC-labeled phalloidin (green), OPN and OCN are stained by rhodamine-labeled antibody (red).

Compared to other display technique such as PD, much longer peptide can be displayed on flagella without losing self-assembly properties [232]. More desirable functions can be conferred upon this bio-template. Moreover, in combination with double or triple display technology [81], multi-functional bacterial flagella could be developed for bone tissue engineering and other applications. Flagella display was applied in basic microbiological research, molecular biology, vaccinology as well as biotechnology [81]. *FliC* can also be used *in vivo* for cancer therapy by binding to toll-like receptor 5 (TLR5) [233]. Based on above data and previous research, bacterial flagella may be an excellent candidate for bone tissue engineering as well as other applications.

In conclusion, bacterial flagella were employed as natural bio-templates for biomimetic mineralization. Their nano-dimension renders them facile to produce a nano-scale mineralized scaffold. Meanwhile, during the biomineralization process, the interaction between bio-template and inorganic particles can direct self-assembly into complex and high-order organic/inorganic nanocomposites. Compared with conventional methods of materials production, biomimetic mineralization is facile, environmentally benign and economic. In the fabrication of new bone materials, molecular self-assembly underlies the “bottom-up” of nanocomposite is a relatively new paradigm. The bioengineered flagella can be defined as the spontaneous organization of individual molecules into an

ordered structure through non-covalent interactions. Moreover, the BMSCs can adhere to flagella scaffold and their differentiation toward osteoblasts is promoted by nanotopography and microenvironment produced by bioengineered flagella.

Chapter 4 Osteogenic Differentiation of Rat Bone Marrow Stem Cells on Biomimetic Nano-Structured Substrates Generated by Bioengineered Flagella

4. 1 Introduction

Natural bone is built from nanoscale molecules that are organized in a hierarchical manner. The smallest building blocks of bone are type I collagen mineralized by HAP nanocrystals [234]. With development of nanotechnology and biotechnology, a “bottom-up” approach has recently been developed which seeks to mimic natural bone compositionally or structurally using strategies found in nature at nano- or molecular-level with biological mineralization process [235]. This approach is considered to be more promising for designing bone-like materials and has sparked increased research interest. Compared to conventional methods, biomimetics offers new combinations of low weight, remarkable mechanical properties and added functionalities [236-238]. These nanocomposites usually require little energy for self-assembly, offer larger surface area-to-volume ratio, and can promote cell attachment, proliferation and differentiation [238-240].

In order to get hierarchical well-defined structure like bone, the bio-inspired materials with self-assembling features have been studied [188]. Some natural and synthetic peptides and proteins with alternating hydrophilic and hydrophobic residues can produce β -sheet structures by self-assembly [186, 188, 241]. Hartgerink et al. [158] reported a designed pH-induced self-assembly of peptide-amphiphiles (PA). It is composed of a hydrophilic head and hydrophobic alkyl tail that can self-assemble into nanoscale fibers in aqueous solutions. The architecture of PA fibers is highly biomimetic of the collagen fibrils found in bone ECM. The surface-exposed head includes 4 cysteine residues (cylindrical nanofiber structure is stabilized by the creation of disulfide bonds between adjacent cysteine groups upon oxidation), a phosphoserine group (capable of promoting HAP nucleation) and an integrin-binding motif, RGD, (which enhances of cell attachment) all of which make them into multi-functional templates. The self-assembly process is driven by weak, non-covalent interactions including hydrogen bonds, ionic bonds (electrostatic interactions), hydrophobic interactions, van der Waals interactions,

etc. under ambient conditions [188, 241]. Thiol groups are also used as assembling driving forces because they are easy to form disulfide bonds upon oxidation. The coupling reaction is reversible, rapid and easy to carry out [241].

In recent years, scientists have begun to take advantage of some naturally occurring nano- or micro- fiber-like biomaterials such as spider-silk, fibrin, virus, which are self-assembled by small molecules, peptides or proteins [188, 242-244]. Meanwhile, natural originated biomaterials with chemical or genetic modifications have been reported to regulate cell-substrates interactions [245-247]. Most recently, we found the M13 phages bioengineered to display an osteogenic peptide (OGP) can highly promote the differentiation of BMSCs toward osteoblast lineages [248].

In this chapter, bacterial flagella bioengineered by peptide display are considered alternative bio-inspired “smart” building blocks of biomaterials. The bacterial flagellum is composed of several thousand copies of the eubacterial *FliC* protein as well as several other minor proteins including a pentamer of the tip-associated *FliD* protein [249]. In flagellum, *FliC* forms a globular structure. The N- and C- terminal regions termed D0 and D1 bind together by non-covalent interactions and face the center of the flagellum fiber. By intermolecular interactions between the α -helical, coiled-coil motifs, *FliC* monomers naturally self-assemble into a linear hollow nanotube with a repeat of 11 monomers per 2 turns [39, 112]. The flagellum has an outer diameter of about 12–25 nm, an inner diameter of ~2 nm, and a length of up to several microns [112]. The N- and C-terminal region (D0 and D1) of *FliC* proteins are highly conserved, however, in the central region (D2 and D3) of *FliC*, the amino acid sequences are highly variable. These two regions can be modified by the insertion or deletion of other sequences without losing self-assembly properties of flagellum [250]. Non-collagen proteins play an important role in the biomineralization process and control calcium phosphate mineral nucleation and growth [251]. The negatively charged amino acids especially E8 from BSP are considered the main factor to attract calcium ions following apatite crystal formation [251]. Herein, based on genetic approach, a peptide with 8 continuous glutamic acids from one of non-collagen proteins-BSP is displayed on the dispensable region of *FliC* and, at the same, it is surface-exposed. After incubated in a supersaturated HAP

solution, the bioengineered E8 flagella can mediate nucleation of nanoscale HAP crystals on their surface. Furthermore, the orientation of HAP nanocrystals is parallel to the *c*-axis of flagella. This arrangement make them quiet similar to the organization of HAP nanocrystals within type I collagen fibrils in bone. Previous studies proved that the short peptide sequences RGD highly enhance cell adhesion and spreading rate [252-257]. Thus, this integrin-binding peptide is also displayed on bioengineered flagella with E8. Finally a RGDEEEEEEEE (RGDE8) peptide was displayed on the surface of flagella.

BMSCs can differentiate into multi-lineage cells such as chondrocytes, osteoblasts, myoblasts and fibroblasts; however, the exact mechanism of the differentiation of these cells is still uncertain [258]. As progenitors of different skeletal tissues, BMSCs have been studied extensively *in vitro* for bone tissue engineering on scaffolds with different topologies and characteristics [259]. In the present study, the effects of nanoscale topographies, surface chemistry and microenvironment built on surface of flagellar scaffold for BMSCs proliferation and differentiation have been investigated.

4. 2 Materials and Methods

4. 2. 1 Layer-by-layer preparation of flagella based substrate:

Flagellar substrates were prepared by the LBL method, which utilizes electrostatic interactions between different layers [260]. Briefly, the pre-cleaned glass coverslips were sited at the bottom of 24-well cell culture plate. Poly-lysine solution (Sigma-Aldrich) allocates to the well of cell culture with coverslips (350 μ L/well) for 30 min, allowing for the adsorption of the first cationic polyelectrolyte layer onto the slides. Then, the coverslips were washed in ultra-pure water (5 min, continuous water flow) and dried under a pressurized air stream. Then 150 μ L flagella in water or supersaturated HAP solution was added into the well and incubated at room temperature for 20 min. The coverslips were then washed with ultra-pure water (5 min) and dried under a pressurized air stream. The previous steps were repeated three times and the final layer was covered by flagella (Figure 4. 1). Coverslips with one layer of poly-lysine were used as the control.

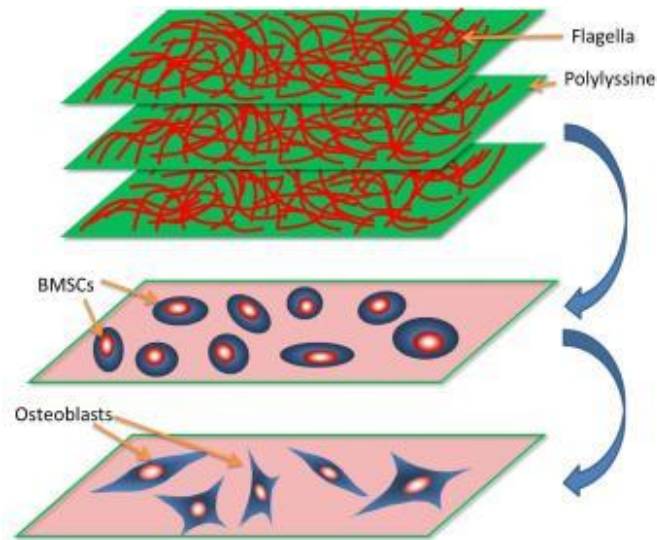


Figure 4.1: Schematic illustration of the formation of the flagella substrate using layer-by-layer method. The positively charged polylysine initiates the first layer of the substrate following the negatively charged flagella layer. After several cycles of deposition, the top layer was ended by flagella. Then, BMSCs seed on this substrate under osteogenic conditions. With the help of nanotopographic surfaces, surface chemistry and microenvironment generated by bioengineered flagella, BMSCs finally differentiate into osteoblasts.

4. 2. 2 BMSCs isolation and culture:

Primary BMSCs were isolated from the bone marrow of a young Fisher 334 adult female rat femur (Harlan) based on the previously described method [261]. Briefly, the isolated bone marrow cells were washed several times with Dulbecco's Modified Eagle Medium (DMEM; GIBCO BRL, Grand Island, NY, USA). After cell viability was tested and the density of the cells confirmed using trypan blue staining, cells were maintained in DMEM (low glucose) supplemented with 10 % fetal bovine serum (FBS) (Invitrogen), penicillin G 100 U/mL, streptomycin 100 μ g/mL, amphotericin B 0.25 μ g/mL. The cells were incubated in humidified atmosphere containing 5 % CO₂ at 37 °C. The non-adherent cells were removed after three days by changing the culture media. The BMSCs passaged no more than three times after isolation and before use.

4. 2. 3 Proliferation assay by MTT test:

The cells were plated at a density of 4×10^3 cells/well in 96-well plates coated with flagella in DMEM for 72 h. The growth of BMSCs was measured by MTT assay, in which 3-(4, 5-dimethyl thiazol-2-yl)-2, 5-diphenyl tetrazolium bromide (MTT) (5 mg/mL, 20 μ L/well, Sigma-Aldrich) was added to the cell cultures and incubated for 4 h at 37 $^{\circ}$ C. All solution was then removed. The blue reaction product was dissolved completely by adding dimethyl sulfoxide (DMSO) (150 μ L/well, Sigma-Aldrich) to each well and agitating for 30 seconds. The absorbance was measured at 490 nm using a Biotek spectrophotometric microplate reader. The coverslips coated with either flagella or polylysine are divided into 4 groups. The first group is RGDE8 flagella coated substrate. The second one is RGDE8 with biomineralization (M-RGDE8). The third one is the substrate coated by wild type flagella (WT) and the last group is a polylysine coated substrate as the control (Con). The following procedures are also separated into 4 groups accordingly.

4. 2. 4 SEM examination:

BMSCs were seeded on flagellar film at a density of 1×10^4 cells/mL. After cultured for 24 hours, the cells were washed with $1 \times$ PBS and fixed with 2.5 % glutaraldehyde in $0.1 \times$ PBS for 1 h. The cells were washed again with $1 \times$ PBS and then dehydrated in a graded series of ethanol (50 %, 70 %, 90 %, and 100 % respectively) for 30 min each. The samples were further dehydrated with a supercritical point CO₂ dryer. The morphology of BMSCs on flagellar film was observed using SEM (XL30, FEI Corporation).

4. 2. 5 Immunofluorescence of OPN and OCN:

The cell culture on the flagella substrates was terminated at 7, 14 and 21 days respectively in osteogenic media. The cells substrates were fixed using 70 % ethanol in $1 \times$ PBS for 30 min at room temperature. After washed by PBST buffer ($1 \times$ PBS containing 0.05 % Tween-20), the samples were then introduced permeability for 15 min (0.1 % Triton X-100 in $1 \times$ PBS solution). Afterwards, the samples were blocked in 5 % BSA (Sigma-Aldrich) for 1 h at room temperature. The primary anti-OPN antibody (1: 500, Abcam Biotechnology) and anti-OCN antibody (1: 1000, Santa Cruz Biotechnology) diluted in 5 % BSA were incubated with cells overnight at 4 $^{\circ}$ C. After washed 3 times for

5 min by 1 × PBST, secondary antibodies of Goat anti-rabbit IgG-TRITC (1: 500, Santa Cruz Biotechnology) at 1: 100 dilutions in blocking buffer were then incubated for 1 h at room temperature. Filamentous actin was stained with FITC-conjugated phalloidin (1: 40, Invitrogen) in 1 × PBS and nuclei were stained with DAPI (1: 1000, Chemicon). The coverslips with samples were then inverted onto glass slides, mounted and the images were collected by a fluorescence microscope (N-storm, Nikon Microsystems).

4. 2. 6 Quantitative Real-time PCR:

The cells are harvested at 7, 14 and 21 days respectively. Total RNA isolation with reverse transcription to cDNA was prepared with Ambion[®] Cells-to-cDNA[™] II Kit (Invitrogen). Power SYBR Green PCR master mix (Applied Biosystems) was applied in this study for monitoring the changes of DNA during qPCR process. Quantitative examination of the samples was done by a mini Fast real-time PCR system (Bio-rad Laboratories) using 10 μL SYBR Green I mastermix, 3 pmol/mL of each forward and reverse primers and 5 μL cDNA templates in a final reaction volume of 50 μL. The PCR reaction conditions described as: 45 cycles of PCR, 95 °C for 30 s, 58 °C for 30 s, and 72°C for 30 s. In our study, acidic ribosomal phosphoprotein P0 (Arbp) was used as the housekeeping gene. Data collection and analysis was performed using the software supplied with the instrument. The specificity of the PCR amplification was confirmed by agarose gel electrophoresis (data not shown). The primers sequences for qPCR were as follows: OPN, Forward primer 5'-GACGGCCGAGGTGATAGCTT-3', Reverse primer 5'-CATGGCTGGTCTTCCCGTTGC-3'; OCN, 5'-AAAGCCCAGCGACTCT-3', 5'-CTAAACGGTGGTGCCATAGAT-3'; Runx2, 5'-GCTTCTCCAACCCACGAATG-3', 5'-GAACTGATAGGACGCTGACGA-3'; Type I collagen, 5'-TCCTGCCGATGTCGCTATC-3', 5'-CAAGTCCGGTGTGACTCGTG-3'; Arbp (Housekeeping gene), 5' -CGACCTGGAAGTCCAACACTAC-3', 5'-ATCTGCTGCATCTGCTTG-3'.

4. 2. 7 Mineralized bone matrix formation assay:

The cells were plated at a density of 4×10^3 cells / well in 96-well plates and coated with flagella and mineralized flagellar samples and cultured in osteogenic media for 2 weeks. The cells were fixed in 4 % paraformaldehyde at room temperature for 40 min and the

mineralized nodules were stained with 0.1 % solution of alizarin red S (Sigma-Aldrich) at pH 4.1-4.5 for 30 min.

4. 2. 8 Statistical analysis:

All experiments were conducted at least 3 times. All quantifiable data is represented as mean \pm standard deviation in all the figures. Student T tests were calculated to determine significant difference. Significant difference was set as a p-value of less than 0.05 in all results.

4. 3 Results

4. 3. 1 Characterization of flagella coated substrates

LBL technique is widely used for the fabrication of a variety of functional thin films [260]. Generally, it involves alternating positively and negatively charged layers to build a film held together by electrostatic interactions. After the addition of each new layer, the excess or remaining solution can be rinsed off. There are many advantages of the LBL assembly technique. It is easy to scale up, very simple and universal with a nanoscale controllable thickness. Here, positively charged polylysine molecules form the first layer to which the negatively charged flagella will adhere to form a second layer. The schematic representation of LBL preparation is depicted in Figure 1. The final flagellar layer was characterized by atomic force microscopy (AFM) at tapping mode (Figure 4. 2). At high concentration (4.264 $\mu\text{g}/\mu\text{L}$) RGDE8 flagella totally covered the substrate with characteristic flagellar curly morphology (Figure 4. 2 A). Wild type flagella exhibited very similar structures as did RGDE8 (data not shown). After nucleation in supersaturated HAP solution, RGDE8 flagella aggregated. The flagella surface shows more compact but rough topographies (Figure 4. 2 B) and have strong inclination to form bundle-like structures as marked in Figure 4. 2 C. This result is consistent with our previous study. With peptide display technique, unlike with chemical modification, every bioengineered *FliC* can theoretically be modified to display a foreign peptide with a specific, desired functionality. Moreover, the inserted peptide is surface-exposed enabling precise control of flagella functionality through homogeneous surface modification.

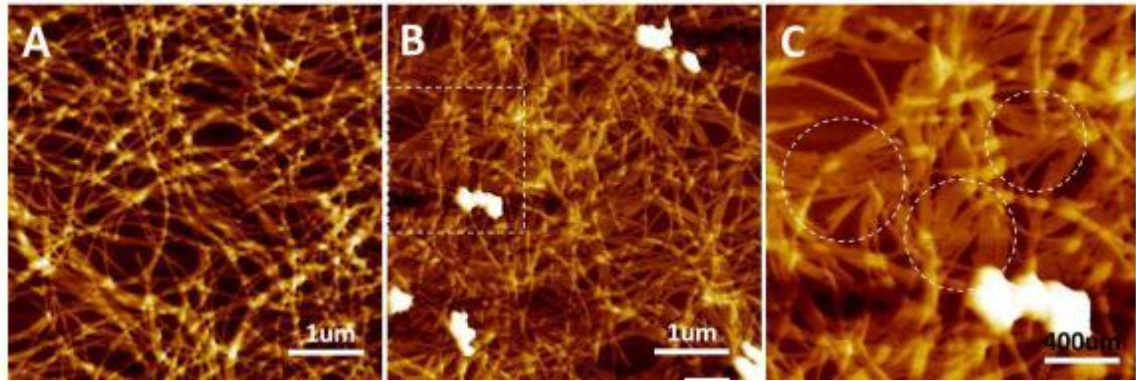


Figure 4.2: AFM micrographs of flagella surfaces prepared by layer-by-layer method. (A) nanotopography coated by bioengineered flagella. Wild type flagella exhibit very similar nanotopographic surfaces. (data not shown); (B, C) AFM micrographs of RGDE8 flagella after nucleation in supersaturated HAP solution. Bundle-like flagella were observed marked by dashed circles in C.

4. 3. 2 Morphology studies of BMSCs

The initial interaction between cells and substrate affects the BMSCs behaviors such as cell proliferation and differentiation. In the present study, changes in BMSCs morphology were monitored using bright field microscopy (Figure 4. 3). After 24 h in culture, BMSCs show characteristic bipolar to polygonal fibroblastic morphology and spread very well on control group (Figure 4. 3A). However, the degree of BMSCs spreading on RGDE8 and M-RGDE8 flagella was less than those on control group (Figure 4. 3B, C). In WT group, BMSCs are much less spread and some of the cells show round-like morphology indicating the wild type flagella may not be very favorable to the cells (Figure 4. 3D). Even though cells did not spread as well in the experimental samples, our results still indicate that the some cells were viable on each of these nanotopographies.

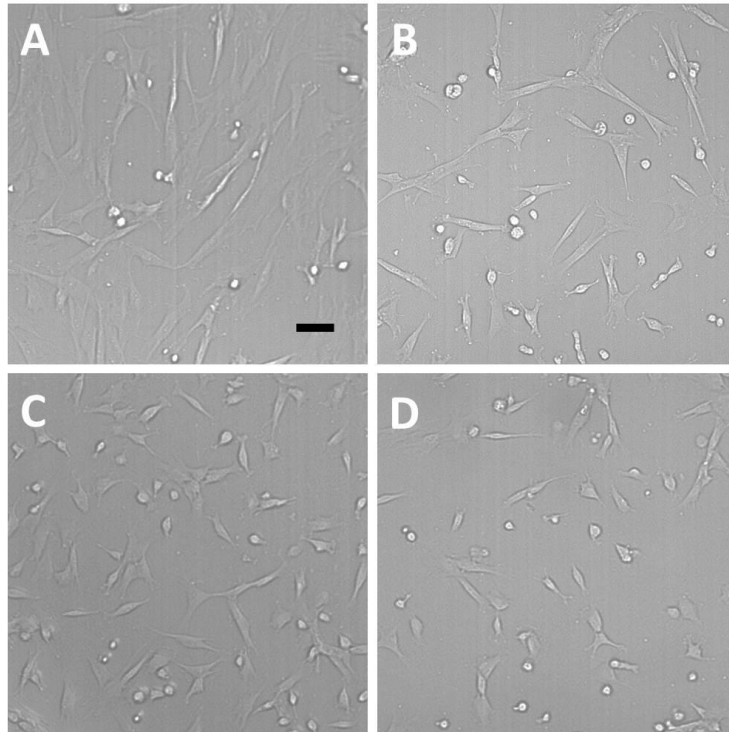


Figure 4.3: Bright field Microscopy of BMSCs on flagella and polylysine coated substrates prepared by LBL at 24 h. A) BMSCs morphology on polylysine coated substrate (Control). The cells totally spread on the substrate. B) BMSCs morphology on RGDE8 coated substrate. The cells are less spread. C) BMSCs on M-RGDE8 coated substrate. Less spread of the cells compared to those on RGDE8 flagella. D) BMSCs on wild type flagella coated substrate. Much less spread of the cells on wild type flagella and some of them only show round morphologies. Scale bar: 100 μm and for all panels

The morphology of BMSCs on the surface of flagella was also monitored using SEM (Figure 4. 4). The spreading of BMSCs on different substrates is similar to those observed by bright field microscopy. The cells are flat and stretched in the control group (Figure 4. 4 A). On flagella coated substrates, BMSCs show less spreading than those in the control group (Figure 4. 4 B, C and D). Especially in wild type group, the cells are much less spread and the cells show bipolar structures (Figure 4. 4 C). This is consistent with another report of cellular morphology on nano-fibrous scaffolding [225]. The SEM revealed that cells strongly adhered to flagellar surface via filopodia-like extensions especially in M-RGDE8 group (Figure 4. 4 B, C, D; Figure 4. 5B). The BMSCs in this

group exhibit longer and more abundant numbers filopodia-like extensions. The structural topography of the flagellar surface was also observed by SEM. Due to resolution constraints, the individual flagella could not be recorded directly. However, some fibrous structures were observed on wild type or RGDE8 flagella coated surfaces (Figure 4. 4 E). At higher magnification (insert), fibrous-like structures, which could be formed by flagella, were observed more clearly. Because flagella were covered with the inorganic calcium phosphates and some flagella formed bundles, more compact but rough surfaces were observed in M-RGDE8 group (Figure 4. 4 F and insert). These results are consistent with AFM examination. There were no similar structural features observed on polylysine coated substrate (Figure 4. 5A).

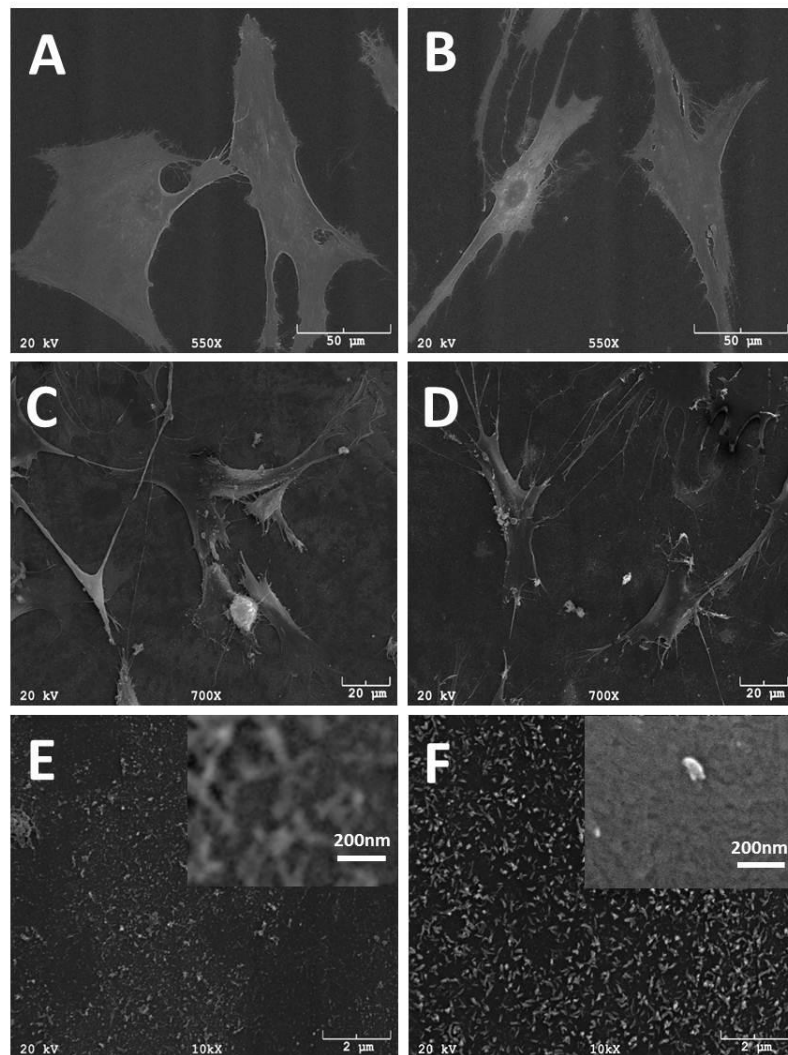


Figure 4.4: BMSCs morphology on flagella coated substrates using SEM. A) Representation of cell morphology after 24 h of incubation on polylysine coated surface (Control); B) SEM micrograph of BMSCs on bioengineered flagella coated substrates; C) shows BMSCs on wild type flagella coated surface and less spread of the cells on this substrate were observed; D) shows BMSCs morphology on bioengineered flagella coated substrate with biomineralization in HAP solution. Much more number and longer filopodia-like extensions appeared around the cells; E) SEM micrograph of bioengineered flagella coated surface and high magnification (inert) show curved fibrous structures which could be formed by flagella or small bundles. WT flagella show very similar surface topology (data not shown); F) shows substrate surface morphology coated by bioengineered flagella with biomineralization and high magnification (inert). After nucleation, the surface became rougher and the thickness of flagella or bundles was increased.

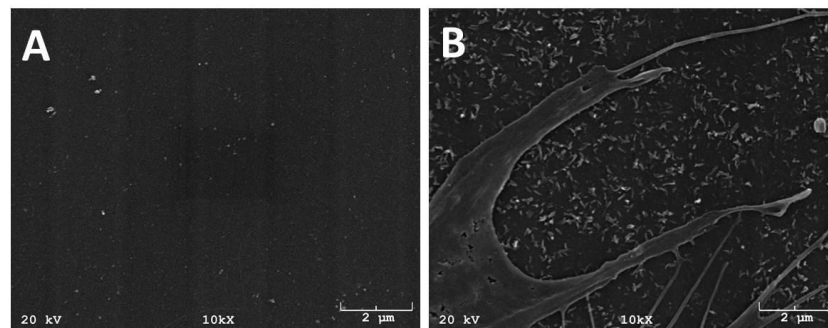


Figure 4.5: A) SEM topographies of polylysine coated substrate. The surface is very flat. B) SEM micrograph shows BMSCs anchor on biomineralized flagella substrate by filopodia-like extensions.

4. 3. 3 Proliferation of BMSCs on flagellar substrates

The proliferation of BMSCs seeded on polylysine and flagellar surfaces was analyzed by MTT assay after 3 days of cell culture (Figure 4. 6). The growth rate of the BMSCs on flagellar substrate was significantly affected by the peptide displayed on the surface of flagella as well as the biomineralization. The growth rate of BMSCs was much higher on RGDE8 and M-RGDE8 flagella than that on wild type ($P < 0.01$ and $P < 0.05$ respectively). After biomineralization of flagella, the proliferation of BMSCs seeded on biomineralized

flagella decreased compared to RGDE8 group, but no significant difference. Polylysine coated substrate promoted the growth of BMSCs better than did wild type and M-RGDE8 flagella coated substrates ($P < 0.01$, $P < 0.05$, respectively).

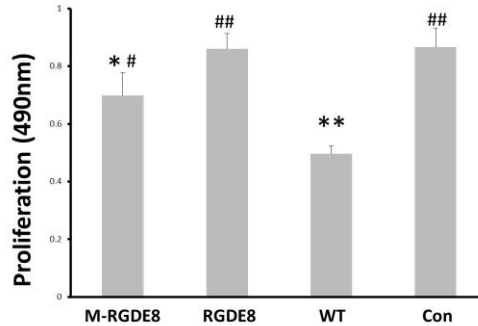


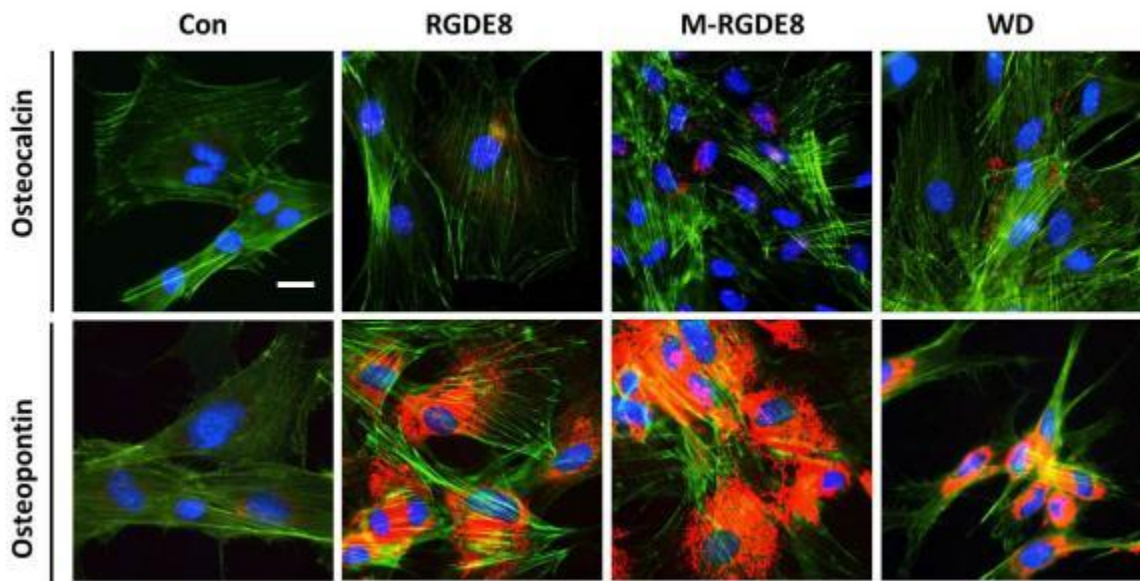
Figure 4.6: Proliferation of BMSCs on flagella coated substrates with control. The growth rate of cells on RGD enriched flagella surface is faster than those on the WT flagella surface. (CON) coverslips coated with polylysine as control; (RGDE8) bioengineered flagella displayed with 8 glutamic acids and RGD integrin binding peptide; (M-RGDE8) displayed the same sequences as RGDE8 and nucleated in supersaturated HAP precursor solution; (WT) wild type flagella. (compared with control group, * $P < 0.05$, ** $P < 0.01$; compared with WT group, # $P < 0.05$, ## $P < 0.01$).

4. 3. 4 Gene expression by immunofluorescence

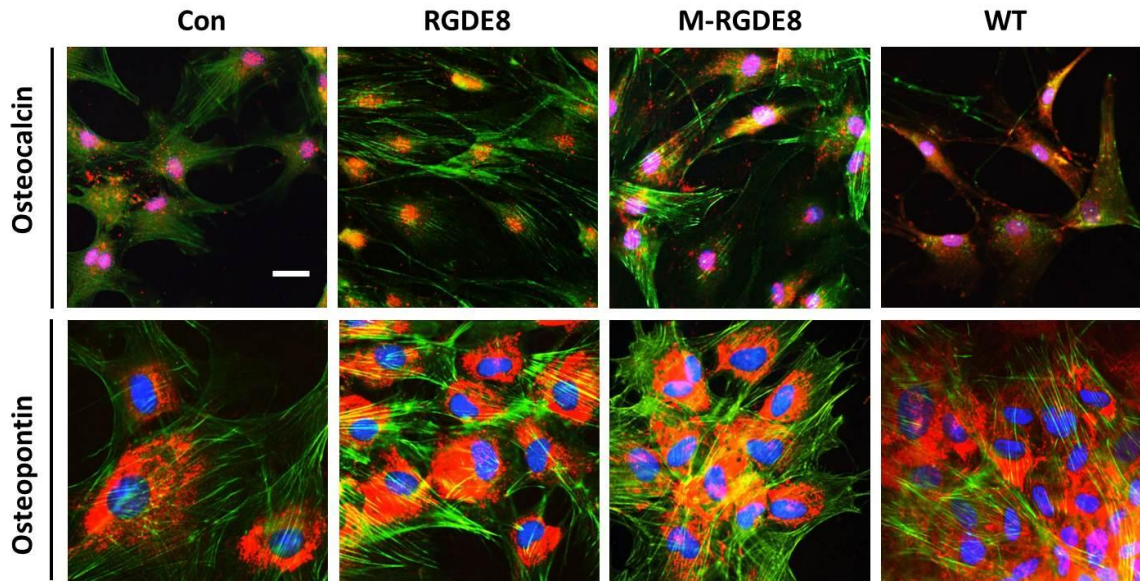
Specific markers can be detected during BMSCs differentiation toward osteoblasts. In this study, we monitored the cellular gene expression of two bone specific formation marker proteins, - OPN and OCN, by immunofluorescence cultured on flagellar substrates. The cell cultures on flagella and polylysine were terminated at 7, 14 and 21 days respectively and the cells were stained for the osteo-specific genes, OPN and OCN. As shown in Figure 4. 7, both OPN and OCN could be detected in cells beginning at day 7. The gene expression levels of OPN and OCN in the cytoplasm on flagellar substrates including RGDE8, M-RGDE8 and WT groups were higher than those on polylysine coated substrate (Figure 4. 7 A). The expression of OPN was especially high in the cells on the biom mineralized RGDE8 flagella. After 14 days, the gene expression of OCN became much higher in all cultures, especially in WT group. Also after 14 days, the cells on wild type and polylysine coated substrate started to express OPN at a high level

(Figure 4. 7 B). After 21 days, the expression of OPN still remained a high level on the RGDE8 and M-RGDE8 flagella substrates; however, it appeared that the expression levels of OPN started to decrease at WT and control groups. The levels of OCN continue to increase at control group. For flagella coated substrates groups, the expression levels of OPN are not as high as those at 14 days, but they still kept at basal levels (Figure 4. 7 C). During 2 weeks culturing process in osteogenic media, the BMSCs seeded on the flagella started to aggregate and form calcified nodule-like structures (Figure 4.7).

(A) 7 days



(B) 14 days



(C) 21 days

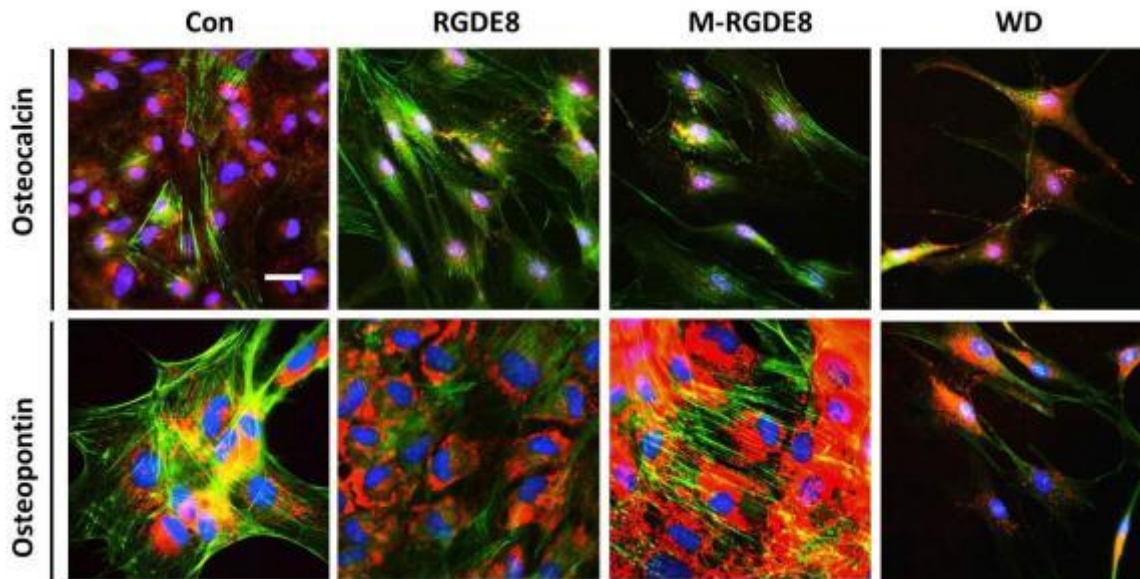


Figure 4.7: Cells grown on flagella and polylysine coated substrates were analyzed for gene expression by immunostaining for 7, 14 and 21 days (scale bar is 25 μ m). A) BMSCs growth for 7 days. B) BMSCs growth for 14 days. C) BMSCs growth for 21 days. Color representation: cell nuclei are stained by DAPI (blue) and the F-actin of cells are stained by FITC-labeled phalloidin (green), OPN and OCN are stained by rhodamine-labeled antibody (red).

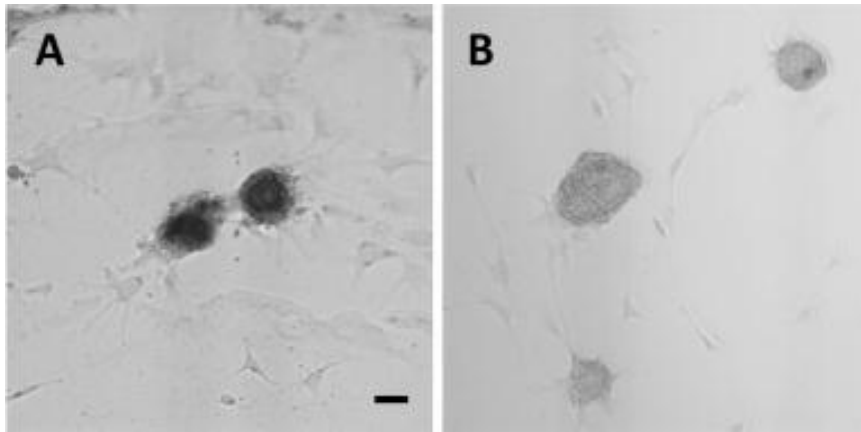


Figure 4.8: Light microscopy of calcified nodule-like structures formed on M-RGDE8 A) and RGD-E8 B) flagella substrates

4. 3. 5 Quantitative real-time PCR

In order to obtain quantitative information for the changes in gene expression during the osteogenic differentiation process, the differences in fold change expressions of selected osteogenic specific gene markers (OCN, OPN, Runx2 and type I collagen) were recorded by quantitative real-time PCR analysis at selected time points (Figure 4. 9 and 4. 10). Because the differentiation markers almost have no expression at 0 day, the day 7 gene expression of BMSCs on polylysine coated substrate was used as the control. At 7 days, significant changes in fold expression of OPN and OCN were observed in cells plated on RGDE8 and M-RGDE8 flagella coated substrates compared to those grown on WT or control groups (RGDE8, M-RGDE8 vs. Con, both $P < 0.01$; RGDE8, M-RGDE8 vs. WT, $P < 0.05$ and $P < 0.01$ respectively). The OPN and OCN expressions in cells on M-RGDE8 flagella is stronger than those on RGDE8 flagellar surface ($P < 0.05$). There is no significant difference of OPN and OCN expression between the cells grown on wild type and on the control and kept at a basal level on both of them (Figure 4. 9 A). These results imply the differentiation of BMSCs to matured osteoblast cells was expedited by RGDE8 and, especially, by M-RGDE8 flagella. At 14 days, the OPN and OCN expression increased significantly to a high level in all groups with no significant differences between the different groups (Figure 4. 9 B). After the cells were cultured for 21 days, the relative fold changes in OPN decreased at all groups except the M-RGDE8 group still remained a comparatively higher level than others ($P < 0.01$) (Figure 4. 9 C). The

expression fold changes of OCN at RGDE8 and M-RGDE8 groups are still higher than WT and control groups. The above data indicates that functionalized flagellar surface could improve and up-regulate osteogenic differentiation of BMSCs toward to osteoblasts. During BMSCs differentiation into osteoblasts, runx2 is expressed as a significant transcription factor. In our results, the expression of runx2 follows a trend similar to that of the expression of OPN in all groups. It is up-regulated in all flagellar substrates including M-RGDE8, RGDE8 and WT groups. In M-RGDE8 group, the expression level of runx2 was up-regulated when compared to the control at as early as at day 7 ($P < 0.01$). At 14 days, the expression of runx2 was also up-regulated in all groups and stayed at this high level until day 21 in the M-RGDE8 group. The expression level of Col I increased significantly on the M-RGDE8 and WT substrates during the first week ($P < 0.01$ vs. WT or Con). The expression of Col I was still expressed at higher level in M-RGDE8 and WT groups at 14 and 21 days. The gene expression of osteogenic markers shows the nanostructure and microenvironment of flagella play an import role for the BMSCs differentiation.

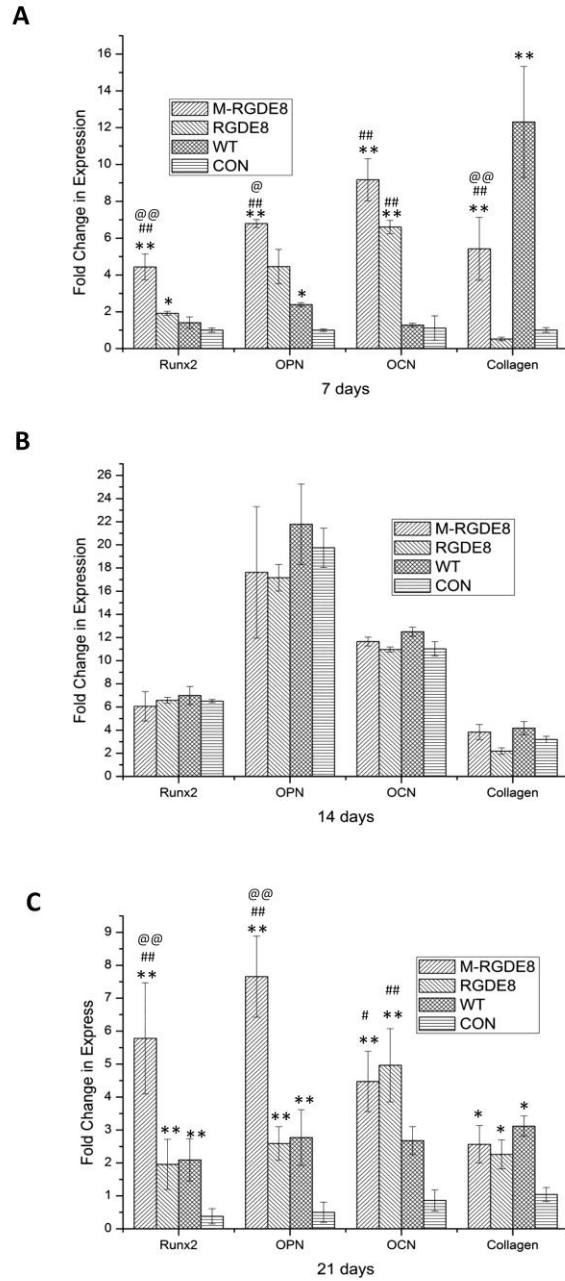


Figure 4.9: Real-time PCR analysis for Runx2, OPN, OCN and type I collagen (Col I) gene expression on flagella and polylysine coated substrate at different time points. A) 7 days; B) 14 days and C) 21 days. Flagella substrates can stimulate and enhance Runx2, OPN, OCN and Col I mRNA expression compared to control. (When compared with Control group, *P<0.05, **P<0.01; When compared with WT group, #P<0.05, ##P<0.01; When compared with RGDE8 group, @P<0.05, @@P<0.01)

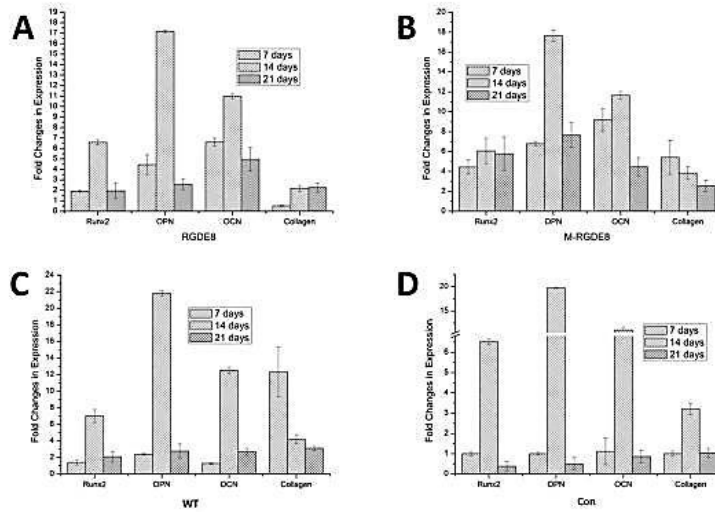


Figure 4.10: Real-time PCR analysis for Runx2, OPN, OCN and type I collagen (Col I) gene expression on flagella and polylysine coated substrates. A) RGDE8 flagella coated substrate; B) biomineralized RGDE8 flagella coated surface; C) wild type flagella coated surface; D) polylysine coated substrate (Control).

4. 3. 6 Mineralized calcium-containing matrix formation

After 14 days culture in osteogenic media, the cells on M-RGDE8 and RGD-E8 started to aggregate and form calcified nodule-like structures (Figure 4. 8). Calcium-containing mineral deposits are also important marker of osteogenic differentiation of BMSCs. The self-mineralized calcium deposits represent the final stages of osteogenic differentiation. In this study, alizarin red stain was used to observe the presence of calcium-containing minerals. The M-RGDE8 group exhibited highest intensity of red color depicting that calcium deposition significantly promoted and totally matured osteoblasts. The calcium-containing mineral deposits were also detected on the RGDE8 and WT flagella substrates. The control group, however, exhibited more fibroblast-like morphology with a few nodule structures (Figure 4. 11). These data show that the flagellar nanostructure, surface chemistry and microenvironment can affect the cells mineralization during the osteogenic differentiation process.

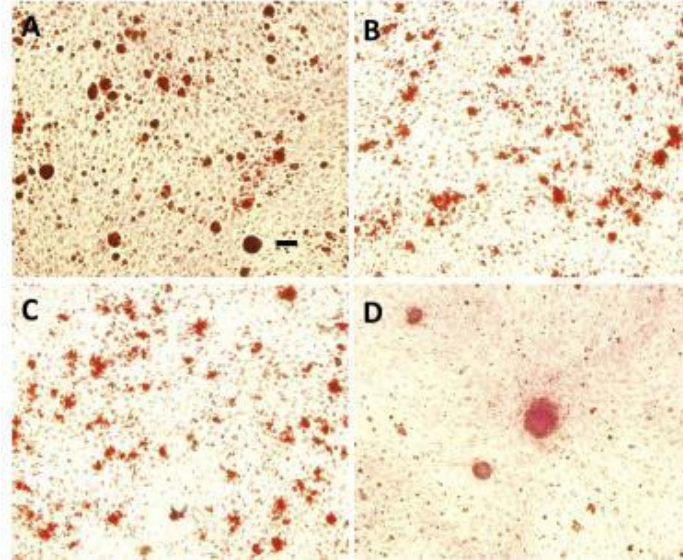


Figure 4.11: Mineralization derived from different flagella coated substrates and polylysine coated surface assayed by Alizarin red S at 14 days. A) biomineralized RGDE8 flagella coated substrate (M-RGDE8); B) RGDE8 flagella coated substrate (RGDE8); C) wild type flagella coated substrate (WT); D) polylysine coated substrate (Con)

4. 4 Discussion

Flagella are naturally occurring bio-nanotubes that self-assemble from *FliC* proteins through non-covalent intermolecular interactions [112]. Flagella from the same host have fixed outer and inner diameters [39] (Figure 4. 12). Using genetic peptide display technique, theoretically, each *FliC* can be bioengineered to display desired functional group, giving rise to a flagella nanotube with homogeneous and controllable surface chemistry [250]. In our study, bioengineered flagella with integrin-binding domain-RGD and E8 peptides are highly biomimetic of the collagen fibrils found in bone ECM. The linear organic flagella combined with inorganic nanoscale HAP crystals on their surface generate structures and organization similar to that of bone ECM to some extent. In order to get more information for potential application as bone substitute materials, the adhesion, proliferation and differentiation of BMSCs on the flagella generated substrates were investigated.

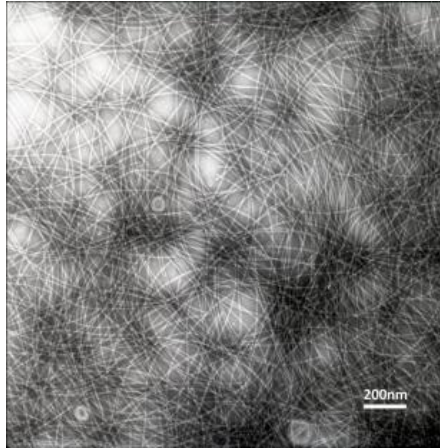


Figure 4.12: TEM images of bacterial flagella from wild type *Salmonella*.

Previous research confirmed that helical proteins can self-assemble into bundles utilizing divalent metal ions or positively charged polymers to laterally cross-link neighboring molecules mediated with [262, 263]. Our results may be based on similar mechanism through which calcium ions in HAP solution interact with the very negatively charged 8 glutamic acids peptide displayed on flagella to induce aggregation and assembly of flagella. After the BMSCs seeded on flagella coated substrates, fibrous structures can still be observed by SEM indicating that the substrates are still stable.

ECM proteins serve as a base for cells to adhere and spread onto substrates [259]. In this study, the surface modified flagella with or without biomineralization, wild type and polylysine coated substrates were investigated for their effect on the osteogenic differentiation of BMSCs. BMSCs could adhere and spread on flagella coated surfaces (Figure 4. 4) indicates that the cells were viable. However, BMSCs exhibited different morphology and spreading levels on different substrates. It is possible for some proteins from serum in the cell culture media to adhere to the substrate and help cell adhesion at the very early stages of cell culture [264]. However, when BMSCs were seeded on tobacco mosaic virus (TMV) (another naturally occurring linear nano-template) in serum free conditions, cells still acquired very spread morphology which was similar to the morphology of cells grown under complete serum conditions [245, 265]. In our study, BMSCs attachment and morphology were observed directly under complete serum conditions.

Polylysine can promote cell attachment by altering the negatively charged surface to positive [266]. Less spreading of BMSCs on flagella coated substrates especially in WT group may be caused by the nanotopographies on flagellar surface. Previous research also found similar results [225, 267]. On the other hand, wild type flagella may not be very favorable for BMSCs attachment. After the surface of flagella was modified with the RGD peptide, improved spreading of BMSCs were observed using bright field microscopy and SEM. As a well-known integrin-binding peptide, RGD can highly promote cell attachment and adhesion [253-257]. It is present in many ECM components such as fibronectin and vitronectin [268]. Moreover, non-collagen proteins of bone OPN and BSP also contain this peptide [269]. The degree of nanoroughness of substrate surfaces also has a significant influence on cell morphology and anchorage. With increased surface roughness and structural complexity, more filopodia-like extensions with greater length appeared [270]. In our study, the rougher flagellar surface after nucleation may induce more filopodia like extensions on the cells.

RGD peptide has also been shown to improve proliferation of the BMSCs [255, 257]. In our results, the growth rate of the BMSCs on RGD containing flagellar substrates were highly enhanced compared to those on wild type flagella. Because the positively charged polylysine surface can also enhance the cells attachment and proliferation [230, 253, 271], there is no significant difference between RGDE8 and control groups. The growth rate of BMSCs decreased on biom mineralized flagellar surfaces. In the previous study, the decreased proliferation rates of BMSCs were also found on the biomimetic mineralized collagen membranes with nanocomposite [272]. A high amount of these cells may start differentiating towards the osteoblastic lineage and inhibit proliferation [273]. The other reason is that after biom mineralization, some of RGD sites on flagellar surface might have been embedded underneath mineral layers and blocked from BMSCs.

The surface chemistry and topography especially at nanoscale play a vital role for initial adhesion, proliferation and differentiation of BMSCs [225, 245, 265]. These effects were further investigated by quantitative analysis of gene expressions of BMSCs during osteogenic differentiation on flagella generated nanotopographies and polylysine coated substrate. Based on q-PCR analysis, during the entire duration of the cell culture, almost

of all the osteo-specific genes were up-regulated. However, the enhancement levels and folds for different genes are surface specific. Previous research confirmed that the topography of nanostructures has significant effects on human mesenchymal stem cell (hMSC) osteogenesis. Nanoscale disorders stimulate MSCs to produce bone mineral *in vitro* without osteogenic supplements [224]. The nano-scaled two dimensional (2D) substrates coated with TMV nanorods and nanofibrous architecture in both 2D poly (L-lactic acid, PLLA) thin matrices and 3D PLLA scaffolds can trigger speedy expression of osteo-specific markers and enhance the osteogenic differentiation [225, 265]. In our study, the physical stresses of flagella topography also accelerate BMSCs differentiation into osteoblastic lineage. Compared to control, higher levels of OPN and OCN were detected in cells on flagellar substrate at 7 days and still maintained similar patterns until 21 days indicating an up-regulated and early osteogenic differentiation of the cells. These results demonstrate the physical nanotopologies generated by flagella can affect the behavior of BMSCs toward osteoblasts. Moreover, the nano-level scaffold can adsorb more proteins such as fibronectin from cell culture media and, in turn, promote up-regulated gene expression and increased mineralization [225].

It has been demonstrated that the surface chemistry not only plays a significant role in initial adhesion but may also control the signaling processes leading to different differentiation pathways depending on the functional group arrangement and its density on the substrate [245, 265]. The RGD peptide can enhance osteogenic differentiation of BMSCs [255] and has been used on a variety of scaffolds, surfaces of bone materials, and surfaces of HAP to enhance cell attachment and proliferation *in vitro* [130, 240, 252, 254] and *in vivo* [256]. In the present study, at M-RGDE8 and RGDE8 groups, we also found early and enhanced gene expression of the OPN and OCN. As the main inorganic composition of bone, HAP exhibits excellent biocompatibility and osteoconductivity and is confirmed to support cell attachment, proliferation, and osteogenesis [274, 275]. BMSCs on calcium phosphate without osteogenic differentiation additives could also differentiate into osteoblasts [276]. On biomaterialized flagellar surface, the OPN as well as OCN is highly up-regulated at an early time and maintains a high level of expression after 3 weeks. This data also confirmed that the surface modified RGDE8 peptide and the microenvironment generated by biomaterialized flagellar surface also participate in

regulating differentiation of BMSCs. On polylysine coated substrate, both of OPN and OCN achieved the highest levels at 14 days, not like the BMSCs cultured on plastic surface, on which the OCN level continued to increase during entire cell culture period [265]. The polylysine substrates may improve the cells adhesion, proliferation and osteogenesis [230].

Runx2 is critical for osteogenic differentiation and maturation of BMSCs toward osteoblasts by binding specific DNA sequences to regulate the transcription of numerous genes for osteogenesis [277]. As a key transcription factor for osteogenesis, runx2 can stimulate OCN gene expression [278]. The highly up-regulated and enhanced expression of runx2 on biomineralized flagellar substrate indicates that the BMSCs differentiate toward osteoblastic lineage. A basal level of runx2 is required for proper osteoblast proliferation and differentiation [277]. In our study, a basal level of runx2 was also found in other groups. Col I exhibited quite different expression pattern. It is highly expressed in the M-RGDE8 and WT groups at 7 days compared to other groups. However, the up-regulation of Col I at these two groups may be based on different mechanisms. In the M-RGDE8 group it may be due to the rough surfaces after biomineralization. Higher levels of type I collagen expression were found on nanoscaffolds than on flat surface [225]. However, in WT group, the surface of wild type flagella may be not very favorable to the cells. The cells have to secrete more ECM proteins such as Col I to survive on the substrate.

Strong mineralization on M-RGDE8 coated substrates was observed. Both of flagellar nanotopographic surfaces and microenvironment by HAP may result in the early maturation of BMSCs. RGDE8 group also showed many biomineralized nodules. The displayed 8 glutamic acids on flagellar surface may attract calcium ion deposition from the media following the biomineralization.

A series of transcription factors and signaling proteins regulate differentiation of BMSCs to osteoblastic lineage in a time-dependent manner. Based on microarray analysis, the BMSCs seeded on substrate with nanotopographies may be activated by different pathways toward osteogenesis [224, 265]. TMV coated substrates show a synchronized effort of various genes through bone morphogenetic protein-2 (BMP-2) signaling

pathway [265]. Cytoskeletal tension was changed when BMSCs seeded on disorder nanosubstrates which in turn effect on indirect mechanotransductive pathways shown by changes in Rho A (an important small G-protein involved in cell signaling and cytoskeletal organization) [224]. The surface chemistry and microenvironment generated by flagella can promote higher and earlier expression of osteogenic genes in BMSCs resulting an early differentiation and mineralization of BMSCs under osteogenic medium.

There are also some other advantages to using bioengineered flagella scaffolds. With the flagella technique, each of subunit of flagella-*FliC* can display the foreign peptide on its surface-exposed side. Moreover, very long peptide can be displayed on *FliC* without losing self-assembly properties. The flagella are also very robust at a variety conditions including stable at pH 2-10 [164] and rigid with a Young's modulus on the order of 10^9 Pa [279]. Porous mineralized scaffolds exhibit more osteoconductivity for various applications in bone engineering [244]. Flagella are naturally occurring bionanotubes which make the scaffold more permeable and may support sufficient nutrient supply and blood vessel ingrowth *in vivo*.

4. 5 Conclusion

We studied BMSCs behavior and gene expression toward osteogenesis on wild type and genetically engineered flagella generated substrates combined with inorganic calcium phosphate under osteogenic conditions. Flagellar substrates can support BMSCs adhesion, proliferation and differentiation meaning that the cells recognize nanotopographic surfaces, microenvironment and surface chemistry produced by flagella. The cell's growth rate, expression levels of genes involved in osteo-differentiation are significantly affected due to the presence of flagella. The early development of mature osteoblast suggests that chemical groups modified on bioengineered flagella promote the osteogenic differentiation of BMSCs. Our data indicate that the biomimetic ECM using genetically engineered flagella incorporated with calcium phosphate may be a promising substitutable scaffold for bone tissue engineering.

Chapter 5 Effects of Phosphorylation of Bioengineered Flagella on Biomimetic Mineralization

5. 1 Introduction

Collagen fibers in bone are considered to provide the organizational three-dimensional framework for inorganic mineral nucleation with spatial constraint [280]. Meanwhile, there are many kinds of non-collagenous macromolecules proteins (NCPs) that might participate in the formation and maturation of HAP nucleation and growth. These proteins are morphologically, structurally, and functionally interact with the collagen fibers through which facilitate primary crystal formation and regulate subsequent mineral crystal growth [281]. Almost all of these proteins are highly acidic which contain aspartic acid (Asp), glutamic acid (Glu) and serine (Ser) [251]. *In vivo*, mineralization of bone starts on the surface of collagen fibrils, nevertheless, a higher mineralization at the surface compared to the interior of the collagen. Moreover, the center-to-center distances between the nanometer-sized particles in the primary biomineralized collagen fibrils correlate with those between the centers of acidic clusters along the chains of the non-collagenous matrix proteins. It can be supposed that apatite mineralization might be induced by the NCPs bound in parallel arranged strands along the collagen fiber surface [281]. A large number of NCPs were found to bind to collagen fibrils such as collagen-binding motif from OPN and BSP [156, 282]. These anionic groups on NCPs may accumulate cations such as calcium ions to generate local supersaturation followed by oriented nucleation and growth of mineral crystals [159, 283]. A specific stereochemical motif on NCPs may recognize the interacting plane of the inorganic minerals which may essential for the mineral nucleation such as β -sheet structure of DMP1 [157] and complementary surface of OCN to calcium ions in an HAP crystal lattice [284].

Among these NCPs, phosphorylation is also important to the mineralization process of bone. Recombinant, non-phosphorylated and chemically dephosphorylated OPN did not affect HAP formation. However, the highly phosphorylated milk OPN promoted HAP formation and stabilized the conversion of amorphous calcium phosphate to HAP [285]. The recombinant DPP, also named DMP2 without phosphorylation possessed much lower calcium binding capacity and could not transform amorphous calcium phosphate to

apatite crystals as native ones [286]. As bone-specific glycoprotein, BSP is also highly phosphorylated containing phosphoserine, sulphotyrosine residues and regions of contiguous glutamic acid residues. The combination of these phosphoserines with the polyglutamic acid residues plays an important role in accumulation of Ca^{2+} and binding to HAP. The full-length rat BSP using a prokaryotic expression system exhibited less potent than native bone BSP [287]. These results unambiguously show that the phosphorylation is important for HAP nucleation and growth. Hartgerink et al also confirmed only amorphous mineral deposited around the fibers after the phosphoserine was replaced by serine on peptide-amphiphile nanofibers [288].

Bacterial flagella grow on surfaces of bacteria and are naturally occurring protein nanotubes which are self-assembled by monomer protein-*FliC*. The *FliC* monomers naturally self-assembled into a linear flagellum tube with a repeat of about 11 monomers per two turns with 15-20 nm in diameter and 10-15 μm in length. This linear structure resembles the collagen fibrils in extracellular matrix (ECM) of bone. Interestingly, the surface of flagella can be modified or inserted by other peptides, however, without losing polymerization and functions [81]. Previously, we demonstrated that the bioengineered flagella with negatively charged 8 glutamic acids or repeated Gly-Pro-Pro sequences could nucleate apatite minerals on their surface. In this study, the negatively charged amino acids with serines were displayed on surface of flagella. The serines on flagella surfaces could be phosphorylated by Casein Kinase II (CK2). Then, the biomimetic nucleation and mineralization of apatite minerals on the phosphorylated flagella were investigated.

5. 2 Materials and Methods

5. 2. 1 Flagella Display:

Briefly, the synthesized single strand oligonucleotides (Invitrogen) which encode target peptide with complementary sequences and sticky ends of *Xho* I and *Bgl* II sites at each end respectively were induced into double strand oligonucleotides by annealing. Then the double strand oligos were inserted in vector PLS411 which contains *FliC* gene with a multicloning site at the central region. The recombinant vector was transformed into competent cell of *Salmonella* SL5928-a *FliC* gene knock out strain. Individual colonies

were picked on agar plate with ampicillin (100 µg/ml) and the recombinant plasmids were confirmed by DNA sequencing (MCLAB). There were three different sequences displayed on surface of flagella: EEEEEEEECSSSSSSSS termed E8+C+S8; ESESESESCSESESESES termed E8CS8; DSDSDSDSCDSDSDSDS termed D8CS8.

5. 2. 2 *Salmonella* flagella purification:

The SL5928 with different recombinant vectors were cultured in LB media at 37 °C with shaking (250 rpm) until OD to 0.6-0.8. The culture was collected and centrifuged at 6000 g for 20 min at 15 °C. The cell pellets were then washed twice by PBS buffer (pH=7.4). Finally, the cell pellet was resuspended in deionized water and cooled on ice-bath. The flagella were then detached from the cells by vortex mixer with highest speed for 3 min. The bacteria were removed by centrifugation at 6000 g for 20-30 min and the supernatant containing detached flagella were collected. The supernatant were centrifuged again at 10,000 g for 20 min to remove debris from solution. High purity flagella were precipitated by ultra-centrifugation at 80,000 g for 2 h. Finally, the flagella were dissolved in deionized water or PBS buffer.

5. 2. 3 Phosphorylation of bioengineered flagella and examination:

The phosphorylation of flagella with serines was carried out in a final volume of 50 µl with 1×CK2 buffer (20 mM Tris-HCl, 50 mM KCl, 10 mM MgCl₂), 20 µl flagella, 1 µl CK2 (New England Biolabs) and 200 µM ATP. The mixture was incubated at 30 °C for 2 h. The phosphorylated flagella proteins were analyzed by SDS-PAGE. The gel was stained in Pro-Q® Diamond phosphoprotein gel stain solution (Invitrogen) following the instruction of the kit. After the gel was totally destained, it was imaged by StormTM 860 (Amersham Biosciences). In order to distinguish the relative amount of phosphorylated portion from total protein, the loaded proteins to each well were adjusted to the same concentration (20 µg/µl).

5. 2. 4 Nucleation of flagella in supersaturated HAP solution:

The buffer and other molecules were removed by dialysis from phosphorylated flagella and were then incubated in supersaturated HAP solution (4 mM) for 3 days at room temperature. Wild type of flagella was used as control. A drop of aqueous solution was

mounted on the carbon TEM grids. After carefully rinsed with double distilled water and dried at room temperature, the samples were subjected to TEM (Zeiss 10) measurements.

5. 3 Results and Discussion

The phosphorylation of flagella with serines was carried out by CK2. CK2 is a constitutively active serine/threonine protein kinase. The CK2 holoenzyme is composed of two 44 kDa catalytic α and/or α' -subunits and two 26 kDa regulatory β -subunits to form stable heterotetramers [289]. The phosphorylation of flagella on E8+C+S8, E8CS8 and D8CS8 was shown on Figure 5. 1. We also displayed a GPSGPSGPSGPSGPSGPSGPS (termed GPS) peptide on flagella as a control. All flagellar proteins in this study were adjusted to the same concentration (2 mg/ml) before loading to SDS-PAGE gel and loaded the same volume to each well. The GPS flagella cannot be phosphorylated by CK2. The total intensity for each band was analyzed by Glyko Bandscan software. The relative intensity for each band was different indicating the variation of relative phosphorylation level over the total amount of protein for different bioengineered flagella. D8CS8 flagella were highly phosphorylated by CK2. E8CS8 flagella were less phosphorylated. However, the intensity of E8+C+S8 flagella band was much less than D8CS8 and E8CS8 ones. The phosphorylation of serine by CK2 is determined by multiple acidic residues located at positions between -2 and +5. The general recognition motif includes SXXE/D. However, SXE/D, S/D and some variations of these sequences could also be phosphorylated by CK2 [290]. At the same time, aspartic acid exhibited higher substrate activity than glutamic acid [291]. In this study, after glutamic acids were replaced by aspartic acids, higher phosphorylation was also observed. Because there is only one glutamic acid at position -2 to serine on E8+C+S8 flagella sequence, this sequence may not be an ideal substrate for CK2 and resulted in low phosphorylation level.

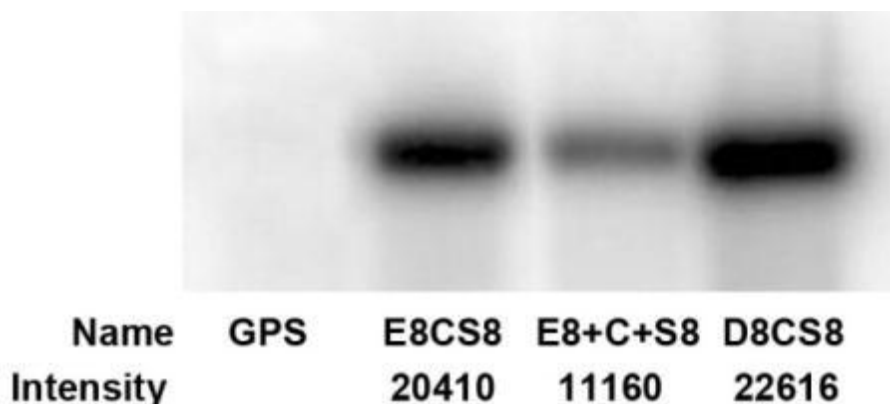


Figure 5.1: Phosphorylation of bioengineered flagella by CK2. Due to the specific requirement for CK2 substrates, GPS cannot be phosphorylated as a control. The total intensity for each band was calculated by Glyko Bandscan software.

The purified flagella were incubated within 4 mM supersaturated HAP solution for 3 days at room temperature. The nucleation of calcium phosphate minerals on flagella before and after phosphorylation by CK2 was depicted on Figure 5. 2. Higher magnification of phosphorylated flagella after biomimetic nucleation was shown on Figure 5. 3. Much less minerals were nucleated on D8CS8 flagella than E8+C+S8 and E8CS8 flagella (Figure 5. 2A). SAED analysis confirmed that most of flagella are only nucleated by a layer of amorphous minerals and some flagella were nucleated by crystal minerals. After phosphorylation, much more calcium phosphate minerals were nucleated on surface of flagella and exhibited high intensity of SAED pattern. The characteristic (002) and (211) planes indicate that the polycrystalline minerals are composed of HAP (Figure 5. 2B). Before phosphorylation, the nucleation of inorganic minerals on E8+C+S8 and E8CS8 flagella was similar. However, SAED analysis indicated more HAP nanocrystals nucleated on E8+C+S8 flagella (Figure 5. 2C, E). E8+C+S8 flagella exhibited curly morphology but E8CS8 flagella are straighter. After phosphorylation, the nucleation ability of calcium phosphate minerals were highly increased on both of E8+C+S8 and E8CS8 flagella. Most of flagella surfaces were covered by a layer of calcium phosphate minerals (Figure 5. 2D, F). Some bundle-like structures could be observed on high concentration of bioengineered flagella which may be caused by the formation of disulfide bond between neighboring flagella (Figure 5. 2D, F). Kumara et al

also demonstrated bundles of flagella by display of cysteine residues on their surface with constrained peptide loops [292]. Because the contrast under TEM is low on amorphous of inorganic minerals nucleated flagella, not much bundle-like morphology can be clearly observed on E8+C+S8 and E8CS8 flagella prior phosphorylation and on D8CS8 flagella.

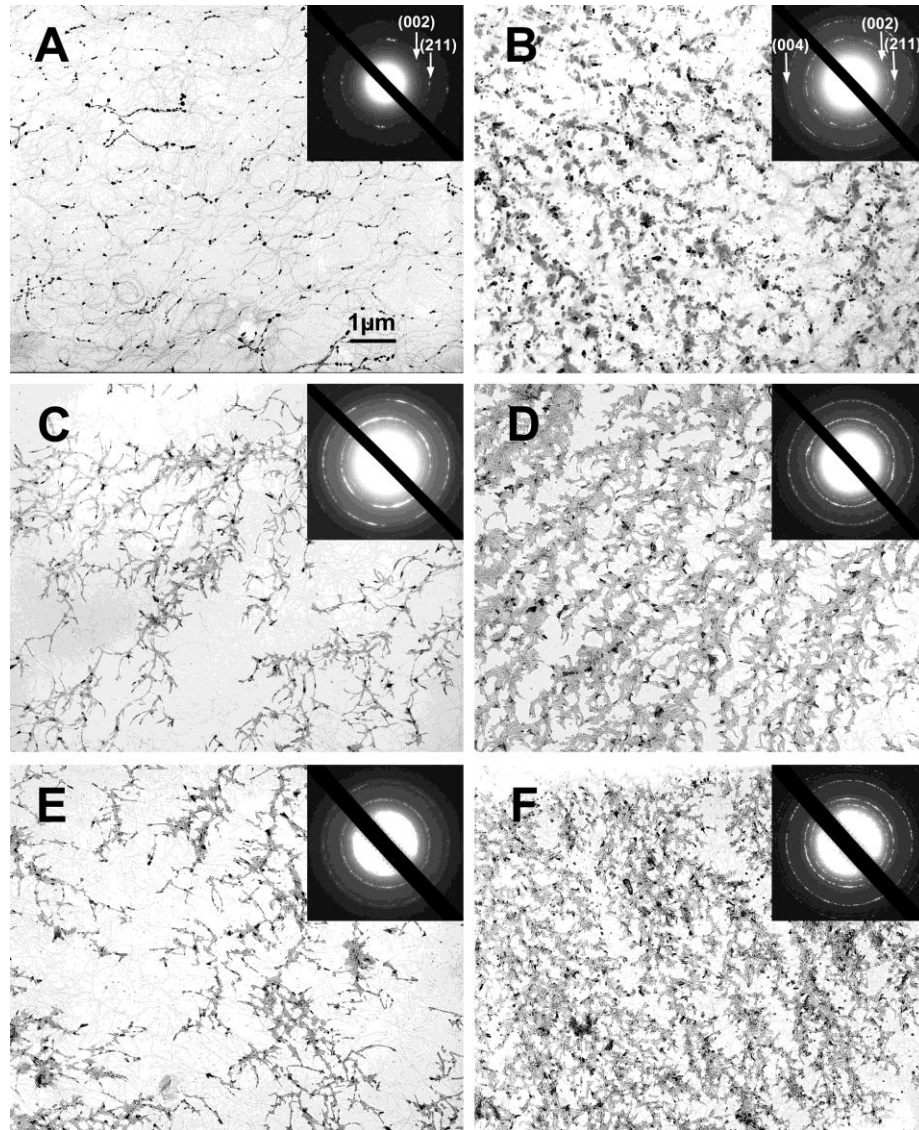


Figure 5.2: TEM images of bioengineered flagella after biomimetic mineralization in supersaturated HAP solution with prior and after phosphorylation. Biomimetic mineralization of D8CS8 flagella before A) and after B) phosphorylation; Biomimetic mineralization of E8+C+S8 flagella before C) and after D) phosphorylation; Biomimetic mineralization of E8CS8 flagella before E) and after F) phosphorylation. Scale bar is for all images.

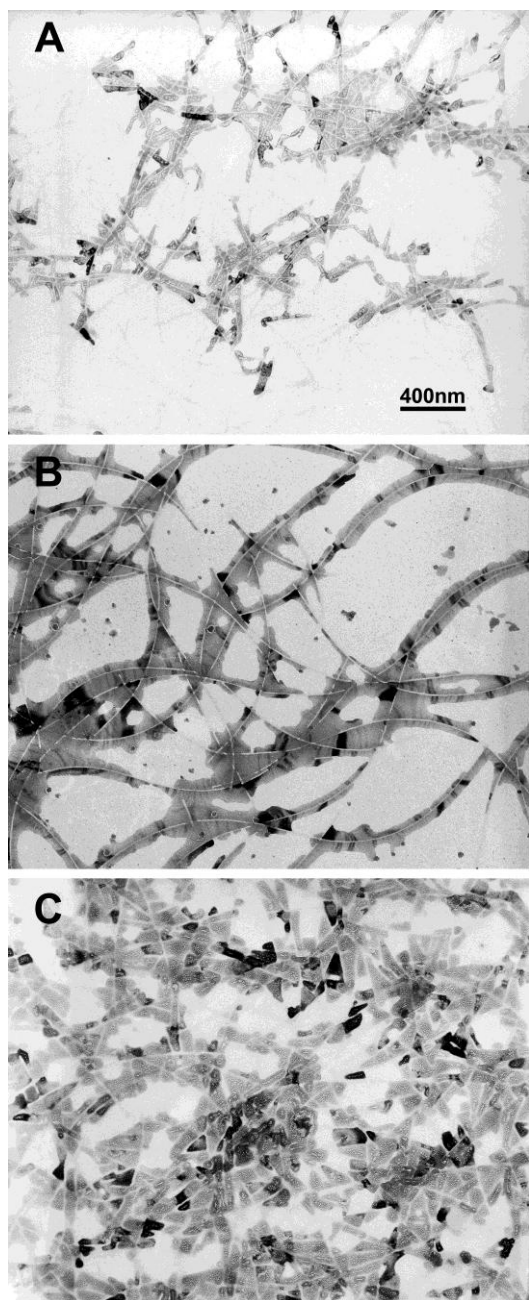


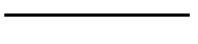


Figure 5.3: High magnification of mineralized flagella after phosphorylation. A) D8CS8; B) E8+C+S8; C) E8CS8.

Poly-L-glutamic acids could accelerate the precipitation of HAP and brushite [293]. The distance between two anionic groups is about 6.0—8.0 Å in poly-L-glutamic acid and the intercationic distance in HAP is ranging from 3.4 to 10.3 Å depending on the crystal faces. It is proposed that the distance between the negatively charged functional groups

matches intercationic distances of the precipitating crystals [294]. Moreover, the conformation of the peptide is of great importance in the formation of HAP. Poly (L-glutamic acid) and poly (D-glutamic acid) can induce the formation of HAP in a steady-state agarose gel system. However, poly (L-aspartic acid) does not have the ability [159]. Poly-glutamic acids exhibited helix confirmation but poly-aspartic acids might be random coil confirmation [159, 295]. In this study, the secondary structures of the inserted peptides were also analyzed by online tools of PSIPRED Protein Structure Prediction (Table 5. 1). Partial helix confirmation was given by both of E8+C+S8 and E8CS8 peptides but not by D8CS8. They may still process the similar confirmation after displayed on surface of flagella.

Peptide sequences	EEEEEEECSSSSSS SS	ESESESESCSESESE S	DSDSDSDSCDSDS DSDS
secondary structure	CHHHHHHHHHHCC CCCC	CCCHHHHHHHHHH HHCC	CCCCCCCCCCCC CCCCC
schematic diagram			

H: Helix; C: Coil

Table 5.1: Secondary structure prediction of peptides displayed on flagella.

In vivo, many NCPs including OPN, OCN, BSP, Dentin Sialoprotein (DSP), DPP, DMP1 and bone acidic glycoprotein 75 (BGA 75) as well as collagen were phosphorylated in mineralizing systems (bone and dentin) and appeared just prior or during mineralization [296]. The non-mineralizing systems (tendon and skin) also contain NCPs. However, they are not or much less phosphorylated [297]. After phosphorylation, the bioengineered flagella exhibited enhanced ability to nucleate HAP nanocrystals. At the same time, the morphology of flagella resemble fibrils of type I collagen in bone. The mineralized bioengineered flagella by HAP are similar to the lowest level of hierarchical organization of bone. They may potentially be an ideal building block for fabrication 2 or 3 dimensional (2D or 3D) scaffold from the bottom up for bone tissue engineering.

Chapter 6 Assembly of Bioengineered Flagella/Collagen Hybrid with Biomimetic Mineralization

6. 1 Introduction

As a bone substitute material, collagen has been studied extensively [272, 298]. In order to fabricate bone-like composites with improved mechanical properties and enhanced biocompatibility, a series of strategies have been developed for synthesis of collagen/HAP hybrid which mimic the natural composition of bone using the self-organization mechanism [299]. The mineralized type I collagen with nano-crystalline HAP exhibited good biocompatibility and bioactivity to BMSCs [272]. Previously, type I collagen is only considered a confined framework for mineral deposition. However, FTIR and circular dichroism (CD) measurement revealed that collagen itself can bind to HAP by chelating Ca^{2+} on carbonyl groups [221, 299]. It is well established, collagen limited to induce apatite formation from metastable calcium phosphate solutions directly. Non-collagen proteins such as BSP [300], DMP1 [301] and OPN [302] play an important role in initiating nucleation of calcium phosphates after binding to collagen matrix. Most recently, Nudelman et al reported inhibitors of HAP nucleation (polyaspartic acid or fetuin) can actively control mineralization of collagen [303].

On the other hand, the integration of bone materials at the interface with bone tissue is also important. If the implant materials are not chemically or biologically bonded with bone tissue, the so-called “inflammation” process will be invoked leading to a non-adherent fibrous capsule around them. Finally, the fibrous tissue result in failure of implants [304]. Lee and co-workers identified a dual functional motif from OPN named collagen-binding motif (CBM, GLRSKSKKFRRPDIQYDPATDEDITSHM) which can specifically bind collagen without chemical conjugation as well as promote apatite nucleation *in vitro* and *in vivo* [282]. After assembled with CBM, collagen-CBM composite can be applied as a bioactive scaffold for bone regeneration. Some polymers have been modified their surface to exhibit bioactivity as tissue engineering scaffold [305, 306]. With surface display technique, naturally occurring materials including phage and spider silk also present bioactivities after bioengineered by bioactive ligands such as RGD (Arg-Gly-Asp) [307-309]. Recently, we reported the osteogenic growth peptide

displayed on M13 phage can accelerate proliferation and differentiation of BMSCs into osteoblasts [194]. We also displayed acidic polyaspartic acid and collagen-like peptide on surface of flagella which can promote nucleation of HAP on their surface and induce early differentiation of BMSCs toward osteoblasts in osteogenic media.

In this report, CBM peptide was displayed on surface of flagella. After mixed with type I collagen, bioengineered flagella formed a new type of fibril with type I collagen. The HAP forming ability of the composite was enhanced in supersaturated HAP precursor solution. The morphology of BMSCs on the flagella/collagen composite was examined by bright field microscopy and SEM.

6. 2 Materials and Methods

6. 2. 1 Surface display of flagella and bioengineered flagella isolation:

Genetically display a foreign peptide on flagella has been described elsewhere [16]. Briefly, the original vector pLS411 contains the gene of *FliC* with a multicloning site including restriction enzymes of *Xho* I and *Bgl* II located in the hypervariable region was digested (New England Biolabs) at 37 °C for 2 h. Then, primers corresponding to encode CBM peptide were synthesized (Invitrogen) with restriction sites of *Xho* I and *Bgl* II at the ends. The synthesized oligonucleotides were inserted in the linearized vector pLS411 by T4 ligase and transformed into competent cell of *FliC* deficient *Salmonella* SL5928. Strain SL5928 is an *aroA* live-vaccine strain of *Salmonella* Dublin. Because its only *FliC* gene- *FliC*(g,p) has been replaced via transduction by *FliC*(i)::Tn10, an allele inactivated by transposon insertion, the functional flagella cannot be expressed. Finally, the ampicillin-resistant clones with recombinant plasmid were selected and confirmed by sequencing. Because only the bacteria with functional flagella can swim in the semisolid medium, the clones were cultured in semisolid medium (1 % tryptone; 1.5 % NaCl; 0.35 % agar) for cell motility test to confirm assembly of recombinant flagella.

The bioengineered bacterial flagella were detached from the bacterial cells by vigorous shaking through vortex with highest speed for 3 times (30 sec/each time). The supernatant containing the sheared flagella was separated by centrifugation at 12,000 g for 20 min. The flagella were precipitated at 100,000 g for 2 h and dissolved in ddH₂O.

6. 2. 2 Assembly of bioengineered flagella/collagen hybrid and biomimetic nucleation:

Type I collagen solution (~4 mg/ml) was diluted 1:20 with 20 mM acetic acid. 300 µl of flagella (800 µg/ml) was mixed with same volume of type I collagen and incubated at 37 °C for 1 h. The mixture was then neutralized by PBS and incubated at 37 °C for 5 h.

Supersaturated HAP solution (4 mM) was prepared as described from HAP power (Sigma). 20 µl of the mixture of flagella and collagen was mixed with 500 µl of supersaturated HAP solution and incubated for 3 days at room temperature. For TEM sample preparation, a drop of aqueous solution was mounted on the carbon TEM grid. After carefully rinsed with double distilled water and dried at room temperature, these grids were subjected to TEM (Zeiss 10) measurements operated at 80 kV.

6. 2. 3 BMSCs isolation and culture:

Primary BMSCs were isolated from the bone marrow of young adult female femur of Fisher 334 rats (Harlan) based on previously described method [33]. Briefly, the isolated bone marrow cells are washed several times with Dulbecco's Modified Eagle Medium (DMEM; GIBCO BRL, Grand Island, NY, USA). After cell viability tested and the density of the cells confirmed using trypan blue staining, cells were maintained in DMEM (low glucose) supplemented with 10 % fetal bovine serum (FBS) (Invitrogen), penicillin G 100 U/mL, streptomycin 100 µg/mL, amphotericin B 0.25 µg/mL. The cells were incubated in humidified atmosphere containing 5 % CO₂ at 37 °C. The non-adherent cells were removed after three days by changing the culture media. The BMSCs passaged no more than three times after isolation before use.

6. 2. 4 SEM examination:

BMSCs were seeded on flagellar film at a density of 1×10^4 cells/mL. After cultured for 24 h, the cells were washed with $1 \times$ PBS and fixed with 2.5 % glutaraldehyde in $0.1 \times$ PBS for 1 h. The cells were washed again with $1 \times$ PBS and then dehydrated in a graded series of ethanol (50 %, 70 %, 90 %, and 100 % respectively) for 30 min each. The samples were further dehydrated by a supercritical point CO₂ dryer. The morphology of BMSCs on flagellar film was observed using SEM (XL30, FEI Corporation).

6. 3 Results and Discussions

Bacterial flagellum has a linear structure about 10-20 μm in length with an outer diameter of 12-25 nm and an inner of 2-3 nm. It is composed of several thousand copies of the eubacterial *FliC*s major protein and some other proteins including a pentamer of the tip-associated *FliD* protein. Bacterial flagellar *FliC* monomers naturally self-assembled into a linear tube with a repeat of about 11 monomers per two turns via non-covalent interactions between α -helical and coiled-coil motifs [310]. The N- and C- terminal region of *FliC* face to the center of the tube and they are highly conserved. However, in the central region of *FliC*, the amino acid sequences are highly variable and surface-exposed. Based on genetic approach, a foreign peptide can be inserted into the variable region of *FliC* [81]. Sequence as long as 302 amino acid residues were successfully displayed on the surface of flagella, without preventing flagellar polymerization and function [232]. Based on this characteristic, a long peptide-CBM with 28 amino acids was displayed on surface of flagella.

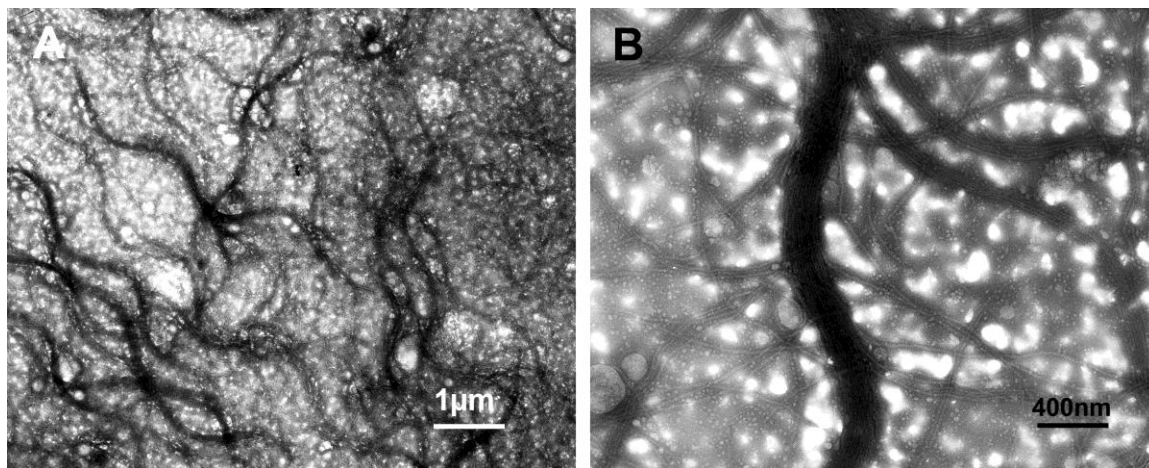


Figure 6.1: TEM micrographs of flagella/collagen composite A) low and B) high magnification.

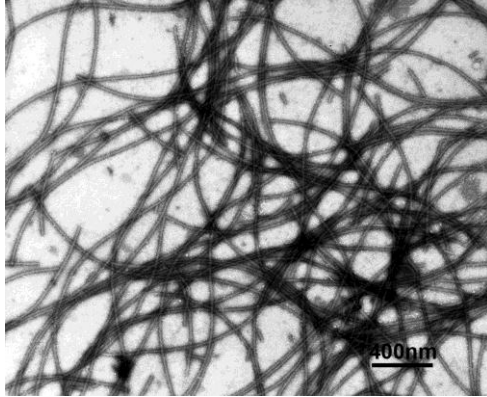


Figure 6.2: TEM micrographs of flagella with CBM. No bundles were observed.

Type I collagen was kept at 20 mM acetic acid to prevent aggregation. The pH is about 3.2. Because the flagella are stable at pH 2-10, the flagella will not depolymerize after mixed with type I collagen. After neutralized by PBS, type I collagen started to self-assembly under entropy-driven process [311]. At the same time, due to the surface of flagella were displayed with CBM flagella combined with collagen and copolymerized into bundles (Figure 6. 1). The bundle exhibited curly morphology which is like morphology of flagellum. The diameter of the bundles can be up to 100 nm. There are still some free flagella in the solution (Figure 6. 1A). At higher magnification, bundled flagella/collagen composite exhibited parallel structures with some branches and these bundles did not exhibit characteristic *D*-periodic cross-striated structures of type I collagen fibrils (Figure 6. 1B). Flagella without collagen did not form into bundles in PBS (Figure 6. 2). Interestingly, after incubated in supersaturated HAP solution, these bundles became “straight” and calcium phosphates nucleated on the surface of bundles (Figure 6. 3). SAED revealed that these calcium phosphates are composed of HAP and the orientation of crystallographic *c*-axes of HAP parallel to the long axes of the flagella/collagen bundles (Figure 6. 3A insert). In a control experiment, type I collagen fibrils without flagella also nucleated by a layer of calcium phosphates. However, SAED revealed that most of these minerals are amorphous (data not shown).

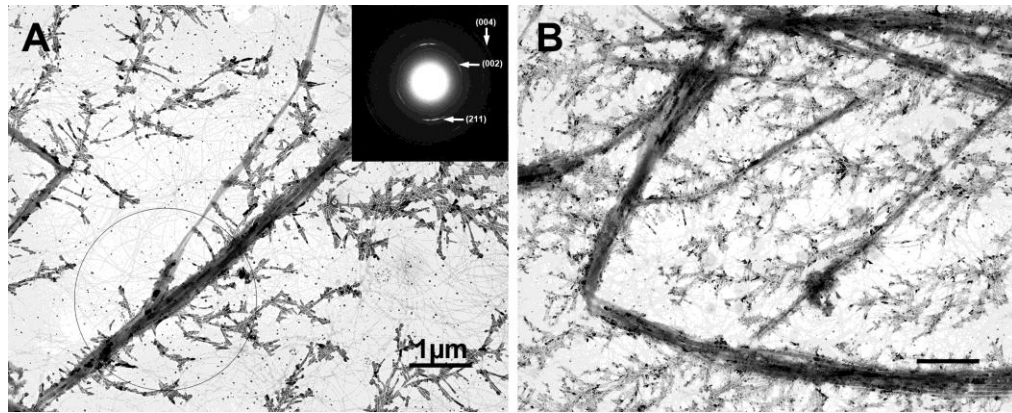


Figure 6.3: TEM micrographs of flagella/collagen hybrid mineralized in supersaturated HAP solution. Inset is the SAED patterns taken from the highlighted section.

It is well established that BMSCs can sense the environment including topographies and surface chemistry during further differentiation [224, 309]. The flagella/collagen composite was coated on plastic cell culture plate. BMSCs were then seeded on surface of the scaffold for 24 h. The morphology of BMSCs was observed by bright field microscopy and SEM. Figure 6. 4 shows the morphology of BMSCs on flagella/collagen composite (Figure 6. 4A) and plastic cell culture plate (Figure 6. 4B) respectively. BMSCs acquired well-spreading morphology on flagella/collagen composite. Some of the cells exhibited spindle-like or bipolar morphology which may attached on flagella/collagen bundles. The “stretched” morphology of BMSCs was proposed by “contact guidance response” [229]. SEM micrographs of BMSCs also revealed similar morphology to the ones under bright field light microscopy (Figure 6. 5). The bundles formed by flagella/collagen co-assembly can be clearly observed (Figure 6. 5A). BMSCs anchored on the substrates by filopodia-like extensions (Figure 6. 5B).

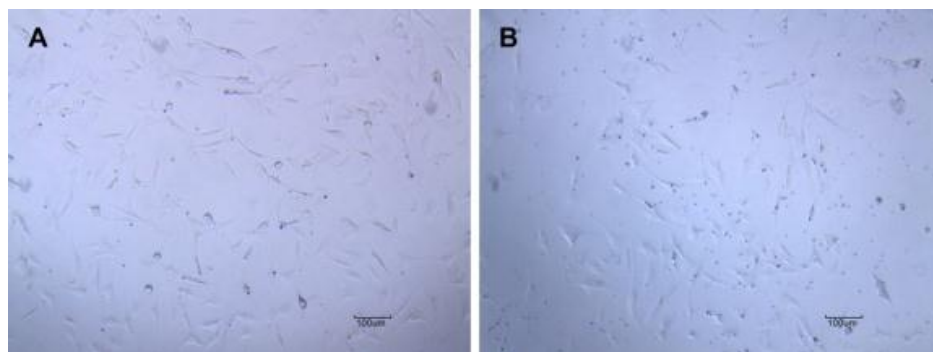


Figure 6.4: Bright field microscopy images of BMSCs on flagella/collagen composite (A) and plastic cell culture plate (B).

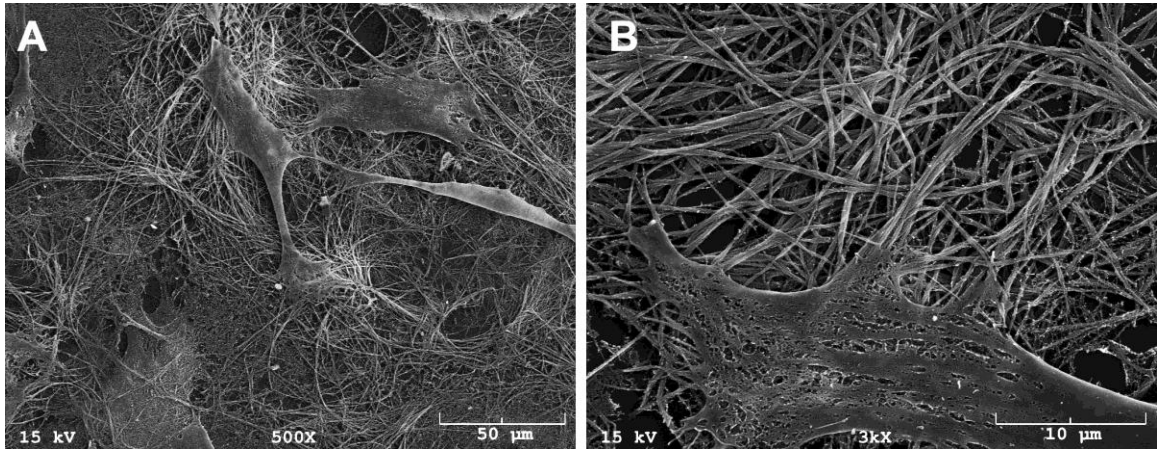


Figure 6.5: SEM micrographs of BMSCs on flagella/collage composite (A); higher magnification (B).

In conclusion, the bioengineered flagella with CBM and collagen can form new type of bundles by co-assembly. The ability of HAP nucleation was highly enhanced on flagella/collagen composite. This composite can support BMSCs adhesion and growth. It may be used as a promising nanocomposite for bone tissue engineering.

Chapter 7 Morphology-Controlled Synthesis of Silica Nanotubes through pH-Sensitive Flagella

7. 1 Introduction

Due to their intrinsic biocompatibility, hydrophilic nature and customizability via simple chemical modifications due to the accessibility of both inner and outer walls, silica nanotubes (SNTs), have gained much attention among a variety of inorganic nanotubes in the last few decades [312, 313]. SNTs have potential applications as chemosensors, adsorbents[314], biosensors [315] and nanoscale reactors [316] as well as in areas such as biospearation, biocatalysis [313, 317] and gene delivery [318]. Among the various strategies and techniques that have been employed to synthesize SNTs, the template-directed synthesis of SNTs exhibits some merits. For example, the dimensions and morphology of the SNTs can be finely controlled through precise manipulation of the templates. The thickness of the silica wall can also be manipulated by tuning the concentration of a precursor solution such as TEOS and the reaction time. Usually, the reaction can be carried out under mild conditions. After the SNTs have been synthesized, the templates can be removed by extraction, heat treatment or chemical reactions. Quite different morphologies and unique surface characteristics of SNTs have been developed based on various templates with examples including straight, helical, curly, chiral, double chiral and pearl-necklace-like SNTs [142, 319-322].

The synthesis of template-based SNTs can be divided into three main categories: inorganic template-directed, organic template-directed and biomolecular template-directed [313]. In nature, there is a great source of biological systems with well-defined structures and complex morphologies which are potentially suitable for the fabrication of inorganic materials. In recent years, biological template-directed synthesis of inorganic materials has gained much attention. Indeed, tobacco mosaic virus (TMV), DNA, peptides and collagen have all been used as templates for SNTs synthesis [323-327]. Hybrid organic-inorganic SNTs with multiple layers have been generated using a lipid template. Multiple layers of SNTs were generated using lipid as a template [328]. In our research, we have utilized flagella, naturally occurring bionanotubes which enable bacteria to swim in aqueous environments, in the synthesis of SNTs. Recently, we

synthesized pearl-necklace-like 1 dimensional (1D) SNTs with uniform diameter using flagella as templates. We also discovered that by modifying the peptide sequence displayed on the flagella surface we can obtain novel morphologies of SNTs [142]. Thus, herein, we expand upon our previous research on utilizing wild type and genetically engineered flagella at different pHs to control the morphology of SNTs.

Flagella filaments have an outer diameter of 12-25 nm and an inner diameter of 2-3 nm. The bacterial flagellum is mainly self-assembled from more than 20,000 copies of identical protein subunits called eubacterial *FliC*s. By intermolecular non-covalent interactions, *FliC* monomers assemble into a linear hollow nanotube with a repeat of 11 monomers per 2 turns [329]. The N- and C- terminal regions of *FliC* located in the center of flagellum bind together by non-covalent interactions and are highly conserved. In contrast, the central regions (D2 and D3 domains) of *FliC*, which are exposed to the surface of flagellum, are highly variable. Some amino acid sequences of *FliC* can be replaced with other functional sequences without losing their self-assembly properties[250]. Unlike other chemically modified nanotubes, such as carbon nanotubes, genetically engineered flagella nanotubes, theoretically, can be designed to display a functional peptide at every monomer-*FliC* at the surface-exposed region, achieving precise control and homogeneous surface modification.

Flagella are very rigid with a modulus of rigidity about 1×10^{11} dyn/cm² [279]. At neutral pH, they exhibit helical structures. When dried on substrate, they flatten to a curly morphology with a sinusoidal wave. The wavelength is constant for each specific strain. Some mutant strains also produce flagella with curly morphology but shorter wavelengths while other mutant strains give rise to straight morphology [330]. The flagella can be depolymerized into monomers by acid or heat treatment (over 60 °C). Repolymerization can be induced by exposing monomers to high anion concentrations, which cause the monomers to be “salted-out”, or to flagella fragments, which serve as seeds upon which monomers can assemble. Flagella can exhibit various stable conformations depending on their environment and constituent monomers. This property is referred as the “polymorphism of flagella” [330, 331]. Both environmental conditions, such as pH, salt concentration, and temperature, and the strain and ratio of *FliC*

monomers to be mixed for copolymerization can be tuned to observe various morphologies of bacterial flagella [164, 332-334]. Interestingly, we observed helical morphological variations of bioengineered flagella that displayed peptides with different charges [142]. In this study, the effects of pH and various peptides displayed on flagellar surfaces on the morphology and surface features of SNTs were investigated.

7. 2 Materials and Methods

7. 2. 1 Flagella display and purification of flagella:

The same procedure as our previous report was followed for the flagella display [142]. The oligonucleotides which encode target peptide with complementary sequences were designed and synthesized (Invitrogen). The primer and encoded peptide sequences are summarized in Table 7. 1. The oligonucleotides also contain sticky ends of *Xho* I and *Bgl* II sites at the 5'-end and 3'-end, respectively and were annealed into double-stranded DNA. The resultant double strand oligos were then inserted into vector pLS411 which contains *FliC* gene with a multicloning site in the central region. The recombinant vector was transformed into competent cell of *Salmonella* SL5928-a *FliC* gene knock out strain. Individual colonies were inoculated on agar plate with ampicillin (AMP) (100 µg/ml) and the recombined plasmids were confirmed by DNA sequencing (MCLAB). The recombinant strains were cultured in LB media with AMP (100 µg/ml) at 37 °C with shaking (250 rpm) until OD to 0.6-0.8. The cell culture was collected and centrifuged at 6000 g for 20 min at 15 °C. The pellets were then washed twice by PBS buffer (pH=7.4). Finally, the cell pellet was resuspended in deionized water and cooled in an ice-bath. The flagella were detached from the cells by vortex mixer at highest speed for 3 min and then subjected to centrifugation at 6000 g for 20-30 min to remove bacteria. The supernatant containing detached flagella was collected. The supernatant was centrifuged again at 10,000 g for 20 min to remove debris from solution. High purity flagella were precipitated by ultra-centrifugation at 80,000 g for 2 h. Finally, the flagella were dissolved in deionized water and kept at -20 °C for further usage.

Table 7.1: Inserted sequences in recombinant plasmid

Name	Oligonucleotides	Encoded peptide sequences
------	------------------	---------------------------

E8+C+S8	5' -GA TCT GAA GAG GAA GAG GAA GAG GAA GAA TGT AGT AGC AGT AGC AGT AGC AGT AGC C-3' 5' -TC GAG GCT ACT GCT ACT GCT ACT GCT ACT ACA TTC TTC CTC TTC CTC TTC CTC TTC A-3'	EEEEEEECSSSSSSSS
E8CS8	5' -GA TCT GAA AGT GAG AGC GAA AGT GAG AGC TGT GAA AGT GAG AGC GAA AGT GAA AGC C-3' 5' -TC GAG GCT TTC ACT TTC GCT CTC ACT TTC ACA GCT CTC ACT TTC GCT CTC ACT TTC A-3'	ESESESECESESESES
D8CS8	5' -GA TCT GAT AGT GAC AGC GAT AGT GAC AGC TGT GAT AGT GAC AGC GAT AGT GAC AGC C-3' 5' -TC GAG GCT GTC ACT ATC GCT GTC ACT ATC ACA GCT GTC ACT ATC GCT GTC ACT ATC A-3'	DSDSDSDSCDSDSDS
GPP8	5' - GA TCT GGA CCA CCT GGT CCA CCT GGT CCT CCA GGT CCA CCT GGA CCA CCT GGT CCA CCT GGT CCT CCA GGT CCA CCT C-3' 5' - TC GAG AGG TGG ACC TGG AGG ACC AGG TGG ACC AGG TGG TCC AGG TGG ACC TGG AGG ACC AGG TGG ACC AGG TGG TCC A-3'	GPPGPPGPPGPPGPPGPPGPPGPPGPP
N-terminal	5' -GA TCT CAG CTG TCT TAT GGC TAT GAT GAG AAA TCA ACC GGA GGA ATT TCC GTG CCT C-3' 5' -TC GAG AGG CAC GGA AAT TCC TCC GGT TGA TTT CTC ATC ATA GCC ATA AGA CAG CTG A-3'	QLSYGYDEKSTGGISVP
C-terminal	5' -GA TCT CAG CGC TGG TTT CGA CTT CAG CTT CCT GCC CCA GCC ACC TCA AGA GAA GGC TCA CGA TGG TGG CCG CTA C-3' 5' -TC GAG TAG CGG CCA CCA TCG TGA GCC TTC TCT TGA GGT GGC TGG GGC AGG AAG CTG AAG TCG AAA CCA GCG CTG A-3'	SAGFDFSFLPQPPQEKAHDGGRYIRA
E8	5' -GA TCT CGA GGT GAT GAA GAG GAA GAG GAA GAG GAA GAA C-3' 5' -TC GAG TTC TTC CTC TTC CTC TTC CTC TTC ATC ACC TCG A-3'	EEEEEEEE
N-Zone	5' -GA TCT GGT TTG GAT GGT GCC AAG GGA GAT GCT GGT CCT GCT GGT CCT AAG GGT GAG CCT GGC AGC CCT GGT GAA AAT C-3' 5' -TC GAG ATT TTC ACC AGG GCT GCC AGG CTC ACC CTT AGG ACC AGC AGG ACC AGC ATC TCC CTT GGC ACC ATC CAA ACC A-3'	GLDGAKGDA GPAGPKGEPGSPGEN
C-Zone	5' -GA TCT GGA CCC CAA GGC CCA CGT GGT GAC AAG GGT GAG ACA GGC GAA CAG GGC GAC AGA GGC ATA AAG GGT CAC CGT C-3' 5' -TC GAG ACG GTG ACC CTT TAT GCC TCT GTC GCC CTG TTC GCC TGT CTC ACC CTT GTC ACC ACG TGG GCC TTG GGG TCC A-3'	GPQPGDGETGEQDGRGIKGHR

KGG4	5' -GA TCT AAA GGC GGT AAA GGC GGT AAA GGC GGT AAA C-3' 5' -TC GAG TTT ACC GCC TTT ACC GCC TTT ACC GCC TTT A-3'	KGGKGGKGGKGG
KS	5' - GA TCT AGC AGC AAA AAG AGC GGT AGC TAC AGC GGT AGC AAA GGT AGC AAA C -3' 5' - TC GAG TTT GCT ACC TTT GCT ACC GCT GTA GCT ACC GCT CTT TTT GCT GCT A-3'	SSKKSGSYSGSKGSK

7. 2. 2 Synthesis of silica on wild type and bioengineered flagella templates:

The method follows our previous report [142] with some modifications. APTES (2×10^{-3} mmol) was mixed and agitated gently with flagella solution (500 mL) by vortex mixer. Then, the pH of the solution was adjusted to set value by HCl or NaOH and cooled in an ice-water bath for 3–5 min. TEOS (2.5×10^{-2} mmol) was added while stirring for at least 3 min. The mixed solution was left in ice-water bath for ~30 min and then aged at room temperature for 8 hr. Because the condensation of TEOS is slow at acidic conditions, longer ageing time (24 h) was applied to solutions of lower pH. The white precipitates were centrifuged at 5000 g for 10 min and washed with ethanol and water several times. The samples were mounted on TEM grids and subjected to examination by TEM (Zeiss 10).

7. 3 Results and Discussion

All bioengineered strains were sequenced at each step to confirm the correct inserts. We observed that the expression of some strains of bioengineered flagella, namely those that were modified to display positively charged amino acids, was severely reduced. That is, for these strains, we observed fewer flagella per bacterium or shortened flagella than on wild type strains. These under-expressed strains were cultured on cell-motility media to select bacteria with best flagella expression. The bacteria that swam to the front edges with enhanced cell motility were inoculated for flagella purification. Finally, we successfully displayed 11 different peptides on surface of flagella. The peptide sequences displayed on all bioengineered flagella are summarized in Table 7. 1.

The formation of silica shell on flagella depends on the absolute rates of hydrolysis and condensation reactions of TEOS as well as the relative rate between these two reactions

[335]. The effect of pH on the hydrolysis and condensation of TEOS was studied [336]. The rate of hydrolysis is catalyzed in both acidic and alkaline conditions with a minimum rate at pH 7.0. The rate of condensation reaches a minimum at a pH of about 2.0. In this study, APTES was first mixed with flagella in aqueous solution then TEOS was added. The APTES should play dual role in directing transcription silica nanotubes on the flagella surface. First, according to the so-called “surface mechanism”, APTES adsorbs on the surface of flagella by hydrogen bonds or electrostatic interactions between the amino group of APTES and the functional groups on flagella surface [337]. The condensed APTES on flagella surface is hydrolyzed, giving rise to the formation of hydroxyl anions and form the thin layers of silica precursors, which serve as nuclei. After TEOS is added, these hydroxyl anions can then mediate the hydrolysis and condensation reactions of TEOS, resulting in the formation of silica shells. The solution pH increased to 10.40 after APTES, a week base, was added to the flagella solution. The alkaline environment promotes the condensation of TEOS. However, in acidic conditions (pH=2-5), hydrolysis of TEOS is favorable but condensation is the rate-determining step [336]. The APTES might not have significant effects on the polycondensation of silica shell. Because of the non-covalent interaction between APTES and flagellar protein on the surfaces, salt affects the binding of APTES on flagella. Different concentrations of NaCl were mixed with the flagella solution. However, no silica shell can be condensed on surface of flagella (data no shown). Moreover, high temperature will render heterogeneous polycondensation of TEOS. In this study, we focus on pH effects on morphology control and surface features of SNTs. In alkaline conditions (pH=8-11.5), after TEOS was added to the solution, white precipitates appeared in 15 min indicating the formation of silica shells on flagella. At pH higher than 11.5 it took less time for white precipitates to form. It took about 24 h in acidic conditions (pH=3-4) to form white precipitates. At pH lower than 3 and pH=5-7, no obvious precipitates could be observed (Figure 7. 1).

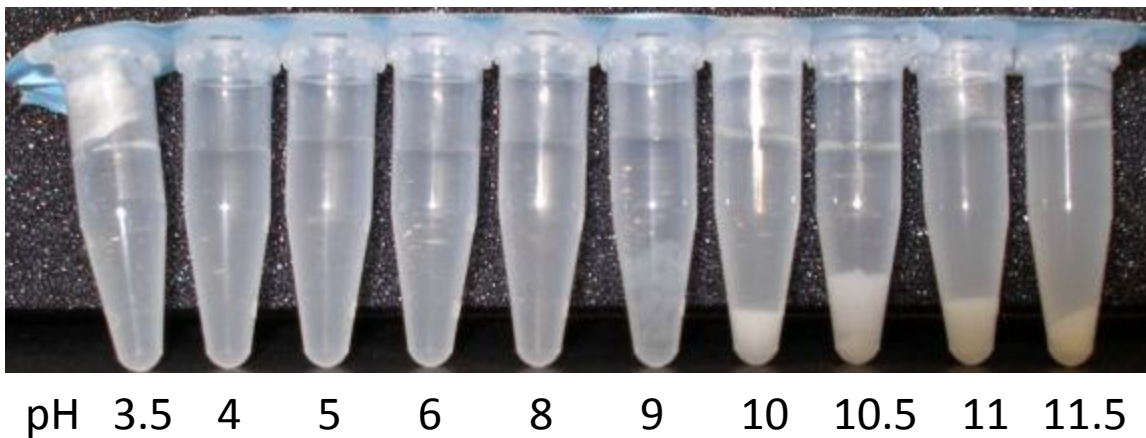


Figure 7.1: White precipitates formed after the reaction at different pHs. At alkaline condition, more precipitates can be observed.

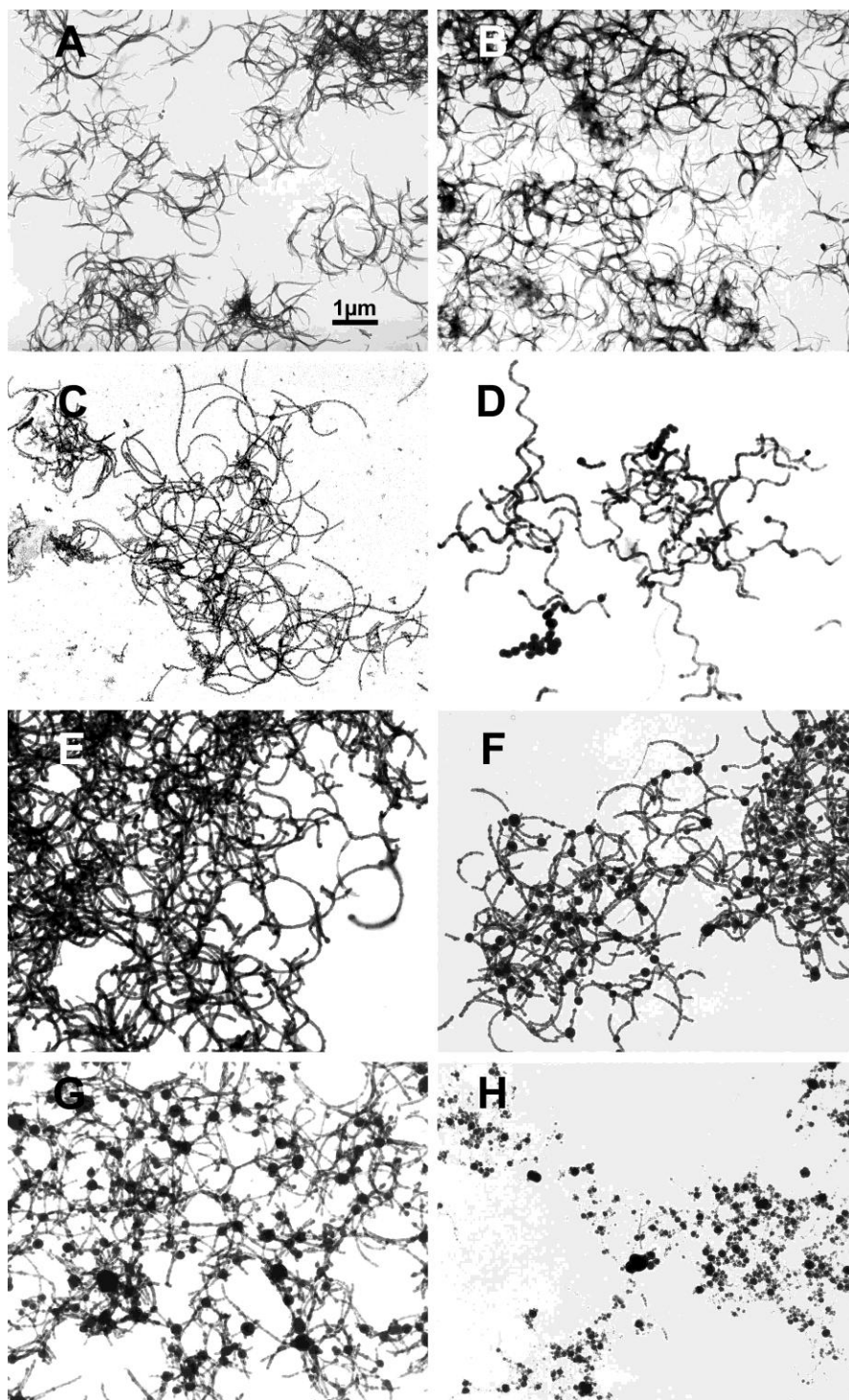


Figure 7.2: TEM images of the resulting silica nanotubes on wild type flagella templates at different pHs. A) pH=3.5; B) pH=4; C) pH=8; D) pH=9; E) pH=10; F) pH=10.5; G) pH=11; H) pH=11.5. Scale bar is for all panels.

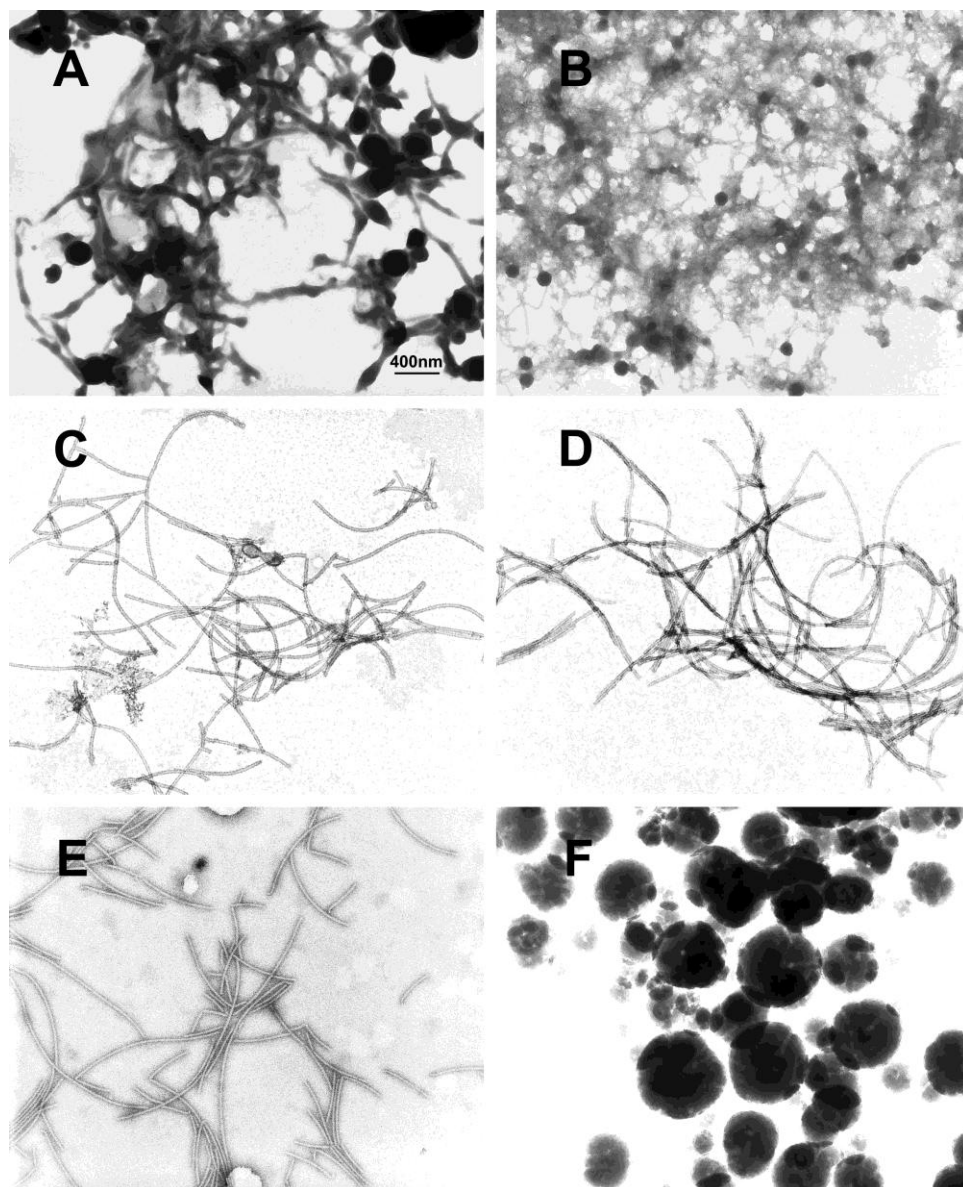


Figure 7.3: TEM images of precipitates formed at different pHs. A) At pH 2, some linear structures and large spherical nanoparticles were observed; B) At pH 2.5, nonspecific aggregation with spherical nanoparticles were precipitated. C) At pH 3, a very thin layer of silica nanoparticles was mineralized on flagella surface and most SNTs are separated. D) At pH 5, similar structure and morphology of SNTs were observed to the SNTs at pH 3 but most SNTs formed into bundles. E) At pH 6 or 7, only a thin layer of amorphous minerals nucleated on the surface of flagella. F) At pH 12, all flagella were degraded into small fragments and wrapped into spherical silica nanoparticles. Scale bar is for all panels.

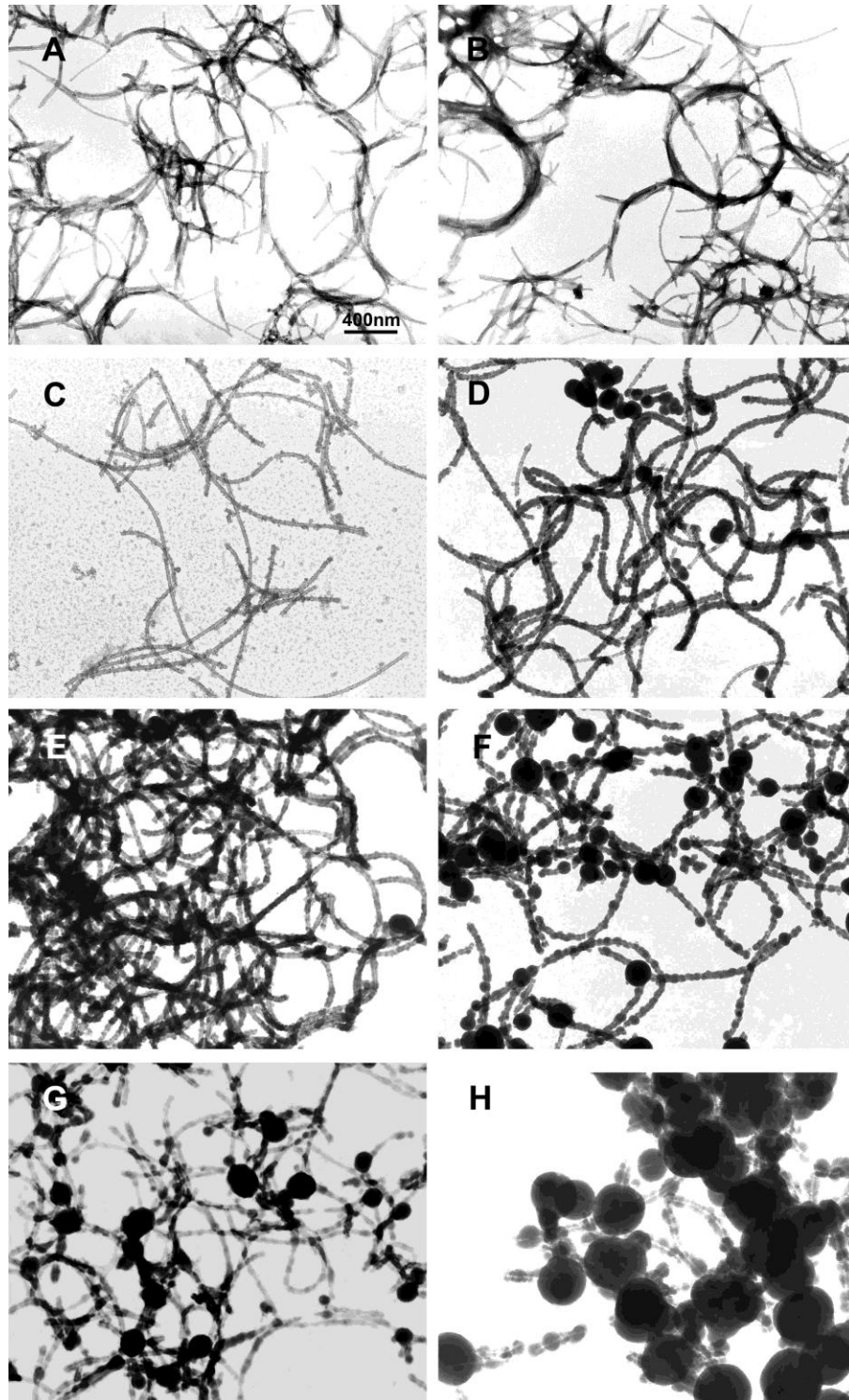


Figure 7.4: Higher magnification of SNTs on wild type flagella templates at different pHs. . A) pH=3.5; B) pH=4; C) pH=8; D) pH=9; E) pH=10; F) pH=10.5; G) pH=11; H) pH=11.5. Scale bar is valid for panels.

The different morphologies of SNTs based on wild type flagella at different pHs are shown in Figure 7. 2 and Figure 7. 3. High magnification of SNTs at different pHs is depicted in Figure 7. 4. Because bacterial flagella are stable at pH=2-10 [332], the effects of pH ranging from 3-11.5 on the morphologies and surface features of SNTs were investigated in this study. At $\text{pH} \leq 3$ or $\text{pH} > 11.5$, the flagella depolymerized and no tubular structures could be observed (Figure 7. 3). In acidic conditions ($\text{pH}=3.5-4$), the bundled SNTs appeared with a thin layer of silica nanoparticles coated on surface of flagella. More SNTs with curly morphology were observed at $\text{pH}=3.5$. Interestingly, there were a great amount of open cyclic silica bundles at $\text{pH}=4$ (Figure 7. 2A, B). At low pH, the hydrolysis of TEOS is catalyzed. The isoelectric point of wild type flagella is 5.3 [338]. The electrostatic interactions between APTES and flagella severely attenuated below $\text{pH}=5.3$. At this moment, the condensation of TEOS may generate on flagella surface directly. The neighboring flagella were bundled together by condensation reaction between hydroxyl anions on each flagellum (Figure 7. 3). In a control experiment, after TEOS was added to flagella solution without APTES at pH below 5.3, similar results was observed (data not shown). At $\text{pH}=5-7$, only a very thin layer of silica formed on surface of flagella, indicating low condensation of TEOS (Figure 7. 2). These results are consistent with previous reports [336, 339].

In alkaline conditions ($\text{pH}=8-11.5$), the polycondensation of TEOS is more favorable and tubular structures of SNTs are observed. At pH 8, polycondensation occurred on the flagella surface and in solution simultaneously. A thin layer of silica particles nucleated on surface of flagella which resulted in a relatively uniform but rough appearance (Figure 7. 2). At the same time, there were also free silica nanoparticles in the solution (Figure 7. 4C). Most of the SNTs exhibited characteristic sinusoidal waves of flagella, but some only exhibited curly morphology. This may have been due to broken flagella. When the pH was increased to 9, the SNTs also showed sinusoidal wave morphology but with a shorter wavelength than those formed at $\text{pH}=8$ (Figure 7. 2D). Some free silica nanoparticles formed on and off the flagella surface. At pH 10, almost all of SNTs were of curly or open cyclic morphology (Figure 7. 2E). At pH 10.5, most SNTs exhibited open cyclic morphology which are similar with our previous report [142]. Actually, after APTES (2×10^{-3} mmol) mixed with wild type flagella, the pH increased to ~ 10.40 . The

surface feature also exhibited pearl-necklace-like morphology with some more free spherical silica nanoparticles (Figure 7. 2F). At pH 11, both curly and straight morphologies of SNTs were observed. There were also some free spherical silica nanoparticles that condensed at intersections of SNTs (Figure 7. 2G). Some of the SNTs were interconnected with each other through large silica spheres. After pH was increased to 11.5, the flagella became unstable with most of the flagella depolymerizing and some being degraded into much shorter fragments (Figure 7. 2H). These short fragments were straight and coated with a layer of granular silica particles. The depolymerization and degradation may also have been caused by stirring the solution during the silica condensation process. In addition to the short fragments, a large number of spherical silica nanoparticles ranging from 40-300 nm with mesostructured interiors were observed.

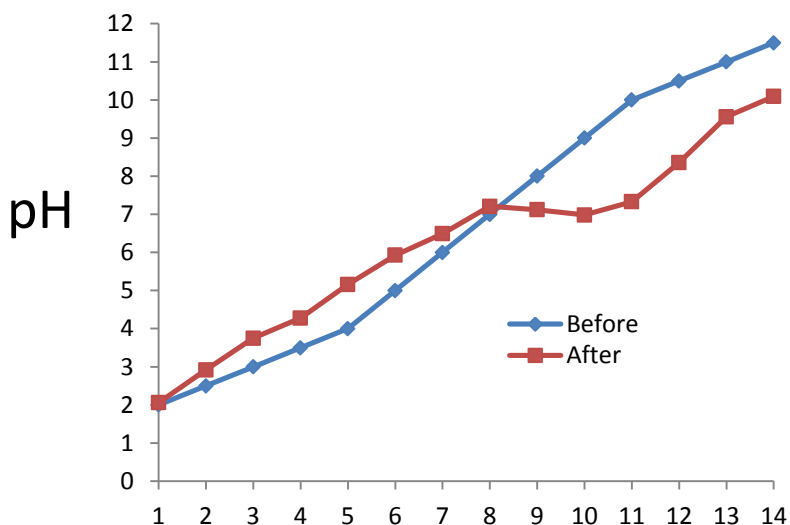


Figure 7.5: pH changes before and after the reaction.

The helical transformation of flagella at different pHs is rapid and the transformation is reversible. Almost all flagella exhibited identical morphology at specific pH [332]. However, we noticed that the morphology of SNTs at given pH was not very uniform. In the reaction, hydrolysis and condensation of TEOS had no effect on the value of pH [336]. In this study, the pH was adjusted to a specific value before TEOS was added. The pH changes during polycondensation of silica on flagella surface were monitored and are summarized in Figure 7. 5. Not only did the pH change after each reaction but the

magnitude and direction of each change also varied with different initial pH values. At pH 2 and 7, no obvious changes in pH were observed before and after the reactions. In acidic conditions, the pH increased after the reaction while the pH decreased in alkaline conditions after the reaction. The ranges of pH changes seems to correspond to the amount of silica precipitates. That more silica precipitates formed reflects that more APTES was involved in the reaction. The changes in pH during the reaction should have been mainly mediated by APTES as it was the only base in the solution. These changes in pH during the reaction explain the occurrence of heterogeneous morphology of SNTs in a single sample. During the reaction, the morphology of flagella is “fixed” by the silica shells. However, some flagella might not have silica shells condensed on their surface at the initial pH. Thus, these uncoated flagella can change their morphology as the pH of the solution changes, resulting in SNTs of aberrant morphology.

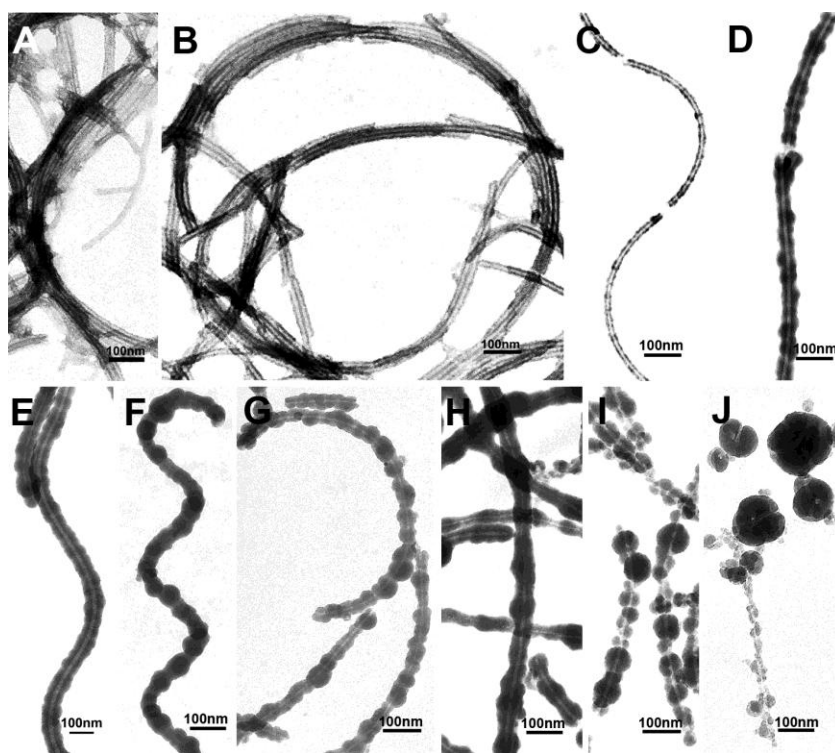


Figure 7.6: TEM images of different morphology with various surface features of SNTs on wild type flagella templates. A, B) At acidic conditions, bundled SNTs were formed; C-I) Different morphology and surface features of SNTs at alkaline conditions.

In addition to the morphological changes of SNTs at different pHs, the surface of the nanotubes also exhibited distinct features which are summarized in Figure 7. 6. At low pH, multi channeled SNTs with curly or open cyclic morphology were observed with a thin layer of tiny SNTs which exhibited uniform inner and outer diameters. (Figure 7. 6A, B). In alkaline conditions, uniform, granular, pearl-necklace-like SNTs with compact or loose surface features that depend on pH could be obtained (Figure 7. 6C-I). At pH=11.5, the straight flagella fragments were coated with a thin layer of granular silica. At high magnification, it was clearly revealed that the mesostructured interiors of the spherical silica nanoparticles are composed of flagella short fragments. The structure of these nanoparticles is very similar to the tobacco mosaic virus based silica nanoparticles of a previous report [340]. The formation of flagella fragment incorporated nanoparticles might be based on similar mechanism. The surface feature of flagella with thickness can also be modulated by different concentration of TEOS (original, 5 \times , 10 \times) (Figure 7. 7). With an increased concentration of TEOS, the thickness of silica shell also increased and the surface of the SNTs became flat. Silica particles grow on the nuclei formed by hydrolysis of APTES on flagella surface until neighboring silica particles meet together [142]. High concentration of TEOS made more packed silica particles on flagella and merged together during growth.

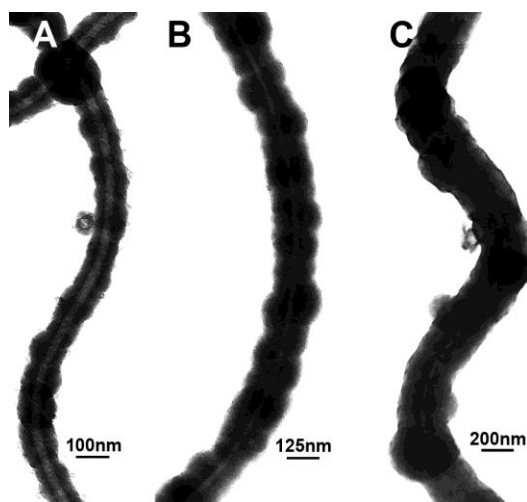


Figure 7.7: TEM images of SNTs on wild type flagella template with different surface features and thickness. A) Original concentration of TEOS; B) 5 \times TEOS; C) 10 \times TEOS

The morphology of SNTs and surface features on bioengineered flagella were also investigated. The SNTs of negatively charged flagella are summarized in Figure 7. 8. Because alkaline conditions are more favorable for the condensation of TEOS [336, 339] and the surface of flagella were modified with negatively charged amino acids, higher pH (11) was also studied. SNTs that used the E8 flagella as a template showed a slightly curved morphology with pearl-necklace-like surface structures (Figure 7. 8A). At higher pH, the SNTs became straighter with granular structures. There were also some large silica spheres attached to the SNTs (Figure 7. 8B). E8+C+S8 flagella template-based SNTs became much thicker and some of the SNTs had two or more flagella inside (insert) due to the formation of disulfide bond between neighboring flagella. The surface of SNTs was granular but no pearl-necklace-like structures were observed (Figure 7. 8C). At higher pH, no bundled flagella mediated SNTs were observed. The morphology was similar to E8 flagella templated SNTs (Figure 7. 8D). E8CS8 flagella template-based SNTs were thicker than E8+C+S8 templated which were attributed to flagella bundle composed of three or more flagella (Insert) and the surface became very smooth (Figure 7. 8E). Interestingly, at higher pH, many bundled open cyclic SNTs were observed (Figure 7. 8F). On the more negatively charged D8CS8 flagella, only a thin layer of granular silica condensed on the surface. Most SNTs were straight and composed of flagella bundles (Figure 7. 8G). The bundled SNTs became monodispersed at higher pH but the morphology did not change significantly (Figure 7. 8H). The above results indicate that negatively charged surface may be not very favorable for the condensation of TEOS. Due to the lower isoelectric point of aspartic acids than that of glutamic acids, less silica was nucleated on D8CS8 flagellar surface than on either the E8+C+S8 or the E8CS8 peptide. Yuwono et al also found that the peptide-amphiphile nanofiber with negatively charged surface was not favorable for the condensation of TEOS [341]. However, the introduction of nucleophilic hydroxyl groups promoted the condensation. The hydroxyl group displayed on surface of flagella may mimic the hydroxyl anion to attack the silicon atom by an SN_2 -Si mechanism [342].

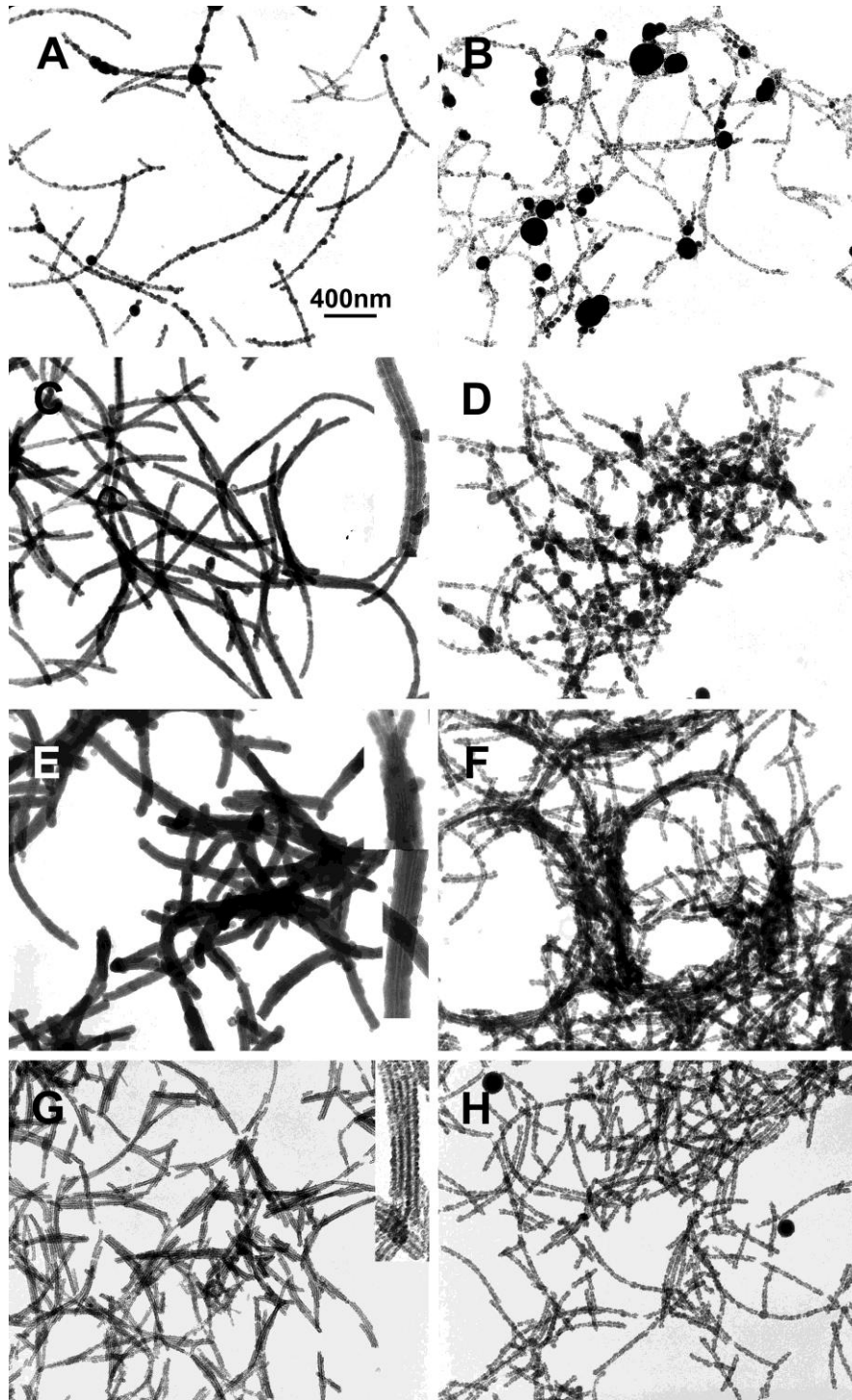


Figure 7.8: The morphology and surface features of SNTs on negatively charged bioengineered flagella. A, B) SNTs on E8 flagella template; C, D) SNTs on E8+C+S8 flagella template; E, F) SNTs on E8CS8 flagella template; G, H) SNTs on D8CS8 flagella template. B, D, F and H are at higher pH.

Positively charged lysine or arginine enriched proteins promote silica mineralization [343-345]. Poly-lysine or histidine synthesized on peptide-amphiphile nanofibers and arginine-lysine loop displayed on flagella catalyzed the silica polymerization on their surface [141, 341]. In this study, the lysine displayed flagella termed KGG4 also directed the condensation of TEOS on their surface (Figure 7. 9A). The thickness of the silica shell is uniform with rough surface and is similar to the previous research on other templates [141, 341]. However, when the serine and lysine modified flagella, termed KS, was used as a template, a novel morphology of SNTs was obtained (Figure 7. 9B). Many silica nanoparticles nucleated around the nanotubes. The ability to induce mineralization of silica may be different for the side functional groups of lysine and serine displayed on flagella. The formation and growth of silica particles are much faster at some nucleation sites. However, the exact mechanism is unexplained for the moment.

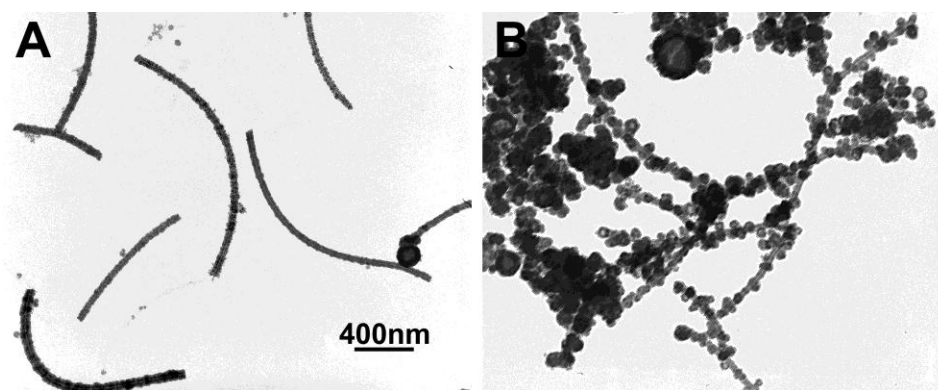


Figure 7.9: The morphology and surface features of SNTs on positively charged bioengineered flagella. A) SNTs morphology on KGG4 flagella; B) SNTs morphology on KS flagella

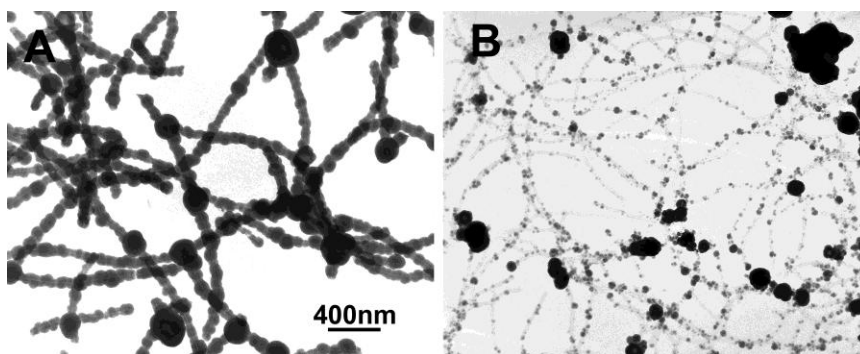


Figure 7.10: TEM images of SNTs on GPP8 flagella template. A) pH=10.4; B) pH=11. Scale bar is for all panels.

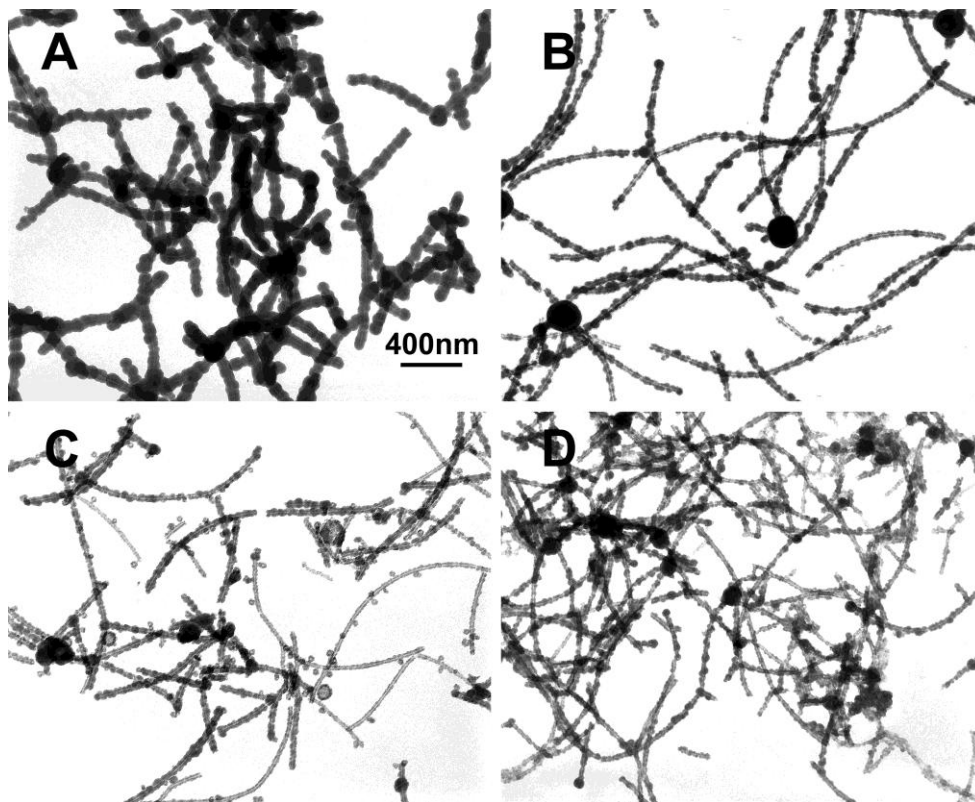


Figure 7.11: SNTs morphology on bioengineered flagella with mixed polar peptides from type I collagen. A) SNTs on N-terminal flagella; B) SNTs on C-terminal flagella; C) SNTs on N-zone flagella; D) SNTs on C-zone flagella.

We also displayed some other sequences on flagella. Flagella with eight continuous GPP sequences can also mediate the mineralization of silica. The morphology is similar to wild type flagella template-based SNTs (Figure 7. 10A). At higher pH, however, the ability to mediate mineralization of silica was severely decreased. Only a very thin layer of silica nucleated on the surface of flagella, indicating the polar amino acids might be important for the silica mineralization (Figure 7. 10B). Flagella with N, C-terminal, N, C-zone sequences with mixed polar amino acids from type I collagen mediated SNTs are summarized in Figure 7. 11. Different morphologies and surface features of SNTs can be observed. The transcription of silica shells we used can also be applied to other biological templates. We also tried to synthesize SNTs on more rigid biological template-pili. The

pili based SNTs are composed of bundled structures inside of SNTs with straight morphology (Figure 7. 12A). Under higher pH, some broken pili fragments were wrapped in spherical silica particles and the fragments were organized radially around a silica core (Figure 7. 12B with insert)

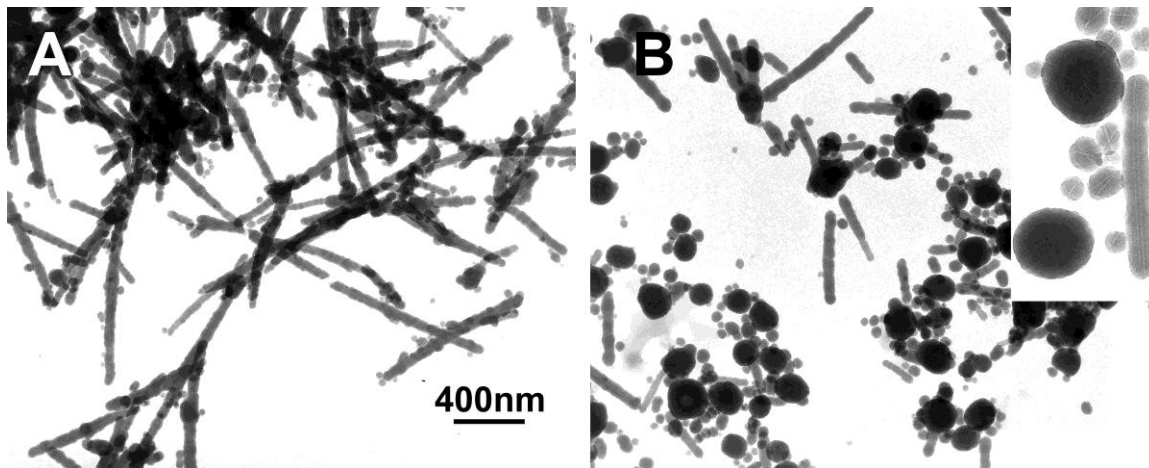


Figure 7.12: TEM images of SNTs on pili template. A) Straight SNTs mineralized pili bundles; B) Some spherical silica nanoparticles with radially organized pili fragments were formed. Scale bar is for all panels.

Conclusion:

In summary, the morphology and surface features of flagella template-based SNTs can be controlled by tuning the pH and concentration of TEOS. At low pH, bundled SNTs were obtained with curly or open cyclic morphology. A layer of tiny nanoparticles mineralized on the surface of flagella. At higher pH, the morphology of SNTs exhibited more variations. Curly, open cyclic, straight, sinusoidal with different wavelength can be observed. The surface feature of SNTs also possessed smooth, rough, pearl-necklace-like and granular structures. The morphology and surface features of SNTs can also be tuned by bioengineered flagella with different functional groups. The negatively charged surface may be not very favorable for the condensation of TEOS. However, when the flagella surface was modified with hydroxyl groups, the thickness of silica shell increased. Moreover, the bundled SNTs were easily obtained by displaying cysteine on the flagella at alkaline conditions. Positively charged surface facilitates the mineralization

of silica and the formation of a silica shell of uniform thickness. Other morphologies of SNTs can be obtained by inserting polar, nonpolar or a mixture of negatively and positively charged amino acids on flagella. This method can also be applied to other biological templates such as pili to obtain straight SNTs. The current work may open new approach towards the facile fabrication of SNTs with controllable morphologies and surface features.

Chapter 8 Biotemplated Synthesis of Hollow Bilayer of TiO₂/SiO₂ Nanotubes at Ambient Conditions

8. 1 Introduction

Nanostructural titanium oxide (titania, TiO₂) nanotubes are one of the most widely studied materials because of their unique and excellent properties. Titania is chemically stable, non-toxic and well known as a wide gap semiconductor oxide. It also has high photocatalytic activity under UV irradiation but not under visible light. Titania nanotubes have a variety of applications as chemical sensing devices, dye-sensitized solar cells, gas sensors, electrodes of solar cells, photocatalysts [346-348]. They are also very promising for biomedical applications, such as tissue engineering, biosensing, and drug delivery, due to their chemical stability and non-toxic characteristics [349-353]. There are two general methods for the synthesis of titania nanotubes: one is through self-assembly of titanium oxide during chemical synthesis processes such as the well-known ‘anodic oxidation’ method [347]; the other one is a template based fabrication of titanium oxide nanotubes [354]. With this latter method, the size of the nanotubes usually depends on the template material and the thickness of the nanotubes can be modified. A liquid-phase deposition method has been widely used to coat the surface of the templates with titania [354]. After deposition, the templates can be chemically or physically removed to generate nanotubes. In recent years, biological systems have been used as supporting templates or catalysts to produce nanoscale titania materials and nanotubes [355-363]. Biological systems are very easy to scale up and the biological templates can be removed at ambient conditions or by heat treatment. They also exhibit precise control over morphology, size distribution and their spatial arrangement. Moreover, most biological templates can self-assemble into highly ordered structures, which is a critical property for materials to be used in nanofabrication and nanotechnology [241, 278, 364]. To date, there are a variety of bio-enabled titania nanoparticles and nanotubes which have been synthesized upon a group of proteins that includes silicatein, silaffins, positively charged lysozymes and peptides. These proteins are used as enzymatic biocatalysts to produce titania nanomaterials [278, 355, 357, 358, 360, 362, 365]. However, this approach is limited by the species of biological templates and does not have enough different

morphology and sizes available. The other method is to for titania nanomaterials upon bio-templates, such as the tobacco mosaic virus and certain lipids [359, 363]. The current approach also has some limitations. Multiple steps have to be employed and the biological templates have to be immobilized on a substrate preventing the scale up of the titania nanomaterials. Furthermore, these reactions cannot be performed in aqueous solution or close to room temperature.

Usually, titania nanoparticles and nanotubes titania are assembled or attached to support scaffolds or substrates for practical applications. However, the application of titania as a photo-catalyst and UV absorbing agent are considerably limited. Due to the excellent photoactivity of titania, in most cases, the organic materials used to support titania are itched or degraded. Consequently, silica as one of photo-catalytically inactive substances has been used to encapsulate titania to fabricate double-layered, core/shell structured, or hybrid materials [366-368]. Silica is UV transparent. Thin shielding layer of silica (20 nm in thickness) on the titania film can improve the photo-catalytic activity toward photooxidation of polystyrene [366]. Another attractive approach to improving the photo-catalytic activity of titania film is to use mesoporous silica and titania nanocrystals which are dispersed within the silica supports. This structure exhibits a large surface area which exposes more active sites of titania [369].

Bacterial flagellum is polymerized mainly from flagellin monomers into a hollow helical structure of 11 units per 2 turns. The outer diameter of the flagella filament varies from 12 nm to 25 nm depending on the species of bacteria. Flagella have an inner diameter of about 2 nm and a length of up to 10-15 μm . Each flagellum is attached to the bacterial cell by a short joint-like hook structure. Recently, we demonstrated the fabrication of silica nanotubes using genetically modified bacterial flagella as a template. By changing the concentration of tetraethoxysilane (TEOS) and the reaction time, we were able to control the thickness of the silica shell. Here, we introduce a new, economically scalable sol-gel method to fabricate silica/titania hollow, double-layered nanotubes with uniform diameter using a bacterial flagella template. In previous research, natural and genetically engineered bacterial flagella have been used as templates to mediate titania nanotube formations [141, 144]. Genetically engineered flagella with a single Tyr loop insert

(HYSYGYSYGYSY) can mediate nucleation of titania on their surface. However, the genetically engineered flagella have to be dried on the TEM grid before applying titanium (IV) ethoxide solution in ethanol [141]. We have confirmed that flagella cannot survive in pure ethanol (data not shown). Hesse et al [144] demonstrated the formation of titania nanotubes using flagella isolated from *Salmonella* typhimurium in aqueous solution. However, hydrolysis of titanium chloride (TiCl_4) will release corrosive hydrogen chloride (HCl). It has been shown that flagella become unstable and depolymerize under low pH [370]. In the present study, we synthesized the titania/silica double-layered nanotubes directly in aqueous solution close to neutral pH at room temperature. After calcification, amorphous titania transformed into crystalline titania nanoparticles (anatase phase) and embedded within the silica shell-tube.

8. 2 Materials and Methods

8. 2. 1 *Salmonella* flagella purification:

The frozen *Salmonella* wild type strain inoculated in 2 ml of LB media at 37 °C with shaking (250 rpm) for overnight. Then the cell culture was inoculated in 1 L of LB media and continues to grow at 37 °C with shaking (250 rpm) until OD reached 0.6-0.8. The culture was collected and centrifuged at 6000 g for 20 min at 4 °C. The cell pellets were washed twice by PBS buffer (pH=7.4). Finally, the cell pellet was resuspended in deionized water and agitated on a vortex mixer at the highest speed for 3 min. The flagella were then detached from the cells and suspended in the solution. The bacteria were removed by centrifugation at 4000 rpm for 20-30 min and the supernatant containing flagella was collected. The supernatant were centrifuged again at 10,000 g for 20 min to remove debris from solution. High purity flagella were precipitated by ultracentrifugation at 80,000 g for 2 h. Finally, the flagella were dissolved in either deionized water or PBS buffer.

8. 2. 2 $\text{TiO}_2/\text{SiO}_2$ growth on flagella templates:

All reagents were purchased from Sigma-Aldrich without any further purification. In a typical experiment, the sol was prepared by titanium (IV) butoxide (TBT) mixed with acetylacetone (AcAc) in ethanol. They were mixed in a molar ratio of TBT: Ethanol: AcAc=1: 100: 5 and stirred for 1 h at room temperature. Then, the solution was then

introduced into deionized water at a volume ratio 1: 8 and stirred for 5 min. AcAc was used as a chelating reagent to slow down the hydrolysis and the condensation reactions. APTES (2×10^{-3} mmol) was added to 500 μ L flagella solution and gently mixed by vortex. The mixed flagella solution cooled down in an ice-water bath for 3-5 min. Then the flagella solution was added drop-wise by sol with stirring for 3 min. The mixed solution was cool in an ice-water bath for about 1 h and then left at room temperature for about 6 h until white precipitates appeared. The titania coated flagella nanotubes were washed with water and ethanol several times by low speed centrifugation. The synthesis of the second SiO₂ layer was based on our previous report [371]. The procedure is similar to TiO₂ synthesis. The only difference is TEOS at a concentration of 2.5×10^{-2} mmol was used as the precursor solution.

8. 2. 3 Calcinations of the bilayer of TiO₂/SiO₂ nanotubes at different temperatures:

Calcination TiO₂ nanotubes were carried out under air in a tube furnace. The air dried TiO₂ nanotubes were transferred to a porcelain boat, and heated at 110 °C for 8 h. Then, the temperature was increase (2 °C/min) to the 150 °C and 200 °C respectively for 2 h. Finally, the samples were cooled to room temperature at a rate of 5 °C/min. Calcination of TiO₂/SiO₂ nanotubes was performed according to the same procedure but at an increased temperature of 500 °C and 700 °C respectively for 4 h. Calcination was carried out in a Lindberg tube furnace (TF55030A)

8. 2. 4 Materials Characterization:

The TiO₂ nanotubes and TiO₂/SiO₂ bilayer nanotubes were examined by using TEM Zeiss 10 and High Resolution TEM JEOL 2010-FX. Morphology and XRD analysis were carried out using SEM JEOL JSM-880.

8. 3 Result and Discussion

High concentrations of flagella can be prepared mainly by one of two methods: The first one is to induce the flagella depolymerization from the bacteria at low pH, remove bacteria through centrifugation, and finally, to induce *FliC* repolymerization into flagella with a high concentration of salt at neutral pH. Usually, some small fragments of flagella are added as seeds to achieve longer flagella polymerization [372]; The other method is

to detach flagella from the bacterial body by high speed vortex [373]. This is facile and easy way to isolate large amount of flagella.

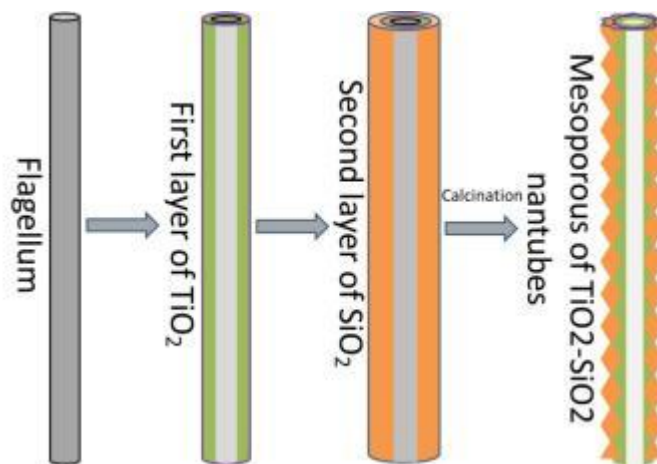


Figure 8.1: Schematic representation of the procedure for fabrication bilayer titania/silica nanotubes and subsequent calcination

The array of TiO₂ nanotubes can be produced by the well-known “electrochemical anodization” method [347]. For the template mediated synthesis of TiO₂ nanotubes, the sol-gel method is widely used [141, 359]. The hydrolysis precursors, such as titanium isopropoxide and titanium butoxide, must be hydrolyzed in organic solvents [374]. However, most of the bioenabled templates cannot survive in organic solvents. Alternative routes have been developed such as immobilizing the templates on substrates [141, 363] or carrying out the reaction at very low temperatures [359]; however, both limit the material’s practical application

Previously, we reported the synthesis of SiO₂ nanotubes mediated by wild type or bioengineered flagella in aqueous solution and at ambient conditions [371]. In the present study, we developed a new sol-gel method for the synthesis TiO₂ nanotubes in which the reaction also occurred in aqueous solution, close to room temperature and neutral pH. APTES is used as the initial nuclei for subsequent TiO₂ nucleation. The second layer of SiO₂ is then coated based on our previous method [371]. The organic flagella templates can be removed by calcination. Finally, hollow bilayer TiO₂/SiO₂ nanotubes were synthesized. After calcination, the amorphous TiO₂ transformed into crystalline

nanoparticles dispersed inside the SiO₂ shell. The entire strategy is depicted in Figure 8.1.

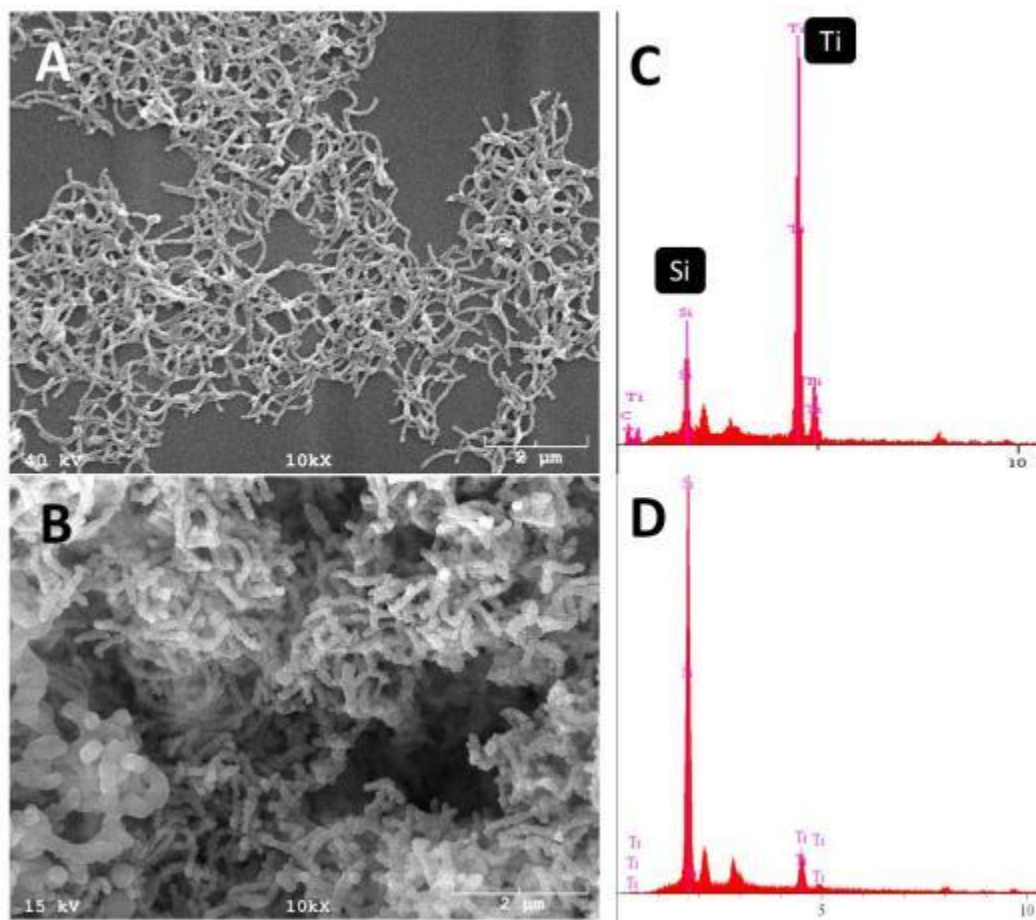


Figure 8.2: SEM micrographs of flagella mediated titania and bilayer titania/silica nanotubes with EDX analysis. A) Titania nanotubes using wild type flagella as template; B) Bilayer titan/silica nanotubes; C) EDX analysis of titania nanotubes. The nanotubes are mainly composed of titania; D) EDX analysis of bilayer titania/silica nanotubes. Both of titania and silica can be observed.

The first layer of TiO₂ nanotubes was characterized by SEM (Figure 8. 2 A). A continuous layer of amorphous TiO₂ with rough surfaces totally covered the surface of the flagella. The nanotubes still kept the characteristic curly morphology of flagella. We propose that the positively charged APTES adsorbed onto the flagella surface by hydrogen bonding or electrostatic interaction [371]. The zeta potential of wild type flagella is about -6 mv indicating the presence of negative charges on the flagella surface.

Partially hydrolyzed APTES form silicic acid as nuclei to mediate the formation of TiO₂ nanotubes. EDX analysis indicates that the amorphous layer is mainly composed of titanium with minor silicon (Figure 8. 2 B). The silicon should come from the hydrolysis of APTES. The SiO₂ shell, or second, layer increased the diameter of the nanotubes and amplified the roughness of the TiO₂ layer upon which the SiO₂ was coated (Figure 8. 2 C). A very high aspect ratio of silica can be observed by EDX. Because the titania layer was covered by the silica layer, The relative ratio of titania to silica significantly decreased (Figure 8. 2 D).

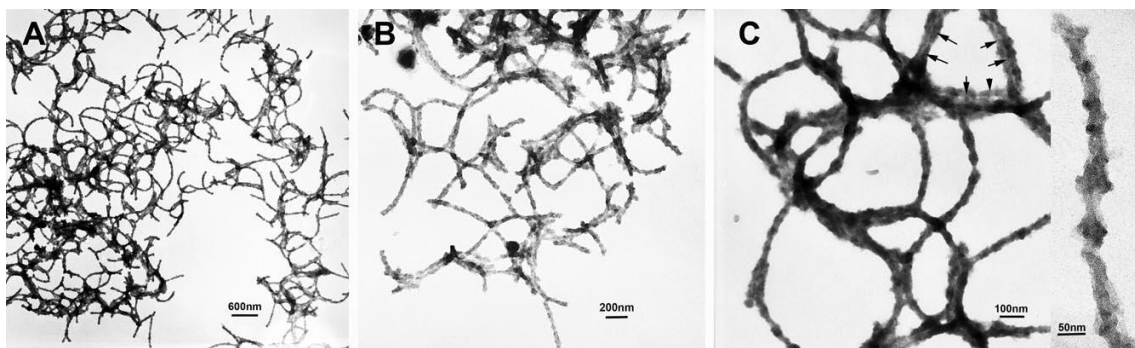


Figure 8.3: TEM micrographs of titania nanotubes. A) Titania nanotubes show characteristic flagella curves; B) The rough surfaces of titania nanotubes exhibit “sticky” properties. Some redundant titania nucleated at the interconnected sites; C) The detailed morphology titania nanotubes. The central pores can barely be observed (as marked by arrows)

Titania and titania/silica bilayer nanotubes were also characterized by TEM as shown in Figure 8. 3. After coating with the first titania layer, the nanotubes exhibit very rough surfaces unlike the flagella based silica nanotubes which exhibit pearl-necklace-like surface feature [371]. The diameter of the titania nanotubes ranges from 30 to 80 nm. Compared to flagella based silica nanotubes, the titania nanotubes appear more “sticky” and some excessive titania is nucleated at the interconnected sites between nanotubes (Figure 8. 3 A, B). This may be ascribed to the low density of titania prepared by the sol-gel method [375]. After coated with amorphous titania, the flagella projected pore at the center of the nanotubes was present but barely observable (Figure 8. 4 C, marked by arrows). In comparison, silica nanotubes with uniform pore size corresponding to the

diameter of flagella can be directly observed under TEM. Interestingly, after the titania nanotubes were coated by the second layer of silica, a uniform pore size with a diameter about 15 nm became visible (Figure 8. 5 A). The high density of silica might enhance the contrast between flagella templates and inorganics. This result is also consistent with our previous research [371]. The diameter of titania/silica bilayer nanotubes increased to 40-90 nm. Meanwhile, the thickness of titania or silica layer is controllable by changing amount and concentration of the precursor solution and/or reaction time (Figure 8. 5 B). After coated by less titania and more silica, the nanotubes became more flat with some free silica nanoparticles nucleated or hanging on the surfaces. If coated with less silica and more titania, the nanotubes exhibited rougher surfaces and the central pores became invisible.

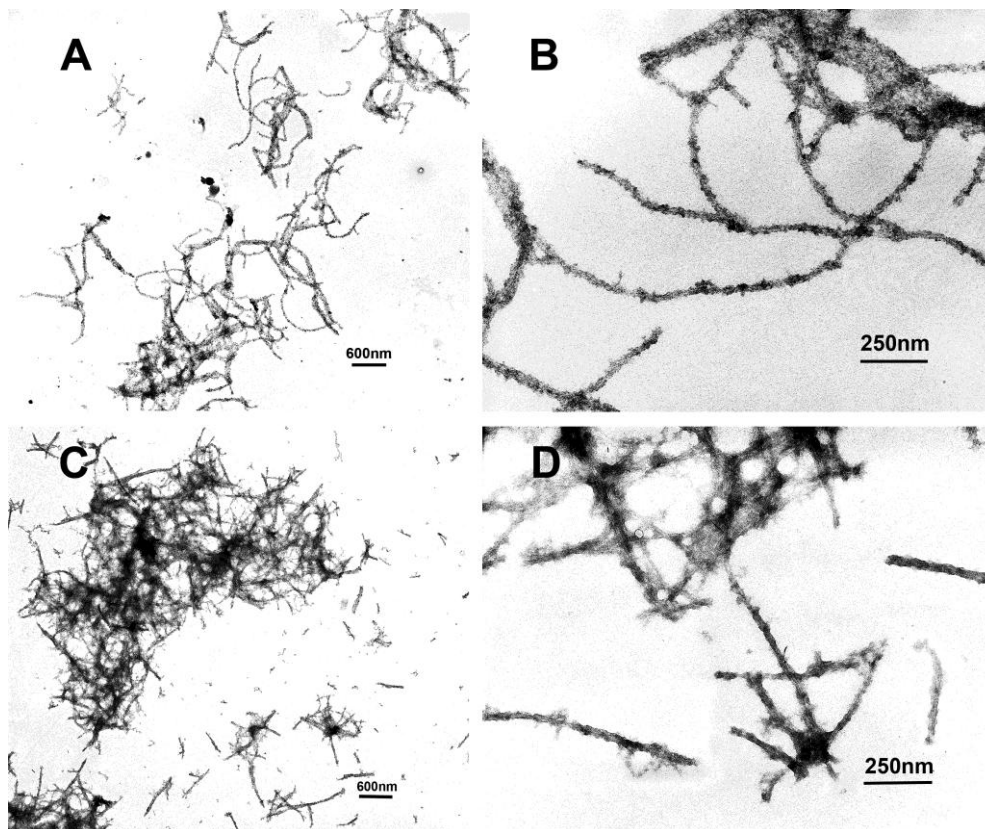


Figure 8.4: TEM micrographs of titania nanotubes based on other biological templates. A, B) Titania nanotubes show some random coils and curved morphology using M13 phage as template. C, D) Straight titania nanotubes can be observed using bacteria pili as template.

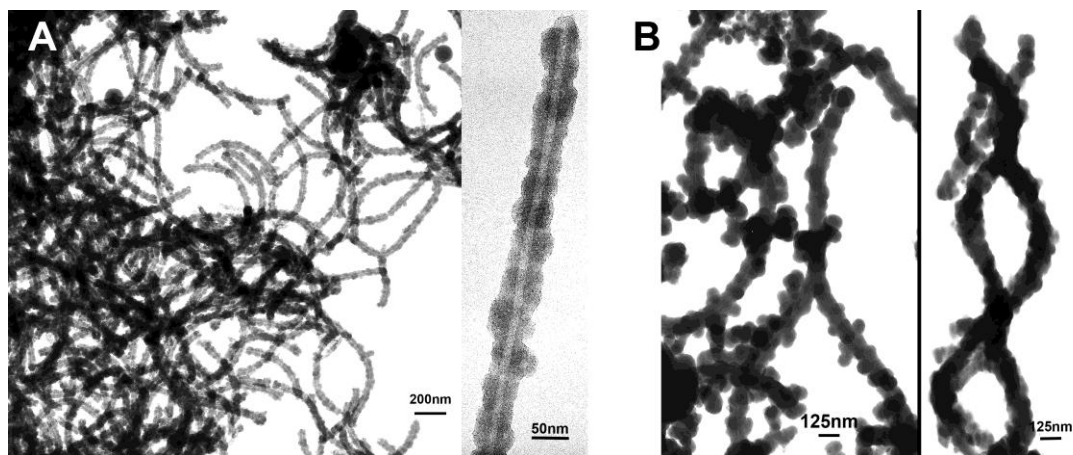


Figure 8.5: TEM micrographs of bilayer titania/silica nanotubes. A) Characteristic morphology of titania/silica nanotubes using wild type flagella as template. B) Tuning thickness of titania or silica by varying the initial precursor concentration and reaction time. Thicker layer of silica (left) shows flat surfaces with some free silica nanoparticles attached. Thicker layer of titania (right) shows rough surfaces due to the first rough titania layer “amplified” by the second silica coating.

Previously, we demonstrated control the morphology of silica nanotubes based on wild type and bioengineered flagella templates [371]. Here we show a different strategy to control the morphology of titania nanotubes by using two other bio-enabled templates, filamentous bacteriophage M13 and bacterial pili. Using the same conditions as were used when coating titania on flagella, both phage and pili have been successfully coated by titania (Figure 8. 4). Because the natural morphologies of phage and pili are quite different than that of flagella, the titania nanotubes based on them exhibited obvious morphological differences. Silica nanotubes based on phage template show some random coils and curves; however, pili based silica nanotubes exhibit straight morphology. The method we used can be extended to other biological templates with different morphologies which may broaden their applications. From this work, a general procedure might be developed for coating titania on bio-enabled templates and/or other templates that cannot survive in organic solvent.

After the flagella were coated by the layer of titania, the samples were washed several times with water and dissolved in ethanol. Then the samples were air dried and annealed

at 150 °C and 200 °C, respectively, for 2 h (Figure 8. 6). At 150 °C, the organic flagella templates start to decompose revealing hollow nanotubes composed of a thin layer of TiO₂ with the curly flagella morphology (Figure 8. 6 A). The diameter of the nanotubes has decreased after heating. The outer diameter of the nanotubes reduced to 40-60 nm with a wall thickness of 10-25 nm and an inner diameter of 20-35 nm. At the higher temperature (200 °C), the TiO₂ nanotubes began to collapse and the characteristic template morphology disappeared. Much shorter but thicker straight nanotubes with corrugated surfaces can be observed (Figure 8. 6 B). A previous study also confirmed that at high temperatures, the amorphous TiO₂ transformed into crystalline nanoparticles [144]. Interestingly, when we subjected the nanotubes to heat treatment at 150 °C for 2 h after coating with a very thin layer of silica, most of the nanotubes remained intact with a pore size fitting the diameter of flagella (Figure 8. 6C). This data demonstrates the ability of silica to support the inner layer of titania and prevent titania nanotubes from collapsing. There were still some nanotubes with a larger pore size because the silica layer on the surface of some flagella was either nonexistent or too thin to preserve the nanotubes.

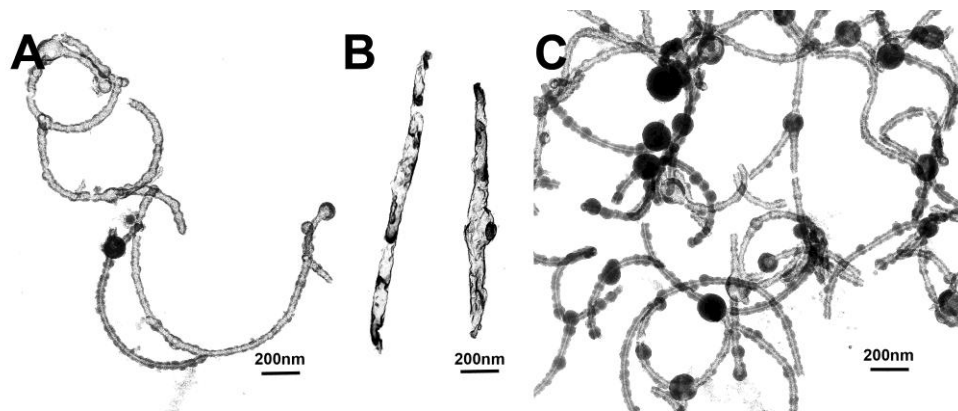


Figure 8.6: TEM micrographs of titania and titania with thin layer of silica nanotubes annealed at low temperature. A) Titian nanotubes annealed at 150 °C for 2 h; B) Annealed at 200 °C for 2 h; C) After the titania nanotubes coated with a thin layer of silica, most nanotubes keep intact.

After coated with a thicker SiO₂ layer, calcinations of the TiO₂/SiO₂ nanotubes at different temperatures (500 °C, 800 °C) were carried out to remove the organic template

under air in a tube furnace (Figure 8. 7). TEM images of the $\text{TiO}_2/\text{SiO}_2$ nanotubes calcined at 500 °C showed hollow structures with a uniform pore size of 10 ± 0.5 nm but very rough outer surfaces. The open-ended tubular structures exhibit outer diameters of about 30-80 nm with a wall thickness of 10–60 nm (Figure 8. 7 A). When the calcination temperature was increased to 800 °C, some of the nanotubes broke into shorter fragment. The diameter of the pore decreased to 8 ± 0.5 nm. The outer diameters also decreased to 25-50 nm (Figure 8. 7 B). However, the thicker layer of silica improved the integrity of titania/silica nanotubes at high temperature (Figure 8. 8). This result also demonstrates that the silica shield has high thermal stability and can support the inner TiO_2 layer as a “skeleton”. The titania prepared by sol-gel method has a tenuous structure and allows silica precursors to penetrate inside the very open network [376]. Without drying the titania core, silica shell could be coated by sol-gel method to form a mixed composition after calcination [376].

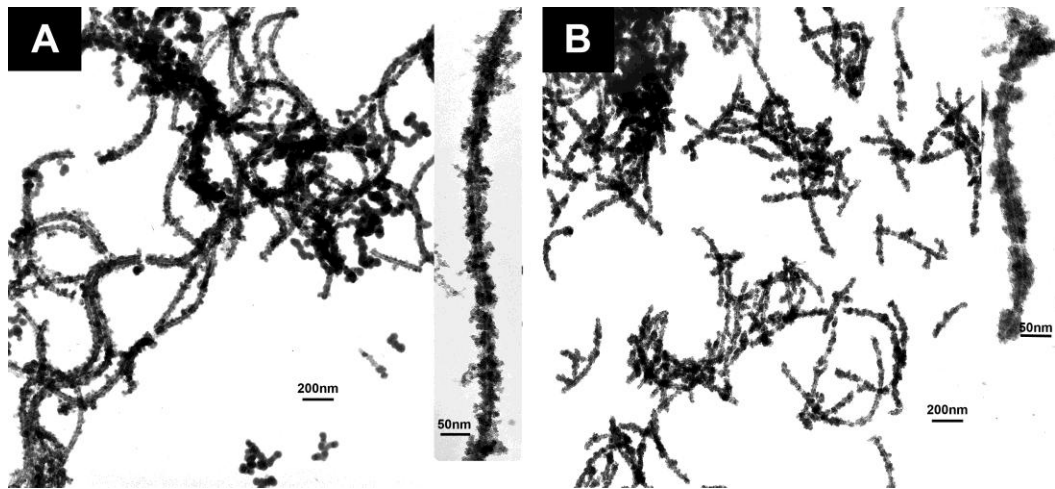


Figure 8.7: TEM micrographs of titania/silica nanotubes calcined at different temperatures. A) Calcined at 500 °C; B) Calcined at 800 °C. (high magnification shows insert)

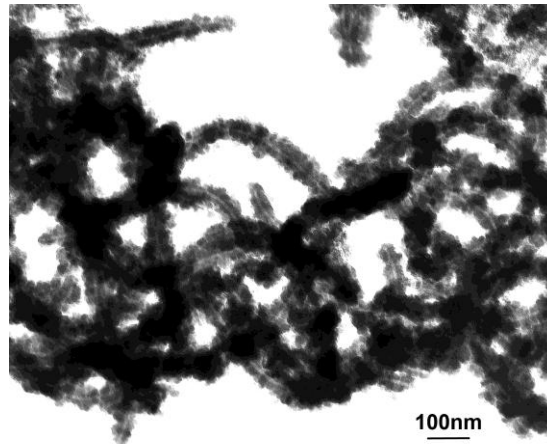


Figure 8.8: TEM micrographs of thicker layer of silica on titania layer nanotubes calcined at 800 °C. The nanotubes still keep intact.

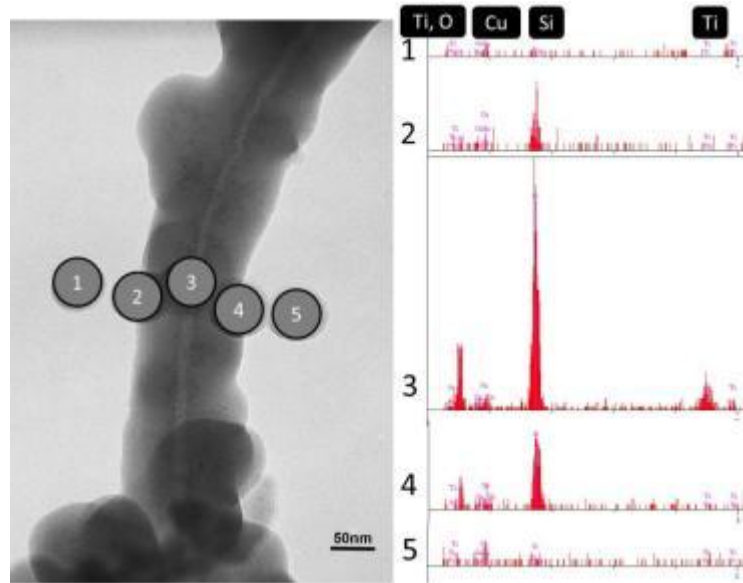


Figure 8.9: HRTEM micrograph with EDX analysis of calcined at 500 °C titania/silica nanotubes

In order to determine whether the titania was still inside of the silica shell, after calcination at 500 °C, the bilayer of $\text{TiO}_2/\text{SiO}_2$ nanotubes was analyzed by EDX using TEM (Figure 8. 9). The thicker layer of SiO_2 was coated for XRD analyses in order to fit the selected sites on and off the axis of nanotubes. It clearly showed that the marginal sides of the nanotubes are only composed of silica. In the center, both titania and silica were detected indicating the presence of a titania layer in side of the silica layer. Before

calcination, we found a very similar pattern of $\text{TiO}_2/\text{SiO}_2$ distributions (Figure 8. 10). Many reports confirmed that amorphous titania start phase transitions upon heating. Yang et al reported the amorphous TiO_2 nanotubes start to initiate phase transition to crystals in the anatase and rutile phases at 300 °C and 500 °C respectively [377]. Polycrystalline anatase phase of the TiO_2 nanotubes prepared by sol-gel method were obtained after calcined at 650 °C for 2 h [354]. Amorphous TiO_2 nanotubes using TiCl_4 as precursor turned into nanoparticle TiO_2 covering the filament after annealing at 200 °C. In our study, the phase transition of $\text{TiO}_2/\text{SiO}_2$ bilayer nanotubes was investigated by high resolution transmission electron microscopy (HRTEM, JEOL-2010) (Figure 8. 11). Figure 8. 11A shows the morphology of the bilayer $\text{TiO}_2/\text{SiO}_2$ nanotubes annealed at 500 °C for 4 h. The outer diameters of the nanotubes with rough surfaces are not very uniform. However, the inner pore sizes created by removing the flagella template are very smooth. High magnification of the TEM images shows some dark small clusters well dispersed in an amorphous background and close to the center. We believe the small clusters are composed of crystalline TiO_2 nanoparticles (Figure 8.10 B). The diameters of the nanoparticles range from 2 to 8 nm. The dashed lines show the hollow pore and direction of the nanotube. The SAED pattern showed in the inset of Figure 8. 7 C indicates that TiO_2 is in the anatase phase. At high resolution, polycrystalline nanoparticles could be clearly observed with identical lattice fringes ($d=0.35\text{nm}$) corresponding to the d-spacing between adjacent (101) crystallographic planes of anatase TiO_2 phase (Figure 8. 11C, D marked in the dash line cycles). Titania nanoparticles are also located near the center pore (as marked by dash line) of the nanotubes. This data demonstrates that after calcination at 500 °C, the amorphous TiO_2 transformed into the crystalline anatase phase. Meanwhile, the crystalline TiO_2 nanoparticles are imbedded inside the amorphous SiO_2 shell. Our previous study proved the amorphous SiO_2 nanotubes prepared by the sol-gel method transformed into the crystalline phase up to a temperature up to 950 °C [371].

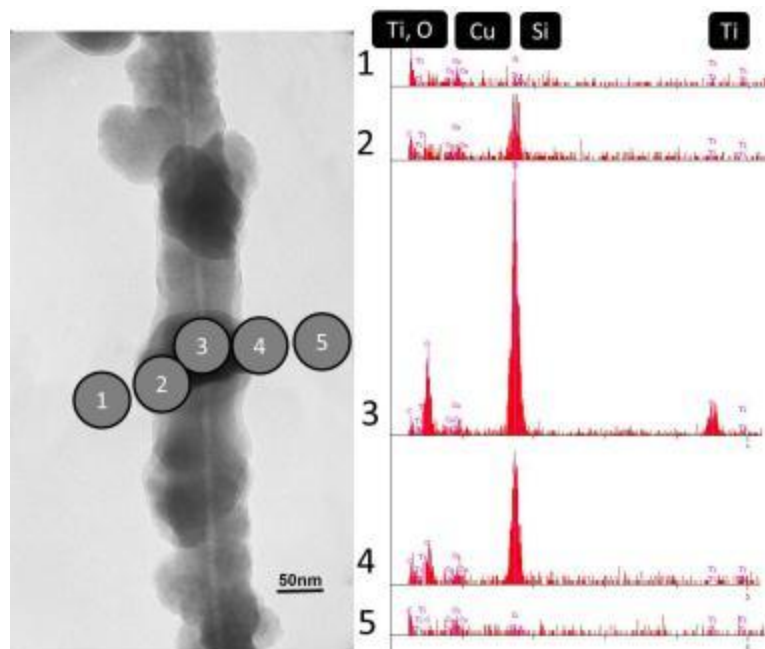


Figure 8.10: HRTEM micrograph with EDX analysis of titania/silica nanotubes before calcination.

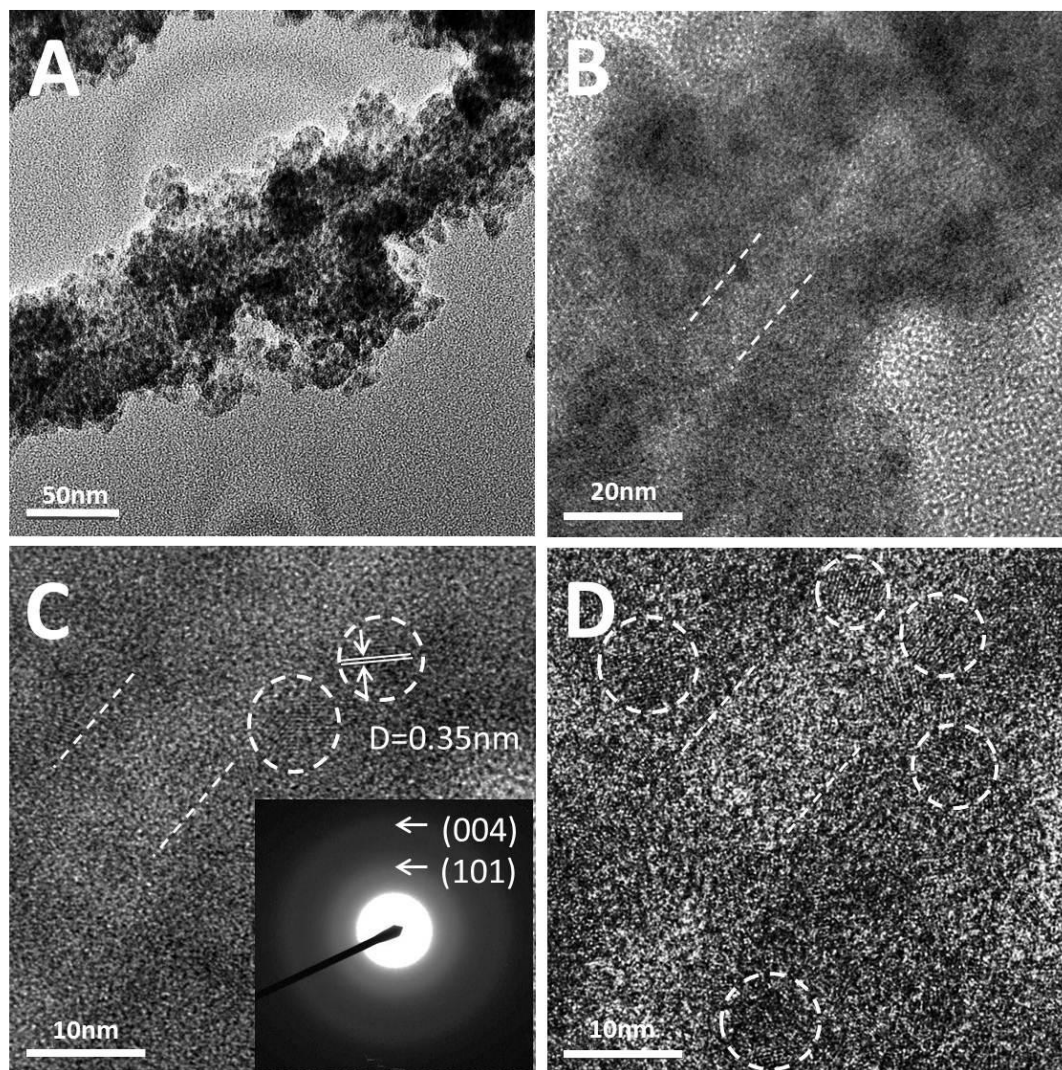


Figure 8.11: HRTEM analysis of titania/silica nanotubes for the phase transition. A) Detailed morphology of titania/silica nanotubes. B) Shows dark nanoparticles dispersed in silica matrix and close to central pore. C, D) Crystal lattice fringes ($d = 0.35 \text{ nm}$) corresponding to the D-spacing between adjacent (101) crystallographic planes of anatase TiO_2 phase (marked in the dash line cycles). SAED pattern of (101) and (004) indicates that anatase phase of titania (insert).

Due to its excellent photocatalytic and photovoltaic properties, TiO_2 has already shown great promise regarding solar energy harvesting, air cleaning and water purification. Because TiO_2 nanoparticles aggregate spontaneously in the reaction system resulting in a rapid loss of their photocatalytic activity, alternative approaches that protect the photocatalytic activity of titania have been developed such as dispersing TiO_2

nanoparticles in porous solids or immobilizing it on the inert surfaces [366-369, 378, 379]. In our study, the titania nanoparticles after calcination were successfully wrapped inside a silica matrix. The photocatalytic activity may be decreased due to the outer silica shell, which may block most of the active sites of TiO_2 [379]. However, after removing the flagella template, the central pores, which mainly composed of TiO_2 nanoparticles becomes surface exposed. An alternative method to maintain the active sites of titania is to coat the titania surface with a titania layer. We also demonstrated titania coated on silica nanotube using flagella as a template and characterized them by SEM (Figure 8. 12). There are multiple features of the flagella mediated synthesis of titania/silica nanotubes that make it technologically advantages: A) Extensive chemistry modifications are available for silane coatings using the SiO_2 exterior. For example, in waste water treatment, nanotube surfaces are functionalized to be hydrophobic which minimize competition between water and organics for sites on the TiO_2 catalyst; B) The silica coating protects TiO_2 particles from abrasive interactions with substrates. C) The thickness of TiO_2 or SiO_2 layers is tunable; D) The central pore create a void space that may facilitate photocatalytic activity; E) After calcination, the SiO_2 serves as a “skeleton” support for TiO_2 nanoparticles; F) The morphology and pore size can also be tuned using different flagella species or other templates such as phage and pili; G) Neither bioengineering nor chemistry modification of template surfaces is required.

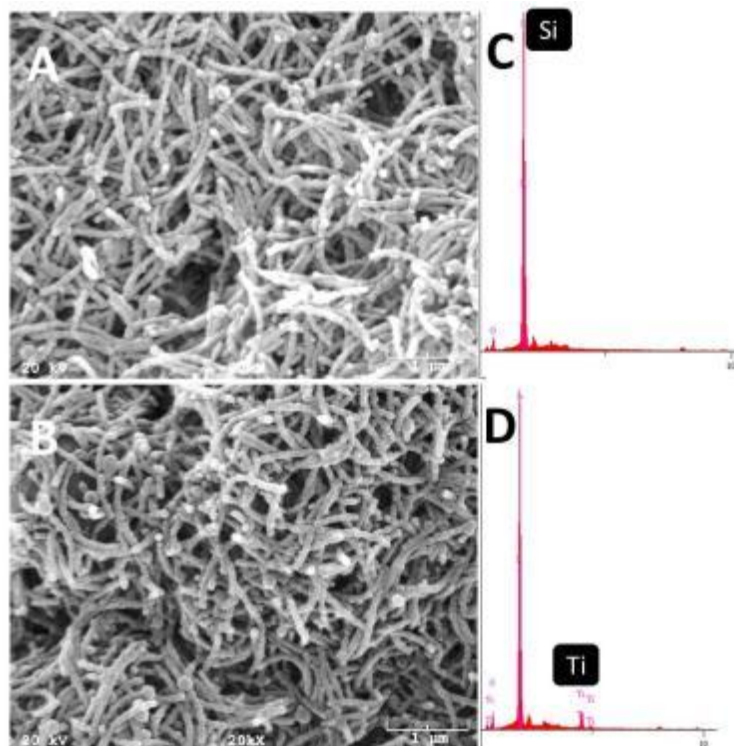


Figure 8.12: SEM micrographs of silica and silica/titania nanotubes using flagella as templates with EDX analysis. A) silica nanotubes based on wild type flagella; B) Bilayer silica/titan nanotubes; C) EDX analysis of silica nanotubes. The nanotubes are only composed of silica; D) EDX analysis of bilayer silica/titania nanotubes. Both of titania and silica can be observed. However, relative small portion of titania can be observed indicating only a very thin layer of titania was coated on surface of silica.

8. 4 Conclusions

In summary, the present research demonstrates a new methodology to prepare hybrid $\text{SiO}_2/\text{TiO}_2$ nanotubes based on bacterial flagella template with uniform pore sizes. All reactions were carried out in aqueous solution at ambient conditions. The thickness of nanotubes could be tuned by varying the initial concentrations of precursor solutions and the reaction time. After calcination, hollow $\text{SiO}_2/\text{TiO}_2$ nanotubes were generated. TiO_2 transformed into crystalline phase and condensed into nanoparticles dispersed inside the SiO_2 matrix. This is a facile method that is easy to scale up and might have potential industry applications.

REFERENCES:

1. Das, I. and S.A. Ansari, *Nanomaterials in science and technology*. J. Sci. Ind. Res. FIELD Full Journal Title:Journal of Scientific & Industrial Research, 2009. **68**(8): p. 657-677.
2. Liu, H. and T.J. Webster, *Nanomaterials as improved implants: a review of recent studies*. Ceram. Eng. Sci. Proc. FIELD Full Journal Title:Ceramic Engineering and Science Proceedings, 2009. **29**(7, Advances in Bioceramics and Porous Ceramics): p. 165-180.
3. Viswanathan, B., *The science of nanomaterials in catalysis*. Chem. Ind. Dig. FIELD Full Journal Title:Chemical Industry Digest, 2009. **22**(9): p. 69-77.
4. Iseli, A., H.-D. Kwen, and S. Rajagopalan, *Nanomaterials for environmental remediation*. Nanoscale Mater. Chem. (2nd Ed.) FIELD Full Journal Title:Nanoscale Materials in Chemistry (2nd Edition), 2009: p. 649-679.
5. Doshi, N. and S. Mitragotri, *Designer Biomaterials for Nanomedicine*. Adv. Funct. Mater. FIELD Full Journal Title:Advanced Functional Materials, 2009. **19**(24): p. 3843-3854.
6. Iancu, C., et al., *Applications of Nanomaterials in Cell Stem Therapies and the Onset of Nanomedicine*. Part. Sci. Technol. FIELD Full Journal Title:Particulate Science and Technology, 2009. **27**(6): p. 562-574.
7. Douglas, K.L., S.D. Carrigan, and M. Tabrizian, *Nanomaterials: perspectives and possibilities in nanomedicine*. Bionanotechnology FIELD Full Journal Title:Bionanotechnology, 2009: p. 269-288.
8. Vasudeo, Y.B. and R. Rangaprasad, *"From nanomaterials and nano technology to polymer nanocomposites" ... chasing a new world of dreams!* Pop. Plast. Packag. FIELD Full Journal Title:Popular Plastics & Packaging, 2005. **50**(11): p. 127-132, 134-140, 142-146.
9. Tamerler, C. and M. Sarikaya, *Molecular biomimetics: nanotechnology and bionanotechnology using genetically engineered peptides*. Philos. Trans. R. Soc., A FIELD Full Journal Title:Philosophical Transactions of the Royal Society, A: Mathematical, Physical & Engineering Sciences, 2009. **367**(1894): p. 1705-1726.
10. Sarikaya, M., et al., *Molecular biomimetics: nanotechnology through biology*. Nat Mater FIELD Full Journal Title:Nature materials, 2003. **2**(9): p. 577-85.
11. Sarikaya, M., et al., *Materials assembly and formation using engineered polypeptides*. Annu. Rev. Mater. Res. FIELD Full Journal Title:Annual Review of Materials Research, 2004. **34**: p. 373-408.
12. Dickerson, M.B., K.H. Sandhage, and R.R. Naik, *Protein- and Peptide-Directed Syntheses of Inorganic Materials*. Chem. Rev. (Washington, DC, U. S.) FIELD Full Journal Title:Chemical Reviews (Washington, DC, United States), 2008. **108**(11): p. 4935-4978.
13. Anon, *Bionanomaterials*. JBIC, J. Biol. Inorg. Chem. FIELD Full Journal Title:JBIC, Journal of Biological Inorganic Chemistry, 2009. **14**(S1): p. 245-254.
14. Chun, A.L., et al., *Self-assembled organic nanotubes: Novel bionanomaterials for orthopedics and tissue engineering*. Nanotechnol. Biol. Med. FIELD Full Journal Title:Nanotechnology in Biology and Medicine, 2007: p. 2/1-2/22.
15. Tamerler, C. and M. Sarikaya, *Molecular biomimetics: linking polypeptides to inorganic structures*. Microb. Bionanotechnol. FIELD Full Journal Title:Microbial Bionanotechnology, 2006: p. 191-221.

16. Sarikaya, M., *Biomimetics: materials fabrication through biology*. Proc. Natl. Acad. Sci. U. S. A. FIELD Full Journal Title:Proceedings of the National Academy of Sciences of the United States of America, 1999. **96**(25): p. 14183-14185.
17. Lowenstam, H.A., *Minerals formed by organisms*. Science (Washington, D. C., 1883-) FIELD Full Journal Title:Science (Washington, DC, United States), 1981. **211**(4487): p. 1126-31.
18. Aizenberg, J., *New nanofabrication strategies: inspired by biomineralization*. MRS Bull. FIELD Full Journal Title:MRS Bulletin. **35**(4): p. 323-330.
19. Alberts B., J.A., Lewis J., Raff M., Roberts K., Walter P., *Molecular biology of the cell*. Garland Science, 2008.
20. Tamerler, C. and M. Sarikaya, *Molecular biomimetics: utilizing nature's molecular ways in practical engineering*. Acta Biomater. FIELD Full Journal Title:Acta Biomaterialia, 2007. **3**(3): p. 289-299.
21. Mao, C., A. Liu, and B. Cao, *Virus-based chemical and biological sensing*. Angew Chem Int Ed Engl FIELD Full Journal Title:Angewandte Chemie (International ed. in English), 2009. **48**(37): p. 6790-810.
22. Petrenko, V., *Evolution of phage display: from bioactive peptides to bioselective nanomaterials*. Expert Opin Drug Deliv FIELD Full Journal Title:Expert opinion on drug delivery, 2008. **5**(8): p. 825-36.
23. Merzlyak, A. and S.-W. Lee, *Phage as templates for hybrid materials and mediators for nanomaterial synthesis*. Curr Opin Chem Biol FIELD Full Journal Title:Current opinion in chemical biology, 2006. **10**(3): p. 246-52.
24. Gerasopoulos, K., et al., *Biofabrication methods for the patterned assembly and synthesis of viral nanotemplates*. Nanotechnology FIELD Full Journal Title:Nanotechnology, 2010. **21**(5): p. 055304.
25. Kumara, M.T., et al., *Bioengineered flagella protein nanotubes with cysteine loops: self-assembly and manipulation in an optical trap*. Nano Lett. FIELD Full Journal Title:Nano Letters, 2006. **6**(9): p. 2121-2129.
26. Kumara Mudalige, T., S. Muralidharan, and C. Tripp Brian, *Generation and characterization of inorganic and organic nanotubes on bioengineered flagella of mesophilic bacteria*. J Nanosci Nanotechnol, 2007. **7**(7): p. 2260-72.
27. Rust, M., T. Schweinitzer, and C. Josenhans, *Helicobacter flagella, motility and chemotaxis*. Helicobacter pylori FIELD Full Journal Title:Helicobacter pylori, 2008: p. 61-85.
28. Spohn, G. and V. Scarlato, *Motility, chemotaxis, and flagella*. Helicobacter pylori FIELD Full Journal Title:Helicobacter pylori, 2001: p. 239-248.
29. Macnab, R. and D.E. Koshland, *Bacterial motility and chemotaxis: Light-induced tumbling response and visualization of individual flagella*. Journal of Molecular Biology, 1974. **84**(3): p. 399-406.
30. Blair, D.F., *How bacteria sense and swim*. Annu Rev Microbiol, 1995. **49**: p. 489-522.
31. Chevance, F.F. and K.T. Hughes, *Coordinating assembly of a bacterial macromolecular machine*. Nat Rev Microbiol, 2008. **6**(6): p. 455-65.
32. Silverman, M. and M. Simon, *Flagellar rotation and the mechanism of bacterial motility*. Nature FIELD Full Journal Title:Nature, 1974. **249**(452): p. 73-4.
33. Vonderviszt, F. and K. Namba, *Structure, function and assembly of flagellar axial proteins*. Fibrous Proteins FIELD Full Journal Title:Fibrous Proteins, 2008: p. 58-76.
34. Macnab, R.M. and S.I. Aizawa, *Bacterial Motility and the Bacterial Flagellar Motor*. Annual Review of Biophysics and Bioengineering, 1984. **13**(1): p. 51-83.
35. Kohl, L., D. Robinson, and P. Bastin, *The flagellum: from cell motility to morphogenesis*. J Soc Biol FIELD Full Journal Title:Journal de la Societe de biologie, 2003. **197**(4): p. 379-87.

36. Chilcott, G.S. and K.T. Hughes, *Coupling of flagellar gene expression to flagellar assembly in Salmonella enterica serovar typhimurium and Escherichia coli*. Microbiol Mol Biol Rev, 2000. **64**(4): p. 694-708.
37. Dingwall, A., J.D. Garman, and L. Shapiro, *Organization and ordered expression of Caulobacter genes encoding flagellar basal body rod and ring proteins*. J Mol Biol, 1992. **228**(4): p. 1147-62.
38. Macnab, R.M., *Genetics, structure, and assembly of the bacterial flagellum*. Symp. Soc. Gen. Microbiol. FIELD Full Journal Title:Symposium of the Society for General Microbiology, 1990. **46**(Biol. Chemotactic Response): p. 77-106.
39. Macnab, R.M., *HOW BACTERIA ASSEMBLE FLAGELLA*. Annual Review of Microbiology, 2003. **57**(1): p. 77-100.
40. Yonekura, K., S. Maki-Yonekura, and K. Namba, *Growth mechanism of the bacterial flagellar filament*. Res. Microbiol. FIELD Full Journal Title:Research in Microbiology, 2002. **153**(4): p. 191-197.
41. Minamino, T., K. Imada, and K. Namba, *Mechanisms of type III protein export for bacterial flagellar assembly*. Mol. BioSyst. FIELD Full Journal Title:Molecular BioSystems, 2008. **4**(11): p. 1105-1115.
42. Namba, K., et al., *Mechanisms of self-assembly and supercoiling of the bacterial flagellum*. Saibo Kogaku FIELD Full Journal Title:Saibo Kogaku, 2001. **20**(10): p. 1371-1379.
43. Namba, K., *Switch mechanism for polymorphic supercoiling of the bacterial flagellar filament*. Seibutsu Butsuri FIELD Full Journal Title:Seibutsu Butsuri, 2003. **43**(3): p. 118-123.
44. Namba, K., *Structural mechanism of self-assembly and polymorphic supercoiling of the bacterial flagellum*. Polym. Prepr. (Am. Chem. Soc., Div. Polym. Chem.) FIELD Full Journal Title:Polymer Preprints (American Chemical Society, Division of Polymer Chemistry), 2002. **43**(1): p. 185-186.
45. Aizawa, S.I., *Flagellar assembly in Salmonella typhimurium*. Mol Microbiol, 1996. **19**(1): p. 1-5.
46. Terashima, H., S. Kojima, and M. Homma, *Flagellar motility in bacteria structure and function of flagellar motor*. Int Rev Cell Mol Biol, 2008. **270**: p. 39-85.
47. Ohnishi, K., et al., *FlgD is a scaffolding protein needed for flagellar hook assembly in Salmonella typhimurium*. J Bacteriol, 1994. **176**(8): p. 2272-81.
48. Yokoseki, T., et al., *Functional analysis of the flagellar genes in the fliD operon of Salmonella typhimurium*. Microbiology, 1995. **141** (Pt 7): p. 1715-22.
49. Ikeda, T., et al., *Localization and stoichiometry of hook-associated proteins within Salmonella typhimurium flagella*. J Bacteriol, 1987. **169**(3): p. 1168-73.
50. Calladine, C.R., *Construction of bacterial flagellar filaments, and aspects of their conversion to different helical forms*. Symp Soc Exp Biol, 1982. **35**: p. 33-51.
51. Turner, L., W.S. Ryu, and H.C. Berg, *Real-Time Imaging of Fluorescent Flagellar Filaments*. J. Bacteriol., 2000. **182**(10): p. 2793-2801.
52. O'Brien, E.J. and P.M. Bennett, *Structure of straight flagella from a mutant Salmonella*. J Mol Biol, 1972. **70**(1): p. 133-52.
53. Yamashita, I., et al., *Structure and switching of bacterial flagellar filaments studied by X-ray fiber diffraction*. Nat Struct Biol, 1998. **5**(2): p. 125-32.
54. Samatey, F.A., et al., *Crystallization of the F41 Fragment of Flagellin and Data Collection from Extremely Thin Crystals*. J. Struct. Biol. FIELD Full Journal Title:Journal of Structural Biology, 2000. **132**(2): p. 106-111.
55. Samatey, F.A., et al., *Structure of the bacterial flagellar protofilament and implications for a switch for supercoiling*. Nature (London, U. K.) FIELD Full Journal Title:Nature (London, United Kingdom), 2001. **410**(6826): p. 331-337.

56. Yonekura, K., S. Maki-Yonekura, and K. Namba, *Complete atomic model of the bacterial flagellar filament by electron cryomicroscopy*. Nature (London, U. K.) FIELD Full Journal Title:Nature (London, United Kingdom), 2003. **424**(6949): p. 643-650.
57. Mimori-Kiyosue, Y., et al., *Direct interaction of flagellin termini essential for polymorphic ability of flagellar filament*. Proc Natl Acad Sci U S A, 1996. **93**(26): p. 15108-13.
58. Namba, K., I. Yamashita, and F. Vonderviszt, *Structure of the core and central channel of bacterial flagella*. Nature, 1989. **342**(6250): p. 648-54.
59. Morgan, D.G., et al., *Structure of Bacterial Flagellar Filaments at 11Å Resolution: Packing of the [alpha]-Helices*. Journal of Molecular Biology, 1995. **249**(1): p. 88-110.
60. Mimori, Y., et al., *The Structure of the R-type Straight Flagellar Filament of Salmonella at 9 Å Resolution by Electron Cryomicroscopy*. Journal of Molecular Biology, 1995. **249**(1): p. 69-87.
61. Tanskanen, J., T.K. Korhonen, and B. Westerlund-Wikstrom, *Construction of a multihybrid display system: flagellar filaments carrying two foreign adhesive peptides*. Appl. Environ. Microbiol. FIELD Full Journal Title:Applied and Environmental Microbiology, 2000. **66**(9): p. 4152-4156.
62. Yonekura, K., S. Maki-Yonekura, and K. Namba, *Building the atomic model for the bacterial flagellar filament by electron cryomicroscopy and image analysis*. Structure, 2005. **13**(3): p. 407-412.
63. Sarikaya, M., et al., *Materials assembly and formation using engineered polypeptides*. Annual Review of Materials Research, 2004. **34**: p. 373-408.
64. Tamerler, C., et al., *Molecular biomimetics: GEPI-based biological routes to technology*. Biopolymers, 2010. **94**(1): p. 78-94.
65. Tamerler, C. and M. Sarikaya, *Molecular biomimetics: utilizing nature's molecular ways in practical engineering*. Acta Biomater, 2007. **3**(3): p. 289-99.
66. Doi, N. and H. Yanagawa, *Screening of conformationally constrained random polypeptide libraries displayed on a protein scaffold*. Cell Mol Life Sci, 1998. **54**(5): p. 394-404.
67. Dani, M., *Peptide display libraries: Design and construction (Reprinted from Combinatorial Chemistry and Technology: Principles, Methods and Applications, pg 301-322, 1999)*. Journal of Receptor and Signal Transduction Research, 2001. **21**(4): p. 469-488.
68. Wernerus, H. and S. Stahl, *Biotechnological applications for surface-engineered bacteria*. Biotechnol Appl Biochem, 2004. **40**(Pt 3): p. 209-28.
69. Benhar, I., *Biotechnological applications of phage and cell display*. Biotechnol Adv, 2001. **19**(1): p. 1-33.
70. Chen, W. and G. Georgiou, *Cell-Surface display of heterologous proteins: From high-throughput screening to environmental applications*. Biotechnol Bioeng, 2002. **79**(5): p. 496-503.
71. Boublik, Y., P. Di Bonito, and I.M. Jones, *Eukaryotic virus display: engineering the major surface glycoprotein of the Autographa californica nuclear polyhedrosis virus (AcNPV) for the presentation of foreign proteins on the virus surface*. Biotechnology (N Y), 1995. **13**(10): p. 1079-84.
72. Yang, Z., et al., *Novel bacterial surface display systems based on outer membrane anchoring elements from the marine bacterium Vibrio anguillarum*. Appl Environ Microbiol, 2008. **74**(14): p. 4359-65.
73. Daugherty, P.S., *Protein engineering with bacterial display*. Curr Opin Struct Biol, 2007. **17**(4): p. 474-80.
74. Kondo, A. and M. Ueda, *Yeast cell-surface display--applications of molecular display*. Appl Microbiol Biotechnol, 2004. **64**(1): p. 28-40.

75. Merzlyak, A. and S.W. Lee, *Phage as templates for hybrid materials and mediators for nanomaterial synthesis*. Current Opinion in Chemical Biology, 2006. **10**(3): p. 246-252.
76. Samuelson, P., et al., *Display of proteins on bacteria*. Journal of Biotechnology, 2002. **96**(2): p. 129-154.
77. Klemm, P. and M.A. Schembri, *Fimbrial surface display systems in bacteria: from vaccines to random libraries*. Microbiology-Uk, 2000. **146**: p. 3025-3032.
78. Gold, L., *mRNA display: Diversity matters during in vitro selection*. Proceedings of the National Academy of Sciences of the United States of America, 2001. **98**(9): p. 4825-4826.
79. Wittrup, K.D., *Protein engineering by cell-surface display*. Curr Opin Biotechnol, 2001. **12**(4): p. 395-9.
80. Hosse, R.J., A. Rothe, and B.E. Power, *A new generation of protein display scaffolds for molecular recognition*. Protein Science, 2006. **15**(1): p. 14-27.
81. Westerlund-Wikstrom, B., *Peptide display on bacterial flagella: principles and applications*. International Journal of Medical Microbiology, 2000. **290**(3): p. 223-230.
82. Kuwajima, G., *Construction of a minimum-size functional flagellin of Escherichia coli*. J Bacteriol, 1988. **170**(7): p. 3305-9.
83. Beatson, S.A., T. Minamino, and M.J. Pallen, *Variation in bacterial flagellins: from sequence to structure*. Trends Microbiol, 2006. **14**(4): p. 151-5.
84. Kuwajima, G., *Flagellin domain that affects H antigenicity of Escherichia coli K-12*. J Bacteriol, 1988. **170**(1): p. 485-8.
85. Stocker, B.A. and S.M. Newton, *Immune responses to epitopes inserted in Salmonella flagellin*. Int Rev Immunol, 1994. **11**(2): p. 167-78.
86. Majander, K., et al., *The Bacterial Flagellum as a Surface Display and Expression Tool*, in *Pili and Flagella: Current Research and Future Trends*, K. Jarrell, Editor. 2009, Caister Academic Press. p. 191-206.
87. Ben-Yedidia, T. and R. Arnon, *Epitope-based vaccine against influenza*. Expert Rev Vaccines, 2007. **6**(6): p. 939-48.
88. Dilts, D.A., et al., *Phase I clinical trials of aroA aroD and aroA aroD htrA attenuated S. typhi vaccines; effect of formulation on safety and immunogenicity*. Vaccine, 2000. **18**(15): p. 1473-84.
89. Lu, Z., et al., *Expression of thioredoxin random peptide libraries on the Escherichia coli cell surface as functional fusions to flagellin: a system designed for exploring protein-protein interactions*. Biotechnology (N Y), 1995. **13**(4): p. 366-72.
90. Brown, C.K., et al., *A novel approach for the identification of unique tumor vasculature binding peptides using an E. coli peptide display library*. Ann Surg Oncol, 2000. **7**(10): p. 743-9.
91. Tripp, B.C., et al., *Investigation of the "switch-epitope" concept with random peptide libraries displayed as thioredoxin loop fusions*. Protein Eng., 2001. **14**(5): p. 367-377.
92. Yoshida, H., S.-H. Baik, and S. Harayama, *An effective peptide screening system using recombinant fluorescent bacterial surface display*. Biotechnol. Lett., 2002. **24**(20): p. 1715-1722.
93. Lu, Z., E.R. LaVallie, and J.M. McCoy, *Using bio-panning of FLITRX peptide libraries displayed on E. coli cell surface to study protein-protein interactions*. Methods Mol. Biol. (Totowa, NJ, U. S.), 2003. **205**(E. coli Gene Expression Protocols): p. 267-280.
94. Xin Zhong, T., et al., *Identification of mimotopes by screening of a bacterially displayed random peptide library and its use in eliciting an immune response to native HBV-preS*. Vaccine, 2003. **21**(27-30): p. 4373-9.
95. Xin, Z.-t., et al., *Isolation of a HBV-PreS2 epitope from a random peptide library displayed on the bacterial flagellin*. Zhongguo Yi Xue Ke Xue Yuan Xue Bao, 2003. **25**(1): p. 56-9.

96. Thai Corrine, K., et al., *Identification and characterization of Cu(2)O- and ZnO-binding polypeptides by Escherichia coli cell surface display: toward an understanding of metal oxide binding*. Biotechnol Bioeng, 2004. **87**(2): p. 129-37.
97. Schwarzman, A.L., et al., *Selection of peptides binding to the amyloid β -protein reveals potential inhibitors of amyloid formation*. Amyloid, 2005. **12**(4): p. 199-209.
98. Zitzmann, S., et al., *Identification of a new prostate-specific cyclic peptide with the bacterial FliTrx system*. J. Nucl. Med., 2005. **46**(5): p. 782-785.
99. Anon, *Selection of peptide ligands specific for baculovirus DNA-binding protein from the flitrax random peptide display library*. Anal. Lett., 2006. **39**(12): p. 2497.
100. Nguyen, K.V., *Peptide ligands specific for baculovirus DNA-binding protein selected from the FliTrx random peptide display library*. 2006, (Vista Biologicals Corporation, USA). Application: US. p. 11 pp.
101. Nguyen, K.V., *Selection of Peptide Ligands Specific for Baculovirus DNA-Binding Protein from the Flitrax Random Peptide Display Library*. Anal. Lett., 2006. **39**(1): p. 99-112.
102. Thattiyaphong, A., et al., *Antibody-binding motif of mimetic peptides to V. cholerae O139 lipopolysaccharide*. Proc. Kasetsart Univ. Annu. Conf., 44th, 2006: p. 42-49.
103. Li, W., et al., *Screening and identification of a novel target specific for hepatoma cell line HepG2 from the FliTrx bacterial peptide library*. Acta Biochim. Biophys. Sin., 2008. **40**(5): p. 443-451.
104. Nakanishi, K., H. Imanaka, and K. Imamura, *Cushioning-property adsorbent containing SS25 peptide, SS25' peptide, and/or cushion protein*. 2008, (Okayama University, Japan). Application: JP. p. 32pp.
105. Shiraishi, K., et al., *Evaluation of surface characteristic of poly(ethylene terephthalate) film modified with thermoresponsible polymers using bacterial random peptide library method*. Kobunshi Ronbunshu, 2008. **65**(2): p. 132-139.
106. Yang, W., et al., *TMTP1, a novel tumor-homing peptide specifically targeting metastasis*. Clin Cancer Res, 2008. **14**(17): p. 5494-502.
107. Galan, J.E. and H. Wolf-Watz, *Protein delivery into eukaryotic cells by type III secretion machines*. Nature, 2006. **444**(7119): p. 567-573.
108. Ikeda, T., S. Yamaguchi, and H. Hotani, *Flagellar growth in a filament-less Salmonella fliD mutant supplemented with purified hook-associated protein 2*. J Biochem, 1993. **114**(1): p. 39-44.
109. Majander, K., et al., *Extracellular secretion of polypeptides using a modified Escherichia coli flagellar secretion apparatus*. Nat Biotech, 2005. **23**(4): p. 475-481.
110. Vegh, B.M., et al., *Localization of the flagellum-specific secretion signal in Salmonella flagellin*. Biochem Biophys Res Commun, 2006. **345**(1): p. 93-8.
111. Lee, S.Y., J.H. Choi, and Z. Xu, *Microbial cell-surface display*. Trends Biotechnol, 2003. **21**(1): p. 45-52.
112. Yonekura, K., S. Maki-Yonekura, and K. Namba, *Complete atomic model of the bacterial flagellar filament by electron cryomicroscopy*. Nature, 2003. **424**(6949): p. 643-50.
113. Kumara, M.T., B.C. Tripp, and S. Muralidharan, *Self-Assembly of Metal Nanoparticles and Nanotubes on Bioengineered Flagella Scaffolds*. Chem. Mater. FIELD Full Journal Title:Chemistry of Materials, 2007. **19**(8): p. 2056-2064.
114. Deplanche, K., et al., *Manufacture of stable palladium and gold nanoparticles on native and genetically engineered flagella scaffolds*. Biotechnol. Bioeng. FIELD Full Journal Title:Biotechnology and Bioengineering, 2008. **101**(5): p. 873-880.

115. Kumara, M.T., B.C. Tripp, and S. Muralidharan, *Exciton Energy Transfer in Self-Assembled Quantum Dots on Bioengineered Bacterial Flagella Nanotubes*. J. Phys. Chem. C FIELD Full Journal Title:Journal of Physical Chemistry C, 2007. **111**(14): p. 5276-5280.
116. Ngweniform, P., D. Li, and C. Mao, *Self-assembly of drug-loaded liposomes on genetically engineered protein nanotubes: a potential anti-cancer drug delivery vector. [Erratum to document cited in CA151:063470]*. Soft Matter FIELD Full Journal Title:Soft Matter, 2009. **5**(24): p. 5044.
117. Yang, J., et al., *Hollow Silica Nanocontainers as Drug Delivery Vehicles*. Langmuir, 2008. **24**(7): p. 3417-3421.
118. Hesse, W.R., et al., *Mineralization of flagella for nanotube formation*. Mater. Sci. Eng., C FIELD Full Journal Title:Materials Science & Engineering, C: Materials for Biological Applications, 2009. **29**(7): p. 2282-2286.
119. Lazzari, M., et al., *Self-assembly: a minimalist route to the fabrication of nanomaterials*. J Nanosci Nanotechnol, 2006. **6**(4): p. 892-905.
120. Ma, H., et al., *Assembly of nanomaterials through highly ordered self-assembled monolayers and peptide-organic hybrid conjugates as templates*. J Nanosci Nanotechnol, 2007. **7**(8): p. 2549-66.
121. Crookes-Goodson, W.J., J.M. Slocik, and R.R. Naik, *Bio-directed synthesis and assembly of nanomaterials*. Chem Soc Rev, 2008. **37**(11): p. 2403-12.
122. Lee, S.-W., et al., *Ordering of Quantum Dots Using Genetically Engineered Viruses*. Science, 2002. **296**(5569): p. 892-895.
123. Barry, E., et al., *Entropy-driven formation of a chiral liquid-crystalline phase of helical filaments*. Phys Rev Lett, 2006. **96**(1): p. 018305.
124. Kumara, M.T., B.C. Tripp, and S. Muralidharan, *Layer-by-Layer Assembly of Bioengineered Flagella Protein Nanotubes*. Biomacromolecules FIELD Full Journal Title:Biomacromolecules, 2007. **8**(12): p. 3718-3722.
125. Woods, R.D., et al., *Bifunctional Nanotube Scaffolds for Diverse Ligands Are Purified Simply from Escherichia coli Strains Coexpressing Two Functionalized Flagellar Genes*. Nano Lett. FIELD Full Journal Title:Nano Letters, 2007. **7**(6): p. 1809-1816.
126. Majander, K., T.K. Korhonen, and B. Westerlund-Wikstrom, *Simultaneous display of multiple foreign peptides in the FliD capping and FliC filament proteins of the Escherichia coli flagellum*. Appl Environ Microbiol, 2005. **71**(8): p. 4263-8.
127. Iino, T., *Assembly of Salmonella flagellin in vitro and in vivo*. J Supramol Struct, 1974. **2**(2-4): p. 372-84.
128. Sergeeva, A., et al., *Display technologies: Application for the discovery of drug and gene delivery agents*. Advanced Drug Delivery Reviews, 2006. **58**(15): p. 1622-1654.
129. Salgado, A.J., O.P. Coutinho, and R.L. Reis, *Bone tissue engineering: state of the art and future trends*. Macromol Biosci, 2004. **4**(8): p. 743-65.
130. Hosseinkhani, H., et al., *Osteogenic differentiation of mesenchymal stem cells in self-assembled peptide-amphiphile nanofibers*. Biomaterials, 2006. **27**(22): p. 4079-4086.
131. Brinckmann, J., *Collagen : primer in structure, processing, and assembly*. 2005: p. 1-56.
132. Rossert, J. and B. de Crombrughe, *Type I collagen: Structure, synthesis, and regulation*. Principles of Bone Biology, 1996: p. 127-142.
133. Taton, T.A., *Nanotechnology. Boning up on biology*. Nature, 2001. **412**(6846): p. 491-2.
134. Murphy, W.L. and D.J. Mooney, *Molecular-scale biomimicry*. Nat Biotechnol, 2002. **20**(1): p. 30-1.
135. He, T., et al., *Nanofibrous Bio-inorganic Hybrid Structures Formed Through Self-Assembly and Oriented Mineralization of Genetically Engineered Phage Nanofibers*. Small, 2010. **6**(20): p. 2230-2235.

136. Wang, F., B. Cao, and C. Mao, *Bacteriophage Bundles with Prealigned Ca²⁺ Initiate the Oriented Nucleation and Growth of Hydroxylapatite*. *Chemistry of Materials*, 2010. **22**(12): p. 3630-3636.
137. Cao, B. and C. Mao, *Oriented Nucleation of Hydroxylapatite Crystals on Spider Dragline Silks*. *Langmuir*, 2007. **23**(21): p. 10701-10705.
138. Newton, S.M., C.O. Jacob, and B.A. Stocker, *Immune response to cholera toxin epitope inserted in Salmonella flagellin*. *Science*, 1989. **244**(4900): p. 70-2.
139. Kumara, M.T., B.C. Tripp, and S. Muralidharan, *Self-Assembly of Metal Nanoparticles and Nanotubes on Bioengineered Flagella Scaffolds*. *Chem. Mater.*, 2007. **19**(8): p. 2056-2064.
140. Kumara, M.T., B.C. Tripp, and S. Muralidharan, *Exciton Energy Transfer in Self-Assembled Quantum Dots on Bioengineered Bacterial Flagella Nanotubes*. *The Journal of Physical Chemistry C*, 2007. **111**(14): p. 5276-5280.
141. Kumara, M.T.M., Subra; Tripp, Brian C., *Generation and Characterization of Inorganic and Organic Nanotubes on Bioengineered Flagella of Mesophilic Bacteria*. *Journal of Nanoscience and Nanotechnology*, 2007. **7**: p. 2260-2272.
142. Wang, F., D. Li, and C. Mao, *Genetically Modifiable Flagella as Templates for Silica Fibers: From Hybrid Nanotubes to 1D Periodic Nanohole Arrays*. *Advanced Functional Materials*, 2009. **19**(21): p. n/a-n/a.
143. Deplanche, K., et al., *Manufacture of stable palladium and gold nanoparticles on native and genetically engineered flagella scaffolds*. *Biotechnology and Bioengineering*, 2008. **101**(5): p. 873-880.
144. Hesse, W.R., et al., *Mineralization of flagella for nanotube formation*. *Materials Science and Engineering: C*, 2009. **29**(7): p. 2282-2286.
145. Weiner, S. and W. Traub, *Crystal size and organization in bone*. *Connect Tissue Res FIELD Full Journal Title:Connective tissue research*, 1989. **21**(1-4): p. 259-65.
146. Hodge, A.J., *Molecular models illustrating the possible distributions of 'holes' in simple systematically staggered arrays of type I collagen molecules in native-type fibrils*. *Connect Tissue Res FIELD Full Journal Title:Connective tissue research*, 1989. **21**(1-4): p. 137-47.
147. Glimcher, M.J. and S.M. Krane, *Organization and structure of bone, and the mechanism of calcification*. *Treatise Collagen FIELD Full Journal Title:*, 1968. **2**(Pt. B): p. 67-251.
148. Weiner, S. and P.A. Price, *Disaggregation of bone into crystals*. *Calcif Tissue Int FIELD Full Journal Title:Calcified tissue international*, 1986. **39**(6): p. 365-75.
149. Landis, W.J., F.H. Silver, and J.W. Freeman, *Collagen as a scaffold for biomimetic mineralization of vertebrate tissues*. *Journal of Materials Chemistry*, 2006. **16**(16): p. 1495-1503.
150. Maitland, M.E. and A.L. Arsenault, *A correlation between the distribution of biological apatite and amino acid sequence of type I collagen*. *Calcified Tissue International*, 1991. **48**(5): p. 341-52.
151. Wiesmann, H.P., et al., *Aspects of collagen mineralization in hard tissue formation*. *International Review of Cytology*, 2005. **242**(Survey of Cell Biology): p. 121-156.
152. Landis, W.J. and F.H. Silver, *Mineral Deposition in the Extracellular Matrices of Vertebrate Tissues: Identification of Possible Apatite Nucleation Sites on Type I Collagen*. *Cells Tissues Organs FIELD Full Journal Title:Cells Tissues Organs*, 2009. **189**(1-4): p. 20-24.
153. Rhee, S.-H., J.D. Lee, and J. Tanaka, *Nucleation of hydroxyapatite crystal through chemical interaction with collagen*. *Journal of the American Ceramic Society*, 2000. **83**(11): p. 2890-2892.
154. Hunter, G.K., et al., *Nucleation and inhibition of hydroxyapatite formation by mineralized tissue proteins*. *Biochem J*, 1996. **317 (Pt 1)**: p. 59-64.

155. Hoang, Q.Q., et al., *Bone recognition mechanism of porcine osteocalcin from crystal structure*. Nature (London, United Kingdom), 2003. **425**(6961): p. 977-980.
156. Harris, N.L., et al., *Functional analysis of bone sialoprotein: identification of the hydroxyapatite-nucleating and cell-binding domains by recombinant peptide expression and site-directed mutagenesis*. Bone, 2000. **27**(6): p. 795-802.
157. He, G., et al., *Nucleation of apatite crystals in vitro by self-assembled dentin matrix protein I*. Nature Materials, 2003. **2**(8): p. 552-558.
158. Hartgerink, J.D., E. Beniash, and S.I. Stupp, *Self-assembly and mineralization of peptide-amphiphile nanofibers*. Science, 2001. **294**(5547): p. 1684-8.
159. Hunter, G.K. and H.A. Goldberg, *Modulation of crystal formation by bone phosphoproteins: role of glutamic acid-rich sequences in the nucleation of hydroxyapatite by bone sialoprotein*. Biochem J, 1994. **302** (Pt 1): p. 175-9.
160. Tye, C.E., et al., *Delineation of the hydroxyapatite-nucleating domains of bone sialoprotein*. J Biol Chem, 2003. **278**(10): p. 7949-55.
161. Goldberg, H.A., et al., *Determination of the hydroxyapatite-nucleating region of bone sialoprotein*. Connect Tissue Res, 1996. **35**(1-4): p. 385-92.
162. West, M., N.M. Burdash, and F. Freimuth, *Simplified silver-plating stain for flagella*. J Clin Microbiol, 1977. **6**(4): p. 414-9.
163. Lu, H.B., et al., *Controlled crystallization of calcium phosphate under stearic acid monolayers*. Journal of Crystal Growth, 1995. **155**(1/2): p. 120-5.
164. Kamiya, R. and S. Asakura, *Flagellar transformations at alkaline pH*. Journal of Molecular Biology, 1976. **108**(2): p. 513-518.
165. De Almeida, M.E.S., S.M. Newton, and L.C.S. Ferreira, *Antibody responses against flagellin in mice orally immunized with attenuated Salmonella vaccine strains*. Arch. Microbiol. FIELD Full Journal Title:Archives of Microbiology, 1999. **172**(2): p. 102-108.
166. Wakabayashi, K., H. Hotani, and S. Asakura, *Polymerization of salmonella flagellin in the presence of high concentrations of salts*. Biochimica et Biophysica Acta (BBA) - Protein Structure, 1969. **175**(1): p. 195-203.
167. Zhang, W., S.S. Liao, and F.Z. Cui, *Hierarchical Self-Assembly of Nano-Fibrils in Mineralized Collagen*. Chemistry of Materials, 2003. **15**(16): p. 3221-3226.
168. Zhang, W., et al., *Nucleation Sites of Calcium Phosphate Crystals during Collagen Mineralization*. Journal of the American Ceramic Society, 2003. **86**(6): p. 1052-1054.
169. Alam, M. and D. Oesterhelt, *Morphology, function and isolation of halobacterial flagella*. J Mol Biol, 1984. **176**(4): p. 459-75.
170. Wang, Y., et al., *Biomimetic formation of hydroxyapatite/collagen matrix composite*. Advanced Engineering Materials, 2006. **8**(1-2): p. 97-100.
171. Landis, W.J., et al., *Mineral and Organic Matrix Interaction in Normally Calcifying Tendon Visualized in Three Dimensions by High-Voltage Electron Microscopic Tomography and Graphic Image Reconstruction*. Journal of Structural Biology, 1993. **110**(1): p. 39-54.
172. Toworfe, G.K., et al., *Nucleation and growth of calcium phosphate on amine-, carboxyl- and hydroxyl-silane self-assembled monolayers*. Biomaterials, 2006. **27**(4): p. 631-42.
173. Gajardo, R., et al., *Two proline residues are essential in the calcium-binding activity of rotavirus VP7 outer capsid protein*. J. Virol., 1997. **71**(3): p. 2211-2216.
174. Mattice, W.L. and L. Mandelkern, *The Conformational Transition Induced in Poly(4-hydroxy-L-proline) by Calcium Chloride*. Macromolecules, 1970. **3**(2): p. 199-201.
175. Chung, W.-J., et al., *Evolutionary Screening of Collagen-like Peptides That Nucleate Hydroxyapatite Crystals*. Langmuir, 2011: p. null-null.
176. Goldberg, H.A., et al., *Binding of bone sialoprotein, osteopontin and synthetic polypeptides to hydroxyapatite*. Connect Tissue Res, 2001. **42**(1): p. 25-37.

177. Zhu, P., Y. Masuda, and K. Koumoto, *The effect of surface charge on hydroxyapatite nucleation*. *Biomaterials*, 2004. **25**(17): p. 3915-21.
178. Iannotti Joseph, P., et al., *Porcine small intestine submucosa augmentation of surgical repair of chronic two-tendon rotator cuff tears. A randomized, controlled trial*. *J. Bone Joint Surgery*, 2006. **88**(6): p. 1238-1244.
179. Tye, C.E., G.K. Hunter, and H.A. Goldberg, *Identification of the Type I Collagen-binding Domain of Bone Sialoprotein and Characterization of the Mechanism of Interaction*. *Journal of Biological Chemistry*, 2005. **280**(14): p. 13487-13492.
180. Tiffany, M.L. and S. Krimm, *New chain conformations of poly(glutamic acid) and polylysine*. *Biopolymers*, 1968. **6**(9): p. 1379-82.
181. Strzelecka-Golaszewska, H., E. PrÓchniewicz, and W. Drabikowski, *Interaction of Actin with Divalent Cations*. *European Journal of Biochemistry*, 1978. **88**(1): p. 219-227.
182. Song, J., V. Malathong, and C.R. Bertozzi, *Mineralization of synthetic polymer scaffolds: a bottom-up approach for the development of artificial bone*. *J Am Chem Soc*, 2005. **127**(10): p. 3366-72.
183. Sarikaya, M., et al., *Molecular biomimetics: nanotechnology through biology*. *Nat Mater*, 2003. **2**(9): p. 577-85.
184. Kumara, M.T., et al., *Bioengineered flagella protein nanotubes with cysteine loops: self-assembly and manipulation in an optical trap*. *Nano Lett*, 2006. **6**(9): p. 2121-9.
185. Sabir, M., X. Xu, and L. Li, *A review on biodegradable polymeric materials for bone tissue engineering applications*. *Journal of Materials Science*, 2009. **44**(21): p. 5713-5724.
186. George, A. and S. Ravindran, *Protein templates in hard tissue engineering*. *Nano Today*, 2010. **5**(4): p. 254-266.
187. Murugan, R. and S. Ramakrishna, *Nanoengineered Biomimetic Bone-Building Blocks*, in *Molecular Building Blocks for Nanotechnology*, G. Mansoori, et al., Editors. 2007, Springer Berlin / Heidelberg. p. 301-352.
188. Semino, C.E., *Self-assembling Peptides: From Bio-inspired Materials to Bone Regeneration*. *Journal of Dental Research*, 2008. **87**(7): p. 606-616.
189. Mata, A., et al., *Bone regeneration mediated by biomimetic mineralization of a nanofiber matrix*. *Biomaterials*, 2010. **31**(23): p. 6004-6012.
190. Jayawarna, V., et al., *Nanostructured Hydrogels for Three-Dimensional Cell Culture Through Self-Assembly of Fluorenylmethoxycarbonyl-Dipeptides*. *Advanced Materials*, 2006. **18**(5): p. 611-614.
191. Mart, R.J., et al., *Peptide-based stimuli-responsive biomaterials*. *Soft Matter*, 2006. **2**(10): p. 822-835.
192. Zhang, S., *Fabrication of novel biomaterials through molecular self-assembly*. *Nat Biotech*, 2003. **21**(10): p. 1171-1178.
193. Sargeant, T.D., et al., *Covalent functionalization of NiTi surfaces with bioactive peptide amphiphile nanofibers*. *Biomaterials*, 2008. **29**(8): p. 1085-1098.
194. Zhu, H., et al., *Controlled growth and differentiation of MSCs on grooved films assembled from monodisperse biological nanofibers with genetically tunable surface chemistries*. *Biomaterials*, 2011. **32**(21): p. 4744-4752.
195. Kaur, G., et al., *Regulation of osteogenic differentiation of rat bone marrow stromal cells on 2D nanorod substrates*. *Biomaterials*, 2010. **31**(7): p. 1732-1741.
196. Zhang, Y., et al., *The osteogenic properties of CaP/silk composite scaffolds*. *Biomaterials*, 2010. **31**(10): p. 2848-2856.
197. Rho, J.-Y., L. Kuhn-Spearing, and P. Zioupos, *Mechanical properties and the hierarchical structure of bone*. *Medical Engineering & Physics*, 1998. **20**(2): p. 92-102.

198. Perret, S., et al., *Unhydroxylated Triple Helical Collagen I Produced in Transgenic Plants Provides New Clues on the Role of Hydroxyproline in Collagen Folding and Fibril Formation*. Journal of Biological Chemistry, 2001. **276**(47): p. 43693-43698.
199. Boudko, S., et al., *Nucleation and propagation of the collagen triple helix in single-chain and trimerized peptides: transition from third to first order kinetics*. Journal of Molecular Biology, 2002. **317**(3): p. 459-470.
200. Cejas, M.A., et al., *Collagen-Related Peptides: Self-Assembly of Short, Single Strands into a Functional Biomaterial of Micrometer Scale*. Journal of the American Chemical Society, 2007. **129**(8): p. 2202-2203.
201. Przybyla, D.E. and J. Chmielewski, *Higher-Order Assembly of Collagen Peptides into Nano- and Microscale Materials*. Biochemistry, 2010. **49**(21): p. 4411-4419.
202. Kotch, F.W. and R.T. Raines, *Self-assembly of synthetic collagen triple helices*. Proceedings of the National Academy of Sciences of the United States of America, 2006. **103**(9): p. 3028-3033.
203. Fallas, J.A., L.E.R. O'Leary, and J.D. Hartgerink, *Synthetic collagen mimics: self-assembly of homotrimers, heterotrimers and higher order structures*. Chemical Society Reviews, 2010. **39**(9): p. 3510-3527.
204. Gauba, V. and J.D. Hartgerink, *Self-Assembled Heterotrimeric Collagen Triple Helices Directed through Electrostatic Interactions*. Journal of the American Chemical Society, 2007. **129**(9): p. 2683-2690.
205. Koide, T., *Triple Helical Collagen-Like Peptides: Engineering and Applications in Matrix Biology*. Connective Tissue Research, 2005. **46**(3): p. 131-141.
206. Olsen, B.E., et al., *The synthetic polytripeptides (Pro-Pro-Gly)₁₀ and (Pro-Pro-Gly)₂₀ form micro-crystalline structures similar to segmental structures formed by collagen*. Journal of Molecular Biology, 1971. **57**(3): p. 589-590.
207. Engel, J., et al., *Polymers of tripeptides as collagen models: II. Conformational changes of poly(L-prolyl-glycyl-L-prolyl) in solution*. Journal of Molecular Biology, 1966. **17**(1): p. 255-272.
208. Kobayashi, Y., et al., *Physicochemical analysis of (Pro-Pro-Gly)_n with defined molecular weight-temperature dependence of molecular weight in aqueous solution*. Biopolymers, 1970. **9**(4): p. 415-425.
209. Bella, J., et al., *Crystal and molecular structure of a collagen-like peptide at 1.9 Å resolution*. Science, 1994. **266**(5182): p. 75-81.
210. Brodsky, B. and J.A.M. Ramshaw, *The collagen triple-helix structure*. Matrix Biology, 1997. **15**(8-9): p. 545-554.
211. Persikov, A.V., et al., *Electrostatic Interactions Involving Lysine Make Major Contributions to Collagen Triple-Helix Stability†*. Biochemistry, 2005. **44**(5): p. 1414-1422.
212. Schnell, J., *Evidence for the existence of hydrophobic interactions as a stabilizing factor in collagen structure*. Archives of Biochemistry and Biophysics, 1968. **127**: p. 496-502.
213. Hulmes, D.J.S., et al., *Analysis of the primary structure of collagen for the origins of molecular packing*. Journal of Molecular Biology, 1973. **79**(1): p. 137-148.
214. Li, S.-T. and E.P. Katz, *An electrostatic model for collagen fibrils. The interaction of reconstituted collagen with Ca⁺⁺, Na⁺, and Cl⁻*. Biopolymers, 1976. **15**(8): p. 1439-1460.
215. Fowler, W.E. and U. Aebi, *Polymorphism of actin paracrystals induced by polylysine*. The Journal of Cell Biology, 1982. **93**(2): p. 452-458.
216. Gorman, J., L.A. Schick, and J. Newman, *The bundling of actin with polyethylene glycol 8000 in the presence and absence of gelsolin*. Biophysical journal, 1996. **71**(3): p. 1485-1492.

217. Cao, B., H. Xu, and C. Mao, *Controlled Self-Assembly of Rodlike Bacterial Pili Particles into Ordered Lattices*. Angewandte Chemie International Edition, 2011: p. n/a-n/a.
218. McMichael, J.C. and J.T. Ou, *Binding of lysozyme to common pili of Escherichia coli*. J. Bacteriol., 1979. **138**(3): p. 976-983.
219. Evans, C.H. and B.J. Drouven, *The promotion of collagen polymerization by lanthanide and calcium ions*. Biochem J, 1983. **213**(3): p. 751-8.
220. Urry, D.W., *Neutral Sites for Calcium Ion Binding to Elastin and Collagen: A Charge Neutralization Theory for Calcification and Its Relationship to Atherosclerosis*. Proceedings of the National Academy of Sciences of the United States of America, 1971. **68**(4): p. 810-814.
221. Cui, F.Z., et al., *Conformation change of collagen during the initial stage of biomineralization of calcium phosphate*. Journal of Materials Chemistry, 2008. **18**(32): p. 3835-3840.
222. Yang, B. and F.Z. Cui, *Molecular modeling and mechanics studies on the initial stage of the collagen-mineralization process*. Current Applied Physics, 2007. **7**(Supplement 1): p. e2-e5.
223. Jones, C., *Structural aspects of recognition and assembly in biological macromolecules. Volumes 1 and 2: Edited by M Balaban. pp 961. Balaban international science services, Rehovot and Philadelphia. 1981 ISBN 0-86689-002-5 and 003-3*. Biochemical Education, 1984. **12**(1): p. 43-43.
224. Dalby, M.J., et al., *The control of human mesenchymal cell differentiation using nanoscale symmetry and disorder*. Nat Mater, 2007. **6**(12): p. 997-1003.
225. Smith, L.A., et al., *The Enhancement of human embryonic stem cell osteogenic differentiation with nano-fibrous scaffolding*. Biomaterials, 2010. **31**(21): p. 5526-5535.
226. Cairns, M.L., et al., *Influence of surface topography on osteoblast response to fibronectin coated calcium phosphate thin films*. Colloids and Surfaces B: Biointerfaces, 2010. **78**(2): p. 283-290.
227. Wang, H., et al., *Biocompatibility and osteogenesis of biomimetic nano-hydroxyapatite/polyamide composite scaffolds for bone tissue engineering*. Biomaterials, 2007. **28**(22): p. 3338-3348.
228. Anderson, J.M., et al., *Osteogenic Differentiation of Human Mesenchymal Stem Cells Directed by Extracellular Matrix-Mimicking Ligands in a Biomimetic Self-Assembled Peptide Amphiphile Nanomatrix*. Biomacromolecules, 2009. **10**(10): p. 2935-2944.
229. Gerecht, S., et al., *The effect of actin disrupting agents on contact guidance of human embryonic stem cells*. Biomaterials, 2007. **28**(28): p. 4068-4077.
230. Galli, D., et al., *In vitro osteoblastic differentiation of human mesenchymal stem cells and human dental pulp stem cells on poly-L-lysine-treated titanium-6-aluminium-4-vanadium*. Journal of Biomedical Materials Research Part A, 2011. **97A**(2): p. 118-126.
231. Tsai, K.-S., et al., *Type I collagen promotes proliferation and osteogenesis of human mesenchymal stem cells via activation of ERK and Akt pathways*. Journal of Biomedical Materials Research Part A, 2010. **94A**(3): p. 673-682.
232. Westerlund-Wikström, B., et al., *Functional expression of adhesive peptides as fusions to Escherichia coli flagellin*. Protein Engineering, 1997. **10**(11): p. 1319-1326.
233. Burdelya, L.G., et al., *An Agonist of Toll-Like Receptor 5 Has Radioprotective Activity in Mouse and Primate Models*. Science, 2008. **320**(5873): p. 226-230.
234. Stevens, M.M., *Biomaterials for bone tissue engineering*. Materials Today, 2008. **11**(5): p. 18-25.
235. Alves, N.M., et al., *Designing biomaterials based on biomineralization of bone*. Journal of Materials Chemistry, 2010. **20**(15): p. 2911-2921.
236. Palmer, L.C., et al., *Biomimetic systems for hydroxyapatite mineralization inspired by bone and enamel*. Chem Rev, 2008. **108**(11): p. 4754-83.

237. Xu, A.-W., Y. Ma, and H. Calfen, *Biomimetic mineralization*. Journal of Materials Chemistry, 2007. **17**(5): p. 415-449.
238. Barthelat, F., *Biomimetics for next generation materials*. Philos Transact A Math Phys Eng Sci, 2007. **365**(1861): p. 2907-19.
239. Ma, P.X., *Biomimetic materials for tissue engineering*. Adv Drug Deliv Rev, 2008. **60**(2): p. 184-98.
240. Shin, H., S. Jo, and A.G. Mikos, *Biomimetic materials for tissue engineering*. Biomaterials, 2003. **24**(24): p. 4353-64.
241. Subramani, K.K., Ameen; George, Anne, *Self-Assembly of Proteins and Peptides and their Applications in Bionanotechnology*. Current Nanoscience, 2008. **4**: p. 201-207.
242. Altman, G.H., et al., *Silk-based biomaterials*. Biomaterials, 2003. **24**(3): p. 401-416.
243. Merzlyak, A. and S.-W. Lee, *Phage as templates for hybrid materials and mediators for nanomaterial synthesis*. Current Opinion in Chemical Biology, 2006. **10**(3): p. 246-252.
244. Osathanon, T., et al., *Microporous nanofibrous fibrin-based scaffolds for bone tissue engineering*. Biomaterials, 2008. **29**(30): p. 4091-4099.
245. Kaur, G., et al., *The synergistic effects of multivalent ligand display and nanotopography on osteogenic differentiation of rat bone marrow stem cells*. Biomaterials, 2010. **31**(22): p. 5813-24.
246. Merzlyak, A., S. Indrakanti, and S.W. Lee, *Genetically engineered nanofiber-like viruses for tissue regenerating materials*. Nano Lett, 2009. **9**(2): p. 846-52.
247. Chung, W.J., et al., *Genetically engineered liquid-crystalline viral films for directing neural cell growth*. Langmuir, 2010. **26**(12): p. 9885-90.
248. Zhu, H., et al., *Controlled growth and differentiation of MSCs on grooved films assembled from monodisperse biological nanofibers with genetically tunable surface chemistries*. Biomaterials, 2011. **In press**.
249. Yonekura, K., S. Maki-Yonekura, and K. Namba, *Growth mechanism of the bacterial flagellar filament*. Res Microbiol, 2002. **153**(4): p. 191-7.
250. Westerlund-Wikstrom, B., *Peptide display on bacterial flagella: principles and applications*. Int J Med Microbiol, 2000. **290**(3): p. 223-30.
251. Termine, J.D., *Non-Collagen Proteins in Bone*. Ciba Foundation Symposium 136 - Cell and Molecular Biology of Vertebrate Hard Tissues. 2007: John Wiley & Sons, Ltd. 178-206.
252. Itoh, D., et al., *Enhancement of osteogenesis on hydroxyapatite surface coated with synthetic peptide (EEEEEEPRGDT) in vitro*. Journal of Biomedical Materials Research, 2002. **62**(2): p. 292-298.
253. VandeVondele, S., J. Vörös, and J.A. Hubbell, *RGD-grafted poly-l-lysine-graft-(polyethylene glycol) copolymers block non-specific protein adsorption while promoting cell adhesion*. Biotechnology and Bioengineering, 2003. **82**(7): p. 784-790.
254. Sawyer, A.A., K.M. Hennessy, and S.L. Bellis, *Regulation of mesenchymal stem cell attachment and spreading on hydroxyapatite by RGD peptides and adsorbed serum proteins*. Biomaterials, 2005. **26**(13): p. 1467-75.
255. Yang, F., et al., *The effect of incorporating RGD adhesive peptide in polyethylene glycol diacrylate hydrogel on osteogenesis of bone marrow stromal cells*. Biomaterials, 2005. **26**(30): p. 5991-5998.
256. Rammelt, S., et al., *Coating of titanium implants with collagen, RGD peptide and chondroitin sulfate*. Biomaterials, 2006. **27**(32): p. 5561-5571.
257. Park, J.S., et al., *Osteogenic differentiation of human mesenchymal stem cells using RGD-modified BMP-2 coated microspheres*. Biomaterials, 2010. **31**(24): p. 6239-6248.
258. Bianco, P., et al., *Bone Marrow Stromal Stem Cells: Nature, Biology, and Potential Applications*. Stem Cells, 2001. **19**(3): p. 180-192.

259. Derubeis, A.R. and R. Cancedda, *Bone Marrow Stromal Cells (BMSCs) in Bone Engineering: Limitations and Recent Advances*. Annals of Biomedical Engineering, 2004. **32**(1): p. 160-165.
260. Lvov, Y., et al., *Assembly of Multicomponent Protein Films by Means of Electrostatic Layer-by-Layer Adsorption*. Journal of the American Chemical Society, 1995. **117**(22): p. 6117-6123.
261. Dezawa, M., et al., *Bone marrow stromal cells generate muscle cells and repair muscle degeneration*. Science, 2005. **309**(5732): p. 314-7.
262. Fowler, W.E. and U. Aebi, *Polymorphism of actin paracrystals induced by polylysine*. J Cell Biol, 1982. **93**(2): p. 452-8.
263. Goverman, J., L.A. Schick, and J. Newman, *The bundling of actin with polyethylene glycol 8000 in the presence and absence of gelsolin*. Biophys J, 1996. **71**(3): p. 1485-92.
264. Oh, S., et al., *Stem cell fate dictated solely by altered nanotube dimension*. Proc Natl Acad Sci U S A, 2009. **106**(7): p. 2130-5.
265. Kaur, G., et al., *Regulation of osteogenic differentiation of rat bone marrow stromal cells on 2D nanorod substrates*. Biomaterials, 2010. **31**(7): p. 1732-41.
266. Mazia, D., G. Schatten, and W. Sale, *Adhesion of cells to surfaces coated with polylysine. Applications to electron microscopy*. The Journal of Cell Biology, 1975. **66**(1): p. 198-200.
267. Teng, S.-H., et al., *Bioactive nanocomposite coatings of collagen/hydroxyapatite on titanium substrates*. Journal of Materials Science: Materials in Medicine, 2008. **19**(6): p. 2453-2461.
268. LeBaron, R.G. and K.A. Athanasiou, *Extracellular matrix cell adhesion peptides: functional applications in orthopedic materials*. Tissue Eng, 2000. **6**(2): p. 85-103.
269. John P. Bilezikian, L.G.R., Gideon A. Rodan, *Index for Volumes 1 and 2*, in *Principles of Bone Biology (Second Edition)*, P.B. John, G.R. Lawrence, and A.R. Gideon, Editors. 2002, Academic Press: San Diego. p. 1667-1696.
270. Padial-Molina, M., et al., *Role of wettability and nanoroughness on interactions between osteoblast and modified silicon surfaces*. Acta Biomaterialia, 2011. **7**(2): p. 771-778.
271. Lu, H.G., Likun; Kawazoe, Naoki; Tateishi, Tetsuya; Chen, Guoping, *Effects of Poly(L-lysine), Poly(acrylic acid) and Poly(ethylene glycol) on the Adhesion, Proliferation and Chondrogenic Differentiation of Human Mesenchymal Stem Cells*. Journal of Biomaterials Science, Polymer Edition, 2009. **20**: p. 577-589.
272. Bernhardt, A., et al., *Mineralised collagen—an artificial, extracellular bone matrix—improves osteogenic differentiation of bone marrow stromal cells*. Journal of Materials Science: Materials in Medicine, 2008. **19**(1): p. 269-275.
273. Bruder, S.P., D.J. Fink, and A.I. Caplan, *Mesenchymal stem cells in bone development, bone repair, and skeletal regeneration therapy*. Journal of Cellular Biochemistry, 1994. **56**(3): p. 283-294.
274. Lin, L., K.L. Chow, and Y. Leng, *Study of hydroxyapatite osteoinductivity with an osteogenic differentiation of mesenchymal stem cells*. Journal of Biomedical Materials Research Part A, 2009. **89A**(2): p. 326-335.
275. Kotobuki, N., et al., *Observation of osteogenic differentiation cascade of living mesenchymal stem cells on transparent hydroxyapatite ceramics*. Biomaterials, 2005. **26**(7): p. 779-785.
276. Müller, P., et al., *Calcium phosphate surfaces promote osteogenic differentiation of mesenchymal stem cells*. Journal of Cellular and Molecular Medicine, 2008. **12**(1): p. 281-291.
277. Schroeder, T.M., E.D. Jensen, and J.J. Westendorf, *Runx2: A master organizer of gene transcription in developing and maturing osteoblasts*. Birth Defects Research Part C: Embryo Today: Reviews, 2005. **75**(3): p. 213-225.

278. Huang, J., et al., *MicroRNA-204 regulates Runx2 protein expression and mesenchymal progenitor cell differentiation*. Stem Cells, 2010. **28**(2): p. 357-64.
279. Hoshikawa, H. and R. Kamiya, *Elastic properties of bacterial flagellar filaments: II. Determination of the modulus of rigidity*. Biophysical Chemistry, 1985. **22**(3): p. 159-166.
280. Hhling, H.J., et al., *Structural Relationship Between the Primary Crystal Formations and the Matrix Macromolecules in Different Hard Tissues. Discussion of a General Principle*. Connective Tissue Research, 1995. **33**(1-3): p. 171-178.
281. Wiesmann, H.P., et al., *Aspects of Collagen Mineralization in Hard Tissue Formation*, in *International Review of Cytology*, W.J. Kwang, Editor. 2004, Academic Press. p. 121-156.
282. Lee, J.-Y., et al., *Assembly of collagen-binding peptide with collagen as a bioactive scaffold for osteogenesis in vitro and in vivo*. Biomaterials, 2007. **28**(29): p. 4257-4267.
283. Lakshminarayanan, R., R.M. Kini, and S. Valiyaveetil, *Investigation of the role of ansocalcin in the biomineralization in goose eggshell matrix*. Proceedings of the National Academy of Sciences, 2002. **99**(8): p. 5155-5159.
284. Hoang, Q.Q., et al., *Bone recognition mechanism of porcine osteocalcin from crystal structure*. Nature, 2003. **425**(6961): p. 977-980.
285. Gericke, A., et al., *Importance of Phosphorylation for Osteopontin Regulation of Biomineralization*. Calcified Tissue International, 2005. **77**(1): p. 45-54.
286. He, G., et al., *Phosphorylation of Phosphoryn Is Crucial for Its Function as a Mediator of Biomineralization*. Journal of Biological Chemistry, 2005. **280**(39): p. 33109-33114.
287. Tye, C.E., et al., *Delineation of the Hydroxyapatite-nucleating Domains of Bone Sialoprotein*. Journal of Biological Chemistry, 2003. **278**(10): p. 7949-7955.
288. Hartgerink, J.D., E. Beniash, and S.I. Stupp, *Self-Assembly and Mineralization of Peptide-Amphiphile Nanofibers*. Science, 2001. **294**(5547): p. 1684-1688.
289. Donella-Deana, A., et al., *Tyrosine phosphorylation of protein kinase CK2 by Src-related tyrosine kinases correlates with increased catalytic activity*. Biochem. J., 2003. **372**(3): p. 841-849.
290. Sarno, S., et al., *Protein Kinase CK2 Mutants Defective in Substrate Recognition*. Journal of Biological Chemistry, 1996. **271**(18): p. 10595-10601.
291. Marin, O., F. Meggio, and L.A. Pinna, *Design and Synthesis of Two New Peptide Substrates for the Specific and Sensitive Monitoring of Casein Kinases 1 and 2*. Biochemical and Biophysical Research Communications, 1994. **198**(3): p. 898-905.
292. Kumara, M.T., et al., *Bioengineered Flagella Protein Nanotubes with Cysteine Loops: Self-Assembly and Manipulation in an Optical Trap*. Nano Letters, 2006. **6**(9): p. 2121-2129.
293. Garca-Ramos, J.V. and P. Carmona, *The effect of some homopolymers on the crystallization of calcium phosphates*. Journal of Crystal Growth, 1982. **57**(2): p. 336-342.
294. Sarig, S. and F. Kahana, *On the association between sparingly soluble carbonates and polyelectrolytes*. Journal of Crystal Growth, 1976. **35**(2): p. 145-152.
295. Hiltner, W.A., A.J. Hopfinger, and A.G. Walton, *Helix-coil controversy for polyamino acids*. Journal of the American Chemical Society, 1972. **94**(12): p. 4324-4327.
296. Boskey, A.L., *Phosphoproteins and Biomineralization*. Phosphorus, Sulfur, and Silicon and the Related Elements, 1999. **144**(1): p. 189 - 192.
297. Veis, A., C. Sfeir, and C.B. Wu, *Phosphorylation of the Proteins of the Extracellular Matrix of Mineralized Tissues By Casein Kinase-Like Activity*. Critical Reviews in Oral Biology & Medicine, 1997. **8**(4): p. 360-379.

298. Ou, K.-L., et al., *Effects of the nanostructure and nanoporosity on bioactive nanohydroxyapatite/reconstituted collagen by electrodeposition*. Journal of Biomedical Materials Research Part A, 2010. **92A**(3): p. 906-912.
299. Kikuchi, M., et al., *Biomimetic synthesis of bone-like nanocomposites using the self-organization mechanism of hydroxyapatite and collagen*. Composites Science and Technology, 2004. **64**(6): p. 819-825.
300. Fujisawa, R., Y. Nodasaka, and Y. Kuboki, *Further characterization of interaction between bone sialoprotein (BSP) and collagen*. Calcified Tissue International, 1995. **56**(2): p. 140-144.
301. He, G. and A. George, *Dentin Matrix Protein 1 Immobilized on Type I Collagen Fibrils Facilitates Apatite Deposition in Vitro*. J. Biol. Chem., 2004. **279**(12): p. 11649-11656.
302. Fujisawa, K. and Y. Kuboki, *Affinity of bone sialoprotein and several other bone and dentin acidic proteins to collagen fibrils*. Calcified Tissue International, 1992. **51**(6): p. 438-442.
303. Nudelman, F., et al., *The role of collagen in bone apatite formation in the presence of hydroxyapatite nucleation inhibitors*. Nat Mater, 2010. **9**(12): p. 1004-1009.
304. Barone, D.T.J., J.M. Raquez, and P. Dubois, *Bone-guided regeneration: from inert biomaterials to bioactive polymer (nano)composites*. Polymers for Advanced Technologies, 2011. **22**(5): p. 463-475.
305. Wang, Y., et al., *In vitro cartilage tissue engineering with 3D porous aqueous-derived silk scaffolds and mesenchymal stem cells*. Biomaterials, 2005. **26**(34): p. 7082-7094.
306. Donzelli, E., et al., *Mesenchymal stem cells cultured on a collagen scaffold: In vitro osteogenic differentiation*. Archives of oral biology, 2007. **52**(1): p. 64-73.
307. Bini, E., et al., *RGD-Functionalized Bioengineered Spider Dragline Silk Biomaterial*. Biomacromolecules, 2006. **7**(11): p. 3139-3145.
308. Chung, W.-J., A. Merzlyak, and S.-W. Lee, *Fabrication of engineered M13 bacteriophages into liquid crystalline films and fibers for directional growth and encapsulation of fibroblasts*. Soft Matter, 2010. **6**(18): p. 4454-4459.
309. Merzlyak, A., S. Indrakanti, and S.-W. Lee, *Genetically Engineered Nanofiber-Like Viruses For Tissue Regenerating Materials*. Nano Letters, 2009. **9**(2): p. 846-852.
310. Yonekura, K., S. Maki-Yonekura, and K. Namba, *Complete atomic model of the bacterial flagellar filament by electron cryomicroscopy*. Nature, 2003. **424**(6949): p. 643-650.
311. Chung, H.J., et al., *Collagen Fibril Formation*. Journal of Biological Chemistry, 2008. **283**(38): p. 25879-25886.
312. Mitchell, D.T., et al., *Smart Nanotubes for Bioseparations and Biocatalysis*. Journal of the American Chemical Society, 2002. **124**(40): p. 11864-11865.
313. Yang, X., et al., *Templated-assisted one-dimensional silica nanotubes: synthesis and applications*. Journal of Materials Chemistry, 2011. **21**(17): p. 6122-6135.
314. Jung, J.H., M. Park, and S. Shinkai, *Fabrication of silica nanotubes by using self-assembled gels and their applications in environmental and biological fields*. Chemical Society Reviews, 2010. **39**(11): p. 4286-4302.
315. He, B., S.J. Son, and S.B. Lee, *Shape-Coded Silica Nanotubes for Biosensing*. Langmuir, 2006. **22**(20): p. 8263-8265.
316. Ogihara, H., et al., *Synthesis of SiO₂ Nanotubes and Their Application as Nanoscale Reactors*. Chemistry of Materials, 2006. **18**(4): p. 996-1000.
317. Lee Sang, B., et al., *Template-Synthesized Bionanotubes for Separations and Biocatalysis*, in *Carrier-Based Drug Delivery*. 2004, American Chemical Society. p. 98-118.
318. Chen, C.C., et al., *Preparation of Fluorescent Silica Nanotubes and Their Application in Gene Delivery*. Advanced Materials, 2005. **17**(4): p. 404-407.

319. Wu, X., et al., *A Novel Route for Synthesizing Silica Nanotubes with Chiral Mesoporous Wall Structures*. Chemistry of Materials, 2007. **19**(7): p. 1577-1583.
320. Zygmunt, J., F. Krumeich, and R. Nesper, *Novel Silica Nanotubes with a High Aspect Ratio—Synthesis and Structural Characterization*. Advanced Materials, 2003. **15**(18): p. 1538-1541.
321. Jung, J.H., K. Yoshida, and T. Shimizu, *Creation of Novel Double-Helical Silica Nanotubes Using Binary Gel System*. Langmuir, 2002. **18**(23): p. 8724-8727.
322. Wan, X. and et al., *The formation of helical mesoporous silica nanotubes*. Nanotechnology, 2008. **19**(31): p. 315602.
323. Shenton, W., et al., *Inorganic–Organic Nanotube Composites from Template Mineralization of Tobacco Mosaic Virus*. Advanced Materials, 1999. **11**(3): p. 253-256.
324. Royston, E., et al., *Characterization of silica-coated tobacco mosaic virus*. Journal of Colloid and Interface Science, 2006. **298**(2): p. 706-712.
325. Numata, M., et al., *Sol–Gel Reaction Using DNA as a Template: An Attempt Toward Transcription of DNA into Inorganic Materials*. Angewandte Chemie International Edition, 2004. **43**(25): p. 3279-3283.
326. Meegan, J.E., et al., *Designed Self-Assembled β -Sheet Peptide Fibrils as Templates for Silica Nanotubes*. Advanced Functional Materials, 2004. **14**(1): p. 31-37.
327. Ono, Y., et al., *Preparation of Novel Hollow Fiber Silica Using Collagen Fibers as a Template*. Chemistry Letters, 1999. **28**(6): p. 475-476.
328. Ji, Q., et al., *Self-assembly of glycolipids on silica nanotube templates yielding hybrid nanotubes with concentric organic and inorganic layers*. Journal of Materials Chemistry, 2005. **15**(7): p. 743-748.
329. Samatey, F.A., et al., *Structure of the bacterial flagellar protofilament and implications for a switch for supercoiling*. Nature, 2001. **410**(6826): p. 331-337.
330. Asakura, S., *Polymerization of flagellin and polymorphism of flagella*. Adv Biophys, 1970. **1**: p. 99-155.
331. Asakura, S. and T. Iino, *Polymorphism of Salmonella flagella as investigated by means of in vitro copolymerization of flagellins derived from various strains*. Journal of Molecular Biology, 1972. **64**(1): p. 251-256.
332. Kamiya, R. and S. Asakura, *Helical transformations of Salmonella flagella in vitro*. Journal of Molecular Biology, 1976. **106**(1): p. 167-186.
333. Alam, M. and D. Oesterhelt, *Purification, reconstitution and polymorphic transition of halobacterial flagella*. Journal of Molecular Biology, 1987. **194**(3): p. 495-499.
334. Hasegawa, E., R. Kamiya, and S. Asakura, *Thermal transition in helical forms of Salmonella flagella*. Journal of Molecular Biology, 1982. **160**(4): p. 609-621.
335. Livage, J., M. Henry, and C. Sanchez, *Sol-gel chemistry of transition metal oxides*. Progress in Solid State Chemistry, 1988. **18**(4): p. 259-341.
336. Cihlár, J., *Hydrolysis and polycondensation of ethyl silicates. 1. Effect of pH and catalyst on the hydrolysis and polycondensation of tetraethoxysilane (TEOS)*. Colloids and Surfaces A: Physicochemical and Engineering Aspects, 1993. **70**(3): p. 239-251.
337. van Bommel, K.J.C. and S. Shinkai, *Silica Transcription in the Absence of a Solution Catalyst: The Surface Mechanism*. Langmuir, 2002. **18**(12): p. 4544-4548.
338. Ikeda, T., R. Kamiya, and S. Yamaguchi, *Excretion of flagellin by a short-flagella mutant of Salmonella typhimurium*. J. Bacteriol., 1983. **153**(1): p. 506-510.
339. SCHAEFER, D.W., *Polymers, Fractals, and Ceramic Materials*. Science, 1989. **243**(4894): p. 1023-1027.
340. Fowler, C.E., et al., *Tobacco Mosaic Virus Liquid Crystals as Templates for the Interior Design of Silica Mesophases and Nanoparticles*. Advanced Materials, 2001. **13**(16): p. 1266-1269.

341. Yuwono, V.M. and J.D. Hartgerink, *Peptide Amphiphile Nanofibers Template and Catalyze Silica Nanotube Formation*. *Langmuir*, 2007. **23**(9): p. 5033-5038.
342. Brinker, C.J., *Hydrolysis and condensation of silicates: Effects on structure*. *Journal of Non-Crystalline Solids*, 1988. **100**(1-3): p. 31-50.
343. Wenzl, S., et al., *Quaternary Ammonium Groups in Silica-Associated Proteins*. *Angewandte Chemie International Edition*, 2004. **43**(44): p. 5933-5936.
344. Sumper, M., E. Brunner, and G. Lehmann, *Biominingalization in diatoms: Characterization of novel polyamines associated with silica*. *FEBS letters*, 2005. **579**(17): p. 3765-3769.
345. Kröger, N., R. Deutzmann, and M. Sumper, *Polycationic Peptides from Diatom Biosilica That Direct Silica Nanosphere Formation*. *Science*, 1999. **286**(5442): p. 1129-1132.
346. Kuang, D., et al., *Application of highly ordered TiO₂ nanotube arrays in flexible dye-sensitized solar cells*. *ACS Nano*, 2008. **2**(6): p. 1113-6.
347. Rani, S., et al., *Synthesis and applications of electrochemically self-assembled titania nanotube arrays*. *Phys Chem Chem Phys*, 2010. **12**(12): p. 2780-800.
348. Sekino, T., *Synthesis and Applications of Titanium Oxide Nanotubes*. *Inorganic and Metallic Nanotubular Materials: Recent Technologies and Applications*, 2010. **117**: p. 17-32.
349. Nicula, R., et al., *Spark plasma sintering synthesis of porous nanocrystalline titanium alloys for biomedical applications*. *Biomol Eng*, 2007. **24**(5): p. 564-7.
350. Popat, K.C., et al., *Titania nanotubes: a novel platform for drug-eluting coatings for medical implants?* *Small*, 2007. **3**(11): p. 1878-81.
351. Roy, S.C., M. Paulose, and C.A. Grimes, *The effect of TiO₂ nanotubes in the enhancement of blood clotting for the control of hemorrhage*. *Biomaterials*, 2007. **28**(31): p. 4667-72.
352. Popat, K.C., et al., *Decreased Staphylococcus epidermis adhesion and increased osteoblast functionality on antibiotic-loaded titania nanotubes*. *Biomaterials*, 2007. **28**(32): p. 4880-8.
353. Peng, L., et al., *Long-term small molecule and protein elution from TiO₂ nanotubes*. *Nano Lett*, 2009. **9**(5): p. 1932-6.
354. Maiyalagan, T., B. Viswanathan, and U.V. Varadaraju, *Fabrication and characterization of uniform TiO₂ nanotube arrays by sol-gel template method*. 2006, Indian Academy of Sciences.
355. Sumerel, J.L., et al., *Biocatalytically Templated Synthesis of Titanium Dioxide*. *Chemistry of Materials*, 2003. **15**(25): p. 4804-4809.
356. Kharlampieva, E., et al., *Bioenabled Surface-Mediated Growth of Titania Nanoparticles*. *Advanced Materials*, 2008. **20**(17): p. 3274-3279.
357. Kröger, N., et al., *Bioenabled Synthesis of Rutile (TiO₂) at Ambient Temperature and Neutral pH*. *Angewandte Chemie International Edition*, 2006. **45**(43): p. 7239-7243.
358. Sewell, S.L. and D.W. Wright, *Biomimetic Synthesis of Titanium Dioxide Utilizing the R5 Peptide Derived from *Cylindrotheca fusiformis**. *Chemistry of Materials*, 2006. **18**(13): p. 3108-3113.
359. Ji, Q. and T. Shimizu, *Chemical synthesis of transition metal oxide nanotubes in water using an iced lipid nanotube as a template*. *Chemical Communications*, 2005(35): p. 4411-4413.
360. Dickerson, M.B., et al., *Identification and Design of Peptides for the Rapid, High-Yield Formation of Nanoparticulate TiO₂ from Aqueous Solutions at Room Temperature*. *Chemistry of Materials*, 2008. **20**(4): p. 1578-1584.
361. Kharlampieva, E., et al., *Protein-Enabled Synthesis of Monodisperse Titania Nanoparticles On and Within Polyelectrolyte Matrices*. *Advanced Functional Materials*, 2009. **19**(14): p. 2303-2311.

362. Luckarift, H.R., et al., *Rapid, room-temperature synthesis of antibacterial bionanocomposites of lysozyme with amorphous silica or titania*. *Small*, 2006. **2**(5): p. 640-3.
363. Fujikawa, S. and T. Kunitake, *Surface Fabrication of Hollow Nanoarchitectures of Ultrathin Titania Layers from Assembled Latex Particles and Tobacco Mosaic Viruses as Templates*. *Langmuir*, 2003. **19**(16): p. 6545-6552.
364. Dickerson, M.B., K.H. Sandhage, and R.R. Naik, *Protein- and peptide-directed syntheses of inorganic materials*. *Chem Rev*, 2008. **108**(11): p. 4935-78.
365. Durupthy, O., J. Bill, and F. Aldinger, *Bioinspired Synthesis of Crystalline TiO₂: Effect of Amino Acids on Nanoparticles Structure and Shape*. *Crystal Growth & Design*, 2007. **7**(12): p. 2696-2704.
366. Miyashita, K., et al., *Spectrum response of the vacuum-deposited SiO₂/TiO₂ multilayer film with improved photocatalytic activity*. *Journal of Materials Science Letters*, 2001. **20**(23): p. 2137-2140.
367. Fujimoto, M., et al., *Nanostructure of TiO₂ Nano-Coated SiO₂ Particles*. *Journal of the American Ceramic Society*, 2005. **88**(11): p. 3264-3266.
368. Teleki, A., M.K. Akhtar, and S.E. Pratsinis, *The quality of SiO₂-coatings on flame-made TiO₂-based nanoparticles*. *Journal of Materials Chemistry*, 2008. **18**(30): p. 3547-3555.
369. Zhan, S., et al., *Mesoporous TiO₂/SiO₂ composite nanofibers with selective photocatalytic properties*. *Chemical Communications*, 2007(20): p. 2043-2045.
370. Kamiya, R., S. Asakura, and S. Yamaguchi, *Formation of helical filaments by copolymerization of two types of /'straight/' flagellins*. *Nature*, 1980. **286**(5773): p. 628-630.
371. Wang, F., D. Li, and C. Mao, *Genetically Modifiable Flagella as Templates for Silica Fibers: From Hybrid Nanotubes to 1D Periodic Nanohole Arrays*. *Advanced Functional Materials*, 2008. **18**(24): p. 4007-4013.
372. Ibrahim, G.F., et al., *Method for the isolation of highly purified Salmonella flagellins*. *J. Clin. Microbiol.*, 1985. **22**(6): p. 1040-1044.
373. Trachtenberg, S. and D.J. DeRosier, *A three-start helical sheath on the flagellar filament of Caulobacter crescentus*. *J. Bacteriol.*, 1992. **174**(19): p. 6198-6206.
374. Davydova, O., et al., *The effect exerted by the type of the solvent and precursor in sol-gel preparation of titanium dioxide on its electrorheological activity*. *Russian Journal of Applied Chemistry*, 2010. **83**(1): p. 14-17.
375. Kumar, K.-N.P., J. Kumar, and K. Keizer, *Effect of Peptization on Densification and Phase-Transformation Behavior of Sol-Gel-Derived Nanostructured Titania*. *Journal of the American Ceramic Society*, 1994. **77**(5): p. 1396-1400.
376. Demiroirs, A.F., A. van Blaaderen, and A. Imhof, *Synthesis of Eccentric Titania-Silica Core-Shell and Composite Particles*. *Chemistry of Materials*, 2009. **21**(6): p. 979-984.
377. Yang, Y., X. Wang, and L. Li, *Crystallization and Phase Transition of Titanium Oxide Nanotube Arrays*. *Journal of the American Ceramic Society*, 2008. **91**(2): p. 632-635.
378. Hwang, S.-T., et al., *Preparation and characterization of poly(MSMA-co-MMA)-TiO₂/SiO₂ nanocomposites using the colloidal TiO₂/SiO₂ particles via blending method*. *Colloids and Surfaces A: Physicochemical and Engineering Aspects*, 2005. **259**(1-3): p. 63-69.
379. Park, O.K. and Y.S. Kang, *Preparation and characterization of silica-coated TiO₂ nanoparticle*. *Colloids and Surfaces A: Physicochemical and Engineering Aspects*, 2005. **257-258**: p. 261-265.